UNIVERSITY OF CALIFORNIA
RIVERSIDE

Pharyngeal Taste in *Drosophila* – From Periphery to Brain

A Dissertation submitted in partial satisfaction
of the requirements for the degree of

Doctor of Philosophy

in

Neuroscience

by

Yu-Chieh Chen

September 2019

Dissertation Committee:
Dr. Anupama Dahanukar, Chairperson
Dr. Michael Adams
Dr. Naoki Yamanaka

The Dissertation of Yu-Chieh Chen is approved:

Committee Chairperson

University of California, Riverside

Acknowledgements

My graduate career would not have been so enjoyable and fruitful without the immense support and assistance of my advisor, colleagues, friends, and family. I would like to express my gratitude to my thesis advisor, Dr. Anupama Dahanukar, for her continuous support on both my personal life and academic development during the past six years. With her guidance, I was fortuned to freely explore scientific questions that excited me the most. She helps me to set the research and career goals, and develop strategies to meet these goals. She always provides her constructive suggestions on my projects, and keeps up the momentum when things are not going so well. She encourages me and provides financial supports to attend conferences, meetings, workshops that extend my scientific network effectively with other scientists. I own my deepest gratitude to her for shaping me as an independent scientist and for sharing this exciting scientific journey with me.

I also own many thanks to my thesis committee members- Dr. Michael Adams and Dr. Naoki Yamanaka for their time and effort they put in to ensure I am on the right track. They always provide me with respectful, positive affirmation and constructive feedback. Special thanks to Dr. Anandasankar Ray, who provides valuable experimental insights as well as career advice throughout my graduate career.

Many thanks to my collaborators for their contributions on various part of this thesis research. Dr. Emily LeDue and Dr. Michael Gordon at University of British Columbia provided their expertise on calcium imaging for characterizing the pharyngeal sweet taste neurons and initiated the use of *Poxn-neuro* mutant flies a model for

pharyngeal taste research that becomes an essential part of my thesis research later on. Ms. Scarlet Park and Dr. William Ja at Scripps Florida provided their expertise on various quantitative feeding assays as well as the optogenetic experiments to reveal the functional roles of pharyngeal bitter taste neurons. Dr. Ryan Joseph at University of California Riverside for setting up the *ex vivo* pharyngeal calcium imaging preparation and measure the response profiles of different pharyngeal taste neurons. Mr. Vaibhav Menon at University of California Riverside for his help on running FLIC assays and optimizing the FLIC analysis R code.

I would like to thank the past and the current members of the Dahanukar lab for providing me a friendly and collaborative environment; the members in Ray lab, Yamanaka lab and Adams lab for their useful feedback on my project during the supergroup lab meeting.

I am heartily thankful to various grant/fellowship/scholarship providers, including Sigma XI Grants-in-Aid of Research, Phi Beta Kappa Alumni in Southern California, Yin Chin Foundation of USA, Howard Hughes Medical Institute, and UC Riverside graduate division for their generous financial supports of my graduate research.

Finally, I am grateful to have many supports from my friends and family. A special thank goes to my wife, Ariel Kuan, for her endless love and support for now and the future.

ABSTRACT OF THE DISSERTATION

Pharyngeal Taste in *Drosophila* – From Periphery to Brain

by

Yu-Chieh Chen

Doctor of Philosophy, Graduate Program in Neuroscience
University of California, Riverside, September 2019
Dr. Anupama Dahanukar, Chairperson

Feeding behaviors, guided by the taste system, serve universal and essential functions in animals. The availability of molecular genetic tools and assays to measure behavioral outcomes at high resolution in real time have made the fly, *Drosophila melanogaster*, an invaluable model to identify molecular components and dissect circuit logic of how the quality and quantity of ingested food is controlled. However, most investigations of taste responses have focused on neurons residing in external taste hairs in the labellum, legs, and wing margins. There remains a complex repertoire of pharyngeal taste neurons lying in an anatomical position to control food intake, which has been largely overlooked. This comparatively limited knowledge of the molecular or functional nature of internal taste neurons in the pharynx represents a critical missing link between taste sensory input and feeding behavior output. Notably, taste-guided feeding behaviors of insect disease vectors and pests impose a substantial economic and health burden in the world. An understanding of taste circuits that regulate feeding may lead to the development of behavior-modifying strategies for insect control. In this dissertation, I

present a receptor-to-neuron map for all pharyngeal organs, comprising in a genetic toolkit that allows manipulation of specific cell types in the pharynx, and genetic dissection experiments to assess the roles of selected classes of pharyngeal taste neurons in food selection and intake. The results uncover mechanisms of combinatorial taste coding in pharyngeal taste neurons that mediate feeding avoidance of aversive compounds such as bitter compounds, acids, and high salts. I then report the development of a taste-blind system to examine function of individual classes of pharyngeal taste neurons in controlling food intake of appetitive tastants, such as sugars and amino acids. Finally, I describe efforts to identify potential higher-order brain neurons that control feeding behaviors, and discovery of a subset of brain neurons that might receive pharyngeal input and mediate regurgitation behavior. Taking advantage of tools established by this study for probing pharyngeal function, future investigations can accomplish a systems-level analysis of pharyngeal taste neurons and circuits, and explore functional intersections between taste input and neuroendocrine function in the brain towards guiding feeding behaviors.

Table of Contents

List of Figures

List of Tables

CHAPTER I

General introduction

Portions of this chapter was submitted as a revision to Cellular and Molecular Life Sciences on August 15, 2019 – **YCD Chen** and A Dahanukar. *Recent advances in the genetic basis of taste detection in Drosophila.*

Portions of this chapter have been published previously – **YCD Chen**, SJ Park, WW Ja, and A Dahanukar. *Using Pox-neuro (Poxn) mutants in Drosophila gustation research: a double-edged sword.* Frontiers in Cellular Neuroscience, October 24, 2018; 12(382).

Drosophila gustation: a powerful model for understanding how animals process sensory inputs to generate behaviors

Animals continuously receive and process massive amounts of sensory information from the surrounding environment via different sensory systems, which direct appropriate behavioral responses. Specialized sensory organs in the body are specifically tuned to various types of sensory stimuli. Sensory information is then decoded in the central nervous system, mainly in the brain. In insects, contact chemosensory cues are sensed by the gustatory system, which is critical for mating, feeding, and oviposition behaviors. *Drosophila melanogaster* has been an excellent model organism for dissecting the genetic underpinnings of behaviors driven by gustatory systems in insects, including agricultural pests and disease vectors. A wealth of behavioral and functional assays, combined with the availability of genetic tools and reagents, offer the means to probe how chemical information is encoded at different levels of the gustatory pathway in *Drosophila*. Recent years have seen significant progress in understanding sensory coding in the periphery as well as in mapping of higher-order taste circuits in the fly brain. In this review, we focus on the adult *Drosophila* gustatory system and its role in detecting food-related cues that control feeding and oviposition behaviors. We provide a general overview of the adult *Drosophila* gustatory system and then present recent advances in our knowledge of chemosensory receptors and neurons underlying peripheral responses to various tastants. We also discuss evidence for multimodal taste sensing properties of *Drosophila* neurons,

and for functional differences between neurons across taste organs towards operating different aspects of feeding behaviors.

Anatomical organization of the gustatory system in adult *Drosophila*

In adult *Drosophila*, taste organs are distributed in different parts of the body (**Figure 1.1.**). External taste organs include the anterior wing margin (**Figure 1.1.A**), distal segments of the legs (**Figure 1.1.B**), and the labellum (**Figure 1.1.C-D**). Internal taste organs include three pharyngeal taste organs located internally in the proboscis: labral sense organ (LSO), ventral cibarial sense organ (VCSO), and dorsal cibarial sense organ (DCSO) (**Figure 1.1.E**). Taste organs are covered by morphologically distinct taste sensilla, the basic functional units of taste detection (**Figure 1.1.F-H**). The *Drosophila* labellum, the most extensively characterized taste organ, consists of two types of taste sensilla: taste hairs (**Figure 1.1.C**) and taste pegs (**Figure 1.1.D**). Labellar taste hairs are located on the distal tip of the labellum. There are ~30 hairs on each half of the labellum that can be further divided into morphological subtypes based on the length of the hairs: L (long), I (intermediate), and S (short). Each taste hair has a single pore at the tip of the sensillum, which allows tastants to enter and make contact with the chemosensory neurons present within. All labellar taste hairs house a single mechanosensory neuron, but the number of chemosensory neurons that reside in them varies from two to four, depending on the subtype (i.e. four neurons in L- and S-hairs, two neurons in I-hairs) (**Figure 1.1.F**). Labellar taste pegs are hairless sensilla located between rows of pseudotrachea. The number of labellar taste pegs is sexually dimorphic, with females

having more than males (Shanbhag et al., 2001). Each labellar taste peg is innervated by one mechanosensory neuron and one chemosensory neuron (**Figure 1.1.G**). During feeding, these taste pegs are thought to access food only when the flies open their labial palps. Besides the labellum, taste hairs are distributed on the five tarsal segments of all six legs as well as the anterior wing margins, all of which are innervated by one mechanosensory neuron and four chemosensory neurons (Shanbhag et al., 2001) (**Figure 1.1.F**). Interestingly, the tarsal taste hairs on the forelegs are sexually dimorphic, with more hairs in males than in females. Perhaps not surprisingly, male-specific taste hairs on the forelegs are involved in pheromone detection during courtship behavior (Thistle et al., 2012, Bray and Amrein, 2003). Unlike external taste hairs, internal taste sensilla in the pharyngeal organs are hairless. They are innervated by one to eight chemosensory neurons, and may or may not be associated with mechanosensory neurons (Stocker, 1994, Stocker and Schorderet, 1981) (**Figure 1.1.H**). In *Drosophila*, most sensory neurons are cholinergic (Salvaterra and Kitamoto, 2001), but recent studies showed that a small fraction of labellar and tarsal chemosensory neurons are glutamatergic (Jaeger et al., 2018, Kallman et al., 2015), suggesting neurochemical and functional heterogeneity within chemosensory neurons. However, further studies are required to systemically characterize neurotransmitters that are used in chemosensory neurons of all taste organs.

Physiological response profiles of chemosensory neurons

Single-sensillum extracellular tip recordings allow measurement of physiological responses of all chemosensory neurons in a single taste sensillum (Hiroi et al., 2004).

Recordings are obtained with tastant solutions in glass micropipette electrodes that are used to contact the tips of taste hairs. The stereotypical arrangement and accessibility of taste hairs in the labellum, tarsi, and wings have lent themselves to systematic surveys of tastant-evoked responses. In general, distinct responses have been recorded with stimuli representing distinct taste modalities, which include water, sugar, salt (high and low), acid, and bitter compounds (Hiroi et al., 2004, Ling et al., 2014, Charlu et al., 2013, Weiss et al., 2011, Dahanukar et al., 2007). Based on characteristic spike amplitudes and responses to tastants, neurons have been classified into water-, sweet-, salt-, and bitter-sensing populations. However, the extent to which each population is selectively tuned to tastants remains to be determined, and recent studies suggest that at least some taste neurons can respond to compounds of different taste categories (see below for details), hinting at multimodal taste detection properties in insect taste neurons. Moreover, gustatory coding information is incomplete because the same type of analysis has not been achieved for internal pharyngeal taste sensilla and hairless taste pegs of the oral surface, which are difficult to access as compared to external taste hairs.

Chemosensory receptor gene expression in adult *Drosophila* taste neurons

Almost two decades ago, the *Gustatory receptor* (*Gr*) gene family was identified as a new family encoding transmembrane proteins as candidate taste receptors expressed in taste organs (Clyne et al., 2000, Scott et al., 2001, Dunipace et al., 2001). In *Drosophila melanogaster*, there are 60 *Gr* genes encoding 68 proteins. Although *Gr* transcript expression was typically too low to be reliably detected by *in situ*

hybridization, a series of transgenic reporter lines using the *GAL4/UAS* binary expression system were soon developed to analyze *Gr* expression (Scott et al., 2001, Dunipace et al., 2001). Receptor-to-neuron maps based on reporter analysis were constructed for the labellum (Weiss et al., 2011, Fujii et al., 2015, Jaeger et al., 2018), tarsi (Ling et al., 2014), and pharynx (Chen and Dahanukar, 2017, Ledue et al., 2015). Patterns of *GAL4* reporter expression have been confirmed by independent means only in a few instances (Moon et al., 2009, Dahanukar et al., 2007). Nevertheless, these reporter lines serve as excellent tools for functional analysis of molecularly defined taste neurons. In addition to members of the *Gr* gene family, recent studies have found that other chemosensory receptors, including those encoded by *Ionotropic receptor* (*Ir*), *pickpocket* (*ppk*), and *Transient receptor potential* (*Trp*) gene families, are involved in tastant detection (Sanchez-Alcaniz et al., 2018, Croset et al., 2010, Jaeger et al., 2018, Zhang et al., 2013a, Steck et al., 2018, Ganguly et al., 2017, Croset et al., 2016, Koh et al., 2014, Liu et al., 2018, Vijayan et al., 2014, Toda et al., 2012, Lu et al., 2012, Chen et al., 2010, Cameron et al., 2010, Guntur et al., 2017, Soldano et al., 2016, Du et al., 2016, Zhang et al., 2013b, Kim et al., 2010, Lee et al., 2017, Kang et al., 2011, Kang et al., 2010, Chen and Amrein, 2017, Ahn et al., 2017, Tauber et al., 2017, Hussain et al., 2016, Rimal et al., 2019, He et al., 2019). Transgenic reporter lines for many of these chemosensory genes, in particular the *Ir* genes, have also been constructed, and a significant fraction of them were found to be expressed in taste organs (Sanchez-Alcaniz et al., 2018, Koh et al., 2014). In general, the expression of different chemosensory receptors showed some degree of overlap, especially in the pharynx where most pharyngeal taste neurons express more than one

type of chemosensory receptor gene family (Chen and Dahanukar, 2017). In the following sections, we will discuss recent findings of chemosensory receptors involved in detecting tastants representing canonical taste categories as well as non-canonical taste modalities (**Table 1.1**). While we have attempted to provide information that is fairly extensive, readers are also encouraged to consult other recent reviews on the general function of these chemosensory receptors (Rimal and Lee, 2018, Joseph and Carlson, 2015, Freeman and Dahanukar, 2015).

Taste detection by chemosensory neurons

Sweet

In *Drosophila*, eight Grs belong to a clade of conserved sweet taste receptors that include Gr5a, Gr61a, and Gr64a-f. Based on transgenic reporter techniques, subsets of sweet taste neurons were found to express distinct combinations of sweet Grs (Dahanukar et al., 2007, Ledue et al., 2015, Fujii et al., 2015). Mutant analyses showed that individual sweet Grs are required for sensing multiple sugars, and each sugar response appears to be dependent on multiple sweet Grs (Fujii et al., 2015, Dahanukar et al., 2007, Jiao et al., 2008, Jiao et al., 2007, Slone et al., 2007). In addition, some sweet gustatory receptor neurons (GRNs) also express Gr43a, a highly conserved Gr that is outside of the sweet clade (Fujii et al., 2015, Miyamoto and Amrein, 2014, Miyamoto et al., 2012, Ledue et al., 2015). *Gr43a* is also expressed in nutrient-sensing neurons in the brain, which monitor fructose levels in the hemolymph (Miyamoto et al., 2012).

Some differences in neuronal activation profiles of sweet GRNs in different taste organs have been reported. D- and L-arabinose, for example, have been found to activate tarsal and pharyngeal *Gr43a* GRNs differentially, but not *Gr43a*-expressing neurons in the brain in which both D- and L-arabinose evoke similar responses in terms of both magnitude and kinetics (Mcginnis et al., 2016). Instances of variation in physiological responses observed between different sweet GRNs have been attributed to distinct chemosensory receptor repertoires (Jiao et al., 2008, Slone et al., 2007, Dahanukar et al., 2007, Miyamoto et al., 2013).

Sweet GRNs originating from different organs exhibit distinct axonal projection patterns in the subesophageal zone (SEZ), the primary taste center in the central nervous system (Wang et al., 2004, Thorne et al., 2004, Chen and Dahanukar, 2017). The organotopic map has been the basis for a model in which input from each taste organ is relayed to distinct higher-order neuronal circuits, which in turn regulate different aspects of feeding behavior. Notably, recent studies have found evidence for such differences in sweet GRN-controlled feeding behaviors. For example, two anatomically distinct classes of tarsal sweet GRNs, one that terminates in the ventral nerve cord (VNC) and a second that passes through the VNC and terminates in the SEZ, have been reported to regulate different behavioral responses to sugars. Those ending in the VNC are responsible for stopping the fly's movements upon encountering sugar, while the ones that project to the SEZ are responsible for initiating feeding (Thoma et al., 2016). In addition, pharyngeal sweet GRNs, which project to a discrete region of the SEZ, are distinct from external

sweet GRNs in terms of the behaviors they regulate (Chen and Dahanukar, 2017, Ledue et al., 2015). Another study reported that sugar detection can elicit local search behavior, and this appears to be mediated primarily by pharyngeal *Gr43a* GRNs and not external GRNs (Murata et al., 2017). A finding that confirms the presence of discrete circuit elements for internal and external taste is the identification of IN1 interneurons that are connected with pharyngeal *Gr43a* GRNs but not with external sweet GRNs. (Yapici et al., 2016). IN1 neurons integrate information about pharyngeal sweet taste and hunger to control meal dynamics. Altogether, these findings suggest that the sweet GRNs in different locations can sense ligands in different ways, convey input to different regions in the CNS, and thereby control different aspects of feeding behaviors in response to carbohydrate cues in food substrates.

Given the extended focus on the study of Gr involvement in sweet taste, it was a surprise when sugar-sensitivity was found in a pair of *Ir60b*-expressing neurons in the pharynx (Joseph et al., 2017). *Ir60b* GRNs are unique in that 1) they do not express sweet *Grs*, but rather a few Irs, including *Ir60b*, *Ir94f*, *Ir94h*, and *Ir25a*; 2) their activation restricts sugar consumption rather than promotes it; and 3) they appear to be selectively involved in cellular and behavioral responses to sucrose and glucose but not to other sugars such as trehalose and fructose. These results evoke several interesting questions for follow up studies. Are there other non-*Gr* expressing neurons that detect sugars, possibly those other than sucrose and glucose? How does Ir60b confer sugar responsiveness? Is it directly involved in detecting sucrose, either alone or in

combination with other Irs? How does activation of pharyngeal *Ir60b* GRNs limit sugar consumption – by directly inhibiting *Gr*-expressing sweet taste circuits or by conveying information for integration in higher-order circuits? Finally, the ethological relevance of such narrow tuning of sugar sensitivity in *Ir60b* pharyngeal GRNs also awaits future research.

Bitter

Bitter taste is mediated by members of the Gr family. Initial analyses of *Gr* mutants as well as *Gr-GAL4* reporters revealed that bitter GRNs expressing several bitter *Grs*, including *Gr32a*, *Gr33a*, *Gr66a*, *Gr89a*, and *Gr93a*, are required for physiological and behavioral responses to bitter compounds (Moon et al., 2009, Lee et al., 2009, Moon et al., 2006, Lee et al., 2010). A number of observations also suggested that multiple Grs are likely to come together in heteromeric complexes to detect various bitter substances, however a minimum Gr subunit composition remained unclear until 2015, when a combination of Gr8a, Gr66a, and Gr98b was reported as a full receptor repertoire for detection of L-canavanine (Shim et al., 2015). All three receptors are required for L-canavanine response in bitter GRNs and co-expression of the three receptors is sufficient to confer L-canavanine response in sweet GRNs as well as in *Drosophila* S2 cells. Subsequently, several other members of Grs have been reported to be involved in detection of specific bitter compounds, such as strychnine, coumarin, umbelliferone, chloroquine, saponin, and nicotine (Poudel et al., 2017, Poudel and Lee, 2016, Poudel et al., 2015, Lee et al., 2015, Sang et al., 2019, Rimal and Lee, 2019). Two recent studies

have further elucidated the molecular basis of bitter detection by characterizing differences in responses of bitter GRNs that have distinct molecular profiles of bitter Gr expression (Sung et al., 2017, Delventhal and Carlson, 2016). One study found that Gr32a, Gr59c, and Gr66a together are sufficient for sensing lobeline, berberine, and denatonium, whereas Gr22e, Gr32a, and Gr66a are sufficient for sensing the same three bitter compounds as well as strychnine. Given that the two combinations differ only in one Gr and show overlapping but distinct bitter response profiles, it was suggested that a selected bitter compound could activate molecularly distinct receptor complexes, and a selected heteromeric receptor complex could detect multiple bitter compounds. Thus, the observed heterogeneity of *Gr* expression in bitter GRNs would contribute to an even greater diversity in cellular responses to bitter tastants (Sung et al., 2017). Consistent with these observations, the presence or absence of a single bitter Gr can alter endogenous responses of bitter GRNs by increasing or decreasing responses to selected bitter tastants or by conferring novel responses to bitter tastants (Delventhal and Carlson, 2016).These findings complicate evaluation of the functional roles of single Grs using mutant or ectopic expression analyses. Extensive studies have been focused on labellar bitter GRNs while leaving other taste organs unexplored, except one pharyngeal GRN labeled by *Gr9a-GAL4* shown to be responsible for behavioral avoidance of L-canavanine (Chen and Dahanukar, 2017). An understanding of behavioral roles of various classes of bitter GRNs in different organs, and how inputs from various bitter GRNs are integrated to mediate selected behaviors, will be facilitated by further elucidation of the molecular profiles and cellular responses of bitter GRNs in different taste organs.

Salt

Salt is an essential nutrient for many physiological processes, including reproduction. However, salt elicits opposite behavioral responses depending on its concentration: low salt (<100 mM) is attractive while high salt (>200 mM) is aversive in binary choice assays (Zhang et al., 2013a). The gustatory response to salt is also sexually dimorphic and mating status dependent – mated females show higher proboscis extension upon stimulation of either the labellum or the tarsi as compared to virgin females or males (Walker et al., 2015). Ir76b was first identified as a salt receptor functioning in labellar taste neurons that mediate salt attraction (Zhang et al., 2013a), but was subsequently also reported to be involved in avoidance of high salt (Lee et al., 2017). Besides *Ir76b*, *Gr2a* and *Gr23a* expressed in the pharyngeal L7-3 GRN of the LSO have been implicated in feeding avoidance of salt in a specific behavioral context, in which mildly starved flies were tested with a moderate level of salt (150 mM-450 mM) (Kim et al., 2017). The complex view of salt coding emerging from these studies was tackled by a recent comprehensive functional imaging analysis of salt responses in labellar GRNs (Jaeger et al., 2018). To begin to decode taste responses to different concentrations of salts, the authors first gathered molecular tools for labeling subsets of taste neurons in all labellar hairs. First, the authors identified a driver, *Ir94e-GAL4*, which labels a single GRN that is distinct from previously characterized *ppk28*, *Gr64f*, or *ppk23*-expressing GRNs neurons in L-type hairs, thus completing a molecular genetic toolkit for accessing all four GRNs in these hairs. The authors then identified two subpopulations of *ppk23*-expressing neurons by labeling either glutamatergic or cholinergic neurons (ppk23^{glut} and

ppk23^{chat}), which represented distinct taste neurons in the S-type labellar hairs. Imaging of salt responses in these GRN subpopulations revealed that most if not all types of GRNs respond to salt at some range of the tested concentrations. Specifically, weak calcium activity in response to low concentrations of salt was observed in *Gr64f* and *Ir94e* neurons, while response to high salt was observed in *Gr64f*, *Gr66a*, and *ppk23* neurons. Notably, previous electrophysiological recordings had found high salt-induced activity in two neurons in labellar L-type hairs (Hiroi et al., 2004). Since there are no *Gr66a*-labeled neurons in these hairs, one possibility is that the L-type responses are derived from *Gr64f* and *ppk23* neurons. In I-type hairs, tip recordings have identified high salt sensitivity in both taste neurons that innervate them (Hiroi et al., 2004), which are labeled by *Gr64f* and *Gr66a*, respectively. Interestingly, only the salt response in *Gr66a* neurons is independent of *Ir76b* function, although it is partially dependent on *Ir25a*, suggesting potential heterogeneity among salt receptor complexes as well (Jaeger et al., 2018). This appears to go hand-in-hand with functional diversity in salt-sensing circuits – although both *ppk23*^{glut} and *ppk23*^{chat} GRNs respond to high salt, only the *ppk23*^{glut} subset is involved in mediating internal state-dependent modulation of high salt avoidance. Altogether, it is conceivable that different concentrations of salt activate distinct populations of GRNs, many of which express Ir76b, which explains the previously observed roles of this receptor in both low and high salt detection.

Acid

Carboxylic acids are detected via both olfactory and gustatory systems in adult *Drosophila* to mediate appropriate selection of food and oviposition sites (Rimal et al., 2019, Devineni et al., 2019, Deshpande et al., 2015, Chen and Amrein, 2014, Charlu et al., 2013, Ai et al., 2010, Joseph et al., 2009, Abuin et al., 2011). Although flies are attracted to vinegar, they avoid high concentrations of acetic acid detected via *Ir64a* neurons in olfactory sensilla in the antennae (Ai et al., 2010). In the gustatory system, several carboxylic acids have been shown to activate labellar bitter GRNs and also to suppress sugar responses in sweet GRNs (Charlu et al., 2013). In contrast to the overlap between bitter and acid detection in labellar GRNs, acid sensing in tarsal hairs occurs via two separate groups of GRNs that do not respond to either sugars or bitter compounds: one is broadly tuned to various carboxylic acids, while the second is narrowly tuned to glycolic and malic acids and to high concentrations of salt (Chen and Amrein, 2017). Acid responses in both these classes of tarsal GRNs require two broadly expressed *Irs*, *Ir25a* and *Ir76b*. Given that *Ir25a* and *Ir76b* are widely expressed in both olfactory and gustatory neurons, the identity of additional *Irs* that may confer ligand specificity remains to be determined. Interestingly, one recent report identified another member of the Ir family, Ir7a, which is only expressed in a subset of labellar bitter GRNs as a receptor for acetic acid (Rimal et al., 2019). A high concentration of acetic acid (5%) was found to evoke feeding aversion in binary choice feeding assays. Although feeding avoidance of acetic acid was disrupted in *Ir7a* mutants, it was not dependent on *Ir25a* or *Ir76b*. The observed defects in feeding avoidance were selective for acetic acid and responses to

other carboxylic acids were not affected in the absence of *Ir7a*, consistent with the idea that different receptors with distinct ligand-binding specificities may be involved in sensing various carboxylic acids. Ectopic expression of *Ir7a* in sweet GRNs conferred acetic acid response as measured with tip recordings (Rimal et al., 2019), an observation that needs to be reconciled with acetic acid-evoked calcium activity in endogenous sweet GRNs (Devineni et al., 2019). Moreover, the restricted expression of *Ir7a* in bitter GRNs indicates that the molecular mechanism of acetic acid detection in sweet GRNs is yet to be determined.

Amino acid/Yeast

Yeast is the primary source of dietary proteins and amino acids for *Drosophila*. Yeast feeding is modulated by mating status and prior yeast feeding experience (Vargas et al., 2010, Ribeiro and Dickson, 2010). Recent reports suggest that amino acids are the principal gustatory cues in yeast extract (Ganguly et al., 2017), and cellular and behavioral responses to amino acids are mediated via Ir76b (Ganguly et al., 2017, Croset et al., 2016), which is broadly expressed in peripheral GRNs. Although Ir76b may act alone for salt detection (Zhang et al., 2013a), it is likely to serve as a co-receptor for amino acid detection given that taste neurons in labellar hairs, many expressing Ir76b, have limited responses to amino acids (Park and Carlson, 2018, Ganguly et al., 2017). An RNAi screen identified one putative amino acid co-receptor, Ir20a. Ectopic expression of *Ir76b* and *Ir20a* together in labellar sweet GRNs conferred amino acid response but not salt response, and expression of *Ir20a* in labellar *Ir76b*-expressing salt GRNs reduced salt

responses but did not confer amino acid response, invoking the contribution of additional receptors/factors present in sweet GRNs but not in salt GRNs in mediating amino acid response. Since *Ir20a* shows a considerably limited domain of expression in comparison with *Ir76b*, and *Ir20a* mutants do not phenocopy the *Ir76b* mutant, it is expected that additional amino acid receptors in other GRNs will be involved in taste detection of amino acids.

Although amino acids might be salient components in yeast extract, another recent study indicates that flies might have distinct pathways for sensing amino acids and yeast (Steck et al., 2018). By using yeast rather than yeast extract, the authors showed that yeast feeding requires *Ir76b*-expressing GRNs in labellar taste hairs and taste pegs but not in tarsal taste hairs. Further, *Ir76b* GRNs in labellar taste hairs are responsible for initiation of yeast feeding (i.e. PER responses), while those in labellar taste pegs are involved in sustaining yeast feeding, providing additional insight into taste organ-specific roles in controlling feeding behavior. Interestingly, yeast-evoked activity in GRNs of both labellar hairs and pegs is modulated by internal amino acids, suggesting that consumption of amino acids and yeast is tightly integrated even though peripheral neuronal detection pathways may be distinct. Future experiments identifying receptors for yeast taste in the two types of labellar GRNs would provide the means to compare mechanisms of amino acid and yeast sensing in peripheral GRNs. In addition to taste-sensing mechanisms, there is evidence that three specific dietary amino acids are detected by brain DH44 neuroendocrine cells which innervate the gut (Yang et al., 2018, Dus et

al., 2015). The proposed fast-acting, post-ingestive mechanism of amino acid detection is independent of *Ir76b* and requires putative amino acid transporters in the DH44 cells.

Fatty acids

Fatty acid taste elicits an appetitive or aversive response depending upon the concentration (Ahn et al., 2017). Recent studies have largely focused on the positive behavioral valence of low concentrations (<1%) of short to medium chain fatty acids (hexanoic, octanoic), which is mediated by a subset of labellar and tarsal sweet GRNs (Tauber et al., 2017, Ahn et al., 2017, Masek and Keene, 2013). Notably, a number of studies have found fatty acid taste to be dependent on several members of the *Ir* family, including *Ir56d*, *Ir25a*, and *Ir76b*. In the labellum, there are two subpopulations of *Ir56d* GRNs: one is a subset of sweet GRNs in taste hairs that responds to both sugars and fatty acids, and another is a subset of GRNs in taste pegs that responds to fatty acids but not sugars. Fatty acid stimulated proboscis extension requires *Ir56d* GRNs in the labellar taste hairs, but not in taste pegs (Tauber et al., 2017), consistent with distinct behavioral roles for the two GRN populations. Tarsal stimulation-evoked proboscis extension response (PER) is also mediated by *Ir56d*-labeled sweet GRNs, whose function is dependent on *Ir56d*, *Ir25a*, and *Ir76b* (Ahn et al., 2017). Notably, tarsal PER to hexanoic and octanoic acids is significantly higher in octuple mutant flies lacking all 8 sweet Grs (Ahn et al., 2017), indicating a possible role in for one or more of these receptors in regulating fatty acid response. Consistent with this idea, a recent study reported that one sweet Gr, Gr64e, is involved in mediating fatty acid taste in the labellum (Kim et al.,

2018). Whether Ir56d and Gr64e act independently or together for mediating fatty acid signaling is still unclear. However, all studies have found that NorpA, which encodes a phospholipase C, is essential for fatty acid signaling in sweet GRNs (Kim et al., 2018, Tauber et al., 2017, Ahn et al., 2017, Masek and Keene, 2013).

Interestingly, hexanoic acid shows dose-dependent activation of tarsal GRNs that express Gr33a, a receptor that broadly marks bitter-sensing GRNs. At concentrations of hexanoic acid exceeding 1%, control flies exhibit a reduction in proboscis extension, which is not the case in flies in which *Gr33a* GRNs are functionally ablated (Ahn et al., 2017), consistent with the idea that tarsal bitter GRNs mediate an aversive response to fatty acids. Whether or not labellar bitter GRNs also respond to fatty acids has not been reported. Notably, tarsal bitter GRN sensitivity to fatty acids does not require *Ir25a* and *Ir76b*, suggesting that other as yet unidentified receptors are involved in fatty acid taste aversion. As in the case of salt, which elicits opposing behaviors at low and high concentrations, it will be of interest to decipher fatty acid coding at the sensory level and dissect how appetitive and aversive fatty acid-sensing pathways are integrated to shape feeding behaviors.

Carbonation

The taste of carbonation was first reported in *Drosophila* and was found to be mediated by *E409-GAL4*-labeled GRNs that innervate labellar taste pegs (Fischler et al., 2007). Surprisingly, a suite of chemosensory receptors involved in fatty acid taste (Ir56d,

Ir25a, and Ir76b) is also required for sensing carbonation (Sanchez-Alcaniz et al., 2018). Unlike fatty acids that can activate *Ir56d* GRNs in labellar hairs, labellar pegs, and tarsal hairs, carbonation mainly activates GRNs in labellar taste pegs. GRNs in taste hairs of the labellum but not tarsi show a weaker response to carbonation; however, *Ir56d*, *Ir25a*, and *Ir76b* are unlikely to be involved in these responses according to mutant and rescue analyses (Sanchez-Alcaniz et al., 2018). Although the three *Irs* are necessary for carbonation detection in taste peg neurons, combined ectopic expression, which was tested in labellar bitter GRNs, did not confer carbonation sensitivity, indicating that additional factors may be involved. How does carbonation taste affect feeding behavior? It was first reported that carbonated solutions trigger mild behavioral attraction in a position-based preference assay (Fischler et al., 2007). However, no behavioral relevance for carbonation has been observed in consumption-based feeding assays such as flyPAD (solid food) and Expresso (liquid food), in which several high-resolution micro-feeding parameters are monitored, including total number of sips, number of sips per feeding burst, feeding success, latency to the first bout, total consumption per fly, number of meal bouts and average bout volume (Sanchez-Alcaniz et al., 2018). Thus carbonation may be used as a gustatory cue for behaviors other than food ingestion.

Polyamines

Taste input is important not only for food consumption and choice, but also for egg laying site selection by female *Drosophila*. Polyamines, such as putrescine or cadaverine, are important nutrients for reproductive success and have been shown to

activate both olfactory and gustatory pathways for long-range positional attraction and short-range oviposition site selection, respectively (Hussain et al., 2016). Interestingly, both short-range and long-range behaviors require a common chemosensory receptor, Ir76b. A more narrowly expressed antennal chemoreceptor, *Ir41a*, is also necessary for polyamine attraction. In fact, *Ir76b* expression in *Ir41a* olfactory neurons is sufficient to rescue polyamine attraction in *Ir76b* mutants. In the gustatory system, there are at least two classes of polyamine-sensing GRNs that mediate oviposition site selection: *Ir76b* GRNs in labellar taste hairs and taste pegs, and *Gr66a* GRNs in labellar taste hairs. *Ir76b* GRNs in taste pegs exhibit stronger responses to polyamines than those in taste hairs, but *Ir76b* is required for the responses in both. However, polyamine response in *Gr66a* GRNs is independent of *Ir76b*, invoking a distinct mechanism for polyamine detection in these GRNs. In dissecting the behavioral contributions of various polyamine-sensing GRNs in controlling egg laying, the authors found that polyamine avoidance during egg laying behavior relied on labellar input. Silencing of *Ir76b* or *Gr66a*-expressing neurons reduced polyamine avoidance to different extents, implicating roles for both classes of neurons. In fact, silencing of *Gr66a* GRNs caused a slight attraction to polyamine substrate, which was lost upon silencing both *Ir76b* and *Gr66a* neurons, indicating some positive behavior component in the *Ir76b* pathway for egg-laying site selection. Functional heterogeneity in *Ir76b* and *Gr66a* neurons might provide multiple substrates for modulation, which could be important for the highly context-dependent egg-laying site selection behavior (Yang et al., 2008).

H_2O_2/Bacterial lipopolysaccharide

Recent research has uncovered functions for *Gr66a* bitter GRNs in detecting other types of aversive stimuli such as UV-induced H_2O_2 (Guntur et al., 2017) and bacterial lipopolysaccharide (LPS) (Soldano et al., 2016). These chemicals are detected by TrpA1, one of the transient receptor potential (Trp) channels, which is expressed in a subset of *Gr66a* GRNs in labellar taste hairs (Kim et al., 2010) and in pharyngeal L8 and L9 GRNs of the LSO (Kang et al., 2010, Soldano et al., 2016). UV-induced H_2O_2 -sensing bitter GRNs in the labellum were found to promote egg-laying avoidance of strong UV. In addition, the nucleophile-sensitive TrpA1 (A) isoform expressed in I-labellar hairs was found to play an important role in suppressing intake of food sources with reactive oxygen species produced by strong UV exposure (Du et al., 2016). Another study reported that pharyngeal L8 and L9 GRNs detect bacterial LPS via TrpA1 and mediate feeding aversion (Soldano et al., 2016). Flies also sense LPS via GRNs in the legs and wing margins that mediate grooming behaviors (Yanagawa et al., 2019, Yanagawa et al., 2014), but a requirement of TrpA1 for LPS sensitivity in these organs has not been tested. Since TrpA1 is a highly conserved channel in many species, the recent observations raise the possibility that it may be an ancient chemoreceptor for various aversive stimuli.

Ammonia

Similar to acid, ammonia has been reported to activate both olfactory and gustatory neurons. While olfactory detection of ammonia as an attractive cue depends on *Ir92a*-expressing olfactory neurons (Min et al., 2013), gustatory responses to ammonia

depend on *Gr66a* GRNs in labellar hairs (Delventhal et al., 2017). In addition, ammonia elicits weak responses in L-labellar hairs in which there are no *Gr66a* GRNs. Given that *ppk23* GRNs that respond to high salt are the only known GRNs to detect aversive stimuli in L-labellar hairs, it is possible that they are the ones that sense ammonia. Experiments with *ppk23-GAL4* would help to resolve this question. However, identification of the molecular basis of ammonia taste will need further investigation.

Calcium

High levels of calcium activate *ppk23* GRNs in S- but not L-type labellar hairs and stimulate aversive behaviors (Lee et al., 2018). At least three *Irs*, *Ir25a*, *Ir62a*, and *Ir76b*, were found to be required for the neuronal response to calcium but ectopic expression of the three in sweet GRNs did not confer calcium sensitivity, suggesting that additional factors may be involved. Similar to the activity of bitter compounds and acids, calcium also inhibits sweet GRNs, providing an additional mechanism for behavioral avoidance of calcium-laced mixtures. The report of calcium taste invites many interesting questions. For example, what is the ligand specificity of Ir62a, since the *ppk23* GRNs in S-labellar hairs also respond to high salt (NaCl and KCl)? Do multiple neurons in S-type hairs respond to calcium? An *Ir62a* reporter is expressed in tarsal GRNs (Koh et al., 2014), which raises the question of whether GRNs in other organs respond to calcium, and if so, how they contribute to behavioral avoidance of calcium. Lastly, is it possible that the mechanism underlying calcium detection is one common to various salts? The

answers to these questions will provide insight into how flies distinguish different salts and mount appropriate feeding responses.

Taste neurons in adult *Drosophila* gustatory system can detect multiple tastants from different conventional modalities

Taste neurons in adult *Drosophila* exhibit complex molecular signatures in terms of chemosensory receptor expression. Accumulating evidence suggests that members of *Gr*, *Ir*, *ppk*, and *Trp* gene families contribute to the detection of various tastants. Overlapping expression patterns of these different chemosensory receptors could be the underlying basis of multimodal taste sensing that has now been reported for many taste neurons (**Table 1.1**). In many cases, tastant-evoked responses rely on Ir25a and Ir76b, which might serve as co-receptors for various categories of tastants. Although transgenic chemosensory reporters have presented valuable tools for interrogating the function and response profiles of taste neurons, it should be noted that there might be further functional sub-division within these molecularly defined groups of taste neurons. For example, *Ir76b-GAL4* and *Ir56d-GAL4* label both labellar taste hairs and pegs that respond to polyamines and fatty acid, respectively. Projection patterns of GRNs originating in these two areas can be prominently distinguished by their positions in the SEZ (posterior vs anterior), but calcium activity observed in termini of GRNs from taste hairs cannot be assigned to one type, (L-, I-, or S-), from among the types that are labeled. Development of genetic tools for further defining subgroups of GRNs, possibly at single neuron resolution, will be helpful to understand the extent of molecular and

functional heterogeneity in GRNs. Single sensillum recordings can be used to better target types of sensilla that are measured, but analysis can be complicated by the fact that this method simultaneously gathers activity from all neurons in a sensillum, and also that direct comparisons between tip recordings and calcium imaging are complicated by the presence of interneurons in the SEZ that modulate pre-synaptic activity from other taste input or internal state (Ledue et al., 2016, Youn et al., 2018, Inagaki et al., 2014, Inagaki et al., 2012, Wang et al., 2016). Finally, since GRNs appear to detect multiple compounds of distinct taste modalities, the idea that population coding mechanisms may be involved in discrimination between tastants has some appeal. In the future, not only will it be of interest to determine how taste neurons in different organs control different aspects of feeding behaviors and connect to different higher-order neuronal circuits, but to understand how input from GRNs is integrated and evaluated for more complex taste-associated behaviors.

Pox-neuro (*Poxn*) mutants as a valuable tool for *Drosophila* gustation research

In *Drosophila*, there are two major types of external sensory bristles distinguished broadly as mono- or poly-innervated based on the number of neurons that are housed within. Mono-innervated external sensory (m-es) bristles, such as mechanosensory bristles, are distributed all over the body. Each is innervated by a single mechanosensory neuron, which extends its dendrite to the base of the shaft and detects deflection of the hair (Falk et al., 1976). Poly-innervated external sensory (p-es) bristles, such as taste bristles, are distributed in various parts of the body, including the labellum, distal

segments of the legs, wing margins, and the ovipositor (Freeman and Dahanukar, 2015, Liman et al., 2014, Stocker, 1994). Within the taste bristles, there are multiple taste neurons (usually 2-4 in the labellar taste bristles) that extend their dendrites up to the tip of the hair shaft, close to a single pore through which tastants can enter the sensillum lymph. During development, sensory mother cells of different lineages generate different type of sensory organs, specified by sets of transcription factors (Ghysen and Dambly-Chaudiere, 2000). One such factor is Pox-neuro (Poxn), which is a transcription factor with a paired DNA-binding domain. During neurogenesis, Poxn is expressed in sensory mother cells that eventually give rise to poly-innervated external sensory (p-es) organs of the peripheral nervous system (Dambly-Chaudiere et al., 1992). In *Poxn* mutants, all external chemosensory bristles are transformed into mechanosensory bristles (Dambly-Chaudiere et al., 1992, Awasaki and Kimura, 1997), offering a model with numerous possible uses in gustatory research.

Poxn **mutants are not taste-blind**

The *Poxn* mutant has been widely used to investigate the importance of taste sensory input in driving behaviors of interest (**Table 1.2**). The underlying assumption for many of these studies was the taste-blind feature of *Poxn* mutant flies. In instances where *Poxn* mutants exhibited behaviors similar to those of wild-type counterparts, the palpable conclusion was that the observed behaviors were generated by taste-independent mechanisms. However, several studies provided hints that internal pharyngeal taste organs are intact in *Poxn* mutants (Chen and Dahanukar, 2017, Ledue et al., 2015,

Galindo and Smith, 2001). Analysis of odorant binding protein (OBP) expression revealed that *Poxn* mutants lose expression of external gustatory-specific OBPs but not of ones in the pharynx, such as OBP56b (Galindo and Smith, 2001). This study, published in 2001, was the first to posit a specific requirement for *Poxn* in cell fate determination of external but not internal taste organs. It was not until much later that a functional demonstration followed, in a study that found intact pharyngeal *Gr43a* taste neurons in *Poxn* mutants and proved their requirement for sugar selection and sustained consumption (Ledue et al., 2015).

Dissertation overview

The vinegar fly, *Drosophila melanogaster*, has been a highly tractable model organism to dissect the cellular basis of taste-mediated behaviors. With the powerful molecular genetic tools and robust behavioral assays that can be applied in this model, scientists have explored how taste information is recognized and processed to control feeding behaviors. However, flies have taste organs distributed in various parts of the body, including the labellum, distal segments of the legs, wing margins, and the ovipositor (Freeman and Dahanukar, 2015, Liman et al., 2014, Stocker, 1994). The external taste organs have been extensively studied while little is known about the internal pharyngeal taste organs. Given the anatomical location of pharyngeal taste organs, it has long been assumed that they act as gatekeepers for monitoring food quality and controlling ingestion, but there is little direct knowledge of the functional roles of sensory neurons that reside within. Thus, this dissertation focuses on characterizing

pharyngeal taste in adult *Drosophila*. By taking advantage of *Poxn* mutants, I developed genetic tools to probe the roles of pharyngeal taste neurons in feeding behaviors. In Chapter II, I first carried out a large-scale, systematic analysis to understand the molecular organization of pharyngeal taste neurons, and established an unprecedented receptor-to-neuron map for the internal taste organs. From comparison with established maps of external taste organs, I described features of molecular organization that are conserved between external and internal taste neurons. More interestingly, I also found molecular signatures and neuronal groupings that may be unique to pharyngeal organs, and lead to the discovery of new sensory functions in pharyngeal neurons. In Chapter III, I took advantage of the receptor-to-neuron map and *Poxn* mutants to understand how different classes of pharyngeal neurons contribute to feeding aversion of compounds such as acids, high salts, and bitter chemicals. My approach was to perform a systematic genetic dissection analysis via silencing of specific classes of pharyngeal taste neurons, which provided an overview of functional roles of different classes of pharyngeal taste neurons in food selection. In studies described in Chapter IV, I focused on how feeding responses to appetitive sugars and amino acids are controlled by pharyngeal neurons. Towards this end, I developed a model in which selected classes of pharyngeal neurons are the only sources of taste input. This model allowed evaluation of the role of canonical appetitive neurons in the pharynx in controlling meal parameters, as well as to test functional interactions between defined classes of pharyngeal neurons. Together, the results of my dissertation research reveal that food intake is determined by a coordinated action of multiple classes of GRNs in the pharynx. We now have a model and the means

to evaluate functions of other “orphan” pharyngeal neurons in regulating various aspects of food consumption.

FIGURE

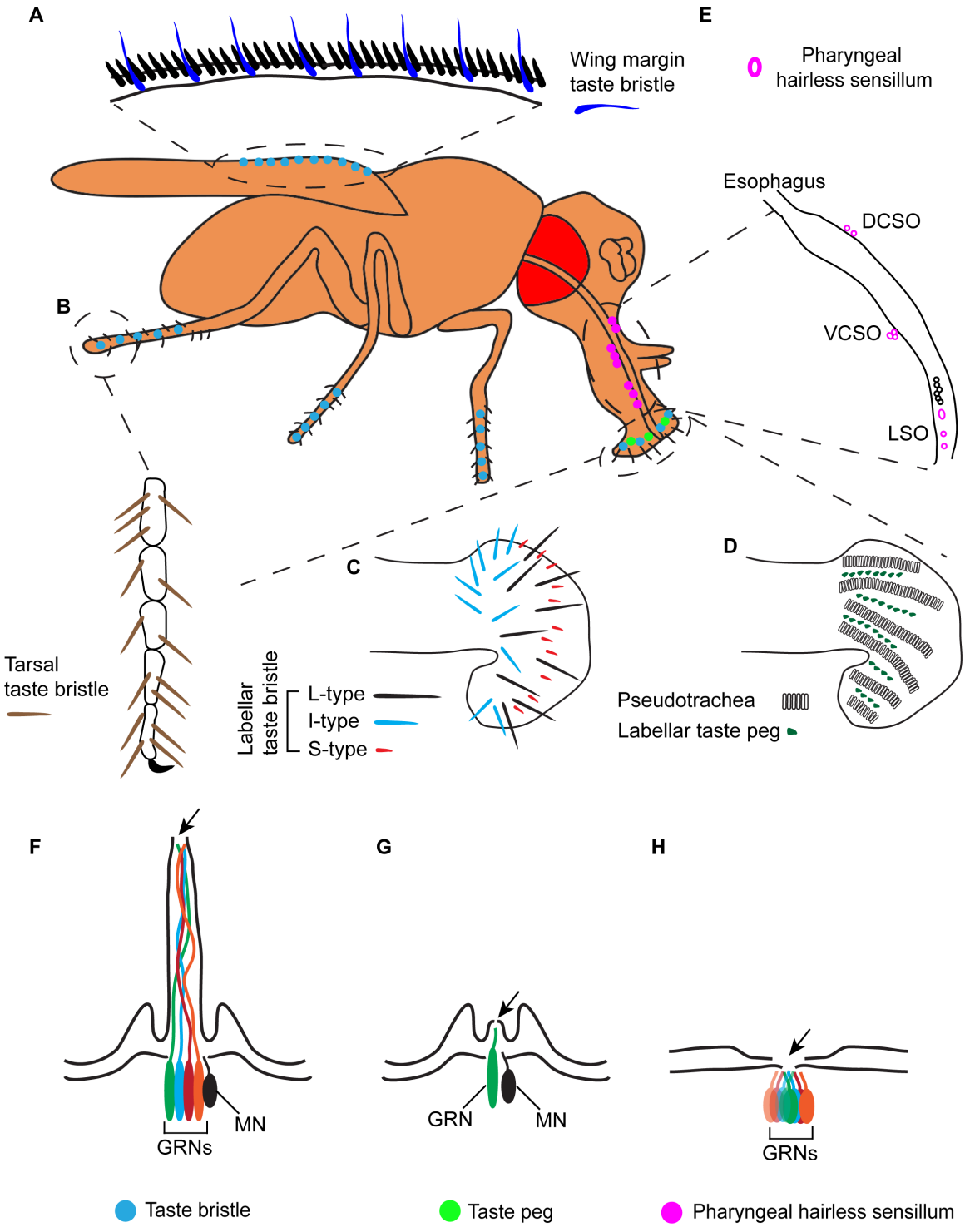
A
Wing margin
taste bristle
B
Tarsal
taste bristle
C
Labellar
taste bristle
L-type
I-type
S-type
D
Pseudotrachea
Labellar taste peg
E
Pharyngeal
hairless sensillum
Esophagus
DCSO
VCSO
LSO
F
MN
GRNs
G
GRN
MN
H
GRNs
Taste bristle
Taste peg
Pharyngeal hairless sensillum

Figure 1.1. Organization of the adult *Drosophila* gustatory system. There are three types of taste sensillum in the different taste organs: taste bristles (blue dots), taste pegs (green dots), and pharyngeal hairless sensillum (magenta dots). The taste bristles are distributed in the anterior wing margins (blue in **A**), the distal segment of the legs (brown in **B**), and the labellum (black, blue and red in **C**). The taste pegs are located between pseudotrachea in the labellum (green in **D**). The hairless sensilla are located in the three internal pharyngeal taste organs: labral sense organs (LSO), ventral and dorsal cibarial sense organs (VCSO and DCSO) (magenta in **E**). (**F-H**) Schematic diagrams showing the structures of three types of taste sensillum. All of them have a terminal pore (arrows) that allows tastants making contact with the taste neurons in each sensillum. The taste bristle has 2-4 gustatory receptor neurons (GRNs) (4 GRNs in this schematic example) whose dendrites extend up to the tip of the taste sensillum (**F**). The taste peg has one GRN (**G**). Both taste bristles and taste pegs have one mechanosensory neuron (MN) at the base of each sensillum (black in **F** and **G**). The pharyngeal hairless sensillum usually does not have mechanosensory neuron, except for the #8 and #9 LSO sensillum. The number of GRNs in the pharyngeal hairless sensillum can vary from 1-8 (8 GRNs in this schematic example) (**H**).

TABLES

Table 1.1. Receptors, neurons and taste responses in adult *Drosophila.*

Tastant	Receptor	Transgenic reporter	Example ligands	Taste organs	Physiological measurement	Behavioral measurement	References
Sweet	Gr5a, Gr43a, Gr61a, Gr64a-f		Trehalose, sucrose, glucose, fructose, glycerol and other sugars	Labellum	Tip recording	PER, food choice	(Dahanukar et al., 2007, Jiao et al., 2007, Dahanukar et al., 2001, Jiao et al., 2008, Hiroi et al., 2002, Wisotsky et al., 2011, Hiroi et al., 2004)
	Gr5a, Gr61a, Gr64a-f			Labellum	None	PER	(Fujii et al., 2015)
		Gr5a-GAL4		Labellum	Ca^{2+} imaging	Food choice	(Marella et al., 2006)
		Gr5a-GAL4			None	PER	(Wang et al., 2004)
	Gr43a			Brain	Ca^{2+} imaging	PER, CAFE	(Fujii et al., 2015, Miyamoto et al., 2012)
		Gr61a-GAL4		Tarsi	Ca^{2+} imaging	PER	(Yavuz et al., 2014, Miyamoto et al., 2013)
		Gr43a-GAL4		Pharynx	Ca^{2+} imaging	Food choice, food consumption	(Ledue et al., 2015)
		Tub-GAL4		Wing	Ca^{2+} imaging	Aggregation	(Raad et al., 2016)
		Gr21a-GAL4, *Gr63a-GAL4*		Ectopic expression system in olfactory sensilla	Tip recording	None	(Freeman et al., 2014)
				Tarsi	Tip recording	None	(Ling et al., 2014)
	Ir60b		Sucrose, glucose	Pharynx	Ca^{2+} imaging	Food consumption, FLIC	(Joseph et al., 2017)
Bitter			Caffeine, quinine, denatonium, DEET, 7-tricosene, and	Labellum, tarsi	Tip recording	Food choice	(Meunier et al., 2003, Weiss et al., 2011, Hiroi et al., 2004, Lacaille et al., 2007)

	Gr32a, Gr33a, Gr66a, Gr93a		other bitter compounds	Labellum	Tip recording	Food choice, courtship	(Lee et al., 2009, Moon et al., 2006, Moon et al., 2009, Lee et al., 2010, Sung et al., 2017)
	Gr2a, Gr10a, Gr22b, Gr28a, Gr28b.a, Gr36a, Gr58c, Gr59c	*Gr89a-GAL4*		Ectopic expression system in labellum	Tip recording	None	(Delventhal and Carlson, 2016)
		Gr66a-GAL4		Labellum	Ca^{2+} imaging	Food choice	(Marella et al., 2006)
		Gr66a-GAL4	Strychnine, L-canavanine	Labellum, tarsi	Tip recording	Food choice, CAFE, PER	(French et al., 2015)
		Gr66a-GAL4	Caffeine, quinine, denatonium, berberine		None	PER	(Wang et al., 2004)
	Gr8a, Gr66a, Gr98b		L-canavanine	Labellum	Tip recording	Food choice	(Shim et al., 2015)
		Gr9a-GAL4	L-canavanine	Pharynx	None	Food choice	(Chen and Dahanukar, 2017)
	Gr47a		Strychnine	Labellum	Tip recording	Food choice, PER	(Lee et al., 2015)
	Gr22e		Strychnine, chloroquine	Labellum	Tip recording	Food choice, PER	(Poudel et al., 2017)
	Gr33a, Gr66a, Gr93a		Umbelliferone, coumarin	Labellum	Tip recording	Food choice, oviposition	(Poudel et al., 2015, Poudel and Lee, 2016)
	Gr28b		Saponin	Labellum	Tip recording	Food choice, PER	(Sang et al., 2019)
	Gr10a		Nicotine	Labellum	Tip recording	PER	(Rimal and Lee, 2019)
	TrpA1		N-methylmaleimide	Labellum	Tip recording	CAFE	(Du et al., 2015)

	TrpA1		Aristolochic acid	Labellum	Tip recording	Food choice	(Zhang et al., 2013b)
	TrpL		Camphor	Labellum	Tip recording	Food choice	(Kim et al., 2010)
	Painless		Isothiocyanate	Labellum, tarsi, pharynx, wing	None	Food choice, PER	(Al-Anzi et al., 2006)
Salt	Ir76b		Sodium chloride	Labellum	Tip recording	Food choice	(Zhang et al., 2013a, Lee et al., 2017)
		Ir76b-GAL4		Tarsi	None	PER	(Walker et al., 2015)
	Gr2a			Pharynx	None	Food choice	(Kim et al., 2017)
				Labellum	Tip recording	Food choice	(Hiroi et al., 2004)
		Gr64f-GAL4, *Gr66a-GAL4*, *ppk23-GAL4*, *Ir94e-GAL4*		Labellum	Ca^{2+} imaging	Food choice	(Jaeger et al., 2018)
Acid	Ir7a		Acetic acid	Labellum	Tip recording	Food choice, PER	(Rimal et al., 2019)
		Gr64f-GAL4, *Gr66a-GAL4*	Acetic acid	Labellum	Ca^{2+} imaging	PER	(Devineni et al., 2019)
	Ir25a, Ir76b		Carboxylic acids, HCl	Tarsi	Ca^{2+} imaging	Oviposition	(Chen and Amrein, 2017)
		Gr89a-GAL4	Carboxylic acids, HCl	Labellum	Tip recording	Food choice, PER	(Charlu et al., 2013)
Amino acids/Yeast	Ir76b		Serine, threonine, phenylalanine, alanine, glycine, yeast extract	Tarsi	Ca^{2+} imaging	Food choice	(Ganguly et al., 2017)
		Ir76b-GAL4	Yeast	Labellum, taste pegs	Ca^{2+} imaging	FlyPAD	(Steck et al., 2018)
		Gr66a-GAL4	Tryptophan, phenylalanine	Labellum	Tip recording	Food choice	(Park and Carlson, 2018)
		AstC-, *Npf*-, and *Dh31*-	Amino acids/yeast	Gut	CaLexA	None	(Park et al., 2016)

		GAL4 (*EE-GAL4*)					
			Amino acids	Labellum, Tarsi	None	Food choice, PER, CAFE	(Toshima and Tanimura, 2012)
Carbonation		*E409-GAL4*	Sodium bicarbonate, cesium bicarbonate (pH 5-6.5)	Taste pegs	Ca^{2+} imaging	Food choice	(Fischler et al., 2007)
	Ir56d			Labellum, taste pegs	Ca^{2+} imaging	Food choice, Positional preference, PER, Expresso, FlyPAD	(Sanchez-Alcaniz et al., 2018)
Fatty acids	Ir56d		Hexanoic acid, octanoic acid, and other fatty acids	Taste pegs, tarsi	Ca^{2+} imaging	PER	(Tauber et al., 2017, Ahn et al., 2017)
	Gr64e			Labellum	Tip recording	PER	(Kim et al., 2018)
		Gr33a$^{[GAL4]}$	Hexanoic acid	Tarsi	Ca^{2+} imaging	PER	(Ahn et al., 2017)
Polyamines	Ir76b	*Gr66a-GAL4*	Putrescine, cadaverine	Labellum	Ca^{2+} imaging, tip recording	Oviposition	(Hussain et al., 2016)
UV/H_2O_2	TrpA1	*Gr66a-GAL4*	UV/H_2O_2	Labellum	Ca^{2+} imaging	Oviposition	(Guntur et al., 2017)
	TrpA1	*Gr66a-GAL4*	UV/H_2O_2	Labellum	Tip recording	Food choice	(Du et al., 2016)
LPS	TrpA1	*Gr66a-GAL4*	LPS	Pharynx	Ca^{2+} imaging	Food choice, PER, oviposition	(Soldano et al., 2016)
		Gr64f-GAL4, *Gr5a-GAL4*, *Gr33a-GAL4*, *Gr66a-GAL4*, *Ir76b-GAL4*	LPS	Wing	None	Grooming	(Yanagawa et al., 2019)
		Gr33a-GAL4	LPS	Wing, tarsi	Tip recording	Grooming	(Yanagawa et al., 2014)
Ammonia		*Gr66a-GAL4*	Ammonium chloride	Labellum	Tip recording	Food choice, food consumption	(Delventhal et al., 2017)
Calcium	Ir62a	*ppk23-GAL4*	Calcium chloride	Labellum	Tip recording	Food choice	(Lee et al., 2018)

CAFE, capillary feeder assay; CaLexA, calcium-dependent nuclear import of LexA; DEET, N,N-Diethl-meta-toluamide; *EE-GAL4*, *enteroendocrine-GAL4*; Expresso, an automated feeding assay for quantification of real time food ingestion; FLIC, fly

liquid food interaction counter; flyPAD, fly proboscis and activity detector; LPS, lipopolysaccharide; PER, proboscis extension response

Table 1.2. *Poxn* mutants for behavioral research

Behaviors	Phenotype	References
Feeding	Nutrient sensing	(Abu et al., 2018, Dus et al., 2013, Dus et al., 2011)
	Sugar	(Murata et al., 2017, Liu et al., 2015, Ledue et al., 2015, Sun et al., 2014, Usui-Aoki et al., 2005)
	Bitter	(Chen and Dahanukar, 2017, Mitri et al., 2009)
	Salt	(Kojima et al., 2018)
	pH	(Deshpande et al., 2015)
	Yeast	(Steck et al., 2018)
	Water	(Chen et al., 2010)
	Ethanol	(Devineni and Heberlein, 2009)
	Fatty acid	(Masek and Keene, 2013)
Social	Aggregation pheromone detection	(Lin et al., 2015)
	Social interaction	(Schneider and Levine, 2014, Schneider et al., 2012)
Reproductive	Oviposition	(Verschut et al., 2017, Hussain et al., 2016, Joseph and Heberlein, 2012, Joseph et al., 2009)
	Courtship	(Krstic et al., 2009, Boll and Noll, 2002)

Others	Grooming	(Yanagawa et al., 2018, Yanagawa et al., 2014)
	Positional preference	(Joseph and Heberlein, 2012, Joseph et al., 2009)
	Starvation-induced hyperactivity	(Yang et al., 2015)

REFERENCES

Abu, F., Wang, J. G., Oh, Y., Deng, J., Neubert, T. A. & Suh, G. S. B. 2018. Communicating the nutritional value of sugar in Drosophila. *Proc Natl Acad Sci U S A,* 115**,** E2829-E2838.

Abuin, L., Bargeton, B., Ulbrich, M. H., Isacoff, E. Y., Kellenberger, S. & Benton, R. 2011. Functional architecture of olfactory ionotropic glutamate receptors. *Neuron,* 69**,** 44-60.

Ahn, J. E., Chen, Y. & Amrein, H. 2017. Molecular basis of fatty acid taste in Drosophila. *Elife,* 6.

Ai, M., Min, S., Grosjean, Y., Leblanc, C., Bell, R., Benton, R. & Suh, G. S. 2010. Acid sensing by the Drosophila olfactory system. *Nature,* 468**,** 691-5.

Al-Anzi, B., Tracey, W. D., Jr. & Benzer, S. 2006. Response of Drosophila to wasabi is mediated by painless, the fly homolog of mammalian TRPA1/ANKTM1. *Curr Biol,* 16**,** 1034-40.

Awasaki, T. & Kimura, K. 1997. pox-neuro is required for development of chemosensory bristles in Drosophila. *J Neurobiol,* 32**,** 707-21.

Boll, W. & Noll, M. 2002. The Drosophila Pox neuro gene: control of male courtship behavior and fertility as revealed by a complete dissection of all enhancers. *Development,* 129**,** 5667-81.

Bray, S. & Amrein, H. 2003. A putative Drosophila pheromone receptor expressed in male-specific taste neurons is required for efficient courtship. *Neuron,* 39**,** 1019-29.

Cameron, P., Hiroi, M., Ngai, J. & Scott, K. 2010. The molecular basis for water taste in Drosophila. *Nature,* 465**,** 91-5.

Charlu, S., Wisotsky, Z., Medina, A. & Dahanukar, A. 2013. Acid sensing by sweet and bitter taste neurons in Drosophila melanogaster. *Nat Commun,* 4**,** 2042.

Chen, Y. & Amrein, H. 2014. Enhancing perception of contaminated food through acid-mediated modulation of taste neuron responses. *Curr Biol,* 24**,** 1969-77.

Chen, Y. & Amrein, H. 2017. Ionotropic Receptors Mediate Drosophila Oviposition Preference through Sour Gustatory Receptor Neurons. *Curr Biol,* 27**,** 2741-2750 e4.

Chen, Y. D. & Dahanukar, A. 2017. Molecular and Cellular Organization of Taste Neurons in Adult Drosophila Pharynx. *Cell Rep,* 21**,** 2978-2991.

Chen, Z., Wang, Q. & Wang, Z. 2010. The amiloride-sensitive epithelial Na+ channel PPK28 is essential for drosophila gustatory water reception. *J Neurosci,* 30**,** 6247-52.

Clyne, P. J., Warr, C. G. & Carlson, J. R. 2000. Candidate taste receptors in Drosophila. *Science,* 287**,** 1830-4.

Croset, V., Rytz, R., Cummins, S. F., Budd, A., Brawand, D., Kaessmann, H., Gibson, T. J. & Benton, R. 2010. Ancient protostome origin of chemosensory ionotropic glutamate receptors and the evolution of insect taste and olfaction. *PLoS Genet,* 6**,** e1001064.

Croset, V., Schleyer, M., Arguello, J. R., Gerber, B. & Benton, R. 2016. A molecular and neuronal basis for amino acid sensing in the Drosophila larva. *Sci Rep,* 6**,** 34871.

Dahanukar, A., Foster, K., Van Der Goes Van Naters, W. M. & Carlson, J. R. 2001. A Gr receptor is required for response to the sugar trehalose in taste neurons of Drosophila. *Nat Neurosci,* 4**,** 1182-6.

Dahanukar, A., Lei, Y. T., Kwon, J. Y. & Carlson, J. R. 2007. Two Gr genes underlie sugar reception in Drosophila. *Neuron,* 56**,** 503-16.

Dambly-Chaudiere, C., Jamet, E., Burri, M., Bopp, D., Basler, K., Hafen, E., Dumont, N., Spielmann, P., Ghysen, A. & Noll, M. 1992. The paired box gene pox neuro: a determinant of poly-innervated sense organs in Drosophila. *Cell,* 69**,** 159-72.

Delventhal, R. & Carlson, J. R. 2016. Bitter taste receptors confer diverse functions to neurons. *Elife,* 5.

Delventhal, R., Menuz, K., Joseph, R., Park, J., Sun, J. S. & Carlson, J. R. 2017. The taste response to ammonia in Drosophila. *Sci Rep,* 7**,** 43754.

Deshpande, S. A., Yamada, R., Mak, C. M., Hunter, B., Soto Obando, A., Hoxha, S. & Ja, W. W. 2015. Acidic Food pH Increases Palatability and Consumption and Extends Drosophila Lifespan. *J Nutr,* 145**,** 2789-96.

Devineni, A. V. & Heberlein, U. 2009. Preferential ethanol consumption in Drosophila models features of addiction. *Curr Biol,* 19**,** 2126-32.

Devineni, A. V., Sun, B., Zhukovskaya, A. & Axel, R. 2019. Acetic acid activates distinct taste pathways in Drosophila to elicit opposing, state-dependent feeding responses. *Elife,* 8.

Du, E. J., Ahn, T. J., Choi, M. S., Kwon, I., Kim, H. W., Kwon, J. Y. & Kang, K. 2015. The Mosquito Repellent Citronellal Directly Potentiates Drosophila TRPA1, Facilitating Feeding Suppression. *Mol Cells,* 38**,** 911-7.

Du, E. J., Ahn, T. J., Wen, X., Seo, D. W., Na, D. L., Kwon, J. Y., Choi, M., Kim, H. W., Cho, H. & Kang, K. 2016. Nucleophile sensitivity of Drosophila TRPA1 underlies light-induced feeding deterrence. *Elife,* 5.

Dunipace, L., Meister, S., Mcnealy, C. & Amrein, H. 2001. Spatially restricted expression of candidate taste receptors in the Drosophila gustatory system. *Curr Biol,* 11**,** 822-35.

Dus, M., Ai, M. & Suh, G. S. 2013. Taste-independent nutrient selection is mediated by a brain-specific Na+ /solute co-transporter in Drosophila. *Nat Neurosci,* 16**,** 526-8.

Dus, M., Lai, J. S., Gunapala, K. M., Min, S., Tayler, T. D., Hergarden, A. C., Geraud, E., Joseph, C. M. & Suh, G. S. 2015. Nutrient Sensor in the Brain Directs the Action of the Brain-Gut Axis in Drosophila. *Neuron,* 87**,** 139-51.

Dus, M., Min, S., Keene, A. C., Lee, G. Y. & Suh, G. S. 2011. Taste-independent detection of the caloric content of sugar in Drosophila. *Proc Natl Acad Sci U S A,* 108**,** 11644-9.

Falk, R., Bleiser-Avivi, N. & Atidia, J. 1976. Labellar taste organs of Drosophila melanogaster. *J Morphol,* 150**,** 327-341.

Fischler, W., Kong, P., Marella, S. & Scott, K. 2007. The detection of carbonation by the Drosophila gustatory system. *Nature,* 448**,** 1054-7.

Freeman, E. G. & Dahanukar, A. 2015. Molecular neurobiology of Drosophila taste. *Curr Opin Neurobiol,* 34**,** 140-8.

Freeman, E. G., Wisotsky, Z. & Dahanukar, A. 2014. Detection of sweet tastants by a conserved group of insect gustatory receptors. *Proc Natl Acad Sci U S A,* 111**,** 1598-603.

French, A. S., Sellier, M. J., Ali Agha, M., Guigue, A., Chabaud, M. A., Reeb, P. D., Mitra, A., Grau, Y., Soustelle, L. & Marion-Poll, F. 2015. Dual mechanism for bitter avoidance in Drosophila. *J Neurosci,* 35**,** 3990-4004.

Fujii, S., Yavuz, A., Slone, J., Jagge, C., Song, X. & Amrein, H. 2015. Drosophila sugar receptors in sweet taste perception, olfaction, and internal nutrient sensing. *Curr Biol,* 25**,** 621-627.

Galindo, K. & Smith, D. P. 2001. A large family of divergent Drosophila odorant-binding proteins expressed in gustatory and olfactory sensilla. *Genetics,* 159**,** 1059-72.

Ganguly, A., Pang, L., Duong, V. K., Lee, A., Schoniger, H., Varady, E. & Dahanukar, A. 2017. A Molecular and Cellular Context-Dependent Role for Ir76b in Detection of Amino Acid Taste. *Cell Rep,* 18**,** 737-750.

Ghysen, A. & Dambly-Chaudiere, C. 2000. A genetic programme for neuronal connectivity. *Trends Genet,* 16**,** 221-6.

Guntur, A. R., Gou, B., Gu, P., He, R., Stern, U., Xiang, Y. & Yang, C. H. 2017. H2O2-Sensitive Isoforms of Drosophila melanogaster TRPA1 Act in Bitter-Sensing Gustatory Neurons to Promote Avoidance of UV During Egg-Laying. *Genetics,* 205**,** 749-759.

He, Z., Luo, Y., Shang, X., Sun, J. S. & Carlson, J. R. 2019. Chemosensory sensilla of the Drosophila wing express a candidate ionotropic pheromone receptor. *PLoS Biol,* 17**,** e2006619.

Hiroi, M., Marion-Poll, F. & Tanimura, T. 2002. Differentiated response to sugars among labellar chemosensilla in Drosophila. *Zoolog Sci,* 19**,** 1009-18.

Hiroi, M., Meunier, N., Marion-Poll, F. & Tanimura, T. 2004. Two antagonistic gustatory receptor neurons responding to sweet-salty and bitter taste in Drosophila. *J Neurobiol,* 61**,** 333-42.

Hussain, A., Zhang, M., Ucpunar, H. K., Svensson, T., Quillery, E., Gompel, N., Ignell, R. & Grunwald Kadow, I. C. 2016. Ionotropic Chemosensory Receptors Mediate the Taste and Smell of Polyamines. *PLoS Biol,* 14**,** e1002454.

Inagaki, H. K., Ben-Tabou De-Leon, S., Wong, A. M., Jagadish, S., Ishimoto, H., Barnea, G., Kitamoto, T., Axel, R. & Anderson, D. J. 2012. Visualizing neuromodulation in vivo: TANGO-mapping of dopamine signaling reveals appetite control of sugar sensing. *Cell,* 148**,** 583-95.

Inagaki, H. K., Panse, K. M. & Anderson, D. J. 2014. Independent, reciprocal neuromodulatory control of sweet and bitter taste sensitivity during starvation in Drosophila. *Neuron,* 84**,** 806-20.

Jaeger, A. H., Stanley, M., Weiss, Z. F., Musso, P. Y., Chan, R. C., Zhang, H., Feldman-Kiss, D. & Gordon, M. D. 2018. A complex peripheral code for salt taste in Drosophila. *Elife,* 7.

Jiao, Y., Moon, S. J. & Montell, C. 2007. A Drosophila gustatory receptor required for the responses to sucrose, glucose, and maltose identified by mRNA tagging. *Proc Natl Acad Sci U S A,* 104**,** 14110-5.

Jiao, Y., Moon, S. J., Wang, X., Ren, Q. & Montell, C. 2008. Gr64f is required in combination with other gustatory receptors for sugar detection in Drosophila. *Curr Biol,* 18**,** 1797-801.

Joseph, R. M. & Carlson, J. R. 2015. Drosophila Chemoreceptors: A Molecular Interface Between the Chemical World and the Brain. *Trends Genet,* 31**,** 683-695.

Joseph, R. M., Devineni, A. V., King, I. F. & Heberlein, U. 2009. Oviposition preference for and positional avoidance of acetic acid provide a model for competing behavioral drives in Drosophila. *Proc Natl Acad Sci U S A,* 106**,** 11352-7.

Joseph, R. M. & Heberlein, U. 2012. Tissue-specific activation of a single gustatory receptor produces opposing behavioral responses in Drosophila. *Genetics,* 192**,** 521-32.

Joseph, R. M., Sun, J. S., Tam, E. & Carlson, J. R. 2017. A receptor and neuron that activate a circuit limiting sucrose consumption. *Elife,* 6.

Kallman, B. R., Kim, H. & Scott, K. 2015. Excitation and inhibition onto central courtship neurons biases Drosophila mate choice. *Elife,* 4**,** e11188.

Kang, K., Panzano, V. C., Chang, E. C., Ni, L., Dainis, A. M., Jenkins, A. M., Regna, K., Muskavitch, M. A. & Garrity, P. A. 2011. Modulation of TRPA1 thermal sensitivity enables sensory discrimination in Drosophila. *Nature,* 481**,** 76-80.

Kang, K., Pulver, S. R., Panzano, V. C., Chang, E. C., Griffith, L. C., Theobald, D. L. & Garrity, P. A. 2010. Analysis of Drosophila TRPA1 reveals an ancient origin for human chemical nociception. *Nature,* 464**,** 597-600.

Kim, H., Jeong, Y. T., Choi, M. S., Choi, J., Moon, S. J. & Kwon, J. Y. 2017. Involvement of a Gr2a-Expressing Drosophila Pharyngeal Gustatory Receptor Neuron in Regulation of Aversion to High-Salt Foods. *Mol Cells,* 40**,** 331-338.

Kim, H., Kim, H., Kwon, J. Y., Seo, J. T., Shin, D. M. & Moon, S. J. 2018. Drosophila Gr64e mediates fatty acid sensing via the phospholipase C pathway. *PLoS Genet,* 14**,** e1007229.

Kim, S. H., Lee, Y., Akitake, B., Woodward, O. M., Guggino, W. B. & Montell, C. 2010. Drosophila TRPA1 channel mediates chemical avoidance in gustatory receptor neurons. *Proc Natl Acad Sci U S A,* 107**,** 8440-5.

Koh, T. W., He, Z., Gorur-Shandilya, S., Menuz, K., Larter, N. K., Stewart, S. & Carlson, J. R. 2014. The Drosophila IR20a clade of ionotropic receptors are candidate taste and pheromone receptors. *Neuron,* 83**,** 850-65.

Kojima, T., Furuyama, A., Isono, K., Hamada, T., Ohsuga, K. & Takada, S. 2018. Effects of salt taste disorder on behavior and lifespan in Drosophila melanogaster. *Journal of Oral Biosciences,* 60**,** 15-20.

Krstic, D., Boll, W. & Noll, M. 2009. Sensory integration regulating male courtship behavior in Drosophila. *PLoS One,* 4**,** e4457.

Lacaille, F., Hiroi, M., Twele, R., Inoshita, T., Umemoto, D., Maniere, G., Marion-Poll, F., Ozaki, M., Francke, W., Cobb, M., Everaerts, C., Tanimura, T. & Ferveur, J. F. 2007. An inhibitory sex pheromone tastes bitter for Drosophila males. *PLoS One,* 2**,** e661.

Ledue, E. E., Chen, Y. C., Jung, A. Y., Dahanukar, A. & Gordon, M. D. 2015. Pharyngeal sense organs drive robust sugar consumption in Drosophila. *Nat Commun,* 6**,** 6667.

Ledue, E. E., Mann, K., Koch, E., Chu, B., Dakin, R. & Gordon, M. D. 2016. Starvation-Induced Depotentiation of Bitter Taste in Drosophila. *Curr Biol,* 26**,** 2854-2861.

Lee, M. J., Sung, H. Y., Jo, H., Kim, H. W., Choi, M. S., Kwon, J. Y. & Kang, K. 2017. Ionotropic Receptor 76b Is Required for Gustatory Aversion to Excessive Na+ in Drosophila. *Mol Cells,* 40**,** 787-795.

Lee, Y., Kim, S. H. & Montell, C. 2010. Avoiding DEET through insect gustatory receptors. *Neuron,* 67**,** 555-61.

Lee, Y., Moon, S. J. & Montell, C. 2009. Multiple gustatory receptors required for the caffeine response in Drosophila. *Proc Natl Acad Sci U S A,* 106**,** 4495-500.

Lee, Y., Moon, S. J., Wang, Y. & Montell, C. 2015. A Drosophila Gustatory Receptor Required for Strychnine Sensation. *Chem Senses,* 40**,** 525-33.

Lee, Y., Poudel, S., Kim, Y., Thakur, D. & Montell, C. 2018. Calcium Taste Avoidance in Drosophila. *Neuron,* 97**,** 67-74 e4.

Liman, E. R., Zhang, Y. V. & Montell, C. 2014. Peripheral coding of taste. *Neuron,* 81**,** 984-1000.

Lin, C. C., Prokop-Prigge, K. A., Preti, G. & Potter, C. J. 2015. Food odors trigger Drosophila males to deposit a pheromone that guides aggregation and female oviposition decisions. *Elife,* 4.

Ling, F., Dahanukar, A., Weiss, L. A., Kwon, J. Y. & Carlson, J. R. 2014. The molecular and cellular basis of taste coding in the legs of Drosophila. *J Neurosci,* 34**,** 7148-64.

Liu, C., Bai, X., Sun, J., Zhang, X. & Li, Y. 2015. Behavioral Switch of Food Preference upon Sugar Deficiency Is Regulated by GPCRs in Drosophila. *J Genet Genomics,* 42**,** 409-12.

Liu, T., Wang, Y., Tian, Y., Zhang, J., Zhao, J. & Guo, A. 2018. The receptor channel formed by ppk25, ppk29 and ppk23 can sense the Drosophila female pheromone 7,11-heptacosadiene. *Genes Brain Behav***,** e12529.

Lu, B., Lamora, A., Sun, Y., Welsh, M. J. & Ben-Shahar, Y. 2012. ppk23-Dependent chemosensory functions contribute to courtship behavior in Drosophila melanogaster. *PLoS Genet,* 8**,** e1002587.

Marella, S., Fischler, W., Kong, P., Asgarian, S., Rueckert, E. & Scott, K. 2006. Imaging taste responses in the fly brain reveals a functional map of taste category and behavior. *Neuron,* 49**,** 285-95.

Masek, P. & Keene, A. C. 2013. Drosophila Fatty Acid Taste Signals through the PLC Pathway in Sugar-Sensing Neurons. *Plos Genetics,* 9.

Mcginnis, J. P., Jiang, H., Agha, M. A., Sanchez, C. P., Lange, J., Yu, Z., Marion-Poll, F. & Si, K. 2016. Immediate perception of a reward is distinct from the reward's long-term salience. *Elife,* 5.

Meunier, N., Marion-Poll, F., Rospars, J. P. & Tanimura, T. 2003. Peripheral coding of bitter taste in Drosophila. *J Neurobiol,* 56**,** 139-52.

Min, S., Ai, M., Shin, S. A. & Suh, G. S. 2013. Dedicated olfactory neurons mediating attraction behavior to ammonia and amines in Drosophila. *Proc Natl Acad Sci U S A,* 110**,** E1321-9.

Mitri, C., Soustelle, L., Framery, B., Bockaert, J., Parmentier, M. L. & Grau, Y. 2009. Plant insecticide L-canavanine repels Drosophila via the insect orphan GPCR DmX. *PLoS Biol,* 7**,** e1000147.

Miyamoto, T. & Amrein, H. 2014. Diverse roles for the Drosophila fructose sensor Gr43a. *Fly (Austin),* 8**,** 19-25.

Miyamoto, T., Chen, Y., Slone, J. & Amrein, H. 2013. Identification of a Drosophila glucose receptor using Ca2+ imaging of single chemosensory neurons. *PLoS One,* 8**,** e56304.

Miyamoto, T., Slone, J., Song, X. & Amrein, H. 2012. A fructose receptor functions as a nutrient sensor in the Drosophila brain. *Cell,* 151**,** 1113-25.

Moon, S. J., Kottgen, M., Jiao, Y., Xu, H. & Montell, C. 2006. A taste receptor required for the caffeine response in vivo. *Curr Biol,* 16**,** 1812-7.

Moon, S. J., Lee, Y., Jiao, Y. & Montell, C. 2009. A Drosophila gustatory receptor essential for aversive taste and inhibiting male-to-male courtship. *Curr Biol,* 19**,** 1623-7.

Murata, S., Brockmann, A. & Tanimura, T. 2017. Pharyngeal stimulation with sugar triggers local searching behavior in Drosophila. *J Exp Biol,* 220**,** 3231-3237.

Park, J. & Carlson, J. R. 2018. Physiological responses of the Drosophila labellum to amino acids. *J Neurogenet,* 32**,** 27-36.

Park, J. H., Chen, J., Jang, S., Ahn, T. J., Kang, K., Choi, M. S. & Kwon, J. Y. 2016. A subset of enteroendocrine cells is activated by amino acids in the Drosophila midgut. *FEBS Lett,* 590**,** 493-500.

Poudel, S., Kim, Y., Gwak, J. S., Jeong, S. & Lee, Y. 2017. Gustatory receptor 22e is essential for sensing chloroquine and strychnine in Drosophila melanogaster. *Insect Biochem Mol Biol,* 88**,** 30-36.

Poudel, S., Kim, Y., Kim, Y. T. & Lee, Y. 2015. Gustatory receptors required for sensing umbelliferone in Drosophila melanogaster. *Insect Biochem Mol Biol,* 66**,** 110-8.

Poudel, S. & Lee, Y. 2016. Gustatory Receptors Required for Avoiding the Toxic Compound Coumarin in Drosophila melanogaster. *Mol Cells,* 39**,** 310-5.

Raad, H., Ferveur, J. F., Ledger, N., Capovilla, M. & Robichon, A. 2016. Functional Gustatory Role of Chemoreceptors in Drosophila Wings. *Cell Rep,* 15**,** 1442-1454.

Ribeiro, C. & Dickson, B. J. 2010. Sex peptide receptor and neuronal TOR/S6K signaling modulate nutrient balancing in Drosophila. *Curr Biol,* 20**,** 1000-5.

Rimal, S. & Lee, Y. 2018. The multidimensional ionotropic receptors of Drosophila melanogaster. *Insect Mol Biol,* 27**,** 1-7.

Rimal, S. & Lee, Y. 2019. Molecular sensor of nicotine in taste of Drosophila melanogaster. *Insect Biochem Mol Biol,* 111**,** 103178.

Rimal, S., Sang, J., Poudel, S., Thakur, D., Montell, C. & Lee, Y. 2019. Mechanism of Acetic Acid Gustatory Repulsion in Drosophila. *Cell Rep,* 26**,** 1432-1442 e4.

Salvaterra, P. M. & Kitamoto, T. 2001. Drosophila cholinergic neurons and processes visualized with Gal4/UAS-GFP. *Brain Res Gene Expr Patterns,* 1**,** 73-82.

Sanchez-Alcaniz, J. A., Silbering, A. F., Croset, V., Zappia, G., Sivasubramaniam, A. K., Abuin, L., Sahai, S. Y., Munch, D., Steck, K., Auer, T. O., Cruchet, S., Neagu-Maier, G. L., Sprecher, S. G., Ribeiro, C., Yapici, N. & Benton, R. 2018. An expression atlas of variant ionotropic glutamate receptors identifies a molecular basis of carbonation sensing. *Nat Commun,* 9**,** 4252.

Sang, J., Rimal, S. & Lee, Y. 2019. Gustatory receptor 28b is necessary for avoiding saponin in Drosophila melanogaster. *EMBO Rep,* 20.

Schneider, J., Dickinson, M. H. & Levine, J. D. 2012. Social structures depend on innate determinants and chemosensory processing in Drosophila. *Proc Natl Acad Sci U S A,* 109 Suppl 2**,** 17174-9.

Schneider, J. & Levine, J. D. 2014. Automated identification of social interaction criteria in Drosophila melanogaster. *Biol Lett,* 10**,** 20140749.

Scott, K., Brady, R., Jr., Cravchik, A., Morozov, P., Rzhetsky, A., Zuker, C. & Axel, R. 2001. A chemosensory gene family encoding candidate gustatory and olfactory receptors in Drosophila. *Cell,* 104**,** 661-73.

Shanbhag, S. R., Park, S. K., Pikielny, C. W. & Steinbrecht, R. A. 2001. Gustatory organs of Drosophila melanogaster: fine structure and expression of the putative odorant-binding protein PBPRP2. *Cell Tissue Res,* 304**,** 423-37.

Shim, J., Lee, Y., Jeong, Y. T., Kim, Y., Lee, M. G., Montell, C. & Moon, S. J. 2015. The full repertoire of Drosophila gustatory receptors for detecting an aversive compound. *Nat Commun,* 6**,** 8867.

Slone, J., Daniels, J. & Amrein, H. 2007. Sugar receptors in Drosophila. *Curr Biol,* 17**,** 1809-16.

Soldano, A., Alpizar, Y. A., Boonen, B., Franco, L., Lopez-Requena, A., Liu, G., Mora, N., Yaksi, E., Voets, T., Vennekens, R., Hassan, B. A. & Talavera, K. 2016. Gustatory-mediated avoidance of bacterial lipopolysaccharides via TRPA1 activation in Drosophila. *Elife,* 5.

Steck, K., Walker, S. J., Itskov, P. M., Baltazar, C., Moreira, J. M. & Ribeiro, C. 2018. Internal amino acid state modulates yeast taste neurons to support protein homeostasis in Drosophila. *Elife,* 7.

Stocker, R. F. 1994. The organization of the chemosensory system in Drosophila melanogaster: a review. *Cell Tissue Res,* 275**,** 3-26.

Stocker, R. F. & Schorderet, M. 1981. Cobalt filling of sensory projections from internal and external mouthparts in Drosophila. *Cell Tissue Res,* 216**,** 513-23.

Sun, F., Wang, Y., Zhou, Y., Van Swinderen, B., Gong, Z. & Liu, L. 2014. Identification of neurons responsible for feeding behavior in the Drosophila brain. *Sci China Life Sci,* 57**,** 391-402.

Sung, H. Y., Jeong, Y. T., Lim, J. Y., Kim, H., Oh, S. M., Hwang, S. W., Kwon, J. Y. & Moon, S. J. 2017. Heterogeneity in the Drosophila gustatory receptor complexes that detect aversive compounds. *Nat Commun,* 8**,** 1484.

Tauber, J. M., Brown, E. B., Li, Y., Yurgel, M. E., Masek, P. & Keene, A. C. 2017. A subset of sweet-sensing neurons identified by IR56d are necessary and sufficient for fatty acid taste. *PLoS Genet,* 13**,** e1007059.

Thistle, R., Cameron, P., Ghorayshi, A., Dennison, L. & Scott, K. 2012. Contact chemoreceptors mediate male-male repulsion and male-female attraction during Drosophila courtship. *Cell,* 149**,** 1140-51.

Thoma, V., Knapek, S., Arai, S., Hartl, M., Kohsaka, H., Sirigrivatanawong, P., Abe, A., Hashimoto, K. & Tanimoto, H. 2016. Functional dissociation in sweet taste receptor neurons between and within taste organs of Drosophila. *Nat Commun,* 7**,** 10678.

Thorne, N., Chromey, C., Bray, S. & Amrein, H. 2004. Taste perception and coding in Drosophila. *Curr Biol,* 14**,** 1065-79.

Toda, H., Zhao, X. & Dickson, B. J. 2012. The Drosophila female aphrodisiac pheromone activates ppk23(+) sensory neurons to elicit male courtship behavior. *Cell Rep,* 1**,** 599-607.

Toshima, N. & Tanimura, T. 2012. Taste preference for amino acids is dependent on internal nutritional state in Drosophila melanogaster. *J Exp Biol,* 215**,** 2827-32.

Usui-Aoki, K., Matsumoto, K., Koganezawa, M., Kohatsu, S., Isono, K., Matsubayashi, H., Yamamoto, M. T., Ueda, R., Takahashi, K., Saigo, K., Mikoshiba, K. & Yamamoto, D. 2005. Targeted expression of Ip3 sponge and Ip3 dsRNA impaires sugar taste sensation in Drosophila. *J Neurogenet,* 19**,** 123-41.

Vargas, M. A., Luo, N., Yamaguchi, A. & Kapahi, P. 2010. A role for S6 kinase and serotonin in postmating dietary switch and balance of nutrients in D. melanogaster. *Curr Biol,* 20**,** 1006-11.

Verschut, T. A., Carlsson, M. A., Anderson, P. & Hamback, P. A. 2017. Sensory mutations in Drosophila melanogaster influence associational effects between resources during oviposition. *Sci Rep,* 7**,** 9352.

Vijayan, V., Thistle, R., Liu, T., Starostina, E. & Pikielny, C. W. 2014. Drosophila pheromone-sensing neurons expressing the ppk25 ion channel subunit stimulate male courtship and female receptivity. *PLoS Genet,* 10**,** e1004238.

Walker, S. J., Corrales-Carvajal, V. M. & Ribeiro, C. 2015. Postmating Circuitry Modulates Salt Taste Processing to Increase Reproductive Output in Drosophila. *Curr Biol,* 25**,** 2621-30.

Wang, Q. P., Lin, Y. Q., Zhang, L., Wilson, Y. A., Oyston, L. J., Cotterell, J., Qi, Y., Khuong, T. M., Bakhshi, N., Planchenault, Y., Browman, D. T., Lau, M. T., Cole, T. A., Wong, A. C., Simpson, S. J., Cole, A. R., Penninger, J. M., Herzog, H. & Neely, G. G. 2016. Sucralose Promotes Food Intake through NPY and a Neuronal Fasting Response. *Cell Metab,* 24**,** 75-90.

Wang, Z., Singhvi, A., Kong, P. & Scott, K. 2004. Taste representations in the Drosophila brain. *Cell,* 117**,** 981-91.

Weiss, L. A., Dahanukar, A., Kwon, J. Y., Banerjee, D. & Carlson, J. R. 2011. The molecular and cellular basis of bitter taste in Drosophila. *Neuron,* 69**,** 258-72.

Wisotsky, Z., Medina, A., Freeman, E. & Dahanukar, A. 2011. Evolutionary differences in food preference rely on Gr64e, a receptor for glycerol. *Nat Neurosci,* 14**,** 1534-41.

Yanagawa, A., Chabaud, M. A., Imai, T. & Marion-Poll, F. 2018. Olfactory cues play a significant role in removing fungus from the body surface of Drosophila melanogaster. *J Invertebr Pathol,* 151**,** 144-150.

Yanagawa, A., Couto, A., Sandoz, J. C., Hata, T., Mitra, A., Ali Agha, M. & Marion-Poll, F. 2019. LPS perception through taste-induced reflex in Drosophila melanogaster. *J Insect Physiol,* 112**,** 39-47.

Yanagawa, A., Guigue, A. M. & Marion-Poll, F. 2014. Hygienic grooming is induced by contact chemicals in Drosophila melanogaster. *Front Behav Neurosci,* 8**,** 254.

Yang, C. H., Belawat, P., Hafen, E., Jan, L. Y. & Jan, Y. N. 2008. Drosophila egg-laying site selection as a system to study simple decision-making processes. *Science,* 319**,** 1679-83.

Yang, Z., Huang, R., Fu, X., Wang, G., Qi, W., Mao, D., Shi, Z., Shen, W. L. & Wang, L. 2018. A post-ingestive amino acid sensor promotes food consumption in Drosophila. *Cell Res,* 28**,** 1013-1025.

Yang, Z., Yu, Y., Zhang, V., Tian, Y., Qi, W. & Wang, L. 2015. Octopamine mediates starvation-induced hyperactivity in adult Drosophila. *Proc Natl Acad Sci U S A,* 112**,** 5219-24.

Yapici, N., Cohn, R., Schusterreiter, C., Ruta, V. & Vosshall, L. B. 2016. A Taste Circuit that Regulates Ingestion by Integrating Food and Hunger Signals. *Cell,* 165**,** 715-29.

Yavuz, A., Jagge, C., Slone, J. & Amrein, H. 2014. A genetic tool kit for cellular and behavioral analyses of insect sugar receptors. *Fly (Austin),* 8**,** 189-96.

Youn, H., Kirkhart, C., Chia, J. & Scott, K. 2018. A subset of octopaminergic neurons that promotes feeding initiation in Drosophila melanogaster. *PLoS One,* 13**,** e0198362.

Zhang, Y. V., Ni, J. & Montell, C. 2013a. The molecular basis for attractive salt-taste coding in Drosophila. *Science,* 340**,** 1334-8.

Zhang, Y. V., Raghuwanshi, R. P., Shen, W. L. & Montell, C. 2013b. Food experience-induced taste desensitization modulated by the Drosophila TRPL channel. *Nat Neurosci,* 16**,** 1468-76.

CHAPTER II

Molecular and cellular organization of taste neurons in adult *Drosophila* pharynx

This chapter has been published previously – **YCD Chen** and A Dahanukar. *Molecular and cellular organization of taste neurons in adult Drosophila pharynx*. Cell Reports, December 5, 2017; 21(10):2978-2991.

SUMMARY

The *Drosophila* pharyngeal taste organs are poorly characterized despite their location at important sites for monitoring food quality. Functional analysis of pharyngeal neurons has been hindered by the paucity of molecular tools to manipulate them, as well as their relative inaccessibility for neurophysiological investigations. Here, we generate receptor-to-neuron maps of all three pharyngeal taste organs by performing a comprehensive *chemoreceptor-GAL4/LexA* expression analysis. The organization of pharyngeal neurons reveals similarities and distinctions in receptor repertoires and neuronal groupings compared to external taste neurons. We validate the mapping results by pinpointing a single pharyngeal neuron required for feeding avoidance of L-canavanine. Inducible activation of pharyngeal taste neurons reveals functional differences between external and internal taste neurons and functional subdivision within pharyngeal sweet neurons. Our results provide road maps of pharyngeal taste organs in an insect model system for probing the role of these understudied neurons in controlling feeding behaviors.

INTRODUCTION

In *Drosophila*, taste neurons located in sensilla in several body regions sense and distinguish nutritive substances such as sugars, amino acids, and low salt, and potentially harmful ones such as high salt, acids, and a diverse variety of bitter compounds (Freeman and Dahanukar, 2015, Liman et al., 2014). Hair-like sensilla on the labellum, the distal segments of the legs (tarsi), the anterior wing margins, and the ovipositor have access to chemicals in external substrates. Pit-like sensilla (taste pegs) on the oral surface have access only once the fly extends its proboscis and opens the labellar palps; similar sensilla in the pharynx have access only when food intake is initiated. Based on its anatomical position, the pharynx is considered to act as a gatekeeper to control ingestion, promoting the intake of appetitive foods and blocking that of toxins.

Three distinct internal taste organs are present in the adult fly pharynx: the labral sense organ (LSO), and the ventral and dorsal cibarial sense organs (VCSO, DCSO). The VCSO and DCSO are paired on opposite sides of the rostrum, whereas the LSO is located in the haustellum (**Figure 2.1A,B**). The organization and neuronal composition of all three organs has been described in detail, based on both light and electron microscopy data (Gendre et al., 2004, Nayak and Singh, 1983, Stocker and Schorderet, 1981). Nine separate sensilla are present in the LSO, of which #1-6 are innervated by a single mechanosensory neuron each. The remaining three, named #7-9, are uniporous sensilla, a feature that ascribes chemosensory function to them. Sensillum #7 is the largest one with eight chemosensory neurons. Sensilla #8 and #9 have two neurons, one mechanosensory

and one chemosensory, each. Although one study reported two sensilla in the VCSO (Nayak and Singh, 1983), we, and two others (Stocker and Schorderet, 1981, Gendre et al., 2004), observed three sensilla in the VCSO, innervated by a total of 8 chemosensory neurons. The DCSO has two sensilla, each containing three chemosensory neurons. Notwithstanding the availability of detailed anatomical descriptions of pharyngeal taste organs, little is known about their function. The internal location of these organs poses challenges for electrophysiological analysis of taste neurons located within them. Additionally, few molecular tools are currently described to manipulate the function of selected pharyngeal taste neurons.

The expression and function of members of several chemosensory receptor gene families such as Gustatory receptors (Grs), Ionotropic receptors (Irs), Pickpocket (Ppk), and Transient receptor potential channels (Trps) have been found in external gustatory receptor neurons (GRNs) of the labellum and the tarsal segments (Freeman and Dahanukar, 2015). A number of *Gr*- and *Ir*-*GAL4* drivers are also shown to label pharyngeal organs (Kwon et al., 2014, Koh et al., 2014), however only a few, including *Gr43a* and members of sweet *Gr* clade, *Gr2a*, *Ir60b*, and *TrpA1*, have been mapped to specific taste neurons (Ledue et al., 2015, Kang et al., 2010, Miyamoto et al., 2012, Kim et al., 2017, Joseph et al., 2017).

Here, we generate receptor-to-neuron maps for three pharyngeal taste organs by a systematic expression analysis of chemoreceptor reporter lines that represent Gr, Ir and

ppk receptor families. The maps reveal a large and diverse chemoreceptor repertoire in the pharynx. Some receptors are expressed in combinations that are predictive of neuronal sweet or bitter taste function based on analysis of external GRNs. By contrast, some pharyngeal taste neurons express receptor combinations that are distinct from any that have been reported in other organs, leaving open questions about their functional roles. We validate the receptor-to-neuron maps derived from reporter gene expression by assessing roles of pharyngeal GRNs predicted to detect L-canavanine, a bitter tastant for which a complete receptor repertoire has been reported (Shim et al., 2015). Interestingly, a systematic activation analysis of different classes of pharyngeal taste neurons reveals functional differences between external and internal taste neurons for bitter avoidance and functional subdivision within pharyngeal sweet neurons for sweet acceptance. Together, our study provides a molecular map of pharyngeal taste organs, which will serve as a resource for future studies of the roles of pharyngeal taste neurons in food evaluation.

RESULTS

Chemoreceptor reporter expression in pharyngeal taste organs

Although adult *Drosophila* pharyngeal taste organs have been anatomically characterized, little is known about receptor expression in sensory neurons housed within these organs. In a previous study, we described neurons in the LSO and VCSO that co-express multiple Grs belonging to the sweet clade (Ledue et al., 2015). However, sweet neurons account for a small fraction (4 of 24) of pharyngeal gustatory receptor neurons (GRNs). We therefore systematically analyzed 43 *Gr-GAL4* drivers reported to label afferents in the pharyngeal nerve and terminate in the SEZ (Kwon et al., 2014). We mapped expression of 36 *Gr-GAL4* lines, which still showed strong expression in the pharynx (**Table 2.1**). We also examined a number of *Ir-GAL4* drivers, focusing on 8 members of the *Ir20a* clade along with *Ir11a* and *Ir100a*, whose expression was reported in the pharynx (Koh et al., 2014, Croset et al., 2010). We included drivers for two broadly expressed Ir co-receptors, *Ir25a* and *Ir76b*, which are expressed in GRNs of external organs (Hussain et al., 2016, Zhang et al., 2013, Croset et al., 2010), and *ppk28-GAL4*, which marks water-sensing neurons in the labellum (Cameron et al., 2010). For most receptors, we tested two independent transgenic lines using *UAS-mCD8-GFP*. First, we identified the number of cells that were GFP positive in the pharynx. Next, we traced labeled dendrites to specific sensilla within each of the three pharyngeal taste organs. By using *MJ94-Gal4*, which labels most if not all chemosensory and mechanosensory neurons in the pharynx (Gendre et al., 2004), we were able to visualize one mechanosensory neuron each in LSO sensilla #1-6 , eight GRNs in LSO sensillum #7,

and one mechanosensory neuron and one GRN each in LSO sensilla #8 and #9 (**Figure 2.1C-F**). In addition, we observed a total of eight GRNs in three VCSO taste sensilla (**Figure 2.1G-J**), and a total of six GRNs in two DCSO taste sensilla (**Figure 2.1K-N**) using *Ir25a-GAL4* and *MJ94-GAL4*, respectively. The three taste sensilla in the LSO, named #7, #8 and #9, are easily distinguishable from each other, as are the two proximal and distal sensilla in the DCSO. We were therefore able to map expression of each driver to one or more identified neurons within each sensillum of the LSO and DCSO (**Figure 2.1F and 1N**). The cuticular pores of the three sensilla in the VCSO, however, are clustered together in a non-linear manner that precluded unambiguous mapping of labeled dendrites to their particular locations (**Figure 2.1G**). Thus, we mapped expression to specific neurons of the VCSO, but did not attest sensillar assignments (**Figure 2.1J**). We introduced a new nomenclature for pharyngeal GRNs, abbreviating location and assigning numbers as follows: L7-1 through L7-8 in the LSO sensillum #7, L8 and L9 in the LSO sensilla #8 and #9; V1 – V8 in the VCSO; DD1 – DD3 in the distal sensillum of the DCSO, and DP1 – DP3 in the proximal sensillum of the DCSO.

In general, we found a total of 12 *Gr-GAL4* lines expressed in the LSO (**Figure 2.2**), including the 5 sweet *Gr-GAL4* drivers that we reported previously (Ledue et al., 2015), and 28 in the VCSO (**Figure 2.3A-H**). A vast majority of the drivers labeled 1–3 neurons in the VCSO; several showed expression in 1–2 neurons in the LSO. We found *Gr-GAL4* lines that were expressed in the LSO alone, in the VCSO alone, as well as in both. Interestingly, the DCSO appeared to exclude *Gr*-expressing neurons (**Figure 2.3I-**

K). *ppk28-GAL4* also labeled cells exclusively in the LSO and VCSO. By contrast, we found *Ir*-expressing neurons in all pharyngeal taste organs. *Ir25a-GAL4*, in particular, labeled all GRNs in the LSO, VCSO and DCSO, whose expression was validated with an Ir25a antibody (**Figures 2.2C, 2.3A,I**). *Ir76b-GAL4* also showed broad expression (**Figures 2.2D, 2.3B,J**). All other drivers were expressed in smaller subsets of neurons (**Figures 2.2E, 2.3F,J**). To further identify GRNs that express each driver, we performed a series of double-driver and double-labeling analyses. For the double-driver analyses, we examined selected pairwise combinations of drivers and compared the number of GFP positive neurons for two *GAL4* drivers with those observed for a single *GAL4* driver alone (**Figures 2.2H-J and 2.3D,G,H**). We also took advantage of several *LexA* drivers to perform two-color analyses to confirm co-expression of drivers in the same neurons (**Figures 2.2B,F,G and 2.3B,C,E,F,K**). Details of the mapping procedure are described in the following sections. Receptor-to-neuron maps generated from analyses of reporter lines are summarized in **Figure 2.1F,J,N**.

Chemoreceptor reporter mapping in the labral sense organ (LSO)

In the LSO, we found that L8 and L9 expressed 3 *Gr-GAL4* lines (*Gr32a*, *Gr66a* and *Gr89a*) (**Figure 2.2A,B**) representing commonly expressed receptors that are broadly expressed in external bitter taste neurons (Ling et al., 2014, Weiss et al., 2011). *Ir76b-* and *Ir25a-GAL4* labeled all taste neurons of the #7-9 sensilla (**Figure 2.2C,D**). The expression of *Ir25a-GAL4* matched with the anti-Ir25a antibody staining (**Figure 2.2C**). In the #7 sensilum of LSO, the L7-1 through L7-8 neurons could be grouped into six

classes based on *GAL4* expression patterns (**Figure 2.2E-J**). As previously described, two neurons, L7-1 and L7-2, expressed *Gr43a* along with other members of the sweet *Gr* clade (Ledue et al., 2015). Double labeling experiments with *Gr43a-LexA* and selected *GAL4* drivers that labeled 1–2 neurons of the #7 sensillum revealed that cells expressing *Gr93d/Ir56a* (L7-3), *ppk28/Ir20a* (L7-4 and L7-5), *Ir67c* (L7-6), *Ir94f/Ir94h* (L7-7) and *Ir100a* (L7-8) were distinct from those expressing *Gr43a* (**Figure 2.2F**). A similar series of experiments with *ppk28-LexA* showed overlap with *GAL4* lines of *Ir20a* but not *Gr93d*, *Ir56a*, *Ir67c, Ir94f, Ir94h* and *Ir100a* (**Figure 2.2G**). Mapping of *Gr93d*, *Ir67c*, *Ir94f* and *Ir100a GAL4* lines to separate neurons was confirmed by examining pairwise combinations of the four drivers – in all cases animals with two drivers showed two labeled neurons, whereas each driver alone labeled only a single neuron. Additional double-driver experiments with either *Gr93d-* or *Ir94f-GAL4* indicated co-expression of four other receptors, *Gr2a*, *Gr23a*, *Gr57a* and *Ir56a*, in the L7-3 neuron, and *Ir94h* in the L7-7 neuron (**Figure 2.2H-J**). We mapped *Ir100a* expression along with *Ir25a* and *Ir76b* in the L7-8 neuron, since *Ir100a* showed no co-expression with driver lines for *Gr43a*, *Gr93d*, *ppk28*, *Ir67c* and *Ir94f*. A receptor-to-neuron map for LSO generated from these results is shown in **Figure 2.1F**.

Chemoreceptor reporter mapping in the ventral cibarial sense organ (VCSO)

In the VCSO, we found *Ir25a-GAL4* to be expressed in all eight neurons of the VCSO as confirmed by an Ir25a antibody (**Figure 2.3A**). By contrast, *Ir76b* was expressed in only 3 of the 8 GRNs. Two *Ir76b*$^{+}$ neurons were identified as V1 and V2,

due to co-expression with *Gr64e-GAL4*. The third *Ir76b*$^{+}$ neuron was identified as V3 – it showed partial overlap with *Ir20a*, but not *ppk28* (V4), *Gr66a* (V5 – V7), *Gr93d* (V7 – V8), *Ir11a*, *Ir94a*, or *Ir94c* (**Figure 2.3B**). Consistent with our previous observations with *Gr43a-GAL4* (Ledue et al., 2015), we found that two neurons, V1 and V2, expressed *Gr43a-LexA*. Double labeling experiments with *Gr43a-LexA* showed overlap with *Ir94h-GAL4* but not with *GAL4* lines for *Gr93d*, *ppk28*, or *Ir20a* (**Figure 2.3C**). Subsequently, we found that *Ir94h-GAL4* and *Gr64c-GAL4* independently marked each of the two *Gr43a*$^{+}$ neurons, identifying them as *Gr64c*$^{+}$ (V1) and *Ir94h*$^{+}$ (V2) (**Figure 2.3D**). We mapped *ppk28* expression to V4, because it was positive for one *Ir20a-GAL4* neuron but not another (V3), nor did it overlap with drivers for *Gr43a*, *Ir76b*, *Gr32a*, *Gr93d* (**Figure 2.3B,C,E,F**).

One of the two cells labeled by *Gr93d-GAL4* overlapped with *Gr32a-LexA*, which was expressed in three cells (**Figure 2.3F**). Thus, *Gr32a* and *Gr93d* together accounted for four additional neurons: V5 (*Gr32a*$^{+}$), V6 (*Gr32a*$^{+}$) and V7 (*Gr32a*$^{+}$, *Gr93d*$^{+}$) and V8 (*Gr32a*$^{-}$, *Gr93d*$^{+}$). We next systematically inspected overlap of *Gr32a-LexA* expression with *GAL4* drivers (**Figure 2.3F**). The three *Gr32a*$^{+}$ neurons also expressed the *Gr33a* and *Gr66a*. The molecular identity of the three *Gr32a*$^{+}$ neurons could be further categorized by *Gr93a-* and *Gr93d-GAL4* (**Table 2.2**). 11 additional *Gr-GAL4* were mapped to V5 by virtue of overlap with *Gr32a-LexA* but exclusion from *Gr93a-* and *Gr93d-GAL4* cells. A single *Gr93a*$^{+}$ neuron was identified as V6, because *Gr93a-GAL4* expression overlapped with *Gr32a-LexA* but not with *Gr93d-GAL4*. Analysis of driver

combinations with *Gr93a-* and *Gr93d-GAL4* mapped a group of 12 additional *Gr-GAL4* to V6 (**Figure 2.3F-H**). The third *Gr32a*$^{+}$ neuron, identified as V7, was characterized as *Gr93a*$^{-}$, *Gr93d*$^{+}$. Double-driver analyses with *Gr93a-* and *Gr93d-GAL4* placed 5 additional *Gr-GAL4* in V7 (**Figure 2.3F-H**). V8 was marked solely by expression of *Gr93d* and no other *Gr-GAL4* drivers were co-expressed in this neuron. This series of experiments resolved mapping of all *Gr-GAL4* drivers expressed in the VCSO. We next turned to other *Ir-GAL4* drivers. Both *Ir94a-GAL4* and *Ir94c-GAL4* were mapped to V5 because of co-expression with *Gr32a-LexA* but not *Gr93d-GAL4* and *Gr93a-GAL4*, and confirmed by double-driver analysis that showed three GFP^{+} neurons in animals that carried *Gr93d-GAL4* with either *Ir94a-GAL4* or *Ir94c-GAL4* (**Figure 2.3G**) and two GFP^{+} neurons in animals that carried *Gr93a-GAL4* with either *Ir94a-GAL4* or *Ir94c-GAL4* (**Figure 2.3H**). *Ir11a-GAL4* was mapped to V6 and V7 because it overlapped with *Gr32a-LexA, Gr93a-GAL4* and partially overlapped with *Gr93d-GAL4* (**Figure 2.3F-H**). A receptor-to-neuron map for VCSO generated from these results is shown in **Figure 2.1J**.

Chemoreceptor reporter mapping in dorsal cibarial sense organ (DCSO)

In the DCSO, we found *Ir25a-GAL4* expression in all six neurons in the proximal and distal sensilla (**Figure 2.3I**). In addition, *Ir76b-GAL4* marked two of the three neurons in each sensillum (**Figure 2.3J**). Notably, *Ir100a-GAL4* showed expression in the one taste neuron in each DCSO sensillum, which overlapped with *Ir76b-LexA* (**Figure 2.3K**). *Gr-GAL4* expression appears to be excluded from the DCSO, although

we inconsistently observed expression of drivers for *Gr22b* and *Gr93d* (**Figure 2.8**). A receptor-to-neuron map for DCSO generated from these results is shown in **Figure 2.1N**.

A pharyngeal taste representation map in the subesophageal zone (SEZ)

Previous studies have shown that axons of taste neurons in pharyngeal taste organs travel via the pharyngeal and accessory pharyngeal nerves and terminate in the dorso-anterior region of the primary taste center, the subesophageal zone (SEZ) (Ledue et al., 2015, Kwon et al., 2014, Stocker and Schorderet, 1981). Our receptor-to-neuron maps gave us an opportunity to examine axonal termini of bilaterally symmetrical pairs of taste neurons utilizing drivers that label single, or a small subset of, identified neurons. We tested all *chemosensory receptor-GAL4* drivers that label every neuronal class identified by mapping analysis, including four main classes of *Gr/Ir*-expressing pharyngeal GRNs: 1) sweet pharyngeal GRNs labeled by *Gr61a-/Gr64d-/Gr64e-GAL4* (**Figure 2.4A**); 2) putative water pharyngeal GRNs labeled by *ppk28-GAL4* (**Figure 2.4B**); 3) putative bitter pharyngeal GRNs labeled by *Gr77a-*/*Gr9a-*/*Gr33a-*/*Gr93d-/Gr66a-GAL4* (**Figure 2.4C**); 4) *Ir*-expressing pharyngeal GRNs labeled by *Ir67c-*/*Ir94f-*/*Ir11a-*/*Ir20a-*/*Ir100a-*/*Ir76b-*/*Ir25a-GAL4* lines (**Figure 2.4D**). Since most of these drivers also showed expression in external GRNs, we examined labeled projections both in wild type and in a *pox-neuro* (*poxn*) mutant background, in which all external taste bristles are transformed into mechanosensory bristles (Awasaki and Kimura, 1997, Nottebohm et al., 1992). As expected, in *poxn* mutants *UAS-mCD8-GFP* driven by *chemosensory receptor-GAL4* drivers showed expression in internal GRNs and their corresponding axonal projections

in the SEZ (**Figure 2.4A-D**). As reported previously (Ledue et al., 2015), *poxn* mutants also retained labeling in a few taste pegs present on the oral surface of the labellum; axons of these neurons terminate in characteristic, bilaterally symmetric S-shaped patterns in the SEZ. Axonal termini of pharyngeal GRNs were all found in the expected dorso-anterior region, with some differences in patterns of axonal arborization. We noticed that neurites of GRNs that are predicted to sense aversive tastants (e.g. *Gr77a-*/*Gr9a-*/*Gr33a-*/*Gr93d-*/*Gr66a-GAL4*) had extensive projections at the midline, whereas those predicted to sense appetitive tastants (e.g. *Gr61a-*/*Gr64d-*/*Gr64e-*/*ppk28-*/*Ir94f-GAL4*) were present in discrete regions on each ipsilateral side.

Pharyngeal taste projections can be separated by neurons and organs

To characterize the projections of different classes of pharyngeal GRNs in the SEZ, we examined the overlap of *Gr43a*, *ppk28*, and *Gr93d* projections by testing combinations of *GAL4/LexA* drivers. We visualized single optical sections of fluorescence images, which revealed little overlap between *Gr43a*, *ppk28* and *Gr93d*-labeled termini (**Figure 2.5A**), consistent with the idea that these GRNs, which are likely to sense different categories of tastants, have distinct representations in the SEZ. To examine whether GRNs of the same taste category originating in different pharyngeal taste organs target discrete areas of the SEZ, we compared axonal projections labeled by *Gr43a-LexA* (LSO and VCSO) and *Gr61a-GAL4* (LSO alone) in *poxn* mutants, using two-color analysis. We note that *Gr43a-LexA* projections of olfactory neurons were also visualized via labial nerves in the antennal lobes of *poxn* mutants. We found *Gr43a-LexA*

taste projections distributed in an anterior zone of the SEZ, labeling neurites in medial and lateral regions. Overlapping *Gr61a-GAL4* projections were found in the lateral areas, but were limited or absent in the medial region, suggesting the pharyngeal sweet neuronal projections from the VCSO terminate medially as compared to those from the LSO (**Figure 2.5B**). The separations between putative bitter pharyngeal GRNs of the LSO and VCSO were less obvious when we compared *Gr32a-LexA* (LSO and VCSO) and *Gr33a-GAL4* (VCSO alone) in labeling in *poxn* flies (**Figure 2.5C**), mainly due to the extensive projections at the midline in these putative bitter pharyngeal GRNs. Overall, these results suggest that pharyngeal GRNs of different classes and/or different pharyngeal taste organs target distinct areas of the SEZ and may represent distinct neural circuits, and possibly distinct functional roles.

Functional validation of pharyngeal taste receptor-to-neuron maps

We next wished to validate the results of our receptor-to-neuron maps, given the caveat that transgenic drivers, which we used to assess receptor expression patterns, may not always reflect endogenous expression patterns of receptors. In a previous study, we confirmed that *Gr64e-GAL4* does in fact label pharyngeal sweet GRNs using calcium imaging and behavior assays (Ledue et al., 2015). We therefore decided to focus on a different taste category to validate other neuronal identities. Specifically, we elected to test a bitter compound, L-canavanine for two reasons. First, L-canavanine is known to activate bitter GRNs but it does not inhibit sweet GRNs (French et al., 2015, Jeong et al., 2013), which can otherwise confound interpretations of feeding assays using sugar/bitter

mixtures. Second, L-canavanine is the only bitter compound for which a complete receptor repertoire has been described (Shim et al., 2015). A recent study reported a high affinity complex comprising Gr8a/Gr66a/Gr98b for detection of L-canavanine (Shim et al., 2015). Perusal of our receptor-to-neuron maps implicated a single *Gr66a* neuron, the V6 neuron in the VCSO, as a high affinity sensor of L-canavanine.

We first silenced all *Gr66a* pharyngeal GRNs using the inwardly rectifying channel, Kir2.1, and tested behavioral responses to various concentrations of L-canavanine mixed with 5 mM sucrose. Experiments were carried out in *poxn* mutants to exclude any contribution from external GRNs. As predicted, control flies showed avoidance of L-canavanine in a dose dependent manner, which was completely abolished in *Gr66a*-silenced flies (**Figure 2.6A**). We then assessed the role of the V6 neuron in sensing L-canavanine using *Gr9a-GAL4*, which is expressed exclusively in this neuron. Notably, in the absence of a functional V6 neuron, flies lost the ability to avoid L-canavanine at all concentrations tested (**Figure 2.6B**), similar to *Gr66a*-silenced flies. This result provides functional evidence for L-canavanine receptor expression in the V6 neuron.

The previous study suggested that *Gr8a* and *Gr66a* together may be sufficient for a weak response to L-canavanine (Shim et al., 2015). We therefore tested the role of the *Gr8a*/*Gr66a*-labeled V7 neuron. Since a *GAL4* driver that is exclusively expressed in V7 is not available, we expressed Kir2.1 with *Gr93d-GAL4*, which would silence V7 along

with two other neurons in the LSO (L7-3) and VCSO (V8). The resulting flies exhibited no difference in feeding avoidance of L-canavanine as compared to the *UAS* control at all concentrations of L-canavanine (**Figure 2.6C**). As an additional control, we silenced the V5 neuron specifically by *Gr77a-GAL4*, which does not express either *Gr8a* or *Gr98b* according to our reporter analysis. As predicted, this manipulation caused no reduction in L-canavanine avoidance (**Figure 2.6D**). We note that *Gr93d-* and *Gr77a*-silenced flies showed a significant difference in feeding avoidance of 1 mM L-canavanine as compared to the corresponding *GAL4* control, but not the *UAS* control, suggesting that the difference is likely due to the background effect of *UAS-Kir2.1*. Taken together, we identified V6 as functional L-canavanine-sensing pharyngeal neurons, with V5 or V7 playing little if any role in sensing L-canavanine, on the basis of their molecular signatures.

Inducible activation of different pharyngeal taste neurons identifies functional differences between and within different taste organs.

To identify the valance that each class of pharyngeal taste neurons might carry in our feeding choice assay, we expressed the mammalian capsaicin receptor (*UAS-$VR1^{E600K}$*) (Marella et al., 2006) under the control of selected *GAL4* drivers in *poxn* mutants and measured feeding preference for capsaicin (**Figure 2.7A**). Flies were tested in binary choice assays with 100 μM capsaicin and ethanol solvent as the two alternatives. All *GAL4* and *UAS* controls were tested, and none showed a preference for capsaicin. We found that *Gr64e>$VR1^{E600K}$* flies had a significant preference for capsaicin,

demonstrating that activation of *Gr64e*$^{+}$ neurons in the LSO and VCSO is sufficient to trigger taste acceptance and ingestion. Interestingly, activation of *Gr64e*$^{+}$ neurons in the LSO alone (via *Gr61a-GAL4*) resulted in preference for capsaicin, whereas that of *Gr64e*$^{+}$ neurons in the VCSO neurons alone (via *Gr64d-GAL4*) did not, suggesting a functional subdivision of pharyngeal sweet GRNs in driving feeding attraction to sugars. One caveat is that a few taste pegs would also be activated in the *Gr64e>VR1*^{E600K} flies, but previous functional calcium imaging of taste pegs projections found no responses to various sugars (Ledue et al., 2015), supporting the view that the residual taste pegs play little role in sugar feeding choice.

Surprisingly, we did not observe significant feeding avoidance of capsaicin with the activation of putative bitter taste neurons using either the *Gr66a-* or *Gr93d-GAL4* drivers. To rule out the possibility that expression via *Gr66a-GAL4* is too weak to drive functional levels of the capsaicin receptor, we confirmed these results using the *Gr32a-GAL4* driver, whose expression overlaps precisely with that of *Gr66a-GAL4*. The activation of *Gr32a* neurons also did not elicit significant capsaicin avoidance (**Figure 2.7A**). Neither did the combined activation of *Gr66a*$^{+}$ and *Gr93d*$^{+}$ neurons. A 10-fold greater concentration of capsaicin (1 mM) did not yield conclusive results, because it affected gelling of the agarose droplets and thwarted participation of adequate numbers of flies. We next tested whether an avoidance function for these neurons could be uncovered when the flies were induced to consume capsaicin. We found that *poxn* flies in which *Gr66a*$^{+}$ neurons were activated simultaneously with *Gr64e*$^{+}$ showed a non-significant

reduction of mean PI for capsaicin, suggesting that pharyngeal *Gr66a* GRNs may be involved in restraining intake that is stimulated by the activity of appetitive neurons. A similar effect was not observed using *Gr64e-GAL4* combined with either *Gr93d* or *Ir94f* drivers. Thus, although not statistically significant, the reduction in mean PI was specifically observed with *Gr66a* driver. While the results are consistent with a role for pharyngeal *Gr66a* neurons in feeding avoidance, it appears that $VR1^{E600K}$-mediated activation of these GRNs does not elicit a strong response of this nature. Although we cannot rule out the possibility that $VR1^{E600K}$ expression or function is weaker in bitter neurons, capsaicin-induced activation of external bitter neurons in wild type flies using *Gr66a-* or *Gr32a-GAL4* caused strong feeding avoidance (**Figure 2.7B**), further supporting the idea of functional differences between internal and external bitter taste circuits.

No discernible phenotypes were observed upon activation or neurons of unknown function marked by *Ir56a*, *Ir67c*, *Ir94f, Ir100a* or *Ir20a*, or of neurons expressing the Ppk28 water receptor. It is possible that these pharyngeal taste neurons may be involved in other behaviors, such as choice of oviposition substrate, as has been reported for *Gr66a* (Joseph and Heberlein, 2012). Alternatively, their roles in feeding behaviors may be dependent on the context, such as prior experience, internal state, or complexity of food substrate.

DISCUSSION

Internal pharyngeal taste organs are the least explored taste organs, despite their obvious importance in insect feeding behaviors, which are crucial drivers for damaging crops and vectoring disease. Here we investigate the organization of pharyngeal taste neurons by generating maps of *chemoreceptor-GAL4* expression, which showcase the complex molecular signatures and groupings of these in the pharynx.

The receptor-to-neuron maps of pharyngeal taste organs suggest a high degree of molecular complexity, with co-expression of different chemoreceptor family members in many pharyngeal GRNs. In particular, none of the pharyngeal GRNs were found to express *Gr* genes alone, rather one or more *Ir* genes were always found in the same neurons. *Gr* and *Ir* genes are also co-expressed in some external sweet and bitter-sensing GRNs (Van Giesen et al., 2016, Croset et al., 2010). Thus, both classes of receptors are likely to contribute to responses of *Gr*/*Ir*-expressing neurons in the LSO and VCSO, but whether they interact functionally or act independently remains to be determined. In the LSO, expression of sweet *Grs* and *Ir76b* overlaps in pharyngeal sweet GRNs, as observed in tarsi as well (Ganguly et al., 2017). In the pharynx, we also found co-expression of *ppk28* with *Ir* genes, which has not been described for external GRNs. These observations invite explorations of possible crosstalk, and its functional significance, between the two classes of receptors.

Pharyngeal GRNs also exhibit distinctive functional groupings. All external bitter GRNs have always been found grouped with sweet GRNs in taste hairs. By contrast, canonical sweet and bitter GRNs appear to segregate in different sensilla in the LSO, which is most well characterized for this perspective. L8 and L9 may be functionally identical, and house only one *Gr66a*-expressing bitter GRN each, whereas L7 contains two sweet GRNs (L7-1, L7-2). Moreover, external hairs typically have 2–4 GRNs, each of which has a distinct functional profile. In the LSO we find duplications – L7-1 and L7-2 are identical, as are L7-4 and L7-5 – although differences between these pairs of GRNs may emerge as additional chemoreceptors are mapped in the pharynx. Finally, it is difficult to ascribe putative functions to most pharyngeal GRNs based on existing knowledge of receptor function in external counterparts. The L7-3 *Gr*-expressing neuron, for example, does not express members of the sweet clade, but neither does it express any of the common bitter Grs (*Gr32a*, *Gr66a* and *Gr89a*) that would corroborate its role as a bitter GRN. Similarly, with the exception of salt neurons that may express *Ir76b* alone, there are few known functions for GRNs that solely express *Ir* genes. One possibility is that some of these GRNs possess novel chemoreceptor family-ligand interactions. For example, L7-7 is involved in sensing sucrose but limiting sugar ingestion, representing an Ir neuron that operates in a negative circuit module for sugar intake (Joseph et al., 2017). In addition, another recent study suggests that TRPA1 expression in L8 and L9 of the LSO is involved in feeding avoidance to bacterial endotoxins lipopolysaccharides (LPS) (Soldano et al., 2016). Alternatively, some pharyngeal GRNs may evaluate characteristics other than palatability, such as temperature or viscosity. *Ir25a*, which is broadly

expressed in all 24 pharyngeal GRNs, is required for cool and temperature sensing (Ni et al., 2016, Chen et al., 2015). It will be worth investigating whether one or more pharyngeal GRNs act to integrate information about temperature and chemical quality of food substrates.

Expression analyses also hint at some functional subdivisions between pharyngeal taste organs. The LSO contains a smaller proportion of *Gr*-expressing neurons as compared to the VCSO, which also expresses a larger number of *Gr* genes that are co-expressed with *Gr66a*. Thus, we might expect broader bitter taste function in the VCSO. By contrast, sweet taste function appears to be more dominant in the LSO – its sweet GRNs express more sweet *Gr-GAL4* drivers than the ones in the VCSO, and their activation is sufficient to drive feeding preference. VCSO sweet GRNs fail to promote ingestion by themselves, but may contribute to an increase in feeding preference when activated simultaneously with those in the LSO. Thus, there may be synergistic or hierarchical interactions between LSO and VCSO sweet taste circuits, with the latter coming into play only once the former is activated. The finding that *Gr* and *Ir* genes are expressed in the LSO and VCSO but only *Ir* genes in the DCSO is also striking, and raises the possibility that the DCSO, which is present at the most internal location relative to the others, may serve a unique role in controlling ingestion.

The afferents of pharyngeal GRNs target regions of the subesophageal zone (SEZ) that are distinct from areas in which afferents from labellar and tarsal GRNs terminate (Kwon

et al., 2014). Interestingly, pharyngeal GRN projections between molecularly different classes of neurons, as well as between GRNs of the LSO and VCSO are also distinct. Projections of sugar-sensing GRNs were found in separate ipsilateral regions, whereas those of neurons predicted to detect aversive tastants were found at the midline, suggesting the presence of contralateral termini. These observations may inform future functional studies of pharyngeal GRNs. L7-6 neurons, for example, would be predicted to sense aversive compounds based on the presence of their termini at the midline. Analysis of pharyngeal GRN projections also suggests distinct connectivity to higher order neuronal circuits (Yapici et al., 2016). With the molecular tools described here, future investigations of pharyngeal GRNs and pharyngeal taste circuits will provide insight into how internal taste is integrated with external taste to control various aspects of feeding behavior.

EXPERIMENTAL PROCEDURES

Fly strains. Flies were reared on standard cornmeal-dextrose-agar food at 25°C and 60-70% relative humidity under a 12 h:12 h dark:light cycle. The following fly lines were used: *MJ94-GAL4* was a gift from L. Griffith at Brandeis University, *Gr-GAL4* (Ling et al., 2014, Weiss et al., 2011), *Gr66a-GAL4* (BDSC#28801), *Ir-GAL4* (Koh et al., 2014), *Ir11a-GAL4* (BDSC#41742), *Ir100a-GAL4* (BDSC#41743), *Ir76b-GAL4* (BDSC#41730), *Ir25a-GAL4* (BDSC#41728), *ppk28-GAL4* (Cameron et al., 2010), *Gr43a-LexA* (Miyamoto and Amrein, 2014), *Gr32a-LexA* (Fan et al., 2013), *Ir76b-LexA* (Ganguly et al., 2017), *ppk28-LexA* (Thistle et al., 2012), *UAS-Kir2.1* (Baines et al., 2001), *UAS-VR1*^{E600K} (Marella et al., 2006), *poxn*$^{\Delta M22\text{-}B5}$ (Boll and Noll, 2002), *poxn*^{70} (Awasaki and Kimura, 1997), *UAS-mCD8-GFP* (Weiss et al., 2011), and *LexAop2-6XmCherry-HA* (BDSC#52271, 52272). For experiments using *poxn* mutants, we confirmed the *poxn* mutant background in all sorted flies by observing the transformed long and bent mechanosensory hairs in the labellum, as well as the fused three tarsal segments in the legs.

Immunohistochemistry. At least 50 flies per genotype were anesthetized on ice, and the proboscis and brain tissue were dissected in 1X PBST (PBS with 0.3% Triton X-100) and fixed for 30 min with 4% paraformaldehyde in 1X PBST at room temperature. After three washes with 1X PBST, samples were blocked with 5% normal goat serum (Sigma, #G9023) in 1X PBST. Tissues were incubated in primary antibody solutions for 3 days at 4^{o}C. Primary antibodies were: chicken anti-GFP (1:5000; Abcam, #ab13970,

RRID:AB_300798), rabbit anti-GFP (1:1000; Invitrogen, #A11122, RRID:AB_221569), rabbit anti-DsRed (1:200; Clontech, #632496, RRID:AB_10013483), rabbit anti-Ir25a (1:500; a gift from L. Vosshall at Rockefeller University), and mouse anti-nc82 (1:20; Developmental Studies Hybridoma Bank, RRID:AB_2314868). Secondary antibodies (1:400; Invitrogen) were: goat anti-chicken Alexa Fluor 488 (RRID:AB_142924), goat anti-rabbit Alexa Fluor 488 (RRID:AB_143165), goat anti-rabbit Alexa Fluor 546 (RRID:AB_143156), goat anti-mouse Alexa Fluor 568 (RRID:AB_141611), and goat anti-mouse Alexa Fluor 647 (RRID:AB_141658). Samples were mounted in 80% glycerol in 1X PBST or VECTASHIELD antifade mounting medium (Vector Laboratories, #H-1000) and stored at 4^{o}C. Fluorescent images were acquired using a Leica SP5 confocal microscope with 400 Hz scan speed in 512x512 or 1024x1024 pixel formats. Image stacks were acquired at 1-μm optical sections. Unless otherwise noted, all images were presented as maximum projections of the *z* stack generated using Leica LAS AF software.

Expression analyses. Expression patterns of *Gr/Ir/ppk-GAL4/LexA* lines were mapped in the three pharyngeal taste organs by using *UAS-mCD8-GFP* and *LexAop2-6XmCherry-HA* reporters. For most of chemosensory receptors, we tested two or more independent reporter lines. Initial analysis was performed through live fluorescence imaging with at least 50 flies per line. The number of pharyngeal GRNs labeled by independent driver lines was consistent, although different signal intensities were observed across individual lines for the same receptor. We selected one representative line with stronger live

fluorescence signal for further immunofluorescence mapping and behavioral experiments. For double-driver analysis, the *UAS-mCD8-GFP* transgene was under the control of two different *Gr-GAL4* drivers and the number of GFP-labeled neurons was compared to flies containing a single *Gr-GAL4* driver alone. Images were acquired using a Leica SP5 confocal microscope.

Binary choice feeding assays. Feeding preference assays were performed as described previously (Charlu et al., 2013). Sucrose (S7903) and L-canavanine (C1625) were obtained from Sigma-Aldrich and were dissolved in water; capsaicin (M2028) was also obtained from Sigma-Aldrich and was prepared in ethanol. Briefly, flies were sorted into groups of 10 males and 10 females upon eclosion and aged for 5-8 days. Since *poxn* mutant male flies are sterile, we added 2 heterozygous males with curly wings (*poxn/CyO*) in each group to ensure that all sorted females were mated. Heterozygous males were discarded during scoring for abdominal color. Flies were starved for 24 hr on water-saturated tissues and then placed in tight-fit Petri dishes (Falcon Cat. #35-1006) with eighteen 10 μL dots of 0.75% agarose that alternated in tastant and color using either 25 mg/mL indigo carmine (Sigma, #I8130) or 50 mg/mL sulforhodamine B (Sigma, #230162). We swapped dyes for each tastant with similar numbers of trials to account for any dye preference. Flies were allowed to feed for 2 hours at 25°C in a dark, humidified chamber, after which they were frozen and scored for abdomen color by dissecting the guts within 24 hours. Trials with participation lower than 50% were excluded. Preference index (PI) was calculated as ((# of flies labeled with the tastant color) – (# of flies labeled

with the control color))/(total number of flies that fed). Thus, a PI of 0 would indicate equal preference between the two choices. In all cases, PI values were calculated for mixed populations of males and females.

Experimental design and statistical analysis. All data are presented as mean ± S.E.M. Statistical tests were conducted using Prism 7 (GraphPad Software). All the experiments were performed in parallel with both control and experimental genotypes. Complete genotypes used in this study are listed in **Table 2.3**. The sample size for each experiment was based on previously published reports. All independent trials were performed over 2 days. To improve normality and homogeneity of variances, we arcsine-transformed the square root of preference indices prior to analysis. Differences between means of different groups were evaluated for statistical significance with parametric ANOVA followed by *post-hoc* Tukey multiple comparisons test.

FIGURES

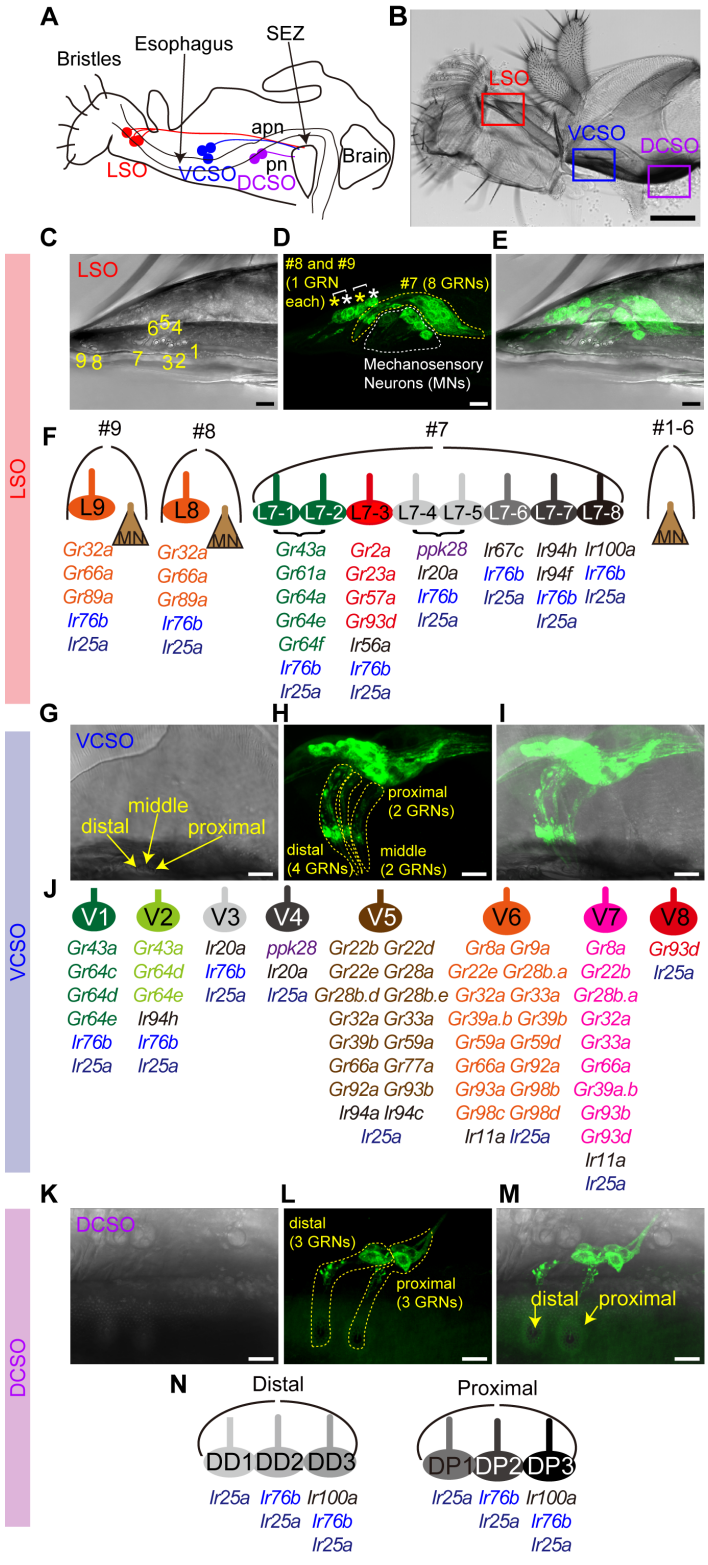
A
Bristles
Esophagus
SEZ
apn
pn
Brain
LSO
VCSO
DCSO
B
LSO
VCSO
DCSO
C
LSO
6 5 4
9 8 7 3 2 1
D
#8 and #9 (1 GRN each)
#7 (8 GRNs)
Mechanosensory Neurons (MNs)
E
F
#9
#8
#7
#1-6
L9
L8
L7-1 L7-2 L7-3 L7-4 L7-5 L7-6 L7-7 L7-8
MN
Gr32a Gr66a Gr89a Ir76b Ir25a
Gr32a Gr66a Gr89a Ir76b Ir25a
Gr43a Gr61a Gr64a Gr64e Gr64f Ir76b Ir25a
Gr2a Gr23a Gr57a Gr93d Ir56a Ir76b Ir25a
ppk28 Ir20a Ir76b Ir25a
Ir67c Ir76b Ir25a
Ir94h Ir94f Ir76b Ir25a
Ir100a Ir76b Ir25a
G
VCSO
middle
distal
proximal
H
proximal (2 GRNs)
distal (4 GRNs)
middle (2 GRNs)
I
J
V1 V2 V3 V4 V5 V6 V7 V8
Gr43a Gr64c Gr64d Gr64e Ir76b Ir25a
Gr43a Gr64d Gr64e Ir94h Ir76b Ir25a
Ir20a Ir76b Ir25a
ppk28 Ir20a Ir25a
Gr22b Gr22d Gr22e Gr28a Gr28b.d Gr28b.e Gr32a Gr33a Gr39b Gr59a Gr66a Gr77a Gr92a Gr93b Ir94a Ir94c Ir25a
Gr8a Gr9a Gr22e Gr28b.a Gr32a Gr33a Gr39a.b Gr39b Gr59a Gr59d Gr66a Gr92a Gr93a Gr98b Gr98c Gr98d Ir11a Ir25a
Gr8a Gr22b Gr28b.a Gr32a Gr33a Gr66a Gr39a.b Gr93b Gr93d Ir11a Ir25a
Gr93d Ir25a
K
DCSO
L
distal (3 GRNs)
proximal (3 GRNs)
M
distal
proximal
N
Distal
Proximal
DD1 DD2 DD3
DP1 DP2 DP3
Ir25a Ir76b Ir100a Ir25a Ir76b Ir25a
Ir25a Ir76b Ir100a Ir25a Ir76b Ir25a

Figure 2.1. Receptor-to-neuron maps of three pharyngeal taste organs. Schematic (**A**) and bright field image of proboscis (**B**) and three pharyngeal taste organs in wild type flies. Taste neurons from the LSO and VCSO project to the subesophageal zone (SEZ) via the accessory pharyngeal nerve (apn); DCSO neurons project via the pharyngeal nerve (pn). Scale bar: 100 μm (**C-E**) *MJ94-GAL4* driven *UAS-mCD8-GFP* labeled neurons in LSO. Numbers in (**C**) indicate the nine LSO sensilla with a linear organization. In (**D**) white dotted line and asterisks indicate mechanosensory neurons; yellow dotted line and asterisks indicate gustatory receptor neurons (GRNs). Scale bar: 10 μm. (**F**) Schematic summary of a receptor-to-neuron map of the LSO as defined by reporter gene expression. MN, Mechanosensory neurons. (**G-I**) *Ir25a-GAL4* driven *UAS-mCD8-GFP* labeled neurons in the VCSO. Yellow arrows mark three VCSO chemosensory sensilla with non-linear organization, which precluded sensillar assignment of individual neurons in the following mapping analysis. Yellow dotted lines delineate groups of GFP labeled neurons in each sensillum. Note that these representative images are the same as shown in **Figure 2.3A**. Scale bar: 10 μm. (**J**) Schematic summary of a receptor-to-neuron map of the VCSO as defined by reporter gene expression. (**K-M**) *MJ94-GAL4* driven *UAS-mCD8-GFP* labeled neurons in the DCSO. Yellow arrows mark two DCSO chemosensory sensilla. Yellow dotted lines delineate groups of GFP labeled neurons in each sensillum. Scale bar: 10 μm. (**N**) Schematic summary of a receptor-to-neuron map of the DCSO as defined by reporter gene expression.

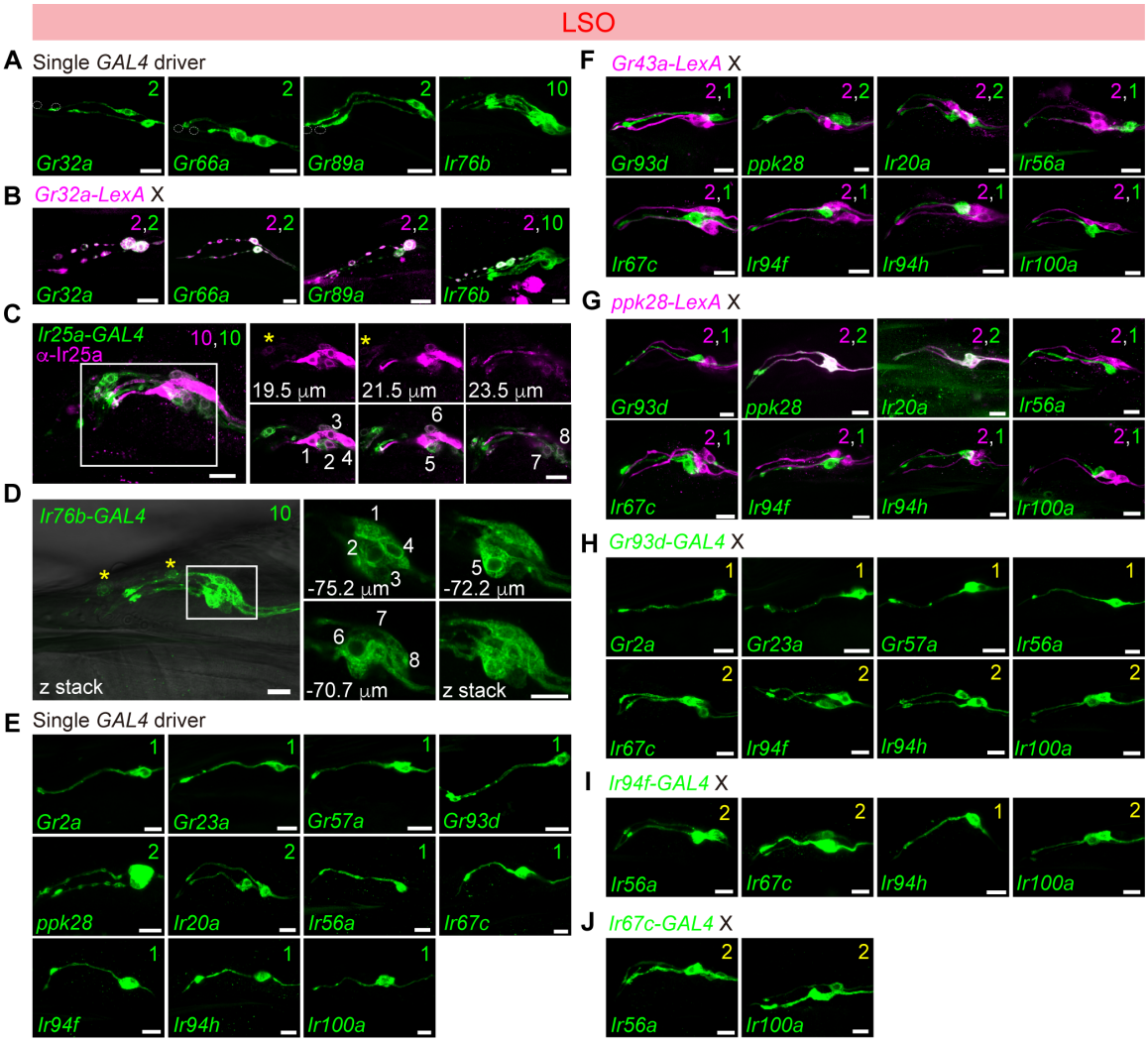

Figure 2.2. *Chemoreceptor-GAL4/LexA* reporter mapping in the labral sense organ (LSO). Expression of *Gr-GAL4* and *Ir-GAL4* lines in the LSO, tested with *UAS-mCD8-GFP* alone (green) (**A, D, E**); co-stained with anti-Ir25a antibody (magenta) (**C**); tested in combination with *LexAop2-mCherry-HA* (magenta) in co-labeling experiments with *Gr32a-LexA* (**B**), *Gr43a-LexA* (**F**), *ppk28-LexA* (**G**); and in double-driver experiments with indicated *GAL4* driver (**H–I**). Numbers in panels in (**C**) and (**D**) are used to label different cells visualized in different optical planes; positions along the *z*-axis are

indicated in μm for the extracted slices. See also **Supplemental movie 1 and 2**. Numbers in top right corners indicate total numbers of green and magenta cells labeled by corresponding *GAL4/LexA* drivers. Numbers in yellow in top right corners in panels (**H**), (**I**) and (**J**) indicate total numbers of GFP^+ cells observed with double *GAL4* driver analysis. Scale bar: 10 μm. All panels show compressed *z*-stacks, with the exception of those labeled with μm in (**C**) and (**D**), which represent single optical slices.

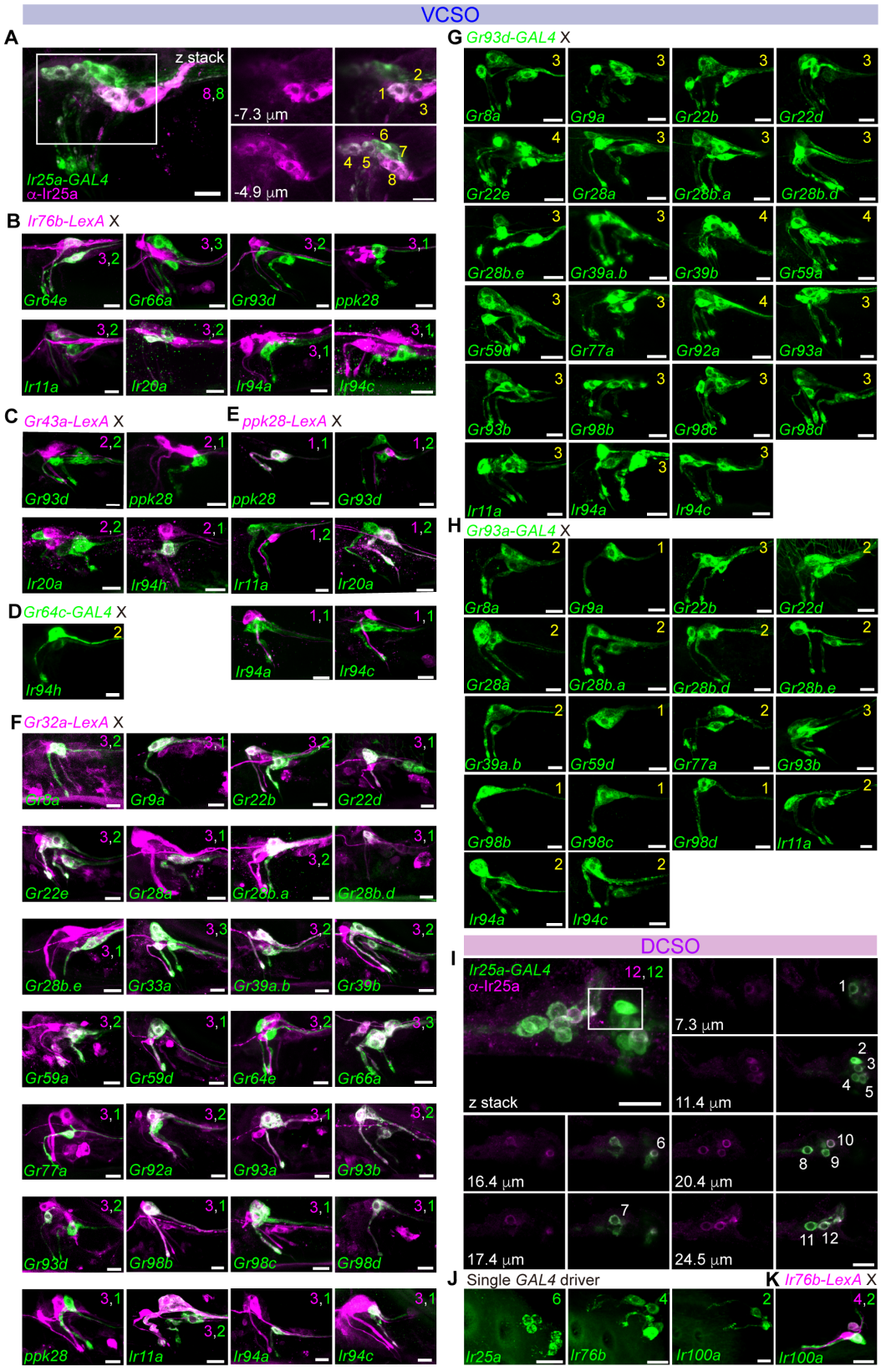
VCSO
A
z stack
8,8
-7.3 μm
-4.9 μm
Ir25a-GAL4
α-Ir25a
B Ir76b-LexA X
Gr64e
Gr66a
Gr93d
ppk28
Ir11a
Ir20a
Ir94a
Ir94c
C Gr43a-LexA X
Gr93d
ppk28
Ir20a
Ir94h
Ir11a
D Gr64c-GAL4 X
Ir94h
E ppk28-LexA X
Ir94a
Ir94c
F Gr32a-LexA X
Gr8a
Gr9a
Gr22b
Gr22d
Gr22e
Gr28a
Gr28b.a
Gr28b.d
Gr28b.e
Gr33a
Gr39a.b
Gr39b
Gr59a
Gr59d
Gr64e
Gr66a
Gr77a
Gr92a
Gr93a
Gr93b
Gr93d
Gr98b
Gr98c
Gr98d
ppk28
Ir11a
Ir94a
Ir94c
G Gr93d-GAL4 X
Gr8a
Gr9a
Gr22b
Gr22d
Gr22e
Gr28a
Gr28b.a
Gr28b.d
Gr28b.e
Gr39a.b
Gr39b
Gr59a
Gr59d
Gr77a
Gr92a
Gr93a
Gr93b
Gr98b
Gr98c
Gr98d
Ir11a
Ir94a
Ir94c
H Gr93a-GAL4 X
Gr8a
Gr9a
Gr22b
Gr22d
Gr28a
Gr28b.a
Gr28b.d
Gr28b.e
Gr39a.b
Gr59d
Gr77a
Gr93b
Gr98b
Gr98c
Gr98d
Ir11a
Ir94a
Ir94c
DCSO
I Ir25a-GAL4
α-Ir25a
12,12
z stack
7.3 μm
11.4 μm
16.4 μm
20.4 μm
17.4 μm
24.5 μm
J Single GAL4 driver
Ir25a
Ir76b
Ir100a
K Ir76b-LexA X
Ir100a

Figure 2.3. *Chemoreceptor-GAL4/LexA* reporter mapping in ventral and dorsal cibarial sense organs (VCSO/DCSO). (**A–H**) GFP expression (green) driven by indicated *Gr-GAL4* and *Ir-GAL4* lines in the VCSO co-stained with anti-Ir25a antibody (magenta) (**A**); tested in combination with *LexAop2-mCherry-HA* (magenta) in co-labeling experiments with *Ir76b-LexA* (**B**), *Gr43a-LexA* (**C**), *ppk28-LexA* (**E**), and *Gr32a-LexA* (**F**); and in double-driver experiments with indicated *GAL4* driver (**D, G, H**). Numbers in panels in (**A**) are used to label different cells visualized in different optical planes; positions along the *z*-axis are indicated in μm for the extracted slices. See also **Supplemental movie 3**. Numbers in top right corners indicate total numbers of green or magenta cells labeled with corresponding *GAL4/LexA* reporters. Numbers in yellow in the top right corners in panels (**D**), (**G**) and (**H**) indicate total numbers of GFP^+ cells observed with double *GAL4* driver analysis. **(I)** GFP expression (green) driven by *Ir25-GAL4* in the DCSO co-stained with anti-Ir25a antibody (magenta). Numbers in panels are used to label different cells visualized in different optical planes; positions along the *z*-axis are indicated in μm for the extracted slices. See also **Supplemental movie 4.** Scale bar: 10 μm. (**J-K**) GFP expression (green) driven by indicated *Ir-GAL4* lines in the DCSO **(J)** or tested in combination with *LexAop2-mCherry-HA* (magenta) in co-labeling experiments with *Ir76b-LexA* (**K**). Numbers in the top right corners indicate total numbers of green and magenta cells labeled by corresponding *GAL4/LexA* reporters. See also **Figure 2.8**. All panels show compressed *z*-stacks, with the exception of those labeled with μm in (**A** and **I**), which represent single optical slices. Scale bar: 10 μm.

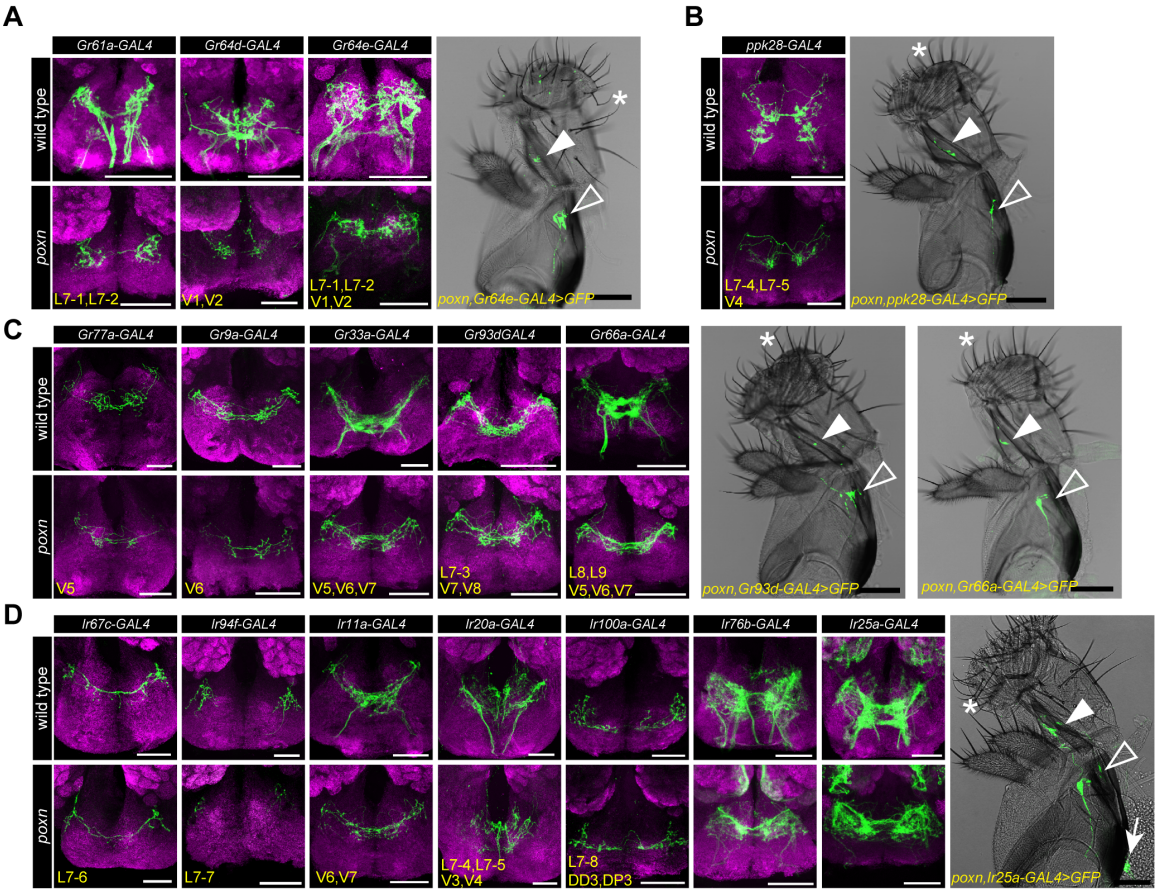

Figure 2.4. Axonal projections of different classes of pharyngeal GRNs in the subesophageal zone (SEZ). (**A-D**) Images of the SEZ showing axonal termini (green) labeled by indicated *Gr*- or *Ir-GAL4* drivers in wild type (w^{1118}, top) and *poxn* ($poxn^{\Delta M22\text{-}B5}/poxn^{70}$, bottom) flies. Four main classes of pharyngeal neuronal projections are presented: sweet pharyngeal GRNs (**A**), putative water pharyngeal GRNs (**B**), putative bitter pharyngeal GRNs (**C**), and *Ir-GAL4* expressing pharyngeal GRNs (**D**). Bright field images of the proboscis show GFP cells (green) labeled by indicated *GAL4* driver in the LSO (closed arrowhead), VCSO (open arrowhead) and DCSO (arrow) in *poxn* mutants. Asterisks point to representative long, bent mechanosensory bristles, which are present in place of external taste hairs in *poxn* mutants. Scale bar: 100 μm. Neuropil is stained with

anti-nc82 (magenta). Subsets of pharyngeal GRNs labeled by *GAL4* drivers named in bottom left corners. Also see **Figure 2.1F, J, N** for nomenclature. Note the presence of a small subset of taste peg projections labeled by *Gr64e-/Ir76b-/Ir25a-GAL4* in the SEZ, and *Ir76b-/Ir25a-GAL4* labeled olfactory projections to antennal lobes in *poxn* mutants.

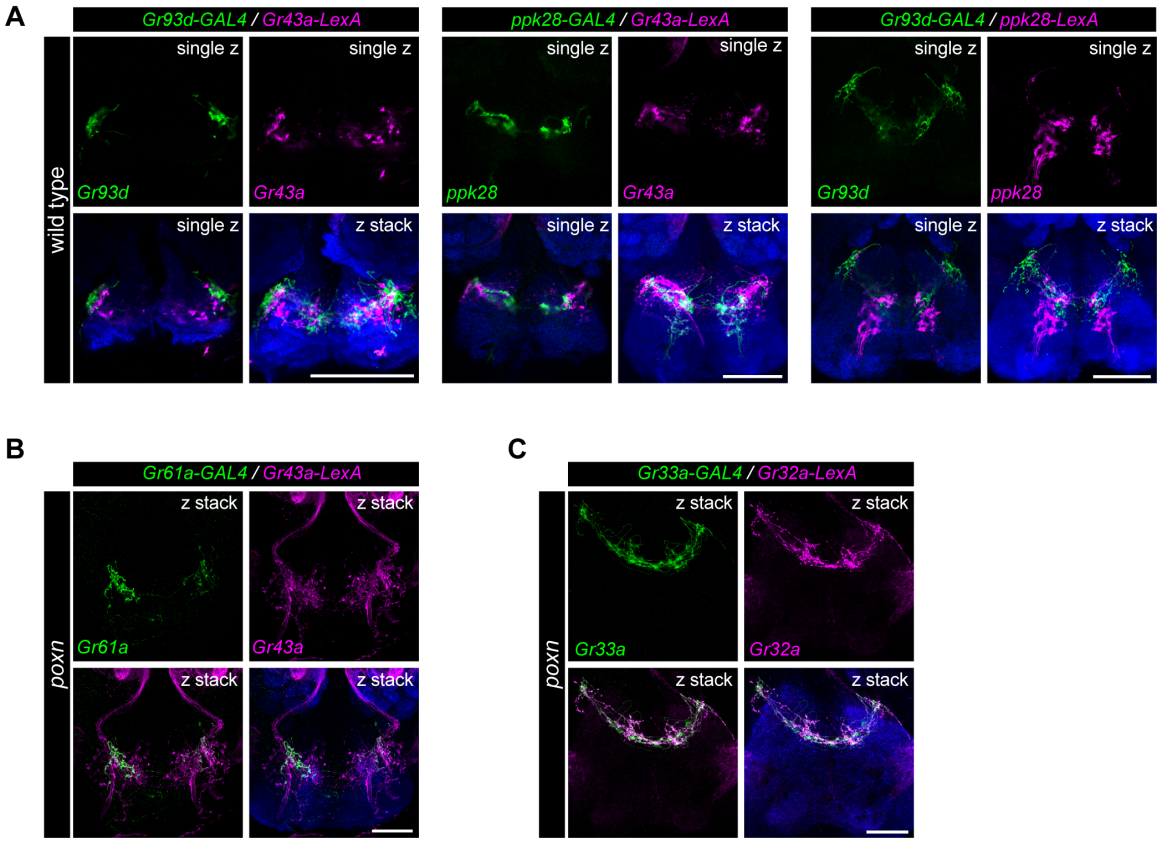

Figure 2.5. Pharyngeal neurons of different categories or location show distinct patterns of axonal projections in the subesophageal zone (SEZ).

(**A**) Axonal projections of pharyngeal GRNs labeled by different *GAL4/LexA* drivers in the SEZ in wild type (w^{1118}) flies. Annotations in top right corners of each image indicate a single optical section (single *z*) to examine reporter co-localization, or compressed *z*-stacks (*z* stack) for comparison. Neuropil is stained with anti-nc82 (blue). In all panels, scale bar: 50 μm. (**B**) Axonal projections labeled by *Gr61a-GAL4* (green) and *Gr43a-LexA* (magenta) in the SEZ in *poxn* ($poxn^{\Delta M22\text{-}B5}/poxn^{70}$) flies. Note the presence of intact olfactory projections to antennal lobes through labial nerves labeled by *Gr43a-LexA* in *poxn* mutants. Neuropil is stained with anti-nc82 (blue). scale bar: 50 μm. (**C**) Axonal

projections labeled by *Gr33a-GAL4* (green) and *Gr32a-LexA* (magenta) in the SEZ in *poxn* (*poxn*$^{\Delta M22\text{-}B5}$/*poxn*^{70}) flies. Neuropil is stained with anti-nc82 (blue). scale bar: 50 μm.

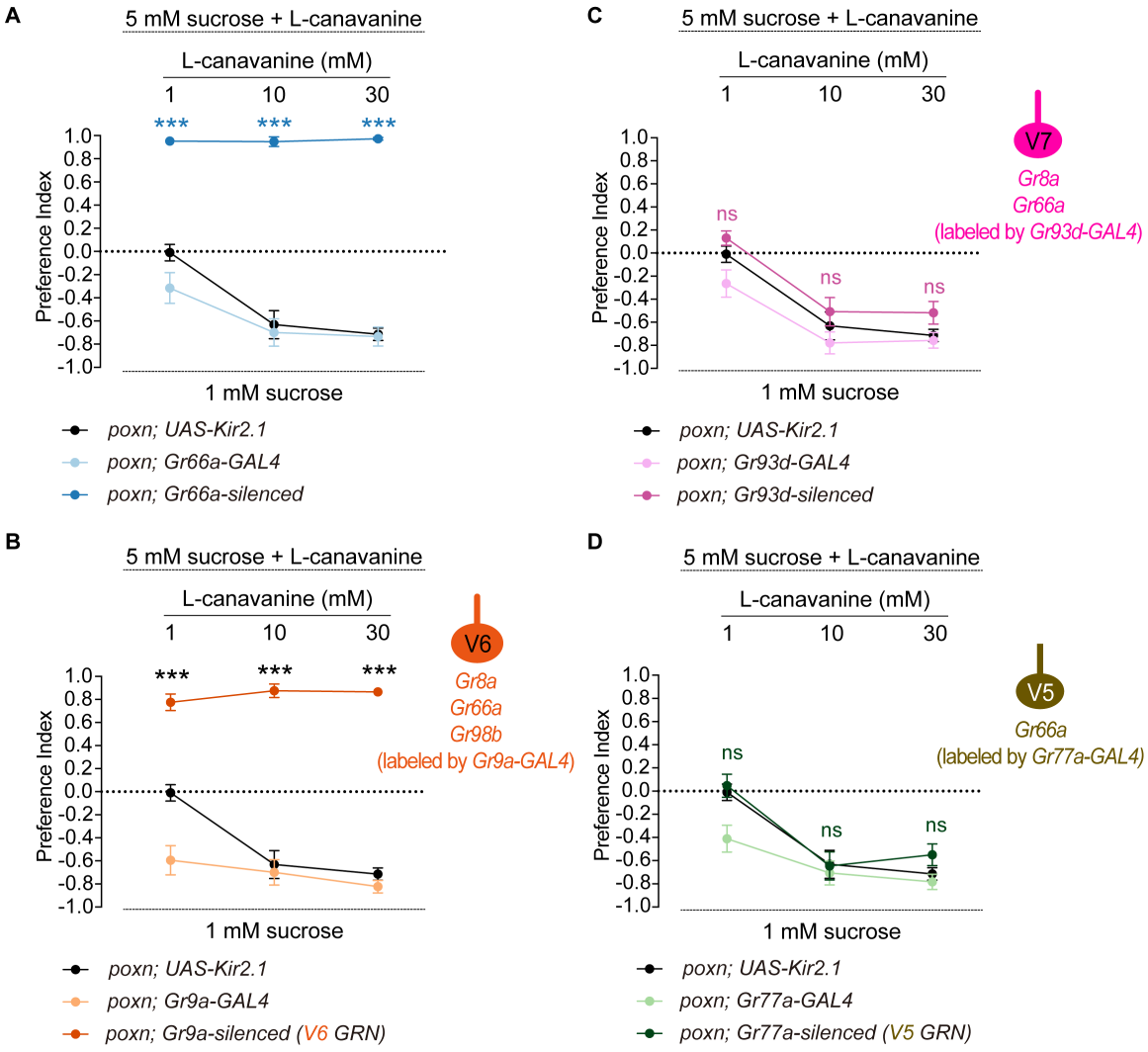

Figure 2.6. Genetic silencing experiments support receptor-to-neuron maps. Mean preference index values from binary choice experiments with sucrose tested against a mixture of sucrose and L-canavanine at indicated concentrations. All genetics manipulations with *Gr66a-GAL4* **(A)**, *Gr9a-GAL4* **(B)**, *Gr93d-GAL4* **(C)**, and *Gr77a-GAL4* **(D)** were performed in a *poxn* mutant background ($poxn^{\Delta M22\text{-}B5}/poxn^{70}$). Schematics of identified VCSO neurons derived from **Figure 2.3** indicating expression of *Gr8a-/Gr66a-/Gr98b-GAL4* are shown on the right of **Figure 2.6B,C,D**. *n*=10-30. Error bars =

SEM. ***$P < 0.0001$ versus *UAS* control, two-way ANOVA with *post-hoc* Tukey test. ns, not significant.

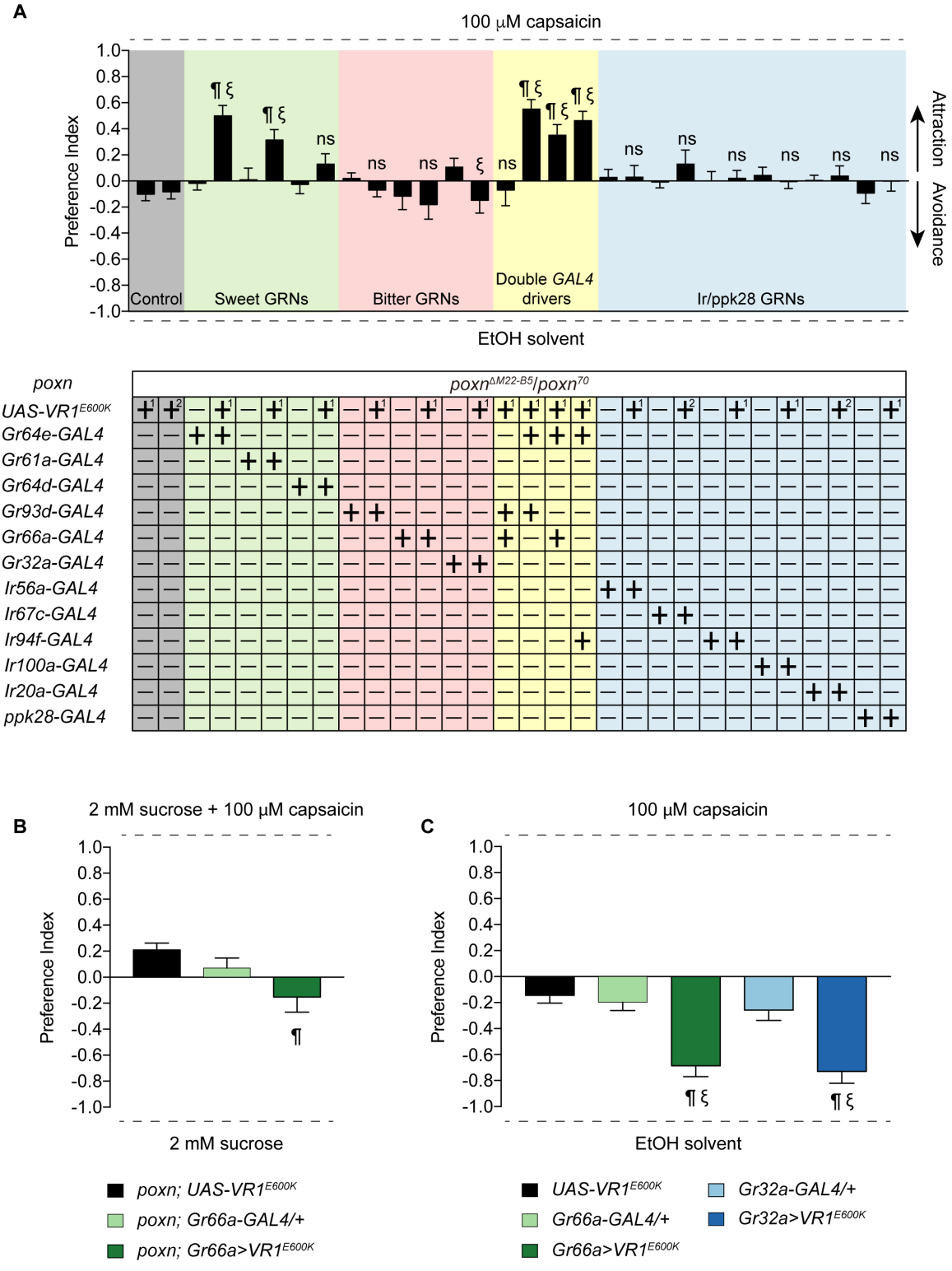
A
100 μM capsaicin
Preference Index
Attraction
Avoidance
Control
Sweet GRNs
Bitter GRNs
Double GAL4 drivers
Ir/ppk28 GRNs
EtOH solvent
poxn
poxn^ΔM22-B5/poxn^70
UAS-VR1^E600K
Gr64e-GAL4
Gr61a-GAL4
Gr64d-GAL4
Gr93d-GAL4
Gr66a-GAL4
Gr32a-GAL4
Ir56a-GAL4
Ir67c-GAL4
Ir94f-GAL4
Ir100a-GAL4
Ir20a-GAL4
ppk28-GAL4
B
2 mM sucrose + 100 μM capsaicin
Preference Index
2 mM sucrose
poxn; UAS-VR1^E600K
poxn; Gr66a-GAL4/+
poxn; Gr66a>VR1^E600K
C
100 μM capsaicin
Preference Index
EtOH solvent
UAS-VR1^E600K
Gr66a-GAL4/+
Gr66a>VR1^E600K
Gr32a-GAL4/+
Gr32a>VR1^E600K

Figure 2.7. A systematically inducible activation of different classes of pharyngeal neurons. (A) Mean preference index values from binary choice experiments with capsaicin tested against ethanol solvent. Genetic manipulations were performed in *poxn* mutant ($poxn^{\Delta M22\text{-}B5}/poxn^{70}$). Two different *UAS-VR1*^{E600K} controls are shown; [1] is a recombinant *of UAS-VR1*^{E600K} with the $poxn^{\Delta M22\text{-}B5}$ allele; [2] is a recombinant with the $poxn^{70}$ allele. *n*=19-30. Error bars indicate SEM. ¶ indicates significant difference from the corresponding *UAS* control; ξ indicates significant difference from the corresponding *GAL4* control (for double driver experiments, ξ indicates significant difference from both *GAL4* controls); *P*<0.05, one-way ANOVA with Tukey test. ns, not significant.
(B) Mean preference index values from binary choice experiments with capsaicin-sucrose mixture tested against sucrose alone. Genetic manipulations were performed in *poxn* mutant ($poxn^{\Delta M22\text{-}B5}/poxn^{70}$). *n*=28-32. Error bars indicate SEM. ¶ indicates significant difference from the corresponding *UAS* control; *P*<0.05, one-way ANOVA with Tukey test. **(C)** Results of binary choice feeding assays performed using flies expressing *VR1*^{E600K} under the control of the indicated *GAL4* drivers in a wild type background with only one $poxn^{\Delta M22\text{-}B5}$ allele. Tastants used were capsaicin and ethanol solvent. *n*=10-20. Error bars = SEM. ¶ indicates significant difference from the *UAS* control; ξ indicates significant difference from the corresponding *GAL4* control; *P*<0.05, one-way ANOVA with Tukey test. ns, not significant.

SUPPLEMENTAL FIGURE

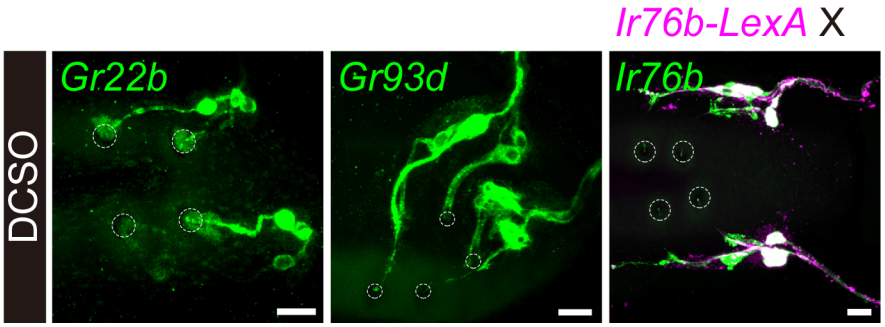

Figure 2.8 Occasional expression of *Gr22b-/Gr93d-GAL4* drivers in pharyngeal neurons of DCSO. Occasional expression in the DCSO of indicated *GAL4* drivers tested with *UAS-mCD8-GFP* (green). Overlap of *Ir76b-GAL4* (green) and *Ir76b-LexA* (magenta) in the DCSO. Scale bar: 10 μm.

TABLES

Table 2.1 Summary of *Gr-GAL4* lines showing pharyngeal expression.

	***Gr-GAL4* labeling of pharyngeal axonal projections (Kwon et al., 2014)**	***Gr-GAL4* labeling of pharyngeal GRNs (this study)**
Gr2a	+	+
Gr8a	+	+
Gr9a	+	+
Gr22b	+	+
Gr22c	+	no expression[a]
Gr22d	+	+
Gr22e	+	+
Gr23a	+	+
Gr28a	+	+
Gr28b.a	+	+
Gr28b.c	+	no expression[a]
Gr28b.d	+	+
Gr28b.e	+	+
Gr32a	+	+
Gr33a	+	+
Gr39a.a	+	no expression[a]
Gr39a.b	+	+
Gr39a.c	+	no expression[a]
Gr39a.d	+	no expression[a]
Gr39b	+	+
Gr43a	+	+
Gr57a	+	+
Gr58b	+	+
Gr59a	+	+
Gr59d	+	+
Gr61a	+	+
Gr64a	+	+
Gr64c	+	+
Gr64d	+	+
Gr64e	+	+
Gr64f	+	+
Gr66a	+	+

Gr77a	+	+
Gr89a	+	+
Gr92a	+	+
Gr93a	+	+
Gr93b	+	+
Gr93c	+	no expression[a]
Gr93d	+	+
Gr94a	+	no expression[a]
Gr98b	+	+
Gr98c	+	+
Gr98d	+	+

[a]We observed no pharyngeal expression for seven *Gr-GAL4* lines that labeled pharyngeal projections in the SEZ previously. The loss of GAL4 expression may be due to the long-term maintenance of the stocks.

Table 2.2. Summary of *Gr/Ir-GAL4* double driver expression in V5-V7 neurons of the VCSO.

	# GFP neurons	**# GFP neurons in combination with *Gr93d-GAL4***	***# GFP neurons in combination with Gr93a-GAL4***
Gr8a	2	3	2
Gr9a	1	3	1
Gr22b	2	3	3
Gr22d	1	3	2
Gr22e	2	4	-
Gr28a	1	3	2
Gr28b.a	2	3	2
Gr28b.d	1	3	2
Gr28b.e	1	3	2
Gr32a	3	-	-
Gr33a	3	-	-
Gr39a.b	2	3	2
Gr39b	2	4	-
Gr59a	2	4	-
Gr59d	1	3	1
Gr66a	3	-	-
Gr77a	1	3	2
Gr92a	2	4	-
Gr93a	1	3	-
Gr93b	2	3	3
Gr93d	2	-	-
Gr98b	1	3	1
Gr98c	1	3	1
Gr98d	1	3	1
Ir11a	2	3	2
Ir94a	1	3	2
Ir94c	1	3	2

Table 2.3. Complete genotypes of flies used in this study.

Figure	Genotype
2.1B	w^{1118}
2.1C-E	*MJ94-GAL4/+; UAS-mCD8GFP/+; UAS-mCD8GFP/+*
2.1G-I	*Ir25a-GAL4/Cyo; UAS-mCD8GFP/UAS-mCD8GFP*
2.1K-M	*Ir25a-GAL4/Cyo; UAS-mCD8GFP/UAS-mCD8GFP*
2.2A	(from left to right)
	UAS-mCD8GFP/UAS-mCD8GFP; Gr32a-GAL4/Gr32a-GAL4
	UAS-mCD8GFP/UAS-mCD8GFP; Gr66a-GAL4/TM3
	Gr89a-GAL4/Cyo; UAS-mCD8GFP/UAS-mCD8GFP
	Ir76b-GAL4/Ir76b-GAL4; UAS-mCD8GFP/UAS-mCD8GFP
2.2B	(from left to right)
	LexAop2-mCherry-HA/UAS-mCD8GFP; Gr32a-LexA/Gr32a-GAL4
	LexAop2-mCherry-HA/UAS-mCD8GFP; Gr32a-LexA/Gr66a-GAL4
	LexAop2-mCherry-HA/Gr89a-GAL4; Gr32a-LexA/UAS-mCD8GFP
	LexAop2-mCherry-HA/Ir76b-GAL4; Gr32a-LexA/UAS-mCD8GFP
2.2C	*Ir25a-GAL4/Cyo; UAS-mCD8GFP/UAS-mCD8GFP*
2.2D	*Ir76b-GAL4/Ir76b-GAL4; UAS-mCD8GFP/UAS-mCD8GFP*
2.2E	(from left to right)
2.2F	(from left to right)
	LexAop2-mCherry-HA/UAS-mCD8GFP; Gr43a-LexA/Gr93d-GAL4
	LexAop2-mCherry-HA/UAS-mCD8GFP; Gr43a-LexA/ppk28-GAL4
	LexAop2-mCherry-HA/Ir20a-GAL4; Gr43a-LexA/UAS-mCD8GFP
	LexAop2-mCherry-HA/UAS-mCD8GFP; Gr43a-LexA/Ir56a-GAL4
	LexAop2-mCherry-HA/Ir67c-GAL4; Gr43a-LexA/UAS-mCD8GFP
	LexAop2-mCherry-HA/UAS-mCD8GFP; Gr43a-LexA/Ir94f-GAL4
	LexAop2-mCherry-HA/UAS-mCD8GFP; Gr43a-LexA/Ir94h-GAL4

	LexAop2-mCherry-HA/UAS-mCD8GFP; Gr43a-LexA/Ir100a-GAL4
2.2G	(from left to right)
	LexAop2-mCherry-HA/UAS-mCD8GFP; ppk28-LexA/Gr93d-GAL4
	LexAop2-mCherry-HA/UAS-mCD8GFP; ppk28-LexA/ppk28-GAL4
	LexAop2-mCherry-HA/Ir20a-GAL4; ppk28-LexA/UAS-mCD8GFP
	LexAop2-mCherry-HA/UAS-mCD8GFP; ppk28-LexA/Ir56a-GAL4
	LexAop2-mCherry-HA/Ir67c-GAL4; ppk28-LexA/UAS-mCD8GFP
	LexAop2-mCherry-HA/UAS-mCD8GFP; ppk28-LexA/Ir94f-GAL4
	LexAop2-mCherry-HA/UAS-mCD8GFP; ppk28-LexA/Ir94h-GAL4
	LexAop2-mCherry-HA/UAS-mCD8GFP; ppk28-LexA/Ir100a-GAL4
2.2H	(from left to right)
	Gr2a-GAL4/UAS-mCD8GFP; Gr93d-GAL4/UAS-mCD8GFP
	UAS-mCD8GFP/UAS-mCD8GFP; Gr93d-GAL4/Gr23a-GAL4
	UAS-mCD8GFP/UAS-mCD8GFP; Gr93d-GAL4/Gr57a-GAL4
	UAS-mCD8GFP/UAS-mCD8GFP; Gr93d-GAL4/Ir56a-GAL4
	Ir67c-GAL4/UAS-mCD8GFP; Gr93d-GAL4/UAS-mCD8GFP
	UAS-mCD8GFP/UAS-mCD8GFP; Gr93d-GAL4/Ir94f-GAL4
	UAS-mCD8GFP/UAS-mCD8GFP; Gr93d-GAL4/Ir94h-GAL4
	UAS-mCD8GFP/UAS-mCD8GFP; Gr93d-GAL4/Ir100a-GAL4
2.2I	(from left to right)
	UAS-mCD8GFP/UAS-mCD8GFP; Ir94f-GAL4/Ir56a-GAL4
	Ir67c-GAL4/UAS-mCD8GFP; Ir94f-GAL4/UAS-mCD8GFP
	UAS-mCD8GFP/UAS-mCD8GFP; Ir94f-GAL4/Ir94h-GAL4
	UAS-mCD8GFP/UAS-mCD8GFP; Ir94f-GAL4/Ir100a-GAL4

2.2J	(from left to right)
	UAS-mCD8GFP/Ir67c-GAL4; Ir56a-GAL4/UAS-mCD8GFP
	UAS-mCD8GFP/Ir67c-GAL4; Ir100a-GAL4/UAS-mCD8GFP
2.3A	*Ir25a-GAL4/Cyo; UAS-mCD8GFP/UAS-mCD8GFP*
2.3B	(from left to right)
	Ir76b-LexA/UAS-mCD8GFP; LexAop2-mCherry-HA/Gr64e-GAL4
	Ir76b-LexA/UAS-mCD8GFP; LexAop2-mCherry-HA/Gr66a-GAL4
	Ir76b-LexA/UAS-mCD8GFP; LexAop2-mCherry-HA/Gr93d-GAL4
	Ir76b-LexA/UAS-mCD8GFP; LexAop2-mCherry-HA/ppk28-GAL4
	Ir76b-LexA/UAS-mCD8GFP; LexAop2-mCherry-HA/Ir11a-GAL4
	Ir76b-LexA/Ir20a-GAL4; LexAop2-mCherry-HA/UAS-mCD8GFP
	Ir76b-LexA/UAS-mCD8GFP; LexAop2-mCherry-HA/Ir94a-GAL4
	Ir76b-LexA/Ir94c-GAL4; LexAop2-mCherry-HA/UAS-mCD8GFP
2.3C	(from left to right)
	LexAop2-mCherry-HA/UAS-mCD8GFP; Gr43a-LexA/Gr93d-GAL4
	LexAop2-mCherry-HA/UAS-mCD8GFP; Gr43a-LexA/ppk28-GAL4
	LexAop2-mCherry-HA/Ir20a-GAL4; Gr43a-LexA/UAS-mCD8GFP
	LexAop2-mCherry-HA/UAS-mCD8GFP; Gr43a-LexA/Ir94h-GAL4
2.3D	*UAS-mCD8GFP/UAS-mCD8GFP; Gr64c-GAL4/Ir94h-GAL4*
2.3E	(from left to right)
	LexAop2-mCherry-HA/UAS-mCD8GFP; ppk28-LexA/ppk28-GAL4
	LexAop2-mCherry-HA/UAS-mCD8GFP; ppk28-LexA/Gr93d-GAL4
	LexAop2-mCherry-HA/UAS-mCD8GFP; ppk28-LexA/Ir11a-GAL4
	LexAop2-mCherry-HA/Ir20a-GAL4; ppk28-LexA/UAS-mCD8GFP

	LexAop2-mCherry-HA/UAS-mCD8GFP; ppk28-LexA/Ir94a-GAL4
	LexAop2-mCherry-HA/Ir94c-GAL4; ppk28-LexA/UAS-mCD8GFP
2.3F	(from left to right)
	LexAop2-mCherry-HA/Gr8a-GAL4; Gr32a-LexA/UAS-mCD8GFP
	LexAop2-mCherry-HA/UAS-mCD8GFP; Gr32a-LexA/Gr9a-GAL4
	LexAop2-mCherry-HA/UAS-mCD8GFP; Gr32a-LexA/Gr22b-GAL4
	LexAop2-mCherry-HA/UAS-mCD8GFP; Gr32a-LexA/Gr22d-GAL4
	LexAop2-mCherry-HA/UAS-mCD8GFP; Gr32a-LexA/Gr22e-GAL4
	LexAop2-mCherry-HA/Gr28a-GAL4; Gr32a-LexA/UAS-mCD8GFP
	LexAop2-mCherry-HA/Gr28b.a-GAL4; Gr32a-LexA/UAS-mCD8GFP
	LexAop2-mCherry-HA/Gr28b.d-GAL4; Gr32a-LexA/UAS-mCD8GFP
	LexAop2-mCherry-HA/Gr28b.e-GAL4; Gr32a-LexA/UAS-mCD8GFP
	LexAop2-mCherry-HA/UAS-mCD8GFP; Gr32a-LexA/Gr33a-GAL4
	LexAop2-mCherry-HA/UAS-mCD8GFP; Gr32a-LexA/Gr39a.b-GAL4
	LexAop2-mCherry-HA/UAS-mCD8GFP; Gr32a-LexA/Gr39b-GAL4
	LexAop2-mCherry-HA/UAS-mCD8GFP; Gr32a-LexA/Gr59a-GAL4
	LexAop2-mCherry-HA/Gr59d-GAL4; Gr32a-LexA/UAS-mCD8GFP
	LexAop2-mCherry-HA/UAS-mCD8GFP; Gr32a-LexA/Gr64e-GAL4
	LexAop2-mCherry-HA/UAS-mCD8GFP; Gr32a-LexA/Gr66a-GAL4
	LexAop2-mCherry-HA/UAS-mCD8GFP; Gr32a-LexA/Gr77a-GAL4
	LexAop2-mCherry-HA/Gr92a-GAL4; Gr32a-LexA/UAS-mCD8GFP
	LexAop2-mCherry-HA/UAS-mCD8GFP; Gr32a-LexA/Gr93a-GAL4

	LexAop2-mCherry-HA/UAS-mCD8GFP; Gr32a-LexA/Gr93b-GAL4
	LexAop2-mCherry-HA/UAS-mCD8GFP; Gr32a-LexA/Gr93d-GAL4
	LexAop2-mCherry-HA/UAS-mCD8GFP; Gr32a-LexA/Gr98b-GAL4
	LexAop2-mCherry-HA/Gr98c-GAL4; Gr32a-LexA/UAS-mCD8GFP
	LexAop2-mCherry-HA/Gr98d-GAL4; Gr32a-LexA/UAS-mCD8GFP
2.3G	(from left to right)
	UAS-mCD8GFP/Gr8a-GAL4; Gr93d-GAL4/UAS-mCD8GFP
	UAS-mCD8GFP/UAS-mCD8GFP; Gr93d-GAL4/Gr9a-GAL4
	UAS-mCD8GFP/UAS-mCD8GFP; Gr93d-GAL4/Gr22b-GAL4
	UAS-mCD8GFP/UAS-mCD8GFP; Gr93d-GAL4/Gr22d-GAL4
	UAS-mCD8GFP/UAS-mCD8GFP; Gr93d-GAL4/Gr22e-GAL4
	UAS-mCD8GFP/Gr28a-GAL4; Gr93d-GAL4/UAS-mCD8GFP
	UAS-mCD8GFP/Gr28b.a-GAL4; Gr93d-GAL4/UAS-mCD8GFP
	UAS-mCD8GFP/Gr28b.d-GAL4; Gr93d-GAL4/UAS-mCD8GFP
	UAS-mCD8GFP/Gr28b.e-GAL4; Gr93d-GAL4/UAS-mCD8GFP
	UAS-mCD8GFP/UAS-mCD8GFP; Gr93d-GAL4/Gr39a.b-GAL4
	UAS-mCD8GFP/UAS-mCD8GFP; Gr93d-GAL4/Gr39b-GAL4
	UAS-mCD8GFP/UAS-mCD8GFP; Gr93d-GAL4/Gr59a-GAL4
	UAS-mCD8GFP/Gr59d-GAL4; Gr93d-GAL4/UAS-mCD8GFP
	UAS-mCD8GFP/UAS-mCD8GFP; Gr93d-GAL4/Gr77a-GAL4
	UAS-mCD8GFP/Gr92a-GAL4; Gr93d-GAL4/UAS-mCD8GFP
	UAS-mCD8GFP/UAS-mCD8GFP; Gr93d-GAL4/Gr93a-GAL4

	UAS-mCD8GFP/UAS-mCD8GFP; Gr93d-GAL4/Gr93b-GAL4
	UAS-mCD8GFP/UAS-mCD8GFP; Gr93d-GAL4/Gr98b-GAL4
	UAS-mCD8GFP/Gr98c-GAL4; Gr93d-GAL4/UAS-mCD8GFP
	UAS-mCD8GFP/Gr98d-GAL4; Gr93d-GAL4/UAS-mCD8GFP
	UAS-mCD8GFP/UAS-mCD8GFP; Gr93d-GAL4/Ir11a-GAL4
	UAS-mCD8GFP/UAS-mCD8GFP; Gr93d-GAL4/Ir94a-GAL4
	Ir94c-GAL4/UAS-mCD8GFP; Gr93d-GAL4/UAS-mCD8GFP
2.3H	(from left to right)
	UAS-mCD8GFP/Gr8a-GAL4; Gr93a-GAL4/UAS-mCD8GFP
	UAS-mCD8GFP/UAS-mCD8GFP; Gr93a-GAL4/Gr9a-GAL4
	UAS-mCD8GFP/UAS-mCD8GFP; Gr93a-GAL4/Gr22b-GAL4
	UAS-mCD8GFP/UAS-mCD8GFP; Gr93a-GAL4/Gr22d-GAL4
	UAS-mCD8GFP/Gr28a-GAL4; Gr93a-GAL4/UAS-mCD8GFP
	UAS-mCD8GFP/Gr28b.a-GAL4; Gr93a-GAL4/UAS-mCD8GFP
	UAS-mCD8GFP/Gr28b.d-GAL4; Gr93a-GAL4/UAS-mCD8GFP
	UAS-mCD8GFP/Gr28b.e-GAL4; Gr93a-GAL4/UAS-mCD8GFP
	UAS-mCD8GFP/UAS-mCD8GFP; Gr93a-GAL4/Gr39a.b-GAL4
	UAS-mCD8GFP/Gr59d-GAL4; Gr93a-GAL4/UAS-mCD8GFP
	UAS-mCD8GFP/UAS-mCD8GFP; Gr93a-GAL4/Gr77a-GAL4
	UAS-mCD8GFP/UAS-mCD8GFP; Gr93a-GAL4/Gr93b-GAL4
	UAS-mCD8GFP/UAS-mCD8GFP; Gr93a-GAL4/Gr98b-GAL4
	UAS-mCD8GFP/Gr98c-GAL4; Gr93a-GAL4/UAS-mCD8GFP

	UAS-mCD8GFP/Gr98d-GAL4; Gr93a-GAL4/UAS-mCD8GFP
	UAS-mCD8GFP/UAS-mCD8GFP; Gr93a-GAL4/Ir11a-GAL4
	UAS-mCD8GFP/UAS-mCD8GFP; Gr93a-GAL4/Ir94a-GAL4
	Ir94c-GAL4/UAS-mCD8GFP; Gr93a-GAL4/UAS-mCD8GFP
2.3I	*Ir25a-GAL4/Cyo; UAS-mCD8GFP/UAS-mCD8GFP*
2.3J	(from left to right)
	Ir25a-GAL4/Cyo; UAS-mCD8GFP/UAS-mCD8GFP
	Ir76b-GAL4/ Ir76b-GAL4; UAS-mCD8GFP/UAS-mCD8GFP
	UAS-mCD8GFP/UAS-mCD8GFP; Ir100a-GAL4/Ir100a-GAL4
2.3K	*Ir76b-LexA/UAS-mCD8GFP; LexAop2-mCherry-HA/Ir100a-GAL4*
2.4A (top)	(from left to right)
	Gr61a-GAL4/ Gr61a -GAL4; UAS-mCD8GFP/UAS-mCD8GFP
	UAS-mCD8GFP/UAS-mCD8GFP; Gr64d-GAL4/Gr64d-GAL4
	Gr64e-GAL4/ Gr64e-GAL4; UAS-mCD8GFP/UAS-mCD8GFP
2.4A (bottom)	(from left to right)
	$poxn^{DM22-B5}$, Gr61a-GAL4/$poxn^{70}$, UAS-mCD8GFP; Dr/TM3
	$poxn^{DM22-B5}$/$poxn^{70}$, UAS-mCD8GFP; Gr64d-GAL4/Dr or TM3
	$poxn^{DM22-B5}$, Gr64e-GAL4/$poxn^{70}$, UAS-mCD8GFP; Dr/TM3
2.4A(proboscis image)	*$poxn^{DM22-B5}$, Gr64e-GAL4/$poxn^{70}$, UAS-mCD8GFP; Dr/TM3*
2.4B (top)	*UAS-mCD8GFP/UAS-mCD8GFP; ppk28-GAL4/ppk28-GAL4*
2.4B (bottom)	*$poxn^{DM22-B5}$/$poxn^{70}$, UAS-mCD8GFP; ppk28-GAL4/Dr or TM3*
2.4B (proboscis image)	*$poxn^{DM22-B5}$/$poxn^{70}$, UAS-mCD8GFP; ppk28-GAL4/Dr or TM3*
2.4C (top)	(from left to right)
	UAS-mCD8GFP/UAS-mCD8GFP; Gr77a-GAL4/Gr77a-GAL4

	UAS-mCD8GFP/UAS-mCD8GFP; Gr9a-GAL4/Gr9a-GAL4
	Gr33a-GAL4/Cyo; UAS-mCD8GFP/UAS-mCD8GFP
	Gr93d-GAL4/Gr93d-GAL4; UAS-mCD8GFP/UAS-mCD8GFP
	UAS-mCD8GFP/UAS-mCD8GFP; Gr66a-GAL4/TM3
2.4C (bottom)	(from left to right)
	$poxn^{DM22-B5}$/$poxn^{70}$, UAS-mCD8GFP; Gr77a-GAL4/Dr or TM3
	$poxn^{DM22-B5}$/$poxn^{70}$, UAS-mCD8GFP; Gr9a-GAL4/Dr or TM3
	$poxn^{DM22-B5}$, Gr33a-GAL4/$poxn^{70}$, UAS-mCD8GFP; Dr/TM3
	$poxn^{DM22-B5}$, Gr93d-GAL4/$poxn^{70}$, UAS-mCD8GFP; Dr/TM3
	$poxn^{DM22-B5}$, Gr66a-GAL4/$poxn^{70}$, UAS-mCD8GFP; Dr/TM3
2.4C (proboscis image)	(from left to right)
	$poxn^{DM22-B5}$, Gr93d-GAL4/$poxn^{70}$, UAS-mCD8GFP; Dr/TM3
	$poxn^{DM22-B5}$, Gr66a-GAL4/$poxn^{70}$, UAS-mCD8GFP; Dr/TM3
2.4D (top)	(from left to right)
	Ir67c-GAL4/Ir67c-GAL4; UAS-mCD8GFP/UAS-mCD8GFP
	UAS-mCD8GFP/UAS-mCD8GFP; Ir94f-GAL4/ Ir94f-GAL4
	UAS-mCD8GFP/UAS-mCD8GFP; Ir11a-GAL4/ Ir11a-GAL4
	Ir20a-GAL4/Cyo; UAS-mCD8GFP/UAS-mCD8GFP
	UAS-mCD8GFP/UAS-mCD8GFP; Ir100a-GAL4/ Ir100a-GAL4
	Ir76b-GAL4/Ir76b-GAL4; UAS-mCD8GFP/UAS-mCD8GFP
	Ir25a-GAL4/Cyo; UAS-mCD8GFP/UAS-mCD8GFP
2.4D (bottom)	(from left to right)
	$poxn^{DM22-B5}$, Ir67c-GAL4/$poxn^{70}$, UAS-mCD8GFP; Dr/TM3
	$poxn^{DM22-B5}$/$poxn^{70}$, UAS-mCD8GFP; Ir94f-GAL4/Dr or TM3
	$poxn^{DM22-B5}$/$poxn^{70}$, UAS-mCD8GFP; Ir11a-GAL4/Dr or TM3
	$poxn^{DM22-B5}$, Ir20a-GAL4/$poxn^{70}$, UAS-mCD8GFP; Dr/TM3
	$poxn^{DM22-B5}$/$poxn^{70}$, UAS-mCD8GFP; Ir100a-GAL4/Dr or TM3
	$poxn^{DM22-B5}$, Ir76b-GAL4/$poxn^{70}$, UAS-mCD8GFP; Dr/TM3
	$poxn^{DM22-B5}$, Ir25a-GAL4/$poxn^{70}$, UAS-mCD8GFP; Dr/TM3

2.4D (proboscis image)	*poxn$^{DM22-B5}$, Ir25a-GAL4/poxn^{70}, UAS-mCD8GFP; Dr/TM3*
2.5A	(from left to right)
	LexAop2-mCherry-HA/UAS-mCD8GFP; Gr43a-LexA/Gr93d-GAL4
	LexAop2-mCherry-HA/UAS-mCD8GFP; Gr43a-LexA/ppk28-GAL4
	LexAop2-mCherry-HA/UAS-mCD8GFP; ppk28-LexA/Gr93d-GAL4
2.5B	*poxn$^{DM22-B5}$, Gr61a-GAL4/poxn^{70}, UAS-mCD8GFP; Gr43a-LexA/LexAop2-mCherry-HA, UAS-mCD8GFP*
2.5C	*poxn$^{DM22-B5}$, Gr33a-GAL4/poxn^{70}, UAS-mCD8GFP; Gr32a-LexA/LexAop2-mCherry-HA, UAS-mCD8GFP*
2.6A	(from top to bottom)
	poxn$^{DM22-B5}$/poxn^{70}; UAS-Kir2.1/+
	poxn$^{DM22-B5}$/poxn^{70}; Gr66a-GAL4/+
	poxn$^{DM22-B5}$/poxn^{70}; Gr66a-GAL4/UAS-Kir2.1
	poxn$^{DM22-B5}$/poxn^{70}; Gr77a-GAL4/+
	poxn$^{DM22-B5}$/poxn^{70}; Gr77a-GAL4/UAS-Kir2.1
	poxn$^{DM22-B5}$/poxn^{70}; Gr9a-GAL4/+
	poxn$^{DM22-B5}$/poxn^{70}; Gr9a-GAL4/UAS-Kir2.1
	poxn$^{DM22-B5}$/poxn^{70}; Gr93d-GAL4/+
	poxn$^{DM22-B5}$/poxn^{70}; Gr93d-GAL4/UAS-Kir2.1
2.6B	(from top to bottom)
	poxn$^{DM22-B5}$/poxn^{70}; UAS-Kir2.1/+
	poxn$^{DM22-B5}$/poxn^{70}; Gr9a-GAL4/+
	poxn$^{DM22-B5}$/poxn^{70}; Gr9a-GAL4/UAS-Kir2.1
2.6C	(from top to bottom)
	poxn$^{DM22-B5}$/poxn^{70}; UAS-Kir2.1/+
	poxn$^{DM22-B5}$/poxn^{70}; Gr93d-GAL4/+
	poxn$^{DM22-B5}$/poxn^{70}; Gr93d-GAL4/UAS-Kir2.1
2.6D	(from top to bottom)
	poxn$^{DM22-B5}$/poxn^{70}; UAS-Kir2.1/+
	poxn$^{DM22-B5}$/poxn^{70}; Gr77a-GAL4/+
	poxn$^{DM22-B5}$/poxn^{70}; Gr77a-GAL4/UAS-Kir2.1
2.4A(proboscis image)	*poxn$^{DM22-B5}$, Gr64e-GAL4/poxn^{70}, UAS-mCD8GFP; Dr/TM3*

2.4B (top)	*UAS-mCD8GFP/UAS-mCD8GFP; ppk28-GAL4/ppk28-GAL4*
2.4B (bottom)	*$poxn^{DM22-B5}$/$poxn^{70}$, UAS-mCD8GFP; ppk28-GAL4/Dr or TM3*
2.4B (proboscis image)	*$poxn^{DM22-B5}$/$poxn^{70}$, UAS-mCD8GFP; ppk28-GAL4/Dr or TM3*
2.4C (top)	(from left to right)
	UAS-mCD8GFP/UAS-mCD8GFP; Gr77a-GAL4/Gr77a-GAL4
	UAS-mCD8GFP/UAS-mCD8GFP; Gr9a-GAL4/Gr9a-GAL4
	Gr33a-GAL4/Cyo; UAS-mCD8GFP/UAS-mCD8GFP
	Gr93d-GAL4/Gr93d-GAL4; UAS-mCD8GFP/UAS-mCD8GFP
	UAS-mCD8GFP/UAS-mCD8GFP; Gr66a-GAL4/TM3
2.4C (bottom)	(from left to right)
	$poxn^{DM22-B5}$/$poxn^{70}$, UAS-mCD8GFP; Gr77a-GAL4/Dr or TM3
	$poxn^{DM22-B5}$/$poxn^{70}$, UAS-mCD8GFP; Gr9a-GAL4/Dr or TM3
	$poxn^{DM22-B5}$, Gr33a-GAL4/$poxn^{70}$, UAS-mCD8GFP; Dr/TM3
	$poxn^{DM22-B5}$, Gr93d-GAL4/$poxn^{70}$, UAS-mCD8GFP; Dr/TM3
	$poxn^{DM22-B5}$, Gr66a-GAL4/$poxn^{70}$, UAS-mCD8GFP; Dr/TM3
2.4C (proboscis image)	(from left to right)
	$poxn^{DM22-B5}$, Gr93d-GAL4/$poxn^{70}$, UAS-mCD8GFP; Dr/TM3
	$poxn^{DM22-B5}$, Gr66a-GAL4/$poxn^{70}$, UAS-mCD8GFP; Dr/TM3
2.4D (top)	(from left to right)
	Ir67c-GAL4/Ir67c-GAL4; UAS-mCD8GFP/UAS-mCD8GFP
	UAS-mCD8GFP/UAS-mCD8GFP; Ir94f-GAL4/ Ir94f-GAL4
	UAS-mCD8GFP/UAS-mCD8GFP; Ir11a-GAL4/ Ir11a-GAL4
	Ir20a-GAL4/Cyo; UAS-mCD8GFP/UAS-mCD8GFP
	UAS-mCD8GFP/UAS-mCD8GFP; Ir100a-GAL4/ Ir100a-GAL4
	Ir76b-GAL4/Ir76b-GAL4; UAS-mCD8GFP/UAS-mCD8GFP
	Ir25a-GAL4/Cyo; UAS-mCD8GFP/UAS-mCD8GFP
2.4D (bottom)	(from left to right)
	$poxn^{DM22-B5}$, Ir67c-GAL4/$poxn^{70}$, UAS-mCD8GFP; Dr/TM3

	poxn$^{DM22-B5}$/poxn^{70}, UAS-mCD8GFP; Ir94f-GAL4/Dr or TM3
	poxn$^{DM22-B5}$/poxn^{70}, UAS-mCD8GFP; Ir11a-GAL4/Dr or TM3
	poxn$^{DM22-B5}$, Ir20a-GAL4/poxn^{70}, UAS-mCD8GFP; Dr/TM3
	poxn$^{DM22-B5}$/poxn^{70}, UAS-mCD8GFP; Ir100a-GAL4/Dr or TM3
	poxn$^{DM22-B5}$, Ir76b-GAL4/poxn^{70}, UAS-mCD8GFP; Dr/TM3
	poxn$^{DM22-B5}$, Ir25a-GAL4/poxn^{70}, UAS-mCD8GFP; Dr/TM3
2.4D (proboscis image)	*poxn$^{DM22-B5}$, Ir25a-GAL4/poxn^{70}, UAS-mCD8GFP; Dr/TM3*
2.5A	(from left to right)
	LexAop2-mCherry-HA/UAS-mCD8GFP; Gr43a-LexA/Gr93d-GAL4
	LexAop2-mCherry-HA/UAS-mCD8GFP; Gr43a-LexA/ppk28-GAL4
	LexAop2-mCherry-HA/UAS-mCD8GFP; ppk28-LexA/Gr93d-GAL4
2.5B	*poxn$^{DM22-B5}$, Gr61a-GAL4/poxn^{70}, UAS-mCD8GFP; Gr43a-LexA/LexAop2-mCherry-HA, UAS-mCD8GFP*
2.5C	*poxn$^{DM22-B5}$, Gr33a-GAL4/poxn^{70}, UAS-mCD8GFP; Gr32a-LexA/LexAop2-mCherry-HA, UAS-mCD8GFP*
2.6A	(from top to bottom)
	poxn$^{DM22-B5}$/poxn^{70}; UAS-Kir2.1/+
	poxn$^{DM22-B5}$/poxn^{70}; Gr66a-GAL4/+
	poxn$^{DM22-B5}$/poxn^{70}; Gr66a-GAL4/UAS-Kir2.1
	poxn$^{DM22-B5}$/poxn^{70}; Gr77a-GAL4/+
	poxn$^{DM22-B5}$/poxn^{70}; Gr77a-GAL4/UAS-Kir2.1
	poxn$^{DM22-B5}$/poxn^{70}; Gr9a-GAL4/+
	poxn$^{DM22-B5}$/poxn^{70}; Gr9a-GAL4/UAS-Kir2.1
	poxn$^{DM22-B5}$/poxn^{70}; Gr93d-GAL4/+
	poxn$^{DM22-B5}$/poxn^{70}; Gr93d-GAL4/UAS-Kir2.1
2.6B	(from top to bottom)
	poxn$^{DM22-B5}$/poxn^{70}; UAS-Kir2.1/+
	poxn$^{DM22-B5}$/poxn^{70}; Gr9a-GAL4/+
	poxn$^{DM22-B5}$/poxn^{70}; Gr9a-GAL4/UAS-Kir2.1
2.6C	(from top to bottom)
	poxn$^{DM22-B5}$/poxn^{70}; UAS-Kir2.1/+

	poxn$^{DM22-B5}$/poxn^{70}; Gr93d-GAL4/+
	poxn$^{DM22-B5}$/poxn^{70}; Gr93d-GAL4/UAS-Kir2.1
2.6D	(from top to bottom)
	poxn$^{DM22-B5}$/poxn^{70}; UAS-Kir2.1/+
	poxn$^{DM22-B5}$/poxn^{70}; Gr77a-GAL4/+
	poxn$^{DM22-B5}$/poxn^{70}; Gr77a-GAL4/UAS-Kir2.1
2.7A	(from left to right)
	poxn$^{DM22-B5}$, UAS-VR1^{E600K}/poxn^{70}; Dr or TM3/+
	poxn$^{DM22-B5}$/poxn^{70}, UAS-VR1 ^{E600K}; Dr or TM3/+
	poxn$^{DM22-B5}$/poxn^{70}; Gr64e-GAL4/+
	poxn$^{DM22-B5}$, UAS-VR1^{E600K}/poxn^{70}; Gr64e-GAL4/+
	poxn$^{DM22-B5}$/poxn^{70}; Gr61a-GAL4/+
	poxn$^{DM22-B5}$, UAS-VR1^{E600K}/poxn^{70}; Gr61a-GAL4/+
	poxn$^{DM22-B5}$/poxn^{70}; Gr64d-GAL4/+
	poxn$^{DM22-B5}$, UAS-VR1^{E600K}/poxn^{70}; Gr64d-GAL4/+
	poxn$^{DM22-B5}$/poxn^{70}; Gr93d-GAL4/+
	poxn$^{DM22-B5}$, UAS-VR1^{E600K}/poxn^{70}; Gr93d-GAL4/+
	poxn$^{DM22-B5}$/poxn^{70}; Gr66a-GAL4/+
	poxn$^{DM22-B5}$, UAS-VR1^{E600K}/poxn^{70}; Gr66a-GAL4/+
	poxn$^{DM22-B5}$/poxn^{70}; Gr32a-GAL4/+
	poxn$^{DM22-B5}$, UAS-VR1^{E600K}/poxn^{70}; Gr32a-GAL4/+
	poxn$^{DM22-B5}$, UAS-VR1^{E600K}/poxn^{70}; Gr93d-GAL4/ Gr66a-GAL4
	poxn$^{DM22-B5}$, UAS-VR1^{E600K}/poxn^{70}; Gr64e-GAL4/ Gr93d-GAL4
	poxn$^{DM22-B5}$, UAS-VR1^{E600K}/poxn^{70}; Gr64e-GAL4/ Gr66a-GAL4
	poxn$^{DM22-B5}$, UAS-VR1^{E600K}/poxn^{70}; Gr64e-GAL4/ Ir94f-GAL4
	poxn$^{DM22-B5}$/poxn^{70}; Ir56a-GAL4/+
	poxn$^{DM22-B5}$, UAS-VR1^{E600K}/poxn^{70}; Ir56a -GAL4/+
	poxn$^{DM22-B5}$, Ir67c-GAL4/poxn^{70}; Dr or TM3/+
	poxn$^{DM22-B5}$, Ir67c-GAL4/poxn^{70}, UAS-VR1^{E600K}; Dr or TM3
	poxn$^{DM22-B5}$/poxn^{70}; Ir94f-GAL4/+
	poxn$^{DM22-B5}$, UAS-VR1^{E600K}/poxn^{70}; Ir94f -GAL4/+
	poxn$^{DM22-B5}$/poxn^{70}; Ir100a-GAL4/+
	poxn$^{DM22-B5}$, UAS-VR1^{E600K}/poxn^{70}; Ir100a -GAL4/+
	poxn$^{DM22-B5}$, Ir20a-GAL4/poxn^{70}; Dr or TM3/+

	poxn$^{DM22-B5}$, Ir20a-GAL4/poxn^{70}, UAS-VR1^{E600K}; Dr or TM3
	poxn$^{DM22-B5}$/poxn^{70}; ppk28-GAL4/+
	poxn$^{DM22-B5}$, UAS-VR1^{E600K}/poxn^{70}; ppk28-GAL4/+
2.7B	(from left to right)
	poxn$^{DM22-B5}$, UAS-VR1^{E600K}/poxn^{70}; Dr or TM3/+
	poxn$^{DM22-B5}$/poxn^{70}; Gr66a-GAL4/+
	poxn$^{DM22-B5}$, UAS-VR1^{E600K}/poxn^{70}; Gr66a-GAL4/+
2.7C	(from left to right)
	poxn$^{DM22-B5}$, UAS-VR1^{E600K}/+; Dr or TM3/+
	poxn$^{DM22-B5}$/+; Gr66a-GAL4/+
	poxn$^{DM22-B5}$, UAS-VR1^{E600K}/+; Gr66a-GAL4/+
	poxn$^{DM22-B5}$/+; Gr32a-GAL4/+
	poxn$^{DM22-B5}$, UAS-VR1^{E600K}/+; Gr32a-GAL4/+
2.8	(from left to right)
	UAS-mCD8GFP/UAS-mCD8GFP; Gr22b-GAL4/TM3
	UAS-mCD8GFP/UAS-mCD8GFP; Gr93d-GAL4/Gr93d-GAL4
	Ir76b-LexA/UAS-mCD8GFP; LexAop2-mCherry-HA/Ir76b-GAL4

REFERENCES

Awasaki, T. & Kimura, K. 1997. pox-neuro is required for development of chemosensory bristles in Drosophila. *J Neurobiol,* 32**,** 707-21.

Baines, R. A., Uhler, J. P., Thompson, A., Sweeney, S. T. & Bate, M. 2001. Altered electrical properties in Drosophila neurons developing without synaptic transmission. *J Neurosci,* 21**,** 1523-31.

Boll, W. & Noll, M. 2002. The Drosophila Pox neuro gene: control of male courtship behavior and fertility as revealed by a complete dissection of all enhancers. *Development,* 129**,** 5667-81.

Cameron, P., Hiroi, M., Ngai, J. & Scott, K. 2010. The molecular basis for water taste in Drosophila. *Nature,* 465**,** 91-5.

Charlu, S., Wisotsky, Z., Medina, A. & Dahanukar, A. 2013. Acid sensing by sweet and bitter taste neurons in Drosophila melanogaster. *Nat Commun,* 4**,** 2042.

Chen, C., Buhl, E., Xu, M., Croset, V., Rees, J. S., Lilley, K. S., Benton, R., Hodge, J. J. & Stanewsky, R. 2015. Drosophila Ionotropic Receptor 25a mediates circadian clock resetting by temperature. *Nature,* 527**,** 516-20.

Croset, V., Rytz, R., Cummins, S. F., Budd, A., Brawand, D., Kaessmann, H., Gibson, T. J. & Benton, R. 2010. Ancient protostome origin of chemosensory ionotropic glutamate receptors and the evolution of insect taste and olfaction. *PLoS Genet,* 6**,** e1001064.

Fan, P., Manoli, D. S., Ahmed, O. M., Chen, Y., Agarwal, N., Kwong, S., Cai, A. G., Neitz, J., Renslo, A., Baker, B. S. & Shah, N. M. 2013. Genetic and neural mechanisms that inhibit Drosophila from mating with other species. *Cell,* 154**,** 89-102.

Freeman, E. G. & Dahanukar, A. 2015. Molecular neurobiology of Drosophila taste. *Curr Opin Neurobiol,* 34**,** 140-8.

French, A. S., Sellier, M. J., Ali Agha, M., Guigue, A., Chabaud, M. A., Reeb, P. D., Mitra, A., Grau, Y., Soustelle, L. & Marion-Poll, F. 2015. Dual mechanism for bitter avoidance in Drosophila. *J Neurosci,* 35**,** 3990-4004.

Ganguly, A., Pang, L., Duong, V. K., Lee, A., Schoniger, H., Varady, E. & Dahanukar, A. 2017. A Molecular and Cellular Context-Dependent Role for Ir76b in Detection of Amino Acid Taste. *Cell Rep,* 18**,** 737-750.

Gendre, N., Luer, K., Friche, S., Grillenzoni, N., Ramaekers, A., Technau, G. M. & Stocker, R. F. 2004. Integration of complex larval chemosensory organs into the adult nervous system of Drosophila. *Development,* 131**,** 83-92.

Hussain, A., Zhang, M., Ucpunar, H. K., Svensson, T., Quillery, E., Gompel, N., Ignell, R. & Grunwald Kadow, I. C. 2016. Ionotropic Chemosensory Receptors Mediate the Taste and Smell of Polyamines. *PLoS Biol,* 14**,** e1002454.

Jeong, Y. T., Shim, J., Oh, S. R., Yoon, H. I., Kim, C. H., Moon, S. J. & Montell, C. 2013. An odorant-binding protein required for suppression of sweet taste by bitter chemicals. *Neuron,* 79**,** 725-37.

Joseph, R. M. & Heberlein, U. 2012. Tissue-specific activation of a single gustatory receptor produces opposing behavioral responses in Drosophila. *Genetics,* 192**,** 521-32.

Joseph, R. M., Sun, J. S., Tam, E. & Carlson, J. R. 2017. A receptor and neuron that activate a circuit limiting sucrose consumption. *Elife,* 6.

Kang, K., Pulver, S. R., Panzano, V. C., Chang, E. C., Griffith, L. C., Theobald, D. L. & Garrity, P. A. 2010. Analysis of Drosophila TRPA1 reveals an ancient origin for human chemical nociception. *Nature,* 464**,** 597-600.

Kim, H., Jeong, Y. T., Choi, M. S., Choi, J., Moon, S. J. & Kwon, J. Y. 2017. Involvement of a Gr2a-Expressing Drosophila Pharyngeal Gustatory Receptor Neuron in Regulation of Aversion to High-Salt Foods. *Mol Cells*.

Koh, T. W., He, Z., Gorur-Shandilya, S., Menuz, K., Larter, N. K., Stewart, S. & Carlson, J. R. 2014. The Drosophila IR20a clade of ionotropic receptors are candidate taste and pheromone receptors. *Neuron,* 83**,** 850-65.

Kwon, J. Y., Dahanukar, A., Weiss, L. A. & Carlson, J. R. 2014. A map of taste neuron projections in the Drosophila CNS. *J Biosci,* 39**,** 565-74.

Ledue, E. E., Chen, Y. C., Jung, A. Y., Dahanukar, A. & Gordon, M. D. 2015. Pharyngeal sense organs drive robust sugar consumption in Drosophila. *Nat Commun,* 6**,** 6667.

Liman, E. R., Zhang, Y. V. & Montell, C. 2014. Peripheral coding of taste. *Neuron,* 81**,** 984-1000.

Ling, F., Dahanukar, A., Weiss, L. A., Kwon, J. Y. & Carlson, J. R. 2014. The molecular and cellular basis of taste coding in the legs of Drosophila. *J Neurosci,* 34**,** 7148-64.

Marella, S., Fischler, W., Kong, P., Asgarian, S., Rueckert, E. & Scott, K. 2006. Imaging taste responses in the fly brain reveals a functional map of taste category and behavior. *Neuron,* 49**,** 285-95.

Miyamoto, T. & Amrein, H. 2014. Diverse roles for the Drosophila fructose sensor Gr43a. *Fly (Austin),* 8**,** 19-25.

Miyamoto, T., Slone, J., Song, X. & Amrein, H. 2012. A fructose receptor functions as a nutrient sensor in the Drosophila brain. *Cell,* 151**,** 1113-25.

Nayak, S. V. & Singh, R. N. 1983. Sensilla on the Tarsal Segments and Mouthparts of Adult Drosophila-Melanogaster Meigen (Diptera, Drosophilidae). *International Journal of Insect Morphology & Embryology,* 12**,** 273-291.

Ni, L., Klein, M., Svec, K. V., Budelli, G., Chang, E. C., Ferrer, A. J., Benton, R., Samuel, A. D. & Garrity, P. A. 2016. The Ionotropic Receptors IR21a and IR25a mediate cool sensing in Drosophila. *Elife,* 5.

Nottebohm, E., Dambly-Chaudiere, C. & Ghysen, A. 1992. Connectivity of chemosensory neurons is controlled by the gene poxn in Drosophila. *Nature,* 359**,** 829-32.

Shim, J., Lee, Y., Jeong, Y. T., Kim, Y., Lee, M. G., Montell, C. & Moon, S. J. 2015. The full repertoire of Drosophila gustatory receptors for detecting an aversive compound. *Nat Commun,* 6**,** 8867.

Soldano, A., Alpizar, Y. A., Boonen, B., Franco, L., Lopez-Requena, A., Liu, G., Mora, N., Yaksi, E., Voets, T., Vennekens, R., Hassan, B. A. & Talavera, K. 2016. Gustatory-mediated avoidance of bacterial lipopolysaccharides via TRPA1 activation in Drosophila. *Elife,* 5.

Stocker, R. F. & Schorderet, M. 1981. Cobalt filling of sensory projections from internal and external mouthparts in Drosophila. *Cell Tissue Res,* 216**,** 513-23.

Thistle, R., Cameron, P., Ghorayshi, A., Dennison, L. & Scott, K. 2012. Contact Chemoreceptors Mediate Male-Male Repulsion and Male-Female Attraction during Drosophila Courtship. *Cell,* 149**,** 1140-1151.

Van Giesen, L., Hernandez-Nunez, L., Delasoie-Baranek, S., Colombo, M., Renaud, P., Bruggmann, R., Benton, R., Samuel, A. D. & Sprecher, S. G. 2016. Multimodal stimulus coding by a gustatory sensory neuron in Drosophila larvae. *Nat Commun,* 7**,** 10687.

Weiss, L. A., Dahanukar, A., Kwon, J. Y., Banerjee, D. & Carlson, J. R. 2011. The molecular and cellular basis of bitter taste in Drosophila. *Neuron,* 69**,** 258-72.

Yapici, N., Cohn, R., Schusterreiter, C., Ruta, V. & Vosshall, L. B. 2016. A Taste Circuit that Regulates Ingestion by Integrating Food and Hunger Signals. *Cell,* 165**,** 715-29.

Zhang, Y. V., Ni, J. & Montell, C. 2013. The molecular basis for attractive salt-taste coding in Drosophila. *Science,* 340**,** 1334-8.

CHAPTER III

Combinatorial pharyngeal taste coding for feeding avoidance in adult *Drosophila*

This chapter was to Cell Reports on August 22, 2019 – **YCD Chen**, SJ Park, RM Joseph, WW Ja, and A Dahanukar. *Combinatorial pharyngeal taste coding for feeding avoidance in adult Drosophila.*

SUMMARY

Taste drives appropriate food preference and intake. In *Drosophila*, taste neurons are housed in both external and internal organs, but the latter have been relatively underexplored. Here we report that *Poxn* mutants with a minimal taste system of pharyngeal neurons can avoid many aversive tastants including bitter compounds, acid, and salt, suggesting that pharyngeal taste is sufficient for rejecting intake of aversive compounds. Optogenetic activation of selected pharyngeal bitter neurons during feeding events elicits changes in feeding parameters that can suppress intake. Functional dissection experiments indicate that multiple classes of pharyngeal neurons are involved in achieving behavioral avoidance, by virtue of being inhibited or activated by aversive tastants. Tracing second-order pharyngeal circuits reveals two main relay centers for processing pharyngeal taste inputs. Together, our results suggest that the pharynx can control the ingestion of harmful compounds by integrating taste input from different classes of pharyngeal neurons.

INTRODUCTION

Insects perceive environmental stimuli through sensory systems and use this information to guide behavioral responses. In some instances, a sensory system encompasses multiple organs, which are thought to have specialized contributions to behavior. In the gustatory system of a well-established genetic model, *Drosophila melanogaster*, there are multiple taste organs, present externally throughout the body (labellum, legs, and wing margins), and internally in pharyngeal organs (Freeman and Dahanukar, 2015, Joseph and Carlson, 2015). Although the labellum and legs may be important for initial assessment of quality due to their first contact with food, pharyngeal taste organs are believed to monitor food quality during ingestion. However, the specific role of pharyngeal taste in controlling feeding has not been explored in depth.

Presumably, pharyngeal taste organs could serve as a final checkpoint to monitor food quality. Pharyngeal taste input is anatomically represented in regions of the central nervous system that are distinct from other taste organs (Kwon et al., 2014, Wang et al., 2004), consistent with potentially separable location-dependent roles of taste input. This notion is supported by recent studies showing that pharyngeal gustatory receptor neurons (GRNs) elicit behavioral responses to appetitive tastants that are distinguishable from those elicited by external GRNs. External GRNs contribute to the initiation of feeding and trigger the proboscis extension reflex (PER), an indication of acceptance behavior, while those in the pharynx sustain feeding bouts (Ledue et al., 2015). Similarly, external GRNs initiate PER to yeast, but those housed in taste pegs lining the inner surface of

labellum sustain feeding (Steck et al., 2018). Pharyngeal GRNs have also been shown to mediate rejection of some compounds (Soldano et al., 2016, Kang et al., 2010), but the extent to which the pharynx controls feeding avoidance is not clear.

Recently, we created receptor-to-neuron maps of pharyngeal taste organs, which revealed the presence of multiple classes of taste neurons (Chen and Dahanukar, 2017), consistent with the idea that the pharynx may independently assess food quality. To investigate how pharyngeal taste input affects feeding behaviors, we take advantage of *Pox-neuro* (*Poxn*) mutants, in which all external taste bristles are transformed into mechanosensory bristles (Awasaki and Kimura, 1997, Nottebohm et al., 1992), but all pharyngeal taste neurons are retained (Chen and Dahanukar, 2017, Chen et al., 2018). We first characterize feeding preference and food intake of *Poxn* mutants, and find that behavioral avoidance of a diverse panel of bitter compounds, high concentrations of salt, and tartaric acid is similar to that of control flies. Notably, we find a strong correlation between *Poxn* and control flies in feeding aversion intensity and food intake suppression, implicating sufficiency of pharyngeal taste for feeding control. Optogenetic activation of two different pharyngeal bitter neurons only during the feeding events, in otherwise wild type flies, either reduces meal size or increases the time to the next meal, supporting the notion that some pharyngeal GRNs play a role as gate-keepers to manage food entry into the digestive tract by suppressing food intake. To further investigate the neuronal basis of feeding avoidance by pharyngeal taste, we use a genetic dissection strategy to silence different classes of pharyngeal GRNs and find that feeding aversion can be achieved by

multiple subsets of pharyngeal GRNs. *Ex vivo* calcium imaging data show that denatonium, tartaric acid, and high salt inhibit sucrose-evoked activity of pharyngeal *Gr43a* sweet GRNs. This inhibition is not a general feature for sugar-sensing pharyngeal GRNs, since denatonium activated rather than inhibited *Ir60b* pharyngeal GRNs, consistent with their role in limiting consumption. Furthermore, feeding avoidance of denatonium, tartaric acid, or high salt is eliminated only when both inhibition of pharyngeal *Gr43a* sweet GRNs and activation of different combinations of aversive pharyngeal GRNs are absent. Tracing pharyngeal second-order circuits reveals that both appetitive and aversive pharyngeal GRNs convey inputs to two common brain areas (pars intercerebralis and lateral protocerebrum), suggesting pharyngeal taste is represented across brain regions. Together, our study demonstrates an important role of pharyngeal taste in controlling food choice and intake, and provides a foundation for further functional investigation of higher-order taste circuits.

RESULTS

RESULTS

Poxn mutants respond to a broad range of bitter compounds

Previous studies have used *Poxn* mutants to understand the role of pharyngeal sweet GRNs, which promote sugar consumption and local search behaviors (Murata et al., 2017, Ledue et al., 2015). To evaluate the role of the pharynx in feeding avoidance, we also took advantage of *Poxn* mutants, which serve as a good model for dissecting the function of pharyngeal taste without other confounding taste inputs (Chen et al., 2018). Specifically, we characterized feeding preferences of *Poxn* mutants in binary choice assays using various categories of aversive tastants, including high concentrations of tartaric acid and salt (Zhang et al., 2013, Charlu et al., 2013), as well as compounds perceived as bitter by humans and avoided by flies (Weiss et al., 2011). All aversive tastants were tested in mixtures with sucrose against sucrose alone, a context in which the reduction in the appetitive value of the mixture as compared to that of sucrose alone can be gauged. *Poxn* flies rejected sucrose mixtures containing tartaric acid (**Figure 3.1A**), or salt at concentrations of 200 mM and above (**Figure 3.1B**), displaying food preferences similar to those of control flies. By contrast, we observed some variation in behavioral responses to bitter compounds between control and *Poxn* mutant flies. Nine bitter compounds were selected on the basis of their ability to elicit different degrees of avoidance in previously reported binary choice assays (Weiss et al., 2011). We tested each compound across a range of concentrations, and measured slopes for trend lines derived from linear regression analyses for each concentration curve for control and *Poxn*

flies. Based on the results, bitter tastants could be broadly separated into two categories depending on the degree to which *Poxn* mutants showed behavioral sensitivity to them. Denatonium, lobeline, quinine, papaverine, and coumarin elicited similar degrees of feeding avoidance in *Poxn* mutants and control flies, although the mutants showed reduced feeding avoidance for some of these compounds at higher concentrations (**Figure 3.1C**). The slopes of trend lines for these compounds, referred to as pharynx-sensitive, ranged from -0.43 to -0.77 for both genotypes. However, *Poxn* mutants showed little or no feeding aversion to caffeine, theophylline, DEET, and strychnine, all of which induced strong concentration-dependent behavioral avoidance in control flies (**Figure 3.1D**). For these compounds, referred to as pharynx-insensitive, the slopes of trend lines ranged from -0.40 to -0.78 in control flies, but -0.11 to -0.22 in the *Poxn* mutants.

Pharyngeal taste controls the intensity of feeding aversion

To better compare behavioral responses to bitter compounds in control and *Poxn* flies, we first extrapolated an iso-attractive concentration for each compound, [IA], a concentration that rendered a mixture with 5 mM sucrose equally as palatable as 1 mM sucrose alone (Preference Index=0 in binary choice assay), based on the linear regression analyses. Thus, a low [IA] value indicates strong aversion and a high [IA] value indicates weak aversion (**Figure 3.1E**). We calculated [IA] values for most compounds for both control and *Poxn* flies, except DEET and strychnine, as *Poxn* mutants did not show concentration-dependent behavioral responses to these compounds. The compounds could be clustered based on the differences in the [IA] between the controls and the

mutants. (**Figure 3.1E**). Control flies generally rejected pharynx-sensitive compounds (e.g., denatonium, lobeline, quinine, papaverine, and coumarin) to a greater extent than those categorized as pharynx-insensitive (e.g., caffeine and theophylline) (**Figure 3.1E**). Surprisingly, we found that the order of aversiveness of the tastants was similar between the control and the mutant flies and there was a strong positive correlation between the [IA] values from *Poxn* mutants and those from control flies (R^2=0.9617, p<0.0001) (**Figure 3.1F**). The similarity in patterns of feeding aversion between *Poxn* and control flies suggests that pharyngeal taste alone can be sufficient for determining overall feeding avoidance of a variety of bitter compounds.

Pharyngeal taste controls the suppression of food intake

Aversive effects of bitter compounds can be observed not only in feeding preference assays but also in suppression of food intake (Weiss et al., 2011, Sellier et al., 2011). Therefore, we next investigated the role of pharyngeal taste in determining ingestion suppression of aversive tastants. We used a newly developed Activity Recording Capillary Feeder or CAFE (ARC) assay in which food intake, meal size, and meal frequency can be measured in individual flies (Murphy et al., 2017). We compared consumption of 100 mM sucrose alone or in mixtures with eight different bitter compounds by control and *Poxn* mutant flies for 24 hours. In control flies, we found that different bitter compounds suppressed food intake to varying degrees. Denatonium, lobeline, strychnine, and quinine evoked strong feeding suppression, whereas papaverine, coumarin, caffeine, and theophylline did so to a weaker extent (**Figure 3.2A**). We noticed

that the aversiveness ranking of bitter compounds in the short-term feeding choice assay (**Figure 3.1E**) was distinct from the ability of bitter compounds to suppress food intake in 24-hours food consumption assay (**Figure 3.2A**). However, the food intake of all tested diets was not significantly different between control and *Poxn* mutant flies (**Figure 3.2A**). In addition, most tested bitter compounds elicited similar degrees of food intake suppression in both *Poxn* mutants and control flies (**Figure 3.2B**), consistent with the idea that pharyngeal taste can be sufficient to mediate food intake suppression. We note that the inhibitory effects of bitter compounds on discrete parameters of food intake (i.e., meal size and meal frequency) were more variable between control and *Poxn* flies (**Figure 3.2C-F**). For example, meal sizes for sucrose alone and for the sucrose/theophylline mixture were significantly larger in *Poxn* mutants than in control flies (**Figure 3.2C**), while meal frequencies for sucrose mixtures with coumarin, caffeine, and theophylline were significantly lower in *Poxn* mutants than in control flies (**Figure 3.2E**). Thus, overall food consumption appears to be normal in *Poxn* mutants, in which taste input is derived solely from the pharynx, however discrete parameters of food intake may be influenced by other factors that are lacking or altered in these flies.

Pharyngeal GRNs mediate feeding avoidance of bitter tastants

We next aimed to test the role of pharyngeal taste in feeding avoidance of bitter compounds, since *Poxn* mutant flies, which have intact pharyngeal GRNs (Chen and Dahanukar, 2017, Ledue et al., 2015), appropriately rejected many tastants. We first silenced all pharyngeal GRNs in *Poxn* mutants by expressing an inwardly rectifying

potassium channel, Kir2.1, under the control of *Ir25a-GAL4*, which labels all pharyngeal GRNs (Chen and Dahanukar, 2017). To measure food intake over 24 hours in fed flies, we labeled fly food with a radioactive ^{32}P tracer (Ja et al., 2009, Deshpande et al., 2014) and quantified radiolabeled food consumption. We tested behavioral responses to two bitter compounds, denatonium and lobeline, which evoked comparable levels of feeding avoidance in both control and *Poxn* mutant flies (**Figure 3.1C**). In control flies, sucrose/bitter mixtures containing denatonium or lobeline almost completely abolished food intake in comparison with sucrose alone (**Figure 3.3A**). We found that *Poxn* mutants in which all pharyngeal GRNs were silenced (*Poxn; Ir25a-silenced*) consumed more sucrose over the same time frame. Notably, they also consumed larger amounts of the sucrose/bitter mixtures, a phenotype consistent with that of bitter-insensitive flies. Nonetheless, intake of sucrose/bitter mixtures in *Ir25a-silenced Poxn* flies was less than observed for sucrose alone (**Figure 3.3A**), suggesting a possible involvement of post-ingestive mechanisms that operate over the 24-hour time frame of this consumption assay. Therefore, we compared bitter feeding avoidance of *Ir25a-silenced Poxn* and control flies in short-term (2-hour) binary choice assays. We found that avoidance of both bitter tastants was significantly reduced in *Ir25a-silenced Poxn* flies as compared to some transgenic controls, barring two exceptions in which denatonium avoidance was not significantly different between *Ir25a-silenced* and *Ir25a-GAL4* control flies (Kruskal-Wallis, uncorrected Dunn's test, P=0. 0892) and lobeline avoidance was not significantly different between *Ir25a-silenced* and *UAS-Kir2.1* control flies (Kruskal-Wallis, uncorrected Dunn's test, P=0. 0853) (**Figure 3.3B**). However, the preference indices of

Ir25a-silenced Poxn flies were not significantly different from zero (Wilcoxon signed rank test, P=0.5542 for denatonium and P=0.5186 for lobeline). In fact, behavioral responses of *Ir25a-silenced Poxn* flies in tests with sucrose alone were no different from those in tests with sucrose/bitter mixtures, consistent with a complete loss of feeding attraction of higher concentration of sugars and avoidance of sugar/bitter mixtures in these assays.

Given that *Gr66a* is broadly expressed in external bitter GRNs and is required for responses to many bitter tastants (Wang et al., 2004, Thorne et al., 2004), we next asked whether pharyngeal *Gr66a* neurons are necessary for feeding avoidance of denatonium and lobeline. We also investigated *Gr93d* neurons, which partially overlap with the *Gr66a* neurons (Chen and Dahanukar, 2017). We expressed Kir2.1 to genetically silence either or both *Gr66a* and *Gr93d* neurons in a *Poxn* mutant background and tested behavioral responses to denatonium and lobeline in food consumption and choice assays. We found that silencing pharyngeal *Gr66a* neurons but not *Gr93d* neurons significantly increased consumption of sucrose/bitter mixtures containing denatonium or lobeline compared to control flies (**Figure 3.3C**). The effect of silencing both *Gr66a* and *Gr93d* neurons was no different from silencing *Gr66a* neurons alone (**Figure 3.3C**), suggesting that *Gr93d* neurons may play little if any role in the suppression of food intake. In feeding preference assays, we found that behavioral avoidance of both denatonium and lobeline was significantly reduced in *Gr66a-silenced* flies as compared to both *GAL4* and *UAS* transgenic controls (**Figure 3.3D**). Unexpectedly, we observed that *Gr93d-silenced*

flies displayed enhanced feeding avoidance of denatonium compared to both transgenic controls and also enhanced feeding avoidance of lobeline compared to *UAS* control. Altogether, our results suggest that pharyngeal *Gr66a* GRNs mediate both negative preference for and intake suppression of bitter compounds.

Pharyngeal GRNs regulate distinct meal parameters to suppress food intake

We next tested whether acute activation of pharyngeal GRNs only during feeding events is sufficient for the suppression of food intake. We elected to test two different *Gr66a* pharyngeal GRNs that are specifically labeled by *GAL4* drivers that are not expressed in external taste organs. These are the V5 (*Gr77a-GAL4*) and the V6 (*Gr9a-GAL4*) neurons. We also tested the L7-3 (*Gr23a-GAL4*) neuron, which is one of the pharyngeal neurons that co-expresses *Gr93d*. We modified the ARC assay to collect meals from freely-feeding fed flies while acutely activating the GRNs by expressing red-shifted channelrhodopsins (*UAS- CsChrimson*) (Klapoetke et al., 2014) under the control of the three *GAL4* drivers. Importantly, the optogenetic activation of the GRNs was tied to consumption events, as the onset of the light stimulus was triggered by automated detection of ingestion (**Figure 3.4A,D**). We offered these transgenic flies 100 mM sucrose and measured meal size and the average time to the next meal with or without light stimulation (**Figure 3.4A,D**). Interestingly, activation of *Gr9a* GRNs significantly decreased meal size as compared to that in counterparts who were feeding without light stimulation (**Figure 3.4B**). However, *Gr9a* GRN activation had no effect on the time to the next meal (**Figure 3.4C**). By contrast, activation of either *Gr23a* or *Gr77a* GRNs

delayed the initiation of the subsequent meal without changing meal size (**Figure 3.4B-C**). *UAS- CsChrimson* transgenic control flies showed no difference, both in meal size and average time to the next meal, upon light stimulation (**Figure 3.4B-C**). Thus, activation of a single pharyngeal *Gr66a* GRN is sufficient to suppress meal size. Moreover, our findings suggest that distinct classes of putative bitter-sensing pharyngeal GRNs may suppress overall food intake by regulating different aspects of micro-feeding behaviors.

Functional redundancies in pharyngeal GRNs for sensing aversive tastants

Thus far, our results showed that feeding avoidance of sucrose/bitter mixtures is not completely lost in *Gr66a-silenced Poxn* flies (**Figure 3.3D**), since silencing *Gr66a* neurons did not completely restore preference indexes to positive values typically observed for 5 mM sucrose alone. This data raises the possibility that other classes of pharyngeal GRNs are involved. To identify such classes of pharyngeal GRNs, we tested the roles of different subsets of pharyngeal GRNs labeled by 8 different *chemosensory receptor-GAL4* drivers (Chen and Dahanukar, 2017). We systematically tested each of these *Gr-silenced Poxn* flies in feeding preference assays using a mixture of 2 mM sucrose and 1 mM denatonium against 2 mM sucrose alone (**Figure 3.8A**). We found that silencing of any one type of pharyngeal GRN did not cause a significant reduction in feeding avoidance of sucrose mixed with denatonium (**Figure 3.8A**). Similar results were obtained when testing the effect of silencing these different pharyngeal GRNs in feeding

choice assays using a mixture of 2 mM sucrose and 10% tartaric acid (**Figure 3.8B**) or 500 mM NaCl (**Figure 3.8C**) against 2 mM sucrose alone.

Aversive tastants inhibit pharyngeal *Gr43a* but not *Ir60b* GRNs

We hypothesized that inhibition of appetitive *Gr43a* pharyngeal GRNs by aversive tastants might contribute to feeding avoidance. Recordings from external taste bristles have demonstrated that various aversive tastants can inhibit sugar-evoked responses in external sugar-sensing GRNs (French et al., 2015, Jeong et al., 2013, Charlu et al., 2013). To directly examine whether aversive compounds can inhibit the sugar-induced activity in pharyngeal *Gr43a* GRNs, we expressed the calcium indicator, GCaMP6s, in *Gr43a* GRNs and measured fluorescence changes in labeled neurons in the LSO after tastant application via an *ex vivo* pharyngeal imaging preparation (Joseph et al., 2017) (**Figures 3.5A and 3.9**).

Consistent with our earlier report (Ledue et al., 2015), pharyngeal *Gr43a* GRNs showed robust activation in response to 1 M sucrose (**Figure 3.5A**). Notably, the response was nearly abolished when any one of the three aversive tastants were included in the stimulus solution. Denatonium (**Figure 3.5B,E**), tartaric acid (**Figure 3.5C,F**) and salt (**Figure 3.5D,G**) were each tested at two different concentrations, both of which caused strong inhibition. Analysis of calcium activity over time revealed dose-dependent differences in the strength of inhibition. For example, while 100 mM denatonium eliminated activation by 1 M sucrose, the addition of a lower concentration of

denatonium (10 mM) still allowed for weak calcium activity (ΔF/F 31%±9%, SEM, *n*=11; *P*=0.0104, Mann-Whitney test versus water, *n*=11-19). We note that all aversive tastants caused a sustained depression of GCaMP6 signal below the pre-stimulus baseline of fluorescent activity, possibly due to the continuous contact with the tastant, once delivered by our perfusion method. The dynamics of depression appeared to be concentration-dependent, with faster depression occurring at higher concentrations of aversive tastants (**Figure 3.5B-G**).

To investigate whether bitter tastants can inhibit other sugar-sensing pharyngeal GRNs, we imaged stimulus-evoked calcium activity in pharyngeal *Ir60b* GRNs, which respond to sugars and act to limit consumption (Joseph et al., 2017). We used a stronger transgenic driver, *Ir94f-GAL4*, to label the pharyngeal *Ir60b* GRNs in LSO and found that application of 100 mM sucrose elicited a significant elevation in GCaMP6 fluorescence as compared to water (**Figures 3.5H and 3.10**), consistent with the previous results (Joseph et al., 2017), Notably, inclusion of 10 mM denatonium did not affect the response to sucrose. However, we observed a significant change in calcium activity with 10 mM denatonium alone, suggesting that *Ir60b* GRNs are activated by bitter tastants in addition to sweet tastants. Although the role of *Ir60b* GRNs in feeding response to aversive tastants alone has not been evaluated, the imaging results are consistent with the negative behavioral role of *Ir60b* GRNs in limiting food consumption. We also noticed some differences in the temporal dynamics of *Gr43a* and *Ir60b* GRN responses; those in the latter are delayed and remain sustained for longer periods of time as compared to

Gr43a GRNs (**Figures 3.5I and 3.10**), in agreement with previous findings (Joseph et al., 2017, Ledue et al., 2015). Overall, our results demonstrate that various categories of aversive tastants can inhibit the activity of pharyngeal *Gr43a* but not *Ir60b* GRNs. In addition, pharyngeal *Ir60b* GRNs sense tastants of at least two different categories.

Distinct combinations of pharyngeal GRNs mediate feeding avoidance of different tastants

We next considered that the inhibition of pharyngeal *Gr43a* GRN activity (**Figure 3.5**) may contribute to behavioral outcomes in binary choice assays, and potentially eclipse the roles of other classes of GRNs in feeding avoidance of aversive tastants. We hypothesized that by simultaneously silencing *Gr66a* neurons, which could be activated by bitter compounds, and *Gr43a* neurons, which are subject to bitter compound-mediated inhibition, we could completely abolish aversion to bitter tastants. Thus, we systematically tested double-silenced flies in which selected neuronal types were silenced in combination with all pharyngeal sweet GRNs labeled by *Gr64e-GAL4*, which is expressed in *Gr43a* GRNs. Indeed, we found that silencing both *Gr64e* and *Gr66a* GRNs abolished avoidance of denatonium (PI was not significantly different from zero, Wilcoxon signed rank test, P=0.1774), suggesting that flies lose the ability to sense denatonium when both *Gr64e* and *Gr66a*-dependent mechanisms are ablated. Similar effects were not observed with any other *Gr64e/GrX or IrX* doubled-silenced flies, except for *Ir76b-silenced* flies in which all *Gr64e* GRNs as well as 13 additional pharyngeal GRNs were functionally abolished (Wilcoxon signed rank test, P=0.2656) (**Figure 3.6A**).

Next, we aimed to identify the classes of pharyngeal GRNs involved in mediating tartaric acid avoidance. As expected from the results of calcium imaging, when both *Gr64e* and *Gr66a* GRNs were silenced, we observed a significant reduction in feeding avoidance of 10% tartaric acid (**Figure 3.6B**). In this instance, *Gr64e-/Gr66a-silenced Poxn* flies retain some ability to avoid tartaric acid (PI was significantly different from zero, Wilcoxon signed rank test, P=0.0085), invoking a role for at least one additional class of *Ir76b* GRNs, since silencing all *Ir76b* pharyngeal GRNs abolished tartaric acid avoidance (PI was not significantly different from zero, Wilcoxon signed rank test, P=0.3696).

Finally, we performed similar analyses to identify pharyngeal GRNs that underlie feeding avoidance of 500 mM salt (**Figure 3.1B**). Surprisingly, none of the tested combinations of *Gr64e* sweet GRNs and other subsets of GRNs was sufficient to eliminate avoidance of high salt (**Figure 3.6C**). Salt avoidance was abolished only when all *Ir76b* pharyngeal GRNs were silenced, signaling broader functional redundancies for high salt avoidance. Together, our results suggest that multiple classes of taste neurons are involved in driving behavioral responses to aversive tastants. Moreover, different categories of aversive tastants may be sensed via overlapping but distinct groups of GRNs. Overall, our results imply a greater degree of functional overlap in these pharyngeal neurons than previously appreciated.

Tracing second-order pharyngeal taste circuits reveals two main taste centers in the brain connecting with different classes of pharyngeal GRNs

To understand how pharyngeal taste information is represented at the second relay, we used the newly developed circuit tracing technique, trans-Tango (Talay et al., 2017), in combination with the molecular toolkit for labeling subsets of pharyngeal GRNs in *Poxn* mutant flies. By recombining trans-Tango cassettes with the $Poxn^{70}$ mutant allele, we were able to specifically trace pharyngeal second-order neurons. We first performed experiments to trace circuits of pharyngeal *Gr32a* bitter GRNs. Notably, the number of *Gr32a* second-order neurons labeled in the brain of a *Poxn* mutant (~20-30) was greatly reduced as compared to that in a wild type brain (>100) (**Figure 3.7A-Ai**), presenting a numerically tractable model for characterizing the anatomy of taste circuits. First, we noticed that neurons lying above the antennal lobes were not labeled in the *Poxn* flies, and thus are likely to be specifically connected with external *Gr32a* GRNs. In addition, second-order neurons connected to pharyngeal *Gr32a* GRNs, or subsets thereof, (**Figure 3.7Aii-Aiii**) showed projections to two main brain regions, pars intercerebralis and lateral protocerebrum. Labeling of second-order neuronal circuits for all possible pharyngeal GRNs showed that most, if not all, pharyngeal GRNs projected to these two brain regions, implicating them as potential relay centers for pharyngeal taste inputs.

Some of the *GAL4* lines (*Gr9a-*, *Gr23a-*, *Ir67c-*, and *Ir94f-GAL4*) used for trans-Tango tracing exclusively labeled single identified pharyngeal neurons (Chen and

Dahanukar, 2017), offering the opportunity to examine the number of second-order taste neurons connected to a single pair of pharyngeal GRNs. We found that each of these neurons connected with multiple second-order neurons (at least 10) and labeled projections in the pars intercerebralis and lateral protocerebrum (**Figure 3.7Aiii, C, Ciii, and Civ**), suggesting that even a specific gustatory input may be broadly conveyed across a few distinct brain regions. Together, our results lay the foundation for further system-wide functional analyses of pharyngeal second-order neurons.

DISCUSSION

Flies have multiple taste organs in the body, present externally and internally. Taste neurons present in organs that line the pharynx have been thought to act as gate-keepers for monitoring food palatability, but they have been less studied in comparison with their external counterparts. Here we assess the role of pharyngeal taste in driving food preference and consumption using *Poxn* mutants, which possess only a "minimal" pharyngeal taste system. We find that *Poxn* flies show behavioral sensitivity to a diverse panel of aversive compounds, including high concentrations of salt, tartaric acid, and several bitter compounds, in a manner that is similar to control flies. Notably, the intensity of feeding aversion evoked by a given bitter tastant is strongly correlated between *Poxn* and control flies, implicating pharyngeal taste as sufficient for determining feeding avoidance. We probe the contributions of pharyngeal GRN classes in feeding aversion to various tastants using genetic dissection studies and find that avoidance of most tastants is achieved via multiple classes of pharyngeal GRNs, including bitter, sweet, and one or more additional classes. Importantly, feeding avoidance of bitter compounds, tartaric acid, and high salts depends on different but overlapping pharyngeal GRN classes, providing a potential mechanism for pharyngeal taste to distinguish different categories of aversive compounds based on combinations of pharyngeal GRNs are activated. We note that pharyngeal GRNs are genetically silenced throughout development and therefore the possibility of potential developmental defects contributing to phenotypic outcomes cannot be ruled out.

Despite extensive, systematic characterization of external taste neuronal responses to large panels of bitter compounds (Ling et al., 2014, Weiss et al., 2011), some questions remain about how these taste inputs are translated to behavior. In particular, why do some robust or broad activators of bitter taste neurons (e.g., caffeine) evoke weaker degrees of aversion in feeding assays as compared to other compounds? Our results, which show that pharyngeal input plays an important role in driving avoidance of aversive tastants, offer one explanation for this conundrum. Although we found differences in the "bitterness" rank order of compounds in binary choice and consumption assays, internal taste input was sufficient for assigning bitterness values and suppressing food intake in patterns that closely resemble those observed in control flies. Features that determine aversion intensity of bitter compounds are not well understood, but a prevailing view is that bitter chemicals signal toxicity. Such a model would predict that compounds that are more toxic would be perceived as more bitter, and consequently avoided to a greater extent. It would be interesting to investigate any potential relationship between pharyngeal sensitivity and toxicity of various bitter compounds.

Our data also suggest that external and internal taste inputs are not functionally redundant. First, even for pharynx-sensitive compounds (e.g., quinine, papaverine, coumarin), *Poxn* mutants can show reduced avoidance at higher concentrations, suggesting that information from both external and internal neurons converges to control overall feeding avoidance. Second, the contribution of external GRNs is more prominent for pharynx-insensitive compounds (e.g., caffeine, theophylline, DEET, strychnine),

suggesting a functional division of bitter taste in organs located in different parts of the body. Whether this is due to differences in activation of bitter GRNs or inhibition of sweet GRNs or both would be interesting to determine in future studies. Lastly, meal size and meal frequency do not correlate well between *Poxn* mutants and control flies, suggesting that these parameters may be influenced by other factors that are altered or lacking in *Poxn* mutants. We also note that some chemosensory receptors are expressed in enteroendocrine cells (Park and Kwon, 2011), and this could also contribute to feeding aversion in long-term (24-hours) assays via unidentified post-ingestive mechanisms.

Previous studies have demonstrated dual mechanisms for cellular detection of aversive compounds – activation of bitter GRNs and inhibition of sweet GRNs (Jeong et al., 2013, French et al., 2015, Charlu et al., 2013). Our results posit that both of these mechanisms exist in pharyngeal GRNs as well. In contrast to a recent study of labellar salt taste, which found that high salt activates sweet neurons (*Gr64f*) (Jaeger et al., 2018), we observe that high salt can inhibit pharyngeal *Gr43a* neurons in calcium imaging experiments, suggesting an intriguing common mechanism for multiple categories of aversive compounds to inhibit neuronal activities of appetitive neurons. A previous study also showed that behavioral avoidance of bitter compounds is well-correlated with the extent of sweet GRN inhibition in the labellum (Sellier et al., 2011), suggesting the sweet GRN inhibition might be a better predictor for behavioral avoidance of sugar/bitter mixtures as compared to bitter GRN activation. Although we did not successfully isolate specific populations of pharyngeal neurons that mediate feeding avoidance of high salt,

we provide evidence that sweet neurons and other *Ir*-expressing neurons are both required for full feeding avoidance of high salt in our behavioral assays. Unlike those of external GRNs (Delventhal et al., 2014, Ling et al., 2014, Weiss et al., 2011, Marella et al., 2006, Shankar et al., 2016), physiological responses of pharyngeal GRNs have not been well studied, in large part due to their inaccessible location for electrophysiological analyses and the necessity of active ingestion for the purposes of calcium imaging of presynaptic terminals (Benton and Dahanukar, 2011, Ledue et al., 2015). New methods that allow for assessing the sensitivity and receptivity of pharyngeal GRNs, and comparing the tastant spaces sampled by internal and external organs, would be invaluable.

By focusing on the minimal pharyngeal taste system, we created a map of pharyngeal inputs and their corresponding second-order pharyngeal taste neurons, using the newly developed circuit-tracing technique, trans-Tango (Talay et al., 2017). We show that pharyngeal second-order neurons convey information to areas (pars intercerebralis and lateral protocerebrum) that also receive external taste input. Thus, pharyngeal taste circuits offer a tractable model to analyze the anatomy and function of taste circuitry and its intersections with higher-order brain functions. Notably, several neuroendocrine cells in the pars intercerebralis, including insulin-producing cells (IPCs), DH44, and SIFamidergic neurons, have been implicated in nutrient-sensing and feeding behaviors (Martelli et al., 2017, Yang et al., 2018, Dus et al., 2015, Soderberg et al., 2012, Broughton et al., 2010). The smaller numbers of pharyngeal second-order neurons

uncovered in our study would facilitate future functional analyses of responses properties of second-order taste neurons and their anatomical connectivity with brain neuroendocrine/nutrient-sensing cells.

Among GRNs, those residing in the pharynx are unique because a subset of them persist through metamorphosis (Gendre et al., 2004). Thus, the pharynx may represent a unique site where information about sensory experience is maintained and transferred from the larval stages to adult stage. Interestingly, taste neurons in the pharynx, but not in other taste organs, regulate oviposition preference for non-appetitive substrates (Joseph and Heberlein, 2012), indicating that flies are capable of remembering a previously encountered non-appetitive substrate to which they return to lay eggs. It would be of interest to examine trans-metamorphic taste memory in flies, and pinpoint the involvement of specific pharyngeal GRNs. Future studies in this direction would yield insight into peripheral taste coding, and may also lead to the discovery of novel deterrent compounds for controlling insect disease vectors and agricultural pests in a manner that abolishes the need to apply repellants or pesticides continually.

EXPERIMENTAL PROCEDURES

Fly strains. Flies were reared on standard cornmeal-dextrose-agar food at 25°C and 60-70% relative humidity under a 12 h:12 h dark:light cycle. The following fly lines were used: *Poxn*$^{\Delta M22\text{-}B5}$ (Boll and Noll, 2002), *Poxn*^{70} (Awasaki and Kimura, 1997), *Gr-GAL4* (Ling et al., 2014, Weiss et al., 2011), *Gr66a-GAL4* (BDSC#28801), *Ir-GAL4* (Koh et al., 2014), *Ir25a-GAL4* (BDSC#41728), *Ir100a-GAL4* (BDSC#41743), *Ir76b-GAL4* (BDSC#41730), *ppk28-GAL4* (Cameron et al., 2010), *UAS-CsChrimson* (BDSC#55136), *UAS-GCaMP6s* (BDSC#42748), *trans-Tango* (Talay et al., 2017). For experiments using *Poxn* mutants, we confirmed the *Poxn* mutant background in all sorted flies by scoring the transformed long and bent mechanosensory hairs in the labellum, and three fused distal segments in the tarsi.

Chemicals. Tastants obtained from Sigma-Aldrich were as follows: sucrose (S7903), denatonium benzoate (D5765), lobeline hydrochloride (141879), coumarin (C4261), quinine hydrochloride dihydrate (22630), papaverine hydrochloride (P3510), caffeine (C8960), theophylline (T1633), DEET (36542), strychnine hydrochloride (S8753) and L-tartaric acid (251380). Sodium chloride was obtained from Macron Chemical (7581-06). All tastants were dissolved in water.

Binary choice feeding assays. Feeding preference assays were performed as described previously (Charlu et al., 2013). Briefly, flies were sorted into groups of 10 males and 10 females upon eclosion and aged for 5-8 days. Since *Poxn* mutant male flies are sterile, we

added 2 heterozygous males with curly wings (*Poxn/CyO*) in each group to ensure that all sorted females were mated. Heterozygous males were discarded while scoring for abdominal color. Flies were starved for 24 hr on water-saturated tissues and then placed in tight-fit Petri dishes (Falcon, #35-1006) with eighteen 10 μL dots of 0.75% agarose that alternated in tastant and color using either 25 mg/mL indigo carmine (Sigma, #I8130) or 50 mg/mL sulforhodamine B (Sigma, #230162). We used sulforhodamine B for aversive tastants and indigo carmine for the sucrose control in **Figure 3.1A-D**. For the binary choice feeding assays in **Figures 3.3, 3.6, and 3.8**, we swapped dyes for each tastant with similar numbers of trials to account for any dye preference. We observed a strong dye preference for sulforhodamine B that resulted in a bimodal distribution of all data points in flies that lost most if not all taste sensing ability (e.g. *Poxn, Ir25a-silenced* flies in **Figure 3.3B**). Flies were allowed to feed for 2 hours at 25°C in a dark, humidified chamber, after which they were frozen and scored for abdomen color by dissecting the guts within 24 hours. Each experiment was performed between ZT 2 and ZT 8. Trials with participation lower than 50% were excluded. Preference index (PI) was calculated as ((# of flies labeled with the tastant color) – (# of flies labeled with the control color))/(total number of flies that fed). Thus, a PI of 0 would indicate an equal preference between the two choices. In all cases, PI values were calculated for mixed populations of males and females.

Activity recording CAFE assay (ARC). Total food intake, meal size, and meal frequency data were collected using the ARC as described previously (Murphy et al.,

2017). Male flies were maintained on standard medium until 5-8 days old. The day before the experiment, the animals were loaded by mouth pipette into standard ARC chambers, one fly per well, and allowed to acclimate overnight with access to 5% sucrose + 5% yeast extract food in a glass capillary pipet (VWR 53432-706). Capillaries were switched the next day to those containing test diets (typically at ZT 6) and the meniscus level of each capillary was tracked for 24 hours. Drops in meniscus position above the threshold were considered feeding events, and feeding bouts less than 2 minutes apart were considered to be part of the same meal. The identity of the test diets was blinded to the experimenters throughout the assay.

Optogenetic activity recording CAFE assay (Optogenetic ARC). Optogenetic stimulation of single pharyngeal GRNs in the ARC was run as described above with the following alterations. Flies were reared and maintained in darkness, and transferred to standard medium containing 400 μM all-trans retinal (ATR, Sigma, #R2500) upon eclosion. Standard ARC chambers were modified such that a red LED (625nm; LEDsupply CREEXPE2-RED-1) was placed directly behind the tip of each experimental capillary. A standard webcam (Microsoft LifeCam Studio), an Arduino microcontroller (Arduino Uno), and a custom Python script based on OpenCV were used to control the LEDs and automatically track food level at 20 Hz. The current position of each meniscus was compared to the average of its positions in the 60 preceding frames (moving average) to account for the discrete nature of pixel values and increase spatial sensitivity. A

suprathreshold drop in the meniscus position, relative to the moving average, was used as a proxy indicator of food consumption for each animal. We used a threshold value of 0.0175 pixel, which was empirically determined to limit false positive rate to below 1.5%. Each detection of feeding immediately triggered the onset of the respective LED for 5 seconds. Thus, all consumption events elicited a minimum of 5 seconds of stimulation, and the duration of stimulation was directly proportional to the duration of the particular feeding event. 100 mM sucrose solution was used as the test diet for all optogenetic experiments in the ARC, and each experiment started around ZT 2 and ran for 6 hours.

Radiolabeled food intake measurement. Total consumption of radiolabeled medium was measured as described previously (Deshpande et al., 2014). Briefly, mixed sex groups of flies were maintained on standard medium until the start of the experiment and the flies were 5-8 days old. Flies were transferred to vials containing [α-32P]-dCTP (PerkinElmer, Cat#NEG013H100UC) labeled diets (typically at ZT 3). After 24 hours, flies were collected in empty vials and frozen. Flies were subsequently sorted by sex for liquid scintillation counting. Total consumption was calculated using aliquots of the radiolabeled medium as a calibration.

Calcium imaging. Calcium imaging of cell bodies in the pharynx was performed as described with some modifications (Joseph et al., 2017). Briefly, 1-week old male and female flies expressing *UAS-GCaMP6s* driven by *Gr43a-GAL4* or *Ir94f-GAL4* were

starved overnight at 25ºC and 60-70% relative humidity. Mated females were then decapitated, and the labial palps of the labellum were carefully excised using a sharp razor blade to increase access to pharyngeal sensilla. Heads were mounted in a minimal volume of water on a microscope slide with three 18×18 mm bridging slips, placed to make two channels between the bridging slips, which allowed liquid to perfuse through the sample. A 22×40 mm coverslip was secured with nail polish on top of the bridging slips, positioned approximately 20 mm from the edge of microscope slide, to allow placement of tastant solution. *UAS-GCaMP6s* fluorescence was viewed with an upright Zeiss 510 confocal or an inverted Leica SP5 confocal microscope. Neurons were visualized with a 10× objective, with a digital zoom of 4-5. Images were acquired at 512×512 resolution with no line averaging, with one frame scanned per second. The pinhole was calibrated to an optical slice of 100 μm, with the 488 nm laser at 25% power. Changes in fluorescent activity were recorded for 4 minutes after delivery of the stimulus. Before stimulus, focal landmarks were identified in the primary channel used to detect green fluorescent activity of the GCaMP reporter, and in a secondary channel (either DIC or a fluorescence channel outside the activation/detection range of GCaMP) used to image the pharyngeal structure during the experiment. These focal landmarks were monitored throughout the assay, to ensure that the sample remained in the correct plane of focus. If the sample shifted slightly out-of-focus along the z-axis, the preparation was refocused to the reference landmarks. The out-of-focus frames were excluded from the $(\Delta F/F)_{MAX}$ calculations, depicted as gaps in representative traces (**Figures 3.9 and 3.10**). Fluorescence intensities were obtained with open-source Fiji/ImageJ software

(https://fiji.sc). A region-of-interest (ROI) was drawn around individual cell bodies; an ROI of identical dimensions was also placed over a non-neuronal area of the image, which was used as a reference for measuring any non-specific background changes in fluorescence. Average pixel intensity for ROIs during each frame was measured with the Time-Series Analyzer Plugin, written by Balaji, J. (https://imagej.nih.gov/ij/plugins/time-series.html). A corrected average intensity for the cell body ROI was measured in each frame by subtracting the average intensity of the background ROI from the average intensity of the cell body ROI. Maximum changes in fluorescent activity were calculated as: $(\Delta F/F)_{MAX}$ = [(corrected intensity of ROI) – (average corrected intensity of 10 frames preceding stimulus)] / (average corrected intensity of 10 frames preceding stimulus). $(\Delta F/F)_{MAX}$ were then determined for either the entire 3-min sampling period or in binned 30-sec intervals, following the stimulus.

trans-Tango. For tracing pharyngeal second-order taste circuits, we recombined *Poxn*^{70} with *trans-Tango* transgenes to create *Poxn*^{70}*, trans-Tango*. Genetic crosses for tracing different pharyngeal *chemoreceptor-GAL4*-labeled GRNs in a *Poxn* mutant background were maintained at 18^{o}C. Flies were tested when about 1-month-old, anesthetized on ice, and dissected for brain tissue in 1× PBST (PBS with 0.3% Triton X-100). Brains were fixed for 30 min with 4% paraformaldehyde in 1× PBST at room temperature. After three washes with 1× PBST, samples were blocked with 5% normal goat serum (Sigma, #G9023) in 1× PBST. Tissues were incubated in primary antibody solutions for 3 days at 4^{o}C. Primary antibodies were: chicken anti-GFP (1:5000; Abcam, #ab13970), rabbit anti-

DsRed (1:200; Clontech, #632496), and mouse anti-nc82 (1:20; Developmental Studies Hybridoma Bank). Secondary antibodies (1:400; Invitrogen) were: goat anti-chicken Alexa Fluor 488, goat anti-rabbit Alexa Fluor 568, and goat anti-mouse Alexa Fluor 647. Samples were mounted in 80% glycerol in 1× PBST or VECTASHIELD antifade mounting medium (Vector Laboratories, #H-1000) and stored at 4^{o}C. Fluorescent images are acquired using a Leica SP5 confocal microscope with 400 Hz scan speed in 512×512 or 1024×1024 pixel formats. Image stacks were acquired at 1 μm optical sections. Unless otherwise noted, all images were presented as maximum projections of *z*-stacks generated using Leica LAS AF software.

Statistical analyses. Unless otherwise noted, all data are presented as median ± interquartile range. Linear regression and correlation analyses were performed using Origin 8.0 software. Statistical tests were conducted using Prism 8. For ARC data in **Figures 3.2 and 3.4**, the differences between means of control and *Poxn* mutant flies were evaluated with two-way ANOVA followed by *post-hoc* Sidak's multiple comparisons test. For Ca^{2+} imaging data in **Figure 3.5**, the GCaMP6s fluorescence changes between different tastants were evaluated with Kruskal-Wallis test followed by Dunn's multiple comparisons test. To analyze the differences between transgene controls and experimental groups (planned comparisons) in **Figures 3.3, 3.6, and 3.8**, we first checked the distribution of the data with a Kolmogorov-Smirnov test for normality. If the data was not normally distributed, a Kruskall-Wallis test followed by the uncorrected Dunn's test was used. If data was normally distributed, we used parametric one-way

ANOVA followed by the uncorrected Fisher's LSD test. In addition, the One sample t test (for normally distributed data) and Wilcoxon signed rank test (for not normally distributed data) were used to compare whether the preference indices in **Figures 3.3, 3.6, and 3.8** were significantly different from 0, which represents no preference for either tastant in the binary choice feeding assays. All experiments were performed in parallel with both control and experimental genotypes. All independent trials were performed over 2 days. Complete genotypes used in this study are listed in **Table 3.1**. The sample size for each experiment was based on previously published reports.

FIGURES

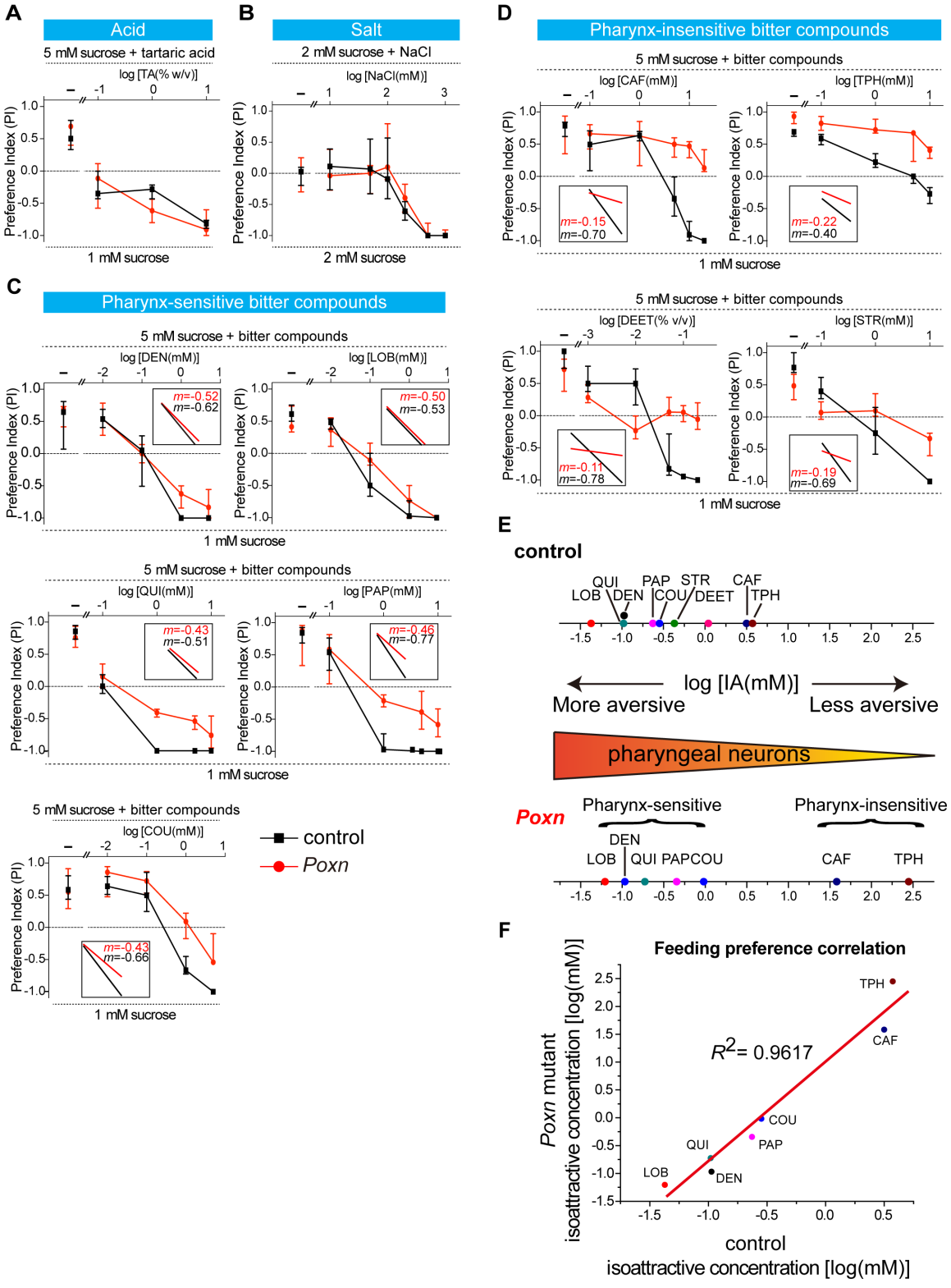
A
Acid
5 mM sucrose + tartaric acid
log [TA(% w/v)]
Preference Index (PI)
1 mM sucrose
B
Salt
2 mM sucrose + NaCl
log [NaCl(mM)]
2 mM sucrose
C
Pharynx-sensitive bitter compounds
5 mM sucrose + bitter compounds
log [DEN(mM)]
m=-0.52
m=-0.62
log [LOB(mM)]
m=-0.50
m=-0.53
log [QUI(mM)]
m=-0.43
m=-0.51
log [PAP(mM)]
m=-0.46
m=-0.77
log [COU(mM)]
m=-0.43
m=-0.66
control
Poxn
D
Pharynx-insensitive bitter compounds
log [CAF(mM)]
m=-0.15
m=-0.70
log [TPH(mM)]
m=-0.22
m=-0.40
log [DEET(% v/v)]
m=-0.11
m=-0.78
log [STR(mM)]
m=-0.19
m=-0.69
E
control
QUI
LOB
DEN
PAP
COU
STR
DEET
CAF
TPH
log [IA(mM)]
More aversive
Less aversive
pharyngeal neurons
Poxn
Pharynx-sensitive
Pharynx-insensitive
F
Feeding preference correlation
Poxn mutant isoattractive concentration [log(mM)]
control isoattractive concentration [log(mM)]
R2= 0.9617

Figure 3.1. *Pox neuro* (*Poxn*) flies display feeding avoidance of aversive tastants.

(**A–D**) Results of binary feeding choice assays with sucrose alone tested against mixtures of sucrose with named aversive compounds; concentrations for all tastants as indicated. The dotted lines at PI=0 indicate an equal preference for the two choices. Insets in (**C-D**) show trend lines and slopes derived from linear regression analysis. Genotypes were control (w^{1118}) and *Poxn* ($Poxn^{\Delta M22\text{-}B5}/Poxn^{70}$). *n*=3-16. Error bars = interquartile range. (**E**) Scale depicting log[IA] values for tested bitter compounds in control (top) and *Poxn* mutant flies (bottom). Compounds are labeled as "pharynx-sensitive" or "pharynx-insensitive" based on an arbitrary cut-off at a value of –0.25 for the slopes (*m*) of trend lines derived from linear regression analyses for *Poxn* mutant data shown in (**C–D**). (**F**) A plot of log[IA] derived from *Poxn* flies versus control flies. The red lines indicate the trend lines derived from the linear regression analysis.

In all plots: CAF, caffeine; COU, coumarin; DEET, N,N-diethyl-*meta*-toluamide; DEN, denatonium; LOB, lobeline; PAP, papaverine; QUI, quinine; STR, strychnine; TA, tartaric acid; TPH, theophylline.

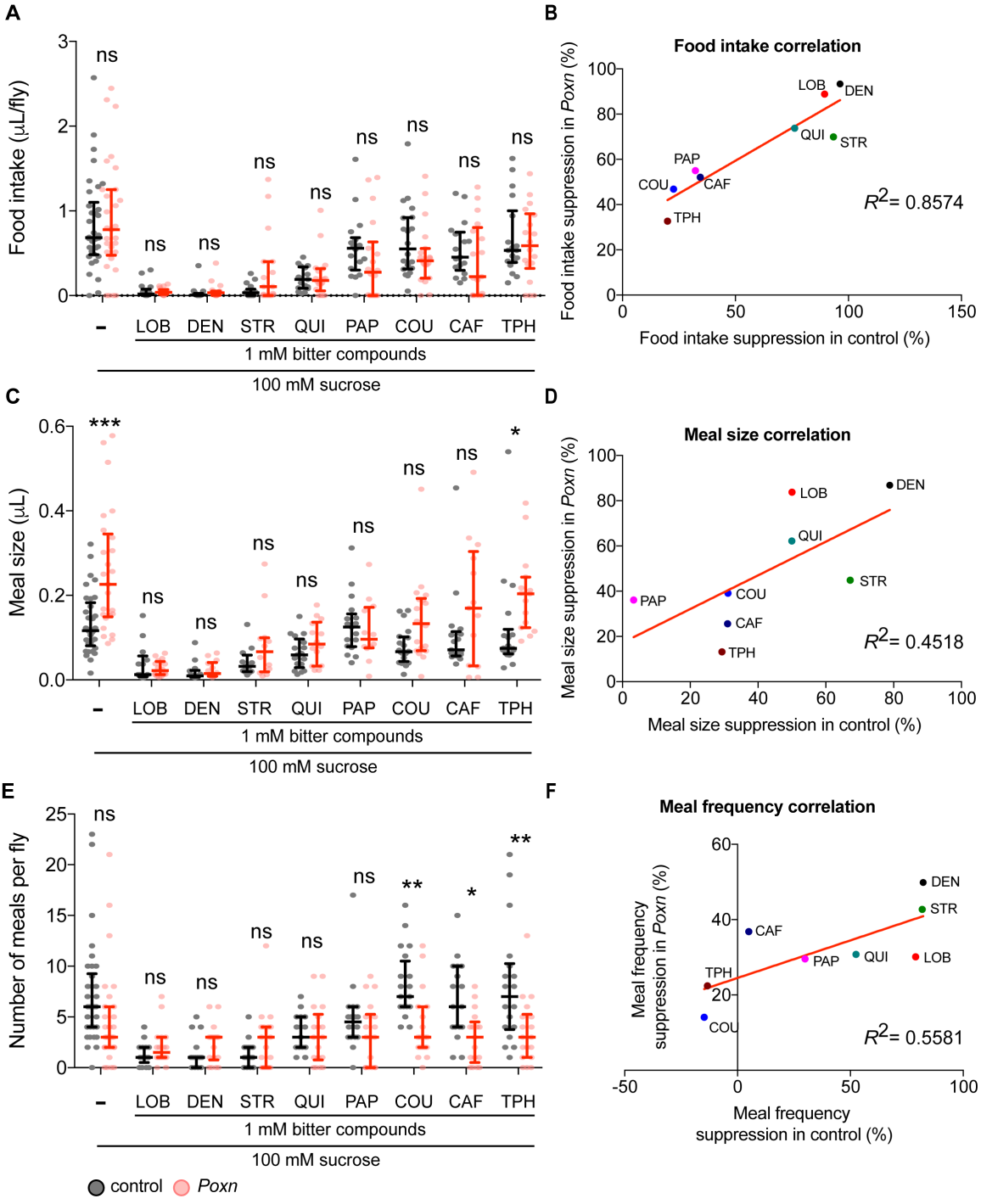

Figure 3.2. *Poxn* flies display suppression of food intake by aversive tastants.

(**A,C,E**) Total food intake (**A**), meal size (**C**), and meal frequency (**E**) of individual flies to 100 mM sucrose alone or 100 mM sucrose with 1 mM bitter mixtures from individual

flies over a 24-hour period. *$P < 0.05$, **$P < 0.01$, ***$P < 0.001$ versus control, two-way ANOVA with *post-hoc* Sidak's multiple comparisons test. ns, not significant. (**B,D,F**) Comparisons of food intake (**B**), meal size (**D**), and meal frequency (**F**) derived from *Poxn* flies versus control flies. Red lines indicate trend lines derived from linear regression analyses. Genotypes were control (w^{1118}) and *Poxn* ($Poxn^{\Delta M22\text{-}B5}/Poxn^{70}$). n=12-34. Error bars = interquartile range.

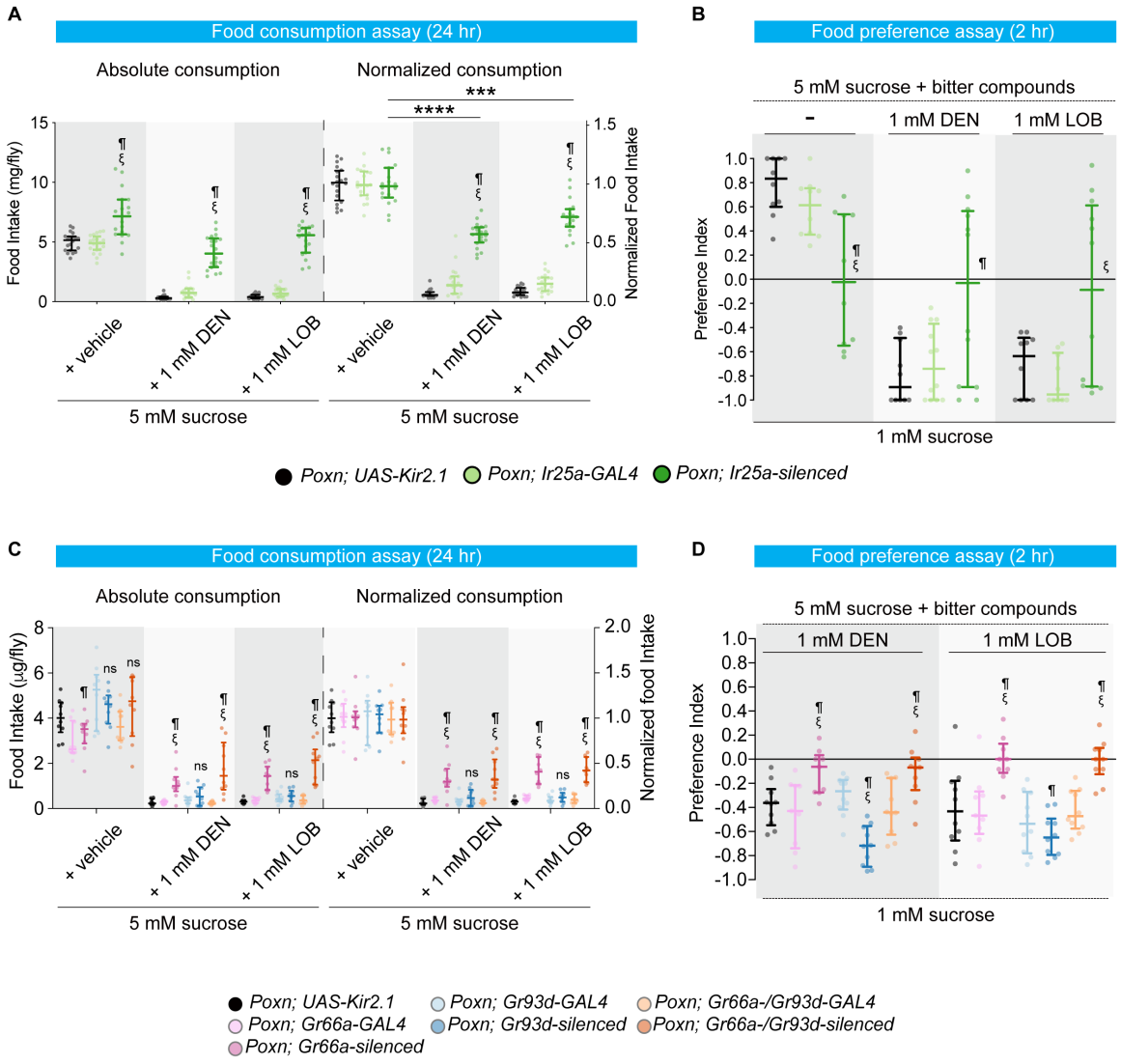

Figure 3.3. Pharyngeal GRNs are required for intake suppression and feeding avoidance of bitter compounds.

(**A,C**) Food intake measurement for 5 mM sucrose alone or mixed with 1 mM bitter compounds over a 24-hour period. The absolute food intake shown on the left was normalized to vehicle control as normalized food intake shown on the right. *n*=10-20. Error bars = interquartile range. All genetics manipulations with *Ir25a-GAL4* (**A**), *Gr66a-GAL4*, *Gr93d-GAL4* (**C**) were performed in a *Poxn* mutant background (*Poxn*$^{\Delta M22-}$

^{B5}/*Poxn*^{70}). ¶ and ξ indicate a statistically significant difference from the *UAS* and *GAL4* controls, respectively, by two-way ANOVA followed by Tukey's multiple comparison test. ***$P < 0.001$, ****$P < 0.0001$ versus vehicle, one-way ANOVA with *post-hoc* Tukey's multiple comparisons test in *Poxn, Ir25a-silenced* flies.

(**B,D**) Feeding preference for 5 mM sucrose mixed with 1 mM denatonium or lobeline against 1 mM sucrose is shown on a scale of -1 to +1. *n*=9-12. Error bars = interquartile range. All genetics manipulations with *Ir25a-GAL4* (**B**), *Gr66a-GAL4*, *Gr93d-GAL4* (**D**) were performed in a *Poxn* mutant background (*Poxn*$^{\Delta M22\text{-}B5}$/*Poxn*^{70}). ¶ and ξ indicate a statistically significant difference from the *UAS* and *GAL4* controls, respectively, by one-way ANOVA followed by uncorrected Fisher's LSD test or Kruskal-Wallis test followed by uncorrected Dunn's test. The One simple t test or Wilcoxon signed-rank test were used for testing whether the median values for each genotype were different from zero.

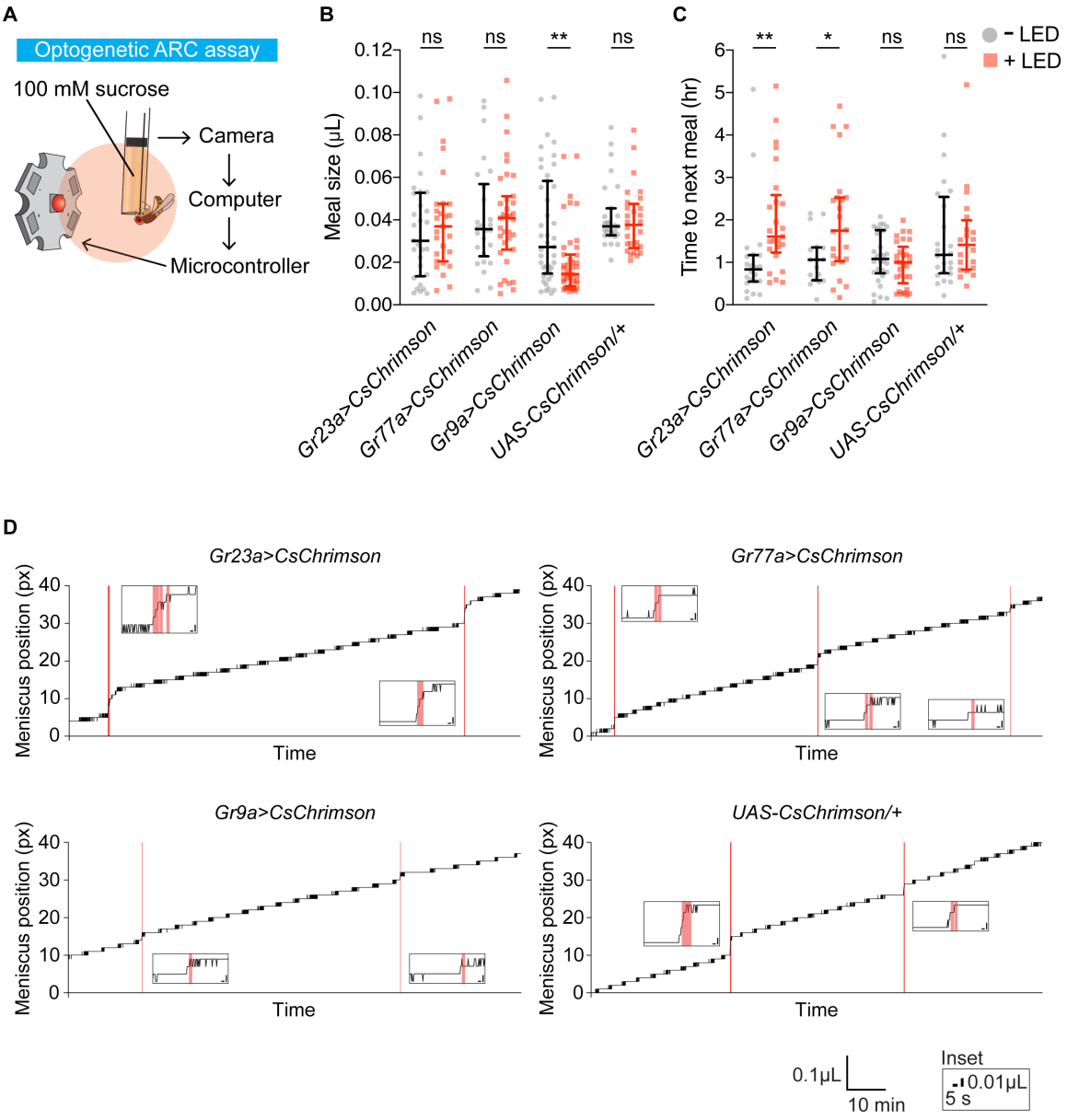

Figure 3.4. Pharyngeal bitter GRNs control different parameters of micro-feeding behaviors to suppress food intake.

(**A**) Schematic diagram of optogenetic ARC showing the setup for closed-looped optical activation of pharyngeal GRNs. Food intake of individual flies is tracked by the computer in real time. When the meniscus of the liquid food drops over a predetermined threshold,

a microcontroller turns on the 625 nm LED for 5 seconds.

(**B-D**) *UAS-CsChrimson* was expressed in single pharyngeal GRNs labeled by *Gr23a-GAL4*, *Gr77a-GAL4*, and *Gr9a-GAL4* in a wild type background. Meal sizes (**B**) and intermeal intervals (**C**) were analyzed. The –LED and +LED groups of the same genotype were compared using two-way ANOVA followed by *post-hoc* Sidak's multiple comparisons test. ns, not significant. n=17-43. *$P < 0.05$, **$P < 0.01$. (**D**) Sample traces of meniscus level tracked over time. A step-like jump in the vertical position of the meniscus represents a feeding event. The red lines indicate the activation of 625 nm LED triggered by food consumption.

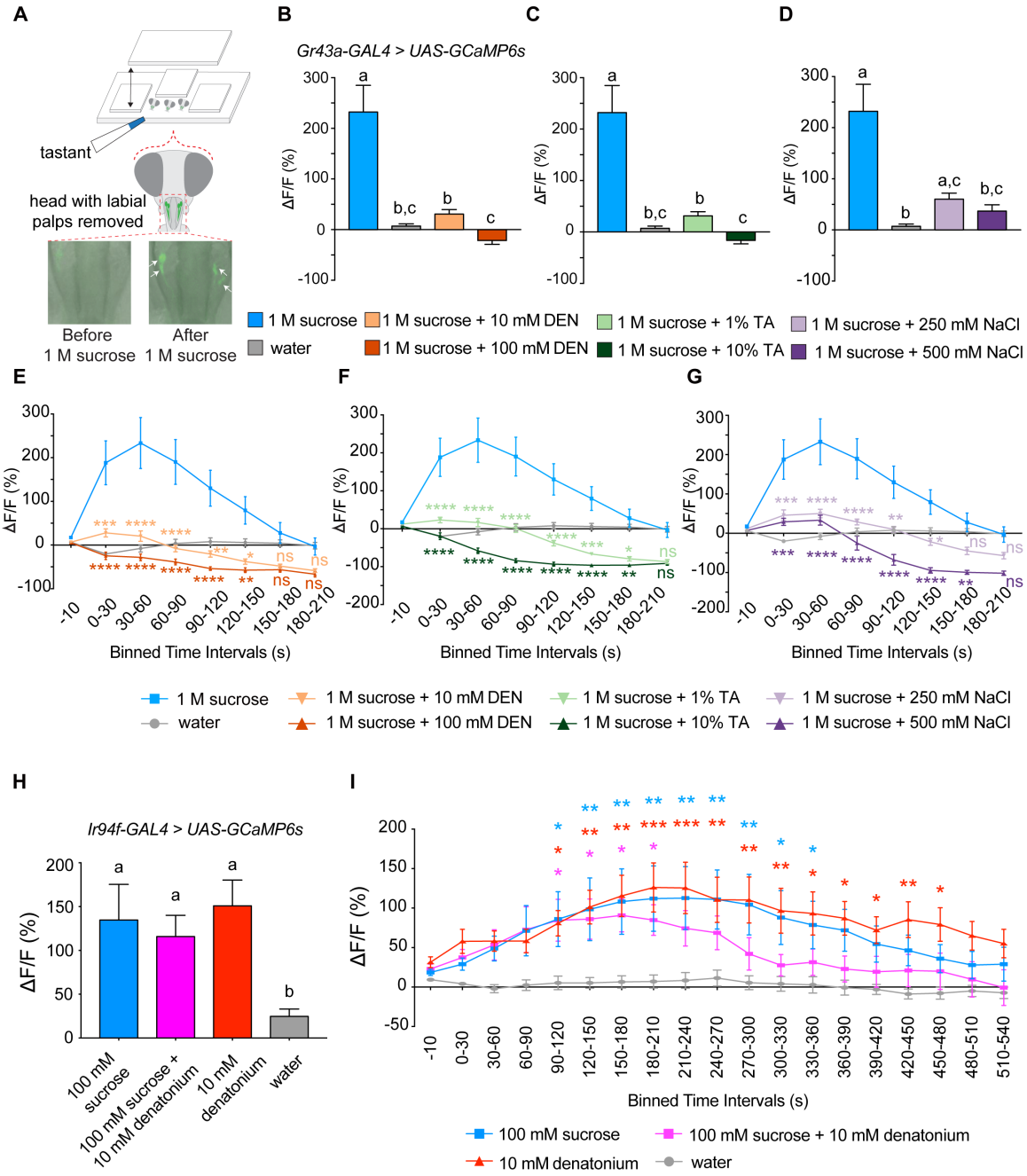

Figure 3.5. Calcium imaging shows that aversive tastants inhibit the activity of pharyngeal sweet GRNs.

(**A**) Schematic diagram of the *ex vivo* pharyngeal calcium imaging setup (top). Flies expressing GCaMP6s calcium indicator in pharyngeal *Gr43a* GRNs were imaged by

confocal microscopy. Representative fluorescence images of pharyngeal *Gr43a* GRNs in the LSO before and after 1 M sucrose stimulus (bottom). Arrows indicate the cell bodies of the pharyngeal *Gr43a* GRNs.

(**B-D**) Peak changes of GCaMP6s fluorescence in pharyngeal *Gr43a* GRNs to 1 M sucrose alone or mixed with 10 mM or 100 mM denatonium (**B**), 1% or 10% tartaric acid (**C**), or 250 mM or 500 mM NaCl (**D**). Different letters indicate significantly different groups by Kruskal-Wallis test followed by Dunn's multiple comparison test. n=11-28. Error bars = SEM.

(E-G) Time course of change in fluorescence (ΔF/F) for samples that received indicated stimuli. ΔF/F values are binned into 30-second intervals after application of stimulus. Asterisks indicate significant difference from 1 M sucrose by two-way ANOVA followed by Tukey *post hoc* test. *$P < 0.05$, **$P < 0.01$, ***$P < 0.001$, ****$P < 0.0001$.

(**H**) Peak changes of GCaMP6s fluorescence in pharyngeal *Ir60b* GRNs labeled by *Ir94f-GAL4* to 100 mM sucrose alone, mixture of 100 mM sucrose with 10 mM denatonium, or 10 mM denatonium alone. Different letters indicate significantly different groups by Kruskal-Wallis test followed by Dunn's multiple comparison test. n=8-10. Error bars = SEM.

(**I**) Time course of change in fluorescence (ΔF/F) for samples that received indicated stimuli. ΔF/F values are binned into 30-second intervals after application of stimulus. Asterisks indicate significant difference from water alone by two-way ANOVA followed by Tukey *post hoc* test. *$P < 0.05$, **$P < 0.01$, ***$P < 0.001$.

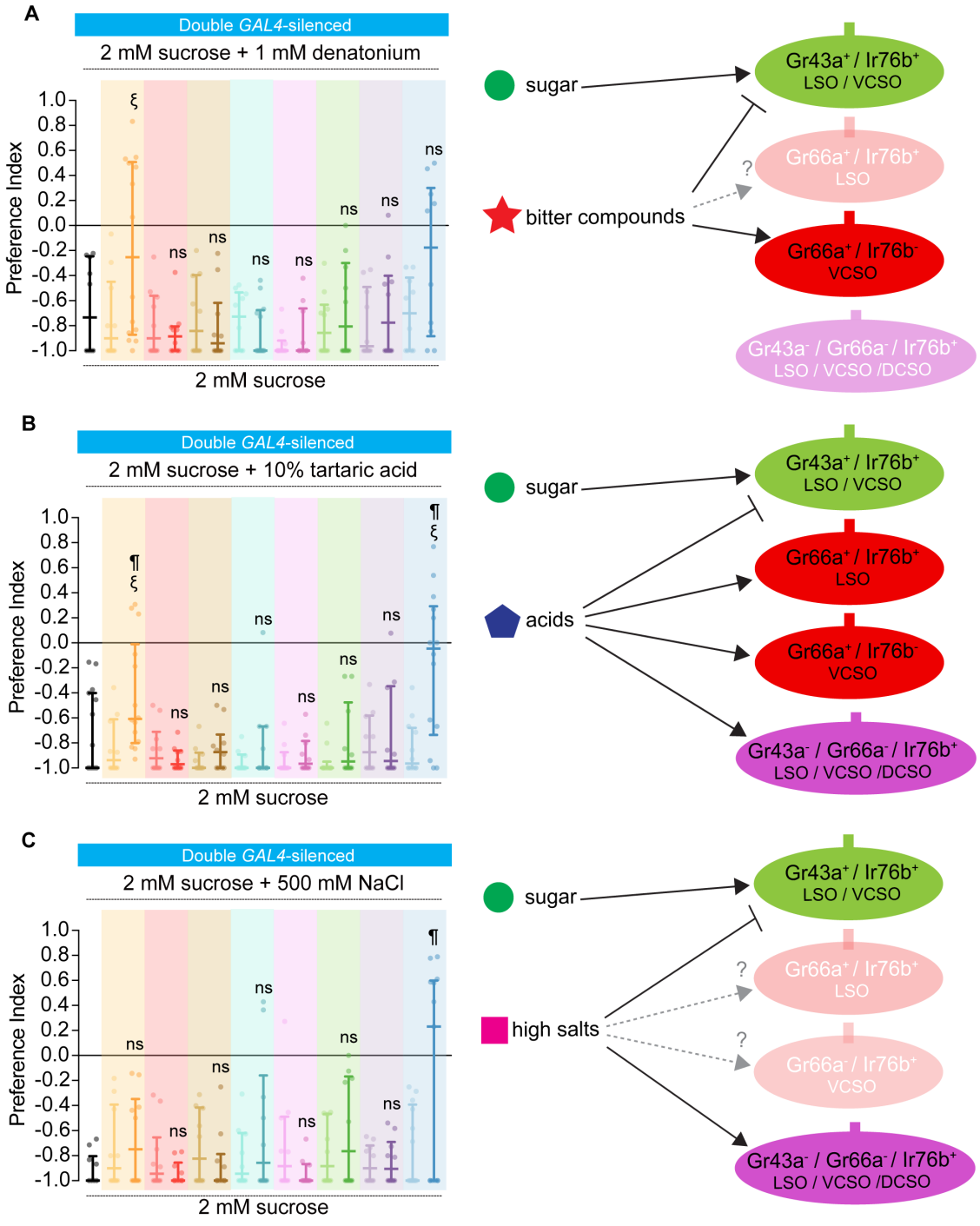

- *Poxn; UAS-Kir2.1*
- *Poxn; Gr64e-/Gr66a-GAL4*
- *Poxn; Gr64e-/Gr66a-silenced*
- *Poxn; Gr64e-/Gr93d-GAL4*
- *Poxn; Gr64e-/Gr93d-silenced*
- *Poxn; Gr64e-/ppk28-GAL4*
- *Poxn; Gr64e-/ppk28-silenced*
- *Poxn; Gr64e-/Ir20a-GAL4*
- *Poxn; Gr64e-/Ir20a-silenced*
- *Poxn; Gr64e-/Ir67c-GAL4*
- *Poxn; Gr64e-/Ir67c-silenced*
- *Poxn; Gr64e-/Ir94f-GAL4*
- *Poxn; Gr64e-/Ir94f-silenced*
- *Poxn; Gr64e-/Ir100a-GAL4*
- *Poxn; Gr64e-/Ir100a-silenced*
- *Poxn; Ir76b-GAL4*
- *Poxn; Ir76b-silenced*

Figure 3.6. Distinct combinations of pharyngeal GRNs are required for feeding avoidance of different aversive tastants.

Mean preference index values of *Poxn* ($Poxn^{\Delta M22\text{-}B5}/Poxn^{70}$) mutants carrying indicated transgenes obtained from binary choice experiments with 2 mM sucrose mixed with 1 mM denatonium (**A**), 10% tartaric acid (**B**), or 500 mM NaCl (**C**) tested against 2 mM sucrose alone. *UAS-Kir2.1* and *Gr/Ir-GAL4* transgenes were tested independently as indicated, or together (*Gr/Ir-silenced*). The schematics on the right depict how bitter compounds, tartaric acid, and high salts are each detected by multiple classes of pharyngeal GRNs. The oval shapes depict different classes of pharyngeal GRNs defined by the chemosensory receptor expression from our previous study (Chen and Dahanukar, 2017). LSO, labral sense organ; VCSO, ventral cibarial sense organ; DCSO, dorsal cibarial sense organ. *n*=10-15. Error bars = interquartile range. ¶ and ξ indicate a statistically significant difference from the *UAS* and *GAL4* controls, respectively, by one-way ANOVA followed by uncorrected Fisher's LSD test or Kruskal-Wallis test followed by uncorrected Dunn's test. The One simple t test or Wilcoxon signed-rank test were used for testing whether the median values for each genotype were different from zero.

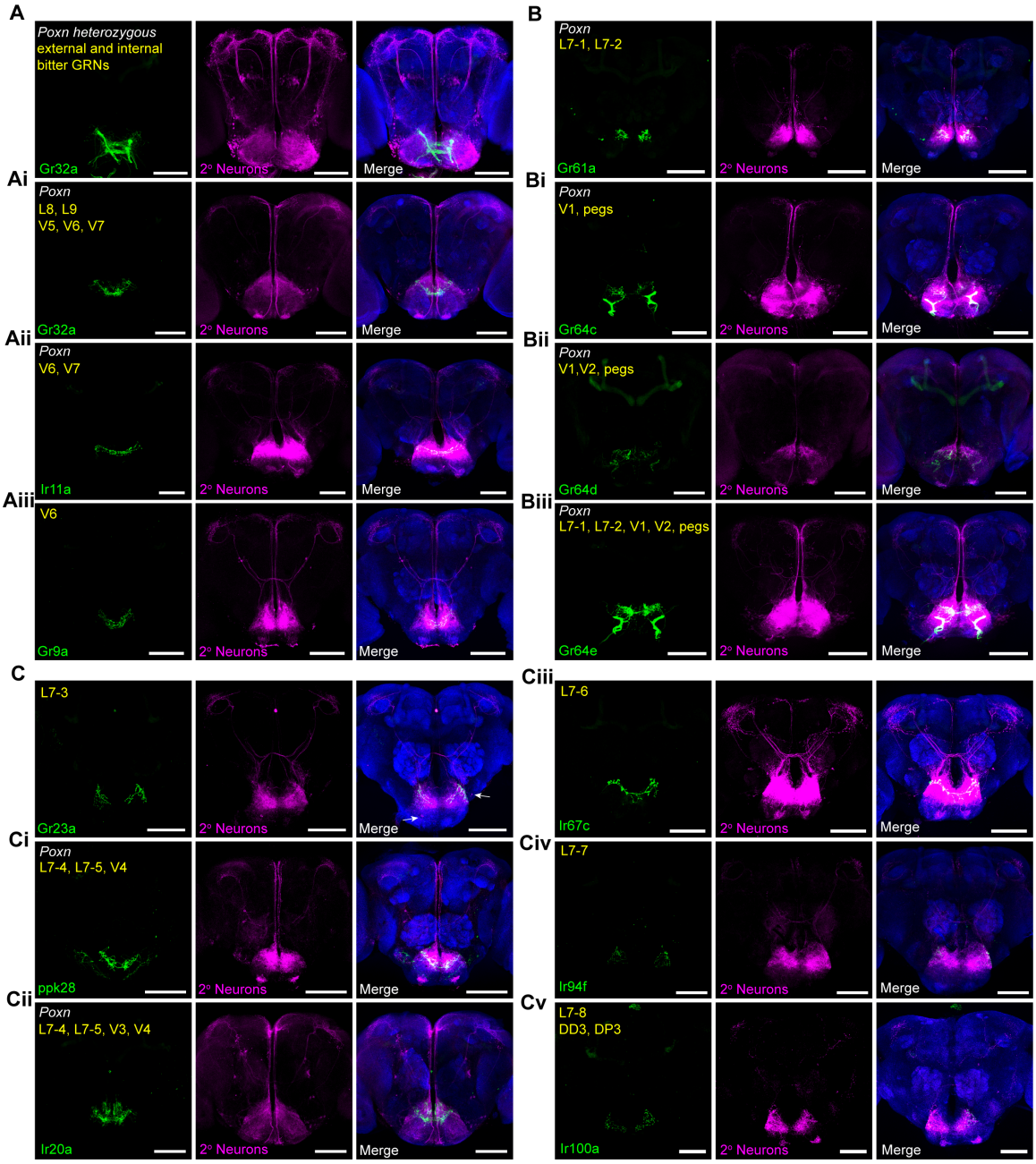

Figure 3.7. trans-Tango tracing of second-order pharyngeal neurons reveals two main higher-order regions that receive taste input.

Examples demonstrating use of trans-Tango system to map second-order taste neurons (magenta) that connect with bitter (**A**), sweet (**B**), or other classes (**C-D**) of pharyngeal

GRNs (green). The nomenclature of pharyngeal GRNs established in our previous study was used (Chen and Dahanukar, 2017). Note the reduced number of second-order taste neurons labeled in *Poxn/Poxn* homozygous versus *Poxn/+* heterozygous backgrounds (**A-Ai**). Unless otherwise noted as *Poxn*, staining was performed in a wild type background for some drivers, such us *Gr9a-*, *Gr23a-*, *Ir67c-*, *Ir94f-* and *Ir100a-GAL4*.

SUPPLEMENTAL FIGURES

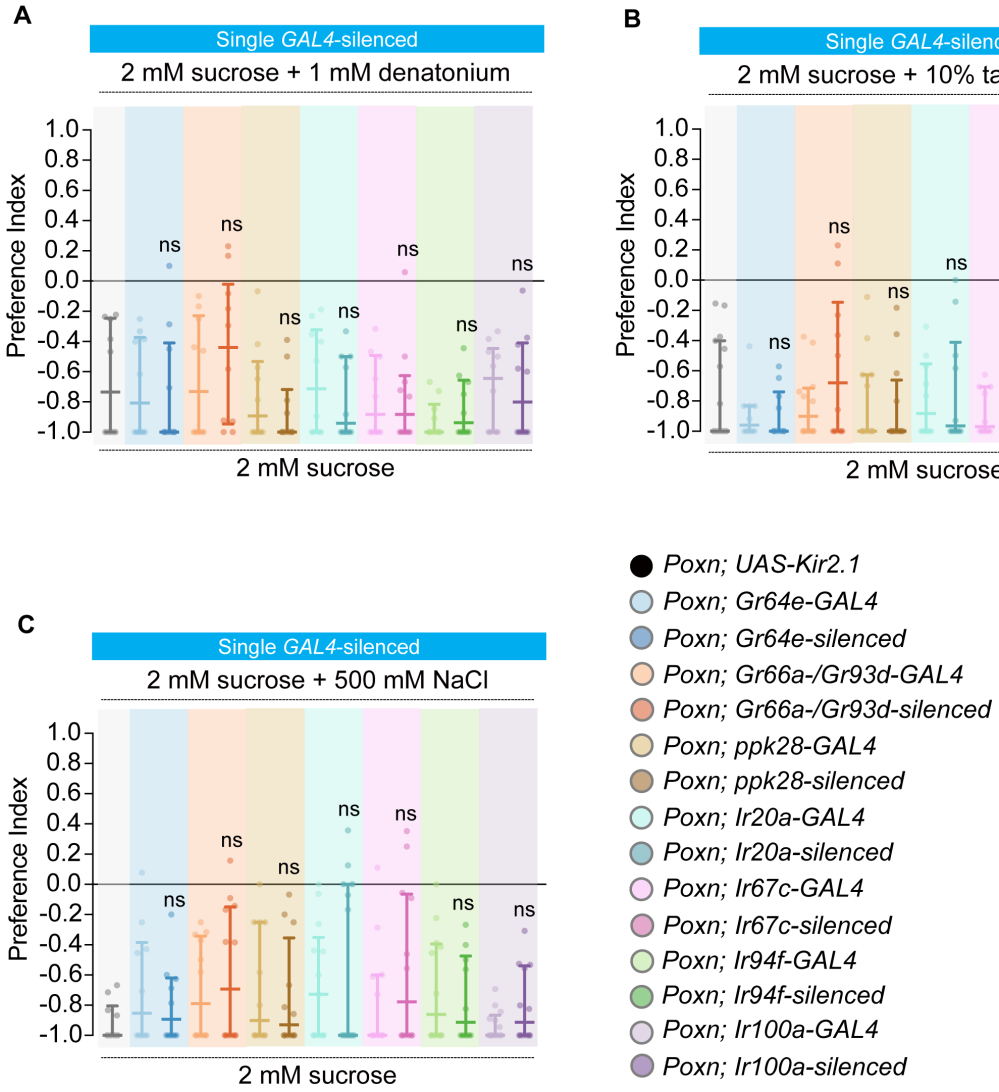

Figure 3.8, related to Figure 3.3. Multiple classes of pharyngeal GRNs are functionally redundant for driving feeding avoidance of aversive compounds.

Preference indices for sucrose/denatonium (**A**), sucrose/tartaric acid (**B**), or sucrose/high salt (**C**) mixtures tested with sucrose alone in *Poxn* ($Poxn^{\Delta M22\text{-}B5}/Poxn^{70}$) mutants carrying indicated transgenes. *UAS-Kir2.1* and *Gr/Ir-GAL4* transgenes were tested independently as indicated, or together (*Gr/Ir-silenced*). *n*=10-14. Error bars = interquartile range. ¶ and

ξ indicate a statistically significant difference from the *UAS* and *GAL4* controls, respectively, by one-way ANOVA followed by uncorrected Fisher's LSD test or Kruskal-Wallis test followed by uncorrected Dunn's test. The One simple t test or Wilcoxon signed-rank test were used for testing whether the median values for each genotype were different from zero.

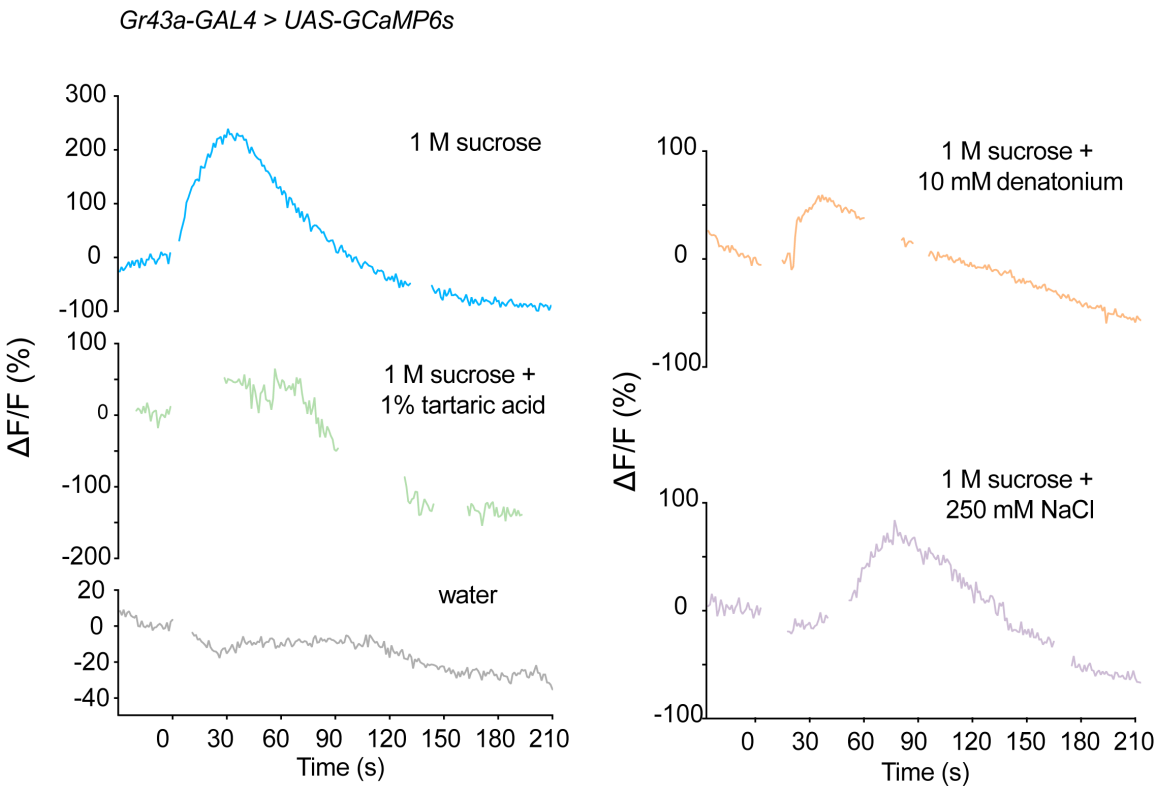

Figure 3.9, related to Figure 3.5. Representative traces of GCaMP6s fluorescence in pharyngeal *Gr43a* GRNs in response to 1 M sucrose alone or mixed with 10 mM denatonium, 1% tartaric acid, 250 mM NaCl, or water alone.

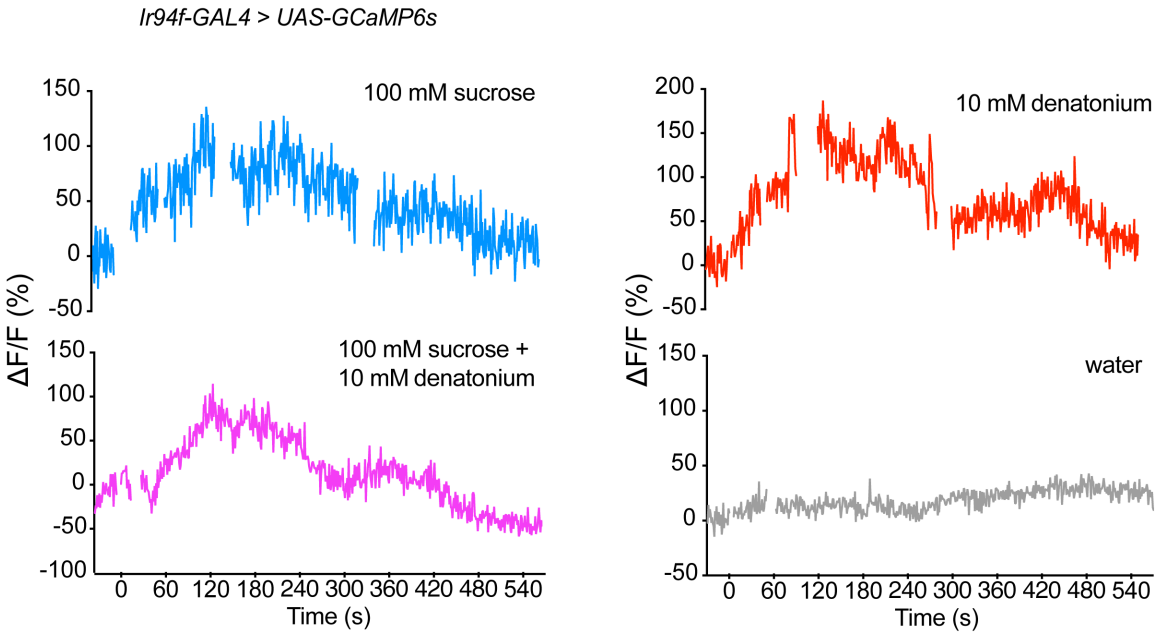

Figure 3.10, related to Figure 3.5. Representative traces of GCaMP6s fluorescence in pharyngeal *Ir60b* GRNs in response to 100 mM sucrose alone, mixture of 100 mM sucrose with 10 mM denatonium, 10 mM denatonium alone, or water alone.

TABLE

Table 3.1. Complete genotypes of flies used in this study.

Figure	Genotype
3.1 and 3.2	control: *w1118*
	Poxn: $Poxn^{\Delta M22\text{-}B5}/Poxn^{70}$
3.3A-B	(from left to right)
	$Poxn^{\Delta M22\text{-}B5}/Poxn^{70}$; *UAS-Kir2.1/+*
	$Poxn^{\Delta M22\text{-}B5}$, *Ir25a-GAL4/*$Poxn^{70}$; *Dr or TM3/+*
	$Poxn^{\Delta M22\text{-}B5}$, *Ir25a-GAL4/*$Poxn^{70}$; *UAS-Kir2.1/UAS-Kir2.1*
3.3C-D	(from left to right)
	$Poxn^{\Delta M22\text{-}B5}/Poxn^{70}$; *UAS-Kir2.1/+*
	$Poxn^{\Delta M22\text{-}B5}/Poxn^{70}$; *Gr66a-GAL4/+*
	$Poxn^{\Delta M22\text{-}B5}/Poxn^{70}$; *Gr66a-GAL4/UAS-Kir2.1*
	$Poxn^{\Delta M22\text{-}B5}/Poxn^{70}$; *Gr93d-GAL4/+*
	$Poxn^{\Delta M22\text{-}B5}/Poxn^{70}$; *Gr93d-GAL4/UAS-Kir2.1*
	$Poxn^{\Delta M22\text{-}B5}$, *Gr66a-GAL4/*$Poxn^{70}$; *Gr93d-GAL4/+*
	$Poxn^{\Delta M22\text{-}B5}$, *Gr66a-GAL4/*$Poxn^{70}$; *Gr93d-GAL4/UAS-Kir2.1*
3.4B-C	(from left to right)
	UAS-CsChrimson/UAS-CsChrimson ; Gr23a-GAL4/Gr23a-GAL4
	UAS-CsChrimson/UAS-CsChrimson ; Gr77a-GAL4/TM3
	UAS-CsChrimson/UAS-CsChrimson ; Gr9a-GAL4/Gr9a-GAL4
3.5A-G	*UAS-GCaMP6s/UAS-GCaMP6s ; Gr43a-GAL4/Gr43a-GAL4*
3.5H-I	*UAS-GCaMP6s/UAS-GCaMP6s ; Ir94f-GAL4/Ir94f-GAL4*
3.6A-C	(from left to right)
	$Poxn^{\Delta M22\text{-}B5}/Poxn^{70}$; *UAS-Kir2.1/+*
	$Poxn^{\Delta M22\text{-}B5}$, *Gr64e-GAL4/*$Poxn^{70}$; *Gr66a-GAL4/+*
	$Poxn^{\Delta M22\text{-}B5}$, *Gr64e-GAL4/*$Poxn^{70}$; *Gr66a-GAL4/UAS-Kir2.1*
	$Poxn^{\Delta M22\text{-}B5}$, *Gr64e-GAL4/*$Poxn^{70}$; *Gr93d-GAL4/+*
	$Poxn^{\Delta M22\text{-}B5}$, *Gr64e-GAL4/*$Poxn^{70}$; *Gr93d-GAL4/UAS-Kir2.1*
	$Poxn^{\Delta M22\text{-}B5}$, *Gr64e-GAL4/*$Poxn^{70}$; *ppk28-GAL4/+*
	$Poxn^{\Delta M22\text{-}B5}$, *Gr64e-GAL4/*$Poxn^{70}$; *ppk28-GAL4/UAS-Kir2.1*
	$Poxn^{\Delta M22\text{-}B5}$, *Ir20a-GAL4/*$Poxn^{70}$; *Gr64e-GAL4/+*
	$Poxn^{\Delta M22\text{-}B5}$, *Ir20a-GAL4/*$Poxn^{70}$; *Gr64e-GAL4/UAS-Kir2.1*

	$Poxn^{\Delta M22\text{-}B5}$, Ir67c-GAL4/$Poxn^{70}$; Gr64e-GAL4/+
	$Poxn^{\Delta M22\text{-}B5}$, Ir67c-GAL4/$Poxn^{70}$; Gr64e-GAL4/UAS-Kir2.1
	$Poxn^{\Delta M22\text{-}B5}$, Gr64e-GAL4/$Poxn^{70}$; Ir94f-GAL4/+
	$Poxn^{\Delta M22\text{-}B5}$, Gr64e-GAL4/$Poxn^{70}$; Ir94f-GAL4/UAS-Kir2.1
	$Poxn^{\Delta M22\text{-}B5}$, Gr64e-GAL4/$Poxn^{70}$; Ir100a-GAL4/+
	$Poxn^{\Delta M22\text{-}B5}$, Gr64e-GAL4/$Poxn^{70}$; Ir100a-GAL4/UAS-Kir2.1
	$Poxn^{\Delta M22\text{-}B5}$, Ir76b-GAL4/$Poxn^{70}$; Dr or TM3/+
	$Poxn^{\Delta M22\text{-}B5}$, Ir76b-GAL4/$Poxn^{70}$; UAS-Kir2.1/UAS-Kir2.1
3.7A	*UAS-myrGFP.QUAS-mtdTomato-3xHA ; $Poxn^{70}$, trans-Tango/Cyo ; Gr32a-GAL4/+*
3.7Ai	*UAS-myrGFP.QUAS-mtdTomato-3xHA ; $Poxn^{\Delta M22\text{-}B5}$/$Poxn^{70}$, trans-Tango ; Gr32a-GAL4/+*
3.7Aii	*UAS-myrGFP.QUAS-mtdTomato-3xHA ; $Poxn^{\Delta M22\text{-}B5}$/$Poxn^{70}$, trans-Tango ; Ir11a-GAL4/+*
3.7Aiii	*UAS-myrGFP.QUAS-mtdTomato-3xHA ; trans-Tango/+ ; Gr9a-GAL4/+*
3.7B	*UAS-myrGFP.QUAS-mtdTomato-3xHA ; $Poxn^{\Delta M22\text{-}B5}$/$Poxn^{70}$, trans-Tango ; Gr61a-GAL4/+*
3.7Bi	*UAS-myrGFP.QUAS-mtdTomato-3xHA ; $Poxn^{\Delta M22\text{-}B5}$/$Poxn^{70}$, trans-Tango ; Gr64c-GAL4/+*
3.7Bii	*UAS-myrGFP.QUAS-mtdTomato-3xHA ; $Poxn^{\Delta M22\text{-}B5}$/$Poxn^{70}$, trans-Tango ; Gr64d-GAL4/+*
3.7Biii	*UAS-myrGFP.QUAS-mtdTomato-3xHA ; $Poxn^{\Delta M22\text{-}B5}$, Gr64e-GAL4/$Poxn^{70}$, trans-Tango ; +/+*
3.7C	*UAS-myrGFP.QUAS-mtdTomato-3xHA ; trans-Tango/+ ; Gr23a-GAL4/+*
3.7Ci	*UAS-myrGFP.QUAS-mtdTomato-3xHA ; $Poxn^{\Delta M22\text{-}B5}$/$Poxn^{70}$, trans-Tango ; ppk28-GAL4/+*
3.7Cii	*UAS-myrGFP.QUAS-mtdTomato-3xHA ; $Poxn^{\Delta M22\text{-}B5}$, Ir20a-GAL4 /$Poxn^{70}$, trans-Tango ; Dr or TM3/+*
3.7Ciii	*UAS-myrGFP.QUAS-mtdTomato-3xHA ; trans-Tango/Ir67c-GAL4 ; Dr or TM3/+*
3.7Civ	*UAS-myrGFP.QUAS-mtdTomato-3xHA ; trans-Tango/+ ; Ir94f-GAL4/+*
3.7Cv	*UAS-myrGFP.QUAS-mtdTomato-3xHA ; trans-Tango/+ ; Ir100a-GAL4/+*
3.8A-C	(from left to right)
	$Poxn^{\Delta M22\text{-}B5}$/$Poxn^{70}$; UAS-Kir2.1/+
	$Poxn^{\Delta M22\text{-}B5}$, Gr64e-GAL4/$Poxn^{70}$

	$Poxn^{\Delta M22\text{-}B5}$, Gr64e-GAL4/$Poxn^{70}$; UAS-Kir2.1/+
	$Poxn^{\Delta M22\text{-}B5}$, Gr66a-GAL4/$Poxn^{70}$; Gr93d-GAL4/+
	$Poxn^{\Delta M22\text{-}B5}$, Gr66a-GAL4/$Poxn^{70}$; Gr93d-GAL4/UAS-Kir2.1
	$Poxn^{\Delta M22\text{-}B5}$/$Poxn^{70}$; ppk28-GAL4/+
	$Poxn^{\Delta M22\text{-}B5}$/$Poxn^{70}$; ppk28-GAL4/UAS-Kir2.1
	$Poxn^{\Delta M22\text{-}B5}$, Ir20a-GAL4/$Poxn^{70}$; Dr or TM3/+
	$Poxn^{\Delta M22\text{-}B5}$, Ir20a-GAL4/$Poxn^{70}$; UAS-Kir2.1/Dr or TM3
	$Poxn^{\Delta M22\text{-}B5}$, Ir67c-GAL4/$Poxn^{70}$; Dr or TM3/+
	$Poxn^{\Delta M22\text{-}B5}$, Ir67c-GAL4/$Poxn^{70}$; UAS-Kir2.1/Dr or TM3
	$Poxn^{\Delta M22\text{-}B5}$/$Poxn^{70}$; Ir94f-GAL4/+
	$Poxn^{\Delta M22\text{-}B5}$/$Poxn^{70}$; Ir94f-GAL4/UAS-Kir2.1
	$Poxn^{\Delta M22\text{-}B5}$/$Poxn^{70}$; Ir100a-GAL4/+
	$Poxn^{\Delta M22\text{-}B5}$/$Poxn^{70}$; Ir100a-GAL4/UAS-Kir2.1
3.9	*UAS-GCaMP6s/UAS-GCaMP6s ; Gr43a-GAL4/Gr43a-GAL4*
3.10	*UAS-GCaMP6s/UAS-GCaMP6s ; Ir94f-GAL4/Ir94f-GAL4*

REFERENCES

Awasaki, T. & Kimura, K. 1997. pox-neuro is required for development of chemosensory bristles in Drosophila. *J Neurobiol,* 32**,** 707-21.

Benton, R. & Dahanukar, A. 2011. Electrophysiological recording from Drosophila taste sensilla. *Cold Spring Harb Protoc,* 2011**,** 839-50.

Boll, W. & Noll, M. 2002. The Drosophila Pox neuro gene: control of male courtship behavior and fertility as revealed by a complete dissection of all enhancers. *Development,* 129**,** 5667-81.

Broughton, S. J., Slack, C., Alic, N., Metaxakis, A., Bass, T. M., Driege, Y. & Partridge, L. 2010. DILP-producing median neurosecretory cells in the Drosophila brain mediate the response of lifespan to nutrition. *Aging Cell,* 9**,** 336-46.

Cameron, P., Hiroi, M., Ngai, J. & Scott, K. 2010. The molecular basis for water taste in Drosophila. *Nature,* 465**,** 91-5.

Charlu, S., Wisotsky, Z., Medina, A. & Dahanukar, A. 2013. Acid sensing by sweet and bitter taste neurons in Drosophila melanogaster. *Nat Commun,* 4**,** 2042.

Chen, Y. D. & Dahanukar, A. 2017. Molecular and Cellular Organization of Taste Neurons in Adult Drosophila Pharynx. *Cell Rep,* 21**,** 2978-2991.

Chen, Y. D., Park, S. J., Ja, W. W. & Dahanukar, A. 2018. Using Pox-Neuro (Poxn) Mutants in Drosophila Gustation Research: A Double-Edged Sword. *Front Cell Neurosci,* 12**,** 382.

Delventhal, R., Kiely, A. & Carlson, J. R. 2014. Electrophysiological recording from Drosophila labellar taste sensilla. *J Vis Exp***,** e51355.

Deshpande, S. A., Carvalho, G. B., Amador, A., Phillips, A. M., Hoxha, S., Lizotte, K. J. & Ja, W. W. 2014. Quantifying Drosophila food intake: comparative analysis of current methodology. *Nat Methods,* 11**,** 535-40.

Dus, M., Lai, J. S., Gunapala, K. M., Min, S., Tayler, T. D., Hergarden, A. C., Geraud, E., Joseph, C. M. & Suh, G. S. 2015. Nutrient Sensor in the Brain Directs the Action of the Brain-Gut Axis in Drosophila. *Neuron,* 87**,** 139-51.

Freeman, E. G. & Dahanukar, A. 2015. Molecular neurobiology of Drosophila taste. *Curr Opin Neurobiol,* 34**,** 140-8.

French, A. S., Sellier, M. J., Ali Agha, M., Guigue, A., Chabaud, M. A., Reeb, P. D., Mitra, A., Grau, Y., Soustelle, L. & Marion-Poll, F. 2015. Dual mechanism for bitter avoidance in Drosophila. *J Neurosci,* 35**,** 3990-4004.

Gendre, N., Luer, K., Friche, S., Grillenzoni, N., Ramaekers, A., Technau, G. M. & Stocker, R. F. 2004. Integration of complex larval chemosensory organs into the adult nervous system of Drosophila. *Development,* 131**,** 83-92.

Ja, W. W., Carvalho, G. B., Zid, B. M., Mak, E. M., Brummel, T. & Benzer, S. 2009. Water- and nutrient-dependent effects of dietary restriction on Drosophila lifespan. *Proc Natl Acad Sci U S A,* 106**,** 18633-7.

Jaeger, A. H., Stanley, M., Weiss, Z. F., Musso, P. Y., Chan, R. C., Zhang, H., Feldman-Kiss, D. & Gordon, M. D. 2018. A complex peripheral code for salt taste in Drosophila. *Elife,* 7.

Jeong, Y. T., Shim, J., Oh, S. R., Yoon, H. I., Kim, C. H., Moon, S. J. & Montell, C. 2013. An odorant-binding protein required for suppression of sweet taste by bitter chemicals. *Neuron,* 79**,** 725-37.

Joseph, R. M. & Carlson, J. R. 2015. Drosophila Chemoreceptors: A Molecular Interface Between the Chemical World and the Brain. *Trends Genet,* 31**,** 683-695.

Joseph, R. M. & Heberlein, U. 2012. Tissue-specific activation of a single gustatory receptor produces opposing behavioral responses in Drosophila. *Genetics,* 192**,** 521-32.

Joseph, R. M., Sun, J. S., Tam, E. & Carlson, J. R. 2017. A receptor and neuron that activate a circuit limiting sucrose consumption. *Elife,* 6.

Kang, K., Pulver, S. R., Panzano, V. C., Chang, E. C., Griffith, L. C., Theobald, D. L. & Garrity, P. A. 2010. Analysis of Drosophila TRPA1 reveals an ancient origin for human chemical nociception. *Nature,* 464**,** 597-600.

Klapoetke, N. C., Murata, Y., Kim, S. S., Pulver, S. R., Birdsey-Benson, A., Cho, Y. K., Morimoto, T. K., Chuong, A. S., Carpenter, E. J., Tian, Z., Wang, J., Xie, Y., Yan, Z., Zhang, Y., Chow, B. Y., Surek, B., Melkonian, M., Jayaraman, V., Constantine-Paton, M., Wong, G. K. & Boyden, E. S. 2014. Independent optical excitation of distinct neural populations. *Nat Methods,* 11**,** 338-46.

Koh, T. W., He, Z., Gorur-Shandilya, S., Menuz, K., Larter, N. K., Stewart, S. & Carlson, J. R. 2014. The Drosophila IR20a clade of ionotropic receptors are candidate taste and pheromone receptors. *Neuron,* 83**,** 850-65.

Kwon, J. Y., Dahanukar, A., Weiss, L. A. & Carlson, J. R. 2014. A map of taste neuron projections in the Drosophila CNS. *J Biosci,* 39**,** 565-74.

Ledue, E. E., Chen, Y. C., Jung, A. Y., Dahanukar, A. & Gordon, M. D. 2015. Pharyngeal sense organs drive robust sugar consumption in Drosophila. *Nat Commun,* 6**,** 6667.

Ling, F., Dahanukar, A., Weiss, L. A., Kwon, J. Y. & Carlson, J. R. 2014. The molecular and cellular basis of taste coding in the legs of Drosophila. *J Neurosci,* 34**,** 7148-64.

Marella, S., Fischler, W., Kong, P., Asgarian, S., Rueckert, E. & Scott, K. 2006. Imaging taste responses in the fly brain reveals a functional map of taste category and behavior. *Neuron,* 49**,** 285-95.

Martelli, C., Pech, U., Kobbenbring, S., Pauls, D., Bahl, B., Sommer, M. V., Pooryasin, A., Barth, J., Arias, C. W. P., Vassiliou, C., Luna, A. J. F., Poppinga, H., Richter, F. G., Wegener, C., Fiala, A. & Riemensperger, T. 2017. SIFamide Translates Hunger Signals into Appetitive and Feeding Behavior in Drosophila. *Cell Rep,* 20**,** 464-478.

Murata, S., Brockmann, A. & Tanimura, T. 2017. Pharyngeal stimulation with sugar triggers local searching behavior in Drosophila. *J Exp Biol,* 220**,** 3231-3237.

Murphy, K. R., Park, J. H., Huber, R. & Ja, W. W. 2017. Simultaneous measurement of sleep and feeding in individual Drosophila. *Nat Protoc,* 12**,** 2355-2366.

Nottebohm, E., Dambly-Chaudiere, C. & Ghysen, A. 1992. Connectivity of chemosensory neurons is controlled by the gene poxn in Drosophila. *Nature,* 359**,** 829-32.

Park, J. H. & Kwon, J. Y. 2011. Heterogeneous expression of Drosophila gustatory receptors in enteroendocrine cells. *PLoS One,* 6**,** e29022.

Sellier, M. J., Reeb, P. & Marion-Poll, F. 2011. Consumption of bitter alkaloids in Drosophila melanogaster in multiple-choice test conditions. *Chem Senses,* 36**,** 323-34.

Shankar, S., Calvert, M. E. & Yew, J. Y. 2016. Measuring Physiological Responses of Drosophila Sensory Neurons to Lipid Pheromones Using Live Calcium Imaging. *J Vis Exp*.

Soderberg, J. A., Carlsson, M. A. & Nassel, D. R. 2012. Insulin-Producing Cells in the Drosophila Brain also Express Satiety-Inducing Cholecystokinin-Like Peptide, Drosulfakinin. *Front Endocrinol (Lausanne),* 3**,** 109.

Soldano, A., Alpizar, Y. A., Boonen, B., Franco, L., Lopez-Requena, A., Liu, G., Mora, N., Yaksi, E., Voets, T., Vennekens, R., Hassan, B. A. & Talavera, K. 2016. Gustatory-mediated avoidance of bacterial lipopolysaccharides via TRPA1 activation in Drosophila. *Elife,* 5.

Steck, K., Walker, S. J., Itskov, P. M., Baltazar, C., Moreira, J. M. & Ribeiro, C. 2018. Internal amino acid state modulates yeast taste neurons to support protein homeostasis in Drosophila. *Elife,* 7.

Talay, M., Richman, E. B., Snell, N. J., Hartmann, G. G., Fisher, J. D., Sorkac, A., Santoyo, J. F., Chou-Freed, C., Nair, N., Johnson, M., Szymanski, J. R. & Barnea, G. 2017. Transsynaptic Mapping of Second-Order Taste Neurons in Flies by trans-Tango. *Neuron,* 96**,** 783-795 e4.

Thorne, N., Chromey, C., Bray, S. & Amrein, H. 2004. Taste perception and coding in Drosophila. *Curr Biol,* 14**,** 1065-79.

Wang, Z., Singhvi, A., Kong, P. & Scott, K. 2004. Taste representations in the Drosophila brain. *Cell,* 117**,** 981-91.

Weiss, L. A., Dahanukar, A., Kwon, J. Y., Banerjee, D. & Carlson, J. R. 2011. The molecular and cellular basis of bitter taste in Drosophila. *Neuron,* 69**,** 258-72.

Yang, Z., Huang, R., Fu, X., Wang, G., Qi, W., Mao, D., Shi, Z., Shen, W. L. & Wang, L. 2018. A post-ingestive amino acid sensor promotes food consumption in Drosophila. *Cell Res,* 28**,** 1013-1025.

Zhang, Y. V., Ni, J. & Montell, C. 2013. The molecular basis for attractive salt-taste coding in Drosophila. *Science,* 340**,** 1334-8.

CHAPTER IV

Control of sugar and amino acid feeding via taste integration of distinct pharyngeal taste neurons

Work in this chapter has produced a manuscript in preparation – **YCD Chen**, V Menon, RM Joseph, and A Dahanukar. *Control of sugar and amino acid feeding via taste integration of distinct pharyngeal taste neurons.*

SUMMARY

Insect gustatory systems comprise of multiple taste organs throughout the body for detecting various chemicals in food mixtures to assess food palatability. How individual taste neurons in each taste organs contribute to feeding control remain poorly defined. Here, we use the *Drosophila* pharynx as a model to investigate the extent to which taste information is integrated at the cellular level and regulates consumption of sugars and amino acids. We generate taste-blind animals and examine the effects of functional restoration of single classes of taste neurons in the adult *Drosophila* pharynx. We report that pharyngeal *Gr43a* neurons integrate information about sweet and amino acid tastants. Genetic dissection experiments uncover additional functionally redundant pharyngeal *Ir20a* neurons in detecting amino acids. Optogenetic activation of sweet taste neurons reveal functional specializations between external and internal taste neurons. Finally, high-resolution behavioral analysis reveals tastant-specific coordination of pharyngeal GRNs in regulating micro-feeding responses to sugars and amino acids. Overall, we identify previously unexplored appetitive taste coding principles in the pharynx and provide evidence of functional overlap and subdivision among taste neurons.

INTRODUCTION

The ability to taste and respond to sugars and amino acids is critical in animals, which allows them to select nutritive food sources in the environment. In the well-established genetic model insect, *Drosophila melanogaster*, the taste system displays remarkable similarity to that of higher animals with its ability to sense and distinguish between nutritive substances such as sugars and amino acids. As such, understanding the neural underpinnings of how *Drosophila* sense sugars and amino acids and translate that into appetitive behavioral responses can be applied across species and will have important global impacts, as numerous insects act as disease vectors or agricultural pests.

Taste sensilla, the functional taste sensory units in *Drosophila*, are distributed in different body parts including the labellum, pharynx, distal segments of the legs (tarsi), wing margins, and ovipositor. A typical taste sensillum contains two to four gustatory receptor neurons (GRNs) that are selectively activated by different categories of tastants such as sugars, salt, water, or bitter compounds. Over the past decade, the expression and function of several chemosensory receptors have been characterized in external taste neurons (Freeman and Dahanukar, 2015, Liman et al., 2014). Systematic electrophysiological analyses of stimulus-evoked responses of labellar and tarsal sensilla have been carried out with panels of food tastants (Ling et al., 2014, Weiss et al., 2011), revealing the presence of distinct functional classes of sensilla. Complementary transgenic reporter gene expression analyses of *Gr* genes and the *Ir20a* clade of *Ir* genes show corresponding molecularly distinct classes of sensilla (Fujii et al., 2015, Ling et al.,

2014, Koh et al., 2014, Weiss et al., 2011, Chen and Dahanukar, 2017). Previous molecular studies have demonstrated taste modality-specific and organ-specific projections of gustatory receptor neurons (GRNs) in the subesophageal zone (SEZ), which is the primary taste center in *Drosophila* (Thorne et al., 2004, Wang et al., 2004). Notably, bitter-sensing *Gr66a* GRNs and sweet-sensing *Gr5a* GRNs send axonal projections to largely non-overlapping areas of the SEZ. The segregation of taste representation has been observed in higher-order centers in the fly brain with calcium imaging (Kirkhart and Scott, 2015, Harris et al., 2015), suggesting that the distinct modality-specific taste information encoded in peripheral GRNs is maintained as it is processed in the brain.

A critical step for understanding principles of taste processing is to determine how responses elicited by distinct functional classes of GRNs are translated into different feeding behaviors. Sensory response profiles of external GRNs and internal pharyngeal GRNs to various sugars have been well characterized (Ledue et al., 2015, Dahanukar et al., 2007, Hiroi et al., 2002, Jiao et al., 2008, Miyamoto et al., 2013). Recent studies also uncover the role of labellar and tarsal GRNs in sensing amino acids (Park and Carlson, 2018, Ganguly et al., 2017). However, much remains to be uncovered about the downstream circuits and behavioral outputs mediated by these taste neurons. It has been shown that sugars induce proboscis extension response and promote feeding consumption through *Gr64f* GRNs (Ledue et al., 2015, Fujii et al., 2015, Jiao et al., 2008, Slone et al., 2007, Dahanukar et al., 2007). Three appetitive amino acid mixtures (Ser, Thr, Phe)

promote food choice by *Ir76b* GRNs (Ganguly et al., 2017). Given that *Gr64f* and *Ir76b* GRNs comprise of a large population of taste neurons in both external and internal pharyngeal taste organs, the functional subdivision between individual GRNs in each taste organ is still unclear. Moreover, some studies have hinted heterogeneous population of *Gr64f*/*Ir56d* GRNs in detecting sugars and fatty acids (Tauber et al., 2017) and functional specialization of *Gr5a*/*Gr64f* GRNs between and within taste organs have been reported (Thoma et al., 2016). Thus, molecularly distinct GRNs in different taste organs would contribute to distinct aspects of feeding responses to sugars and amino acids. Notably, we recently described an unprecedented complexity of molecular organization in the pharyngeal GRNs (Chen and Dahanukar, 2017), which might present a complex functional heterogeneity in feeding control. However, little is known about the functional role of pharyngeal GRNs in feeding behaviors even though they lie in important anatomical positions for evaluating food before ingestion.

Studies into which specific GRNs are necessary for mediating different aspects of feeding are further complicated because most chemosensory receptors and their associated promoter-*GAL4* lines are expressed in multiple taste organs, which pose challenges for assessment of organ-specific roles using mutants or genetic dissection techniques. The detailed molecular map for all the pharyngeal GRNs has provided an important and powerful development to overcome these challenge (Chen and Dahanukar, 2017). *Ir25a-GAL4* was previously shown to be expressed in all pharyngeal GRNs and we propose to employ *Ir25a-GAL4* as a tool to manipulate all pharyngeal GRN activity in

a *Pox-neuro* (*Poxn*) mutant background, in which external taste bristles are transformed into mechanosensory bristles (Awasaki and Kimura, 1997, Nottebohm et al., 1992). Thus, we would be able to generate taste-blind flies in which both internal and external GRNs were inactivated via genetic silencing and to protect specific classes of pharyngeal GRNs in the taste-blind flies to investigate the taste coding and functional heterogeneity of GRNs in the pharynx.

In this study, we report that appropriate feeding responses to five different tastant categories —sweet, amino acid, bitter, acid, and salt — were abolished in taste-blind (*Ir25a*-silenced *Poxn*) flies in binary feeding preference assays, demonstrating a critical role for taste input in short-term behavioral decisions regarding food choice. Interestingly, flies with only pharyngeal sugar-sensing *Gr43a* GRNs exhibited normal preference not only for sucrose but also for amino acids and the ability to promote sugar consumption is based on sweet taste instead of nutritional value of sugars. We also find the behavioral responses correlated with functional responses of *Gr43a* GRNs – calcium imaging experiments showed that both sugar and amino acids activated these GRNs. Genetic silencing experiments further identify the involvement of pharyngeal *Ir20a* GRNs together with *Gr43a* GRNs in promoting amino acid consumption. Optogenetic activation of external sweet GRNs causes proboscis extension, whereas that of pharyngeal *Gr43a* GRNs does not, suggesting distinct roles for sweet GRNs based on their location in external or internal taste organs. Finally, high-resolution quantitative analysis of micro-feeding behaviors reveals that tastant-specific feeding features are

regulated by coordinated activities of different pharyngeal GRNs. Among different subsets of the pharyngeal GRNs tested, the *Gr43a* GRNs play the major role in regulating multiple features of feeding responses to appetitive tastants. Together, our results reveal the appetitive taste coding in the pharyngeal GRNs and the functional heterogeneity of different pharyngeal GRNs in regulating different facets of appetitive feeding responses to sugars and amino acids.

RESULTS

Flies lacking functional taste neurons fail to distinguish tastants in feeding choice assays

We recently described detailed receptor-to-neuron maps for the three pharyngeal taste organs, in which we found that *Ir25a-GAL4* labeled all 24 GRNs in the adult pharynx (Chen and Dahanukar, 2017). Taking advantage of the *Pox-neuro* (*Poxn*) mutant, in which all external taste bristles are transformed into mechanosensory bristles (Awasaki and Kimura, 1997, Nottebohm et al., 1992), we created flies that lack all functional GRNs in external sensory bristles of the labellum, tarsi and wing, and in the internal labral, ventral cibarial, and dorsal cibarial sense organs (LSO, VCSO, and DCSO, respectively) by expressing the inwardly rectifying potassium channel *Kir2.1* via *Ir25a-GAL4* (**Figure 4.1A–C**). We tested the *Ir25a*-silenced *Poxn* flies, which are predicted to be true "taste-blind" flies, in a series of binary choice feeding assays to determine whether they were capable of making appropriate food choices in terms of appetitive responses to sugars and amino acids, and aversive responses to bitter compounds or high concentrations of acid and salt, when present in mixtures with sucrose.

As expected, *GAL4* and *UAS* controls, which possess functional GRNs in the pharynx, showed robust preference for 5 mM sucrose over 1 mM sucrose, as well as for a higher concentration of an appetitive amino acid mixture (Ganguly et al., 2017) of serine, threonine and phenylalanine (3AA, 25 mM each), over a lower concentration of the same

mixture (3AA, 5 mM each). By contrast, *Ir25a*-silenced *Poxn* flies were behaviorally neutral in terms of feeding preference in both sucrose and amino acid assays (**Figure 4.1D-E**). These results suggest that taste input is critical for discriminating between the palatability of different concentrations of sweet and amino acid tastants.

We next tested whether *Ir25a*-silenced *Poxn* flies exhibited feeding avoidance of bitter (denatonium), acid (tartaric acid), and high salt (500 mM NaCl). Our previous study shows that *Ir25a*-silenced *Poxn* flies did not show any feeding preference when testing between 5 mM sucrose mixed with 1 mM denatonium or lobeline against 1 mM sucrose. In this study, we used a lightly modified feeding choice paradigm to dissect the feeding avoidance of aversive tastants using a background of the same concentration of sucrose (2 mM) in all tastant solutions (**Figure 4.1F-H**). Control flies showed robust avoidance of 1 mM denatonium, 10% tartaric acid, and 500 mM NaCl mixed with 2 mM sucrose, and chose 2 mM sucrose alone. By contrast, avoidance of all three tastants was completely abolished in *Ir25a*-silenced *Poxn* flies (in each case, the mean preference index was not significantly different from zero, Wilcoxon signed rank test or One simple *t* test, $P>0.05$) (**Figure 4.1F-H**), which is consistent with our previous finding that taste input is critical for discriminating the sugar/antifeedant mixtures from sugar alone. Altogether, the results suggest that pharyngeal GRNs detect both appetitive and aversive tastants, and are capable of driving appropriate food choice in the absence of external taste input from the labellum and tarsi. Furthermore, the complete lack of preference exhibited by *Ir25a*-silenced *Poxn* flies suggests that any post-ingestive mechanisms such

as those described recently (Dus et al., 2015, Miyamoto et al., 2012, Dus et al., 2011) are insufficient to promote selection of appetitive tastants or avoidance of aversive tastants in short-term binary choice feeding assays.

Pharyngeal sugar-sensing *Gr43a* GRNs are sufficient for promoting food choice of sucrose and amino acids

Ir25a-silenced *Poxn* flies provided a tool to investigate how tastants are encoded by individual neuron types via a genetic background in which function could be selectively restored in defined classes of taste neurons. By expressing the GAL80 suppressor of the GAL4/UAS binary expression system under the control of specific *chemoreceptor-LexA* drivers, we created flies in which selected classes of pharyngeal GRNs labeled by each *chemoreceptor-LexA* driver were the only functional GRNs. To verify that the *chemoreceptor-LexA > LexAop2-GAL80* strategy would indeed suppress *GAL4*-dependent transgene expression in pharyngeal GRNs, we examined VCSO expression of *UAS-GFP* and *LexAop2-mCherry* in flies carrying *Ir76b-GAL4, Gr43a-LexA*, and *LexAop2-GAL80* transgenes. As described in our previous mapping results (Chen and Dahanukar, 2017), *Ir76b-GAL4* labeled three neurons (V1-V3) in the VCSO, including two (V1 and V2) that are also labeled by *Gr43a-LexA* (**Figure 4.2A**). In the presence of *LexAop2-GAL80*, we found GFP expression in V3 but not in the V1 and V2 neurons, confirming that *GAL4* activity was successfully restricted to pharyngeal *Gr43a* GRNs (**Figure 4.2B-C**).

In addition to three published *chemosensory-LexA* drivers (*Gr43a-LexA*, *Gr32a-LexA*, and *ppk28-LexA*) (Thistle et al., 2012, Fan et al., 2013, Miyamoto and Amrein, 2014), we generated two additional *chemosensory-LexA* drivers that label single pharyngeal GRNs in the LSO (*Ir60b-LexA* and *Ir67c-LexA*). Consistent with previous expression results (Chen and Dahanukar, 2017), we validated expression of the *Ir60b-LexA* and *Ir67c-LexA* drivers by examining co-labeling of *Ir60b-LexA* and *Ir94f-GAL4* in the L7-7 neuron (**Figure 4.2D**), and of *Ir67c-LexA* and *Ir67c-GAL4* in the L7-6 neuron (**Figure 4.2E**). We crossed the five *chemosensory-LexA* drivers into the *Ir25a*-silenced *Poxn* taste-blind background, in order to prevent expression of *UAS-Kir2.1* and protect selective GRNs from being silenced (*Poxn, GrX/IrX/ppk28*-protected).

We next tested *Poxn, GrX/IrX/ppk28*-protected flies for behavioral sensitivity to sugars and amino acids in binary choice assays. Since pharyngeal *Gr43a* GRNs are required for robust sugar consumption in *Poxn* mutants (Ledue et al., 2015), we first asked whether they were sufficient to drive selection of a higher, more appetitive, concentration of sugar. As predicted, *Poxn Gr43a*-protected flies exhibited a strong preference for 5 mM sucrose over 1 mM sucrose (**Figure 4.2F**), showing that pharyngeal sugar-sensing *Gr43a* GRNs are sufficient for intensity discrimination and ingestion of sucrose. Unexpectedly, we found that feeding preference for a higher concentration of the 3AA mixture was also indistinguishable between *Poxn Gr43a*-protected flies and transgenic controls (**Figure 4.2G**). Complementary experiments with similarly engineered flies carrying only one of the other four pharyngeal GRN types (*Gr32a*,

Ir60b, *Ir67c*, and *ppk28* GRNs) showed complete abolishment of behavioral responses to both sucrose and 3AA (in all cases, the mean preference index was not significantly different from zero, Wilcoxon signed rank test, $P>0.05$) (**Figure 4.2F-G**). These results posit that pharyngeal *Gr43a* GRNs have the capacity to sense not only sugars but also amino acids.

Pharyngeal *Gr43a* GRNs are activated by both sugar and amino acids

Since we observed that pharyngeal *Gr43a* GRNs can drive amino acid intake (**Figure 4.2G**), we examined whether *Gr43a* GRNs respond to amino acids using calcium imaging. We expressed the calcium indicator, GCaMP6s, in *Gr43a* GRNs and measured fluorescence changes in labeled soma in the LSO after tastant application via an *ex vivo* pharyngeal imaging preparation (Joseph et al., 2017). Consistent with the results of imaging from axonal termini (Ledue et al., 2015), we observed that pharyngeal *Gr43a* GRNs showed robust activation in response to 1 M sucrose (**Figure 4.3A**). As previously described, occasional shifts in the sample caused by the perfusion-delivery method necessitated refocusing of the preparation according to pre-selected visual landmarks (Joseph et al., 2017). Frames during a refocusing event were excluded from the analysis, depicted as gaps in representative traces (**Figure 4.3B**). We also note that application of water typically caused an initial depression in GCaMP6s fluorescence, which returned to and stabilized at the stimulus pre-application baseline within 1-2 minutes (**Figure 4.3B**).

Interestingly, pharyngeal *Gr43a* GRNs were also activated by a 150 mM 3AA mixture (**Figure 4.3C**). The mean value for maximum change in fluorescence upon addition of the 3AA mixture was comparable to that achieved with 100 mM sucrose (**Figure 4.3C**). Further analysis revealed differences in the temporal dynamics of response to the 3AA mixture as compared to that of sucrose, with the latter exhibiting a higher level of calcium activity sustained over a longer period of time (**Figure 4.3D**). For both tastants, calcium activity was significantly different from that observed with water solvent (**Figure 4.3C-D**). These results are consistent with the behavioral data, and demonstrate that pharyngeal sugar-sensing *Gr43a* GRNs are activated by both sugar and amino acids.

Functional redundancies in pharyngeal GRNs for sensing amino acids

An expectation from the observation that pharyngeal *Gr43a* GRNs sense both sugars and amino acids is that silencing of these neurons will disrupt behavioral responses to sugars as well as amino acids. As reported previously (Ledue et al., 2015), genetic inactivation of pharyngeal GRNs in *Poxn* flies via *Gr64e-GAL4,* which labels the same pharyngeal *Gr43a* GRNs (Chen and Dahanukar, 2017), abolished feeding preference for the higher concentration of sucrose, indicating that these neurons are necessary for intensity discrimination of sugar (**Figure 4.4A**). However, in similar experiments with 3AA mixtures, mean preference for the higher concentration was not significantly reduced in *Poxn Gr64e*-silenced flies (**Figure 4.4B**), arguing that other classes of pharyngeal GRNs may also be involved in sensing amino acids.

To identify these additional pharyngeal GRNs, we selected a toolkit based on our previous mapping results (Chen and Dahanukar, 2017) and manipulated different, and in some instances overlapping, subsets of pharyngeal GRNs including: putative bitter GRNs labeled by *Gr66a-/Gr93d-GAL4* (L7-3, L8, L9, V5-V8), putative water GRNs labeled by *ppk28-GAL4* (L7-4, L7-5, V4), and other *Ir*-expressing GRNs labeled by *GAL4* drivers for *Ir20a* (L7-4, L7-5, V3, V4), *Ir67c* (L7-6)*, Ir94f* (L7-7) and *Ir100a* (L7-8, DD3, DP3). We found that independently silencing any of these subsets of pharyngeal GRNs did not diminish behavioral sensitivity to the 3AA mixture (**Figure 4.4B**). One possible explanation for this observation is that more than one class of amino acid-sensing pharyngeal GRNs act in redundant neural circuits to promote amino acid intake.

Given that pharyngeal *Gr43a* GRNs drive amino acid intake (**Figure 4.2G**), we next silenced pharyngeal GRNs in pairwise combinations with *Gr64e* GRNs and tested resulting "double-silenced" flies for feeding response to amino acids. Notably, silencing of both *Gr64e* and *Ir20a* GRNs affected the flies' ability to discriminate between 5 mM and 25 mM 3AA mixtures as compared to *GAL4* controls (**Figure 4.4C**). No other driver combinations had a similar effect. Consistent with these results, behavioral sensitivity to amino acids was reduced in *Ir76b*-silenced *Poxn* flies, generated with an *Ir76b-GAL4* driver that labels pharyngeal *Gr43a* GRNs as well as other *Ir* GRNs, including *Ir20a* GRNs. Taken together, our results suggest that appetitive amino acids are sensed by at least two different types of pharyngeal GRNs, *Gr43a* and *Ir20a* (**Figure 4.4D**).

Inducible activation of pharyngeal *Gr43a* GRNs indicates functional subdivision by locations

Anatomical and functional differences between sweet taste neurons in the legs have been reported previously, in that sweet taste neurons projecting to the ventral nerve cord control locomotion whereas those projecting to the subesophageal zone control proboscis extension (Thoma et al., 2016). We therefore wondered whether functional differences exist in internal and external taste circuits. To address this question, we examined behavioral outcomes of inducible activation of different subsets of sweet taste neurons. We expressed red-shifted channelrhodopsin (*UAS-CsChrimson*) (Klapoetke et al., 2014) in selected neurons, induced activation by exposure to 626 nm red LEDs (**Figure 4.5A**), and scored the number of proboscis extensions (**Figure 4.5B-C**). Similar to previous reports (Inagaki et al., 2014, Dawydow et al., 2014, Keene and Masek, 2012), activation of all *Gr64e* neurons in otherwise wild type flies, which includes external and internal sweet GRNs, resulted in proboscis extensions (**Figure 4.5D**). Activation of *Gr64e* GRNs in *Poxn* mutants, which includes only pharyngeal sweet GRNs, did not induce proboscis extensions (**Figure 4.5E**), suggesting a functional separation of sweet taste circuits based on their location of origin. These results are consistent with the idea that external sweet GRNs, but not pharyngeal sweet GRNs, play a role in proboscis extension and initiation of feeding behavior.

Pharyngeal *Gr43a* GRNs promote food choice based on sweet taste but not nutritional value of sugars

Food choice is immediately influenced by sweet taste, and over time by caloric content of food (Stafford et al., 2012). Several nutrient sensors that play a part in the latter have been identified in the fly brain, including DH44 neurons in the pars intercerebralis (Dus et al., 2015) and *Gr43a* neurons in the posterior superior lateral protocerebrum (Miyamoto et al., 2012), both of which sense nutrient sugar levels in the hemolymph. Although peripheral sweet GRNs are known to detect chemicals perceived as sweet to human (Ledue et al., 2015, Fujii et al., 2015, Jiao et al., 2008, Slone et al., 2007, Dahanukar et al., 2007), little is known about whether they can distinguish sugars based on nutritional value. We therefore wished to investigate the relative contribution of sweet taste and nutritive value in sugar feeding choice mediated by pharyngeal *Gr43a* GRNs. We first tested behavioral sensitivity to L-glucose, an enantiomer of the natural D-glucose with no caloric value (**Figure 4.6A**), and D-glucose (**Figure 4.6B**), in choice assays with 50 mM and 200 mM concentrations. Wild type (w^{1118}), *Poxn UAS-Kir2.1* control and *Poxn Gr43a*-protected flies showed a strong preference for 200 mM L-glucose over 50 mM L-glucose, consistent with previous reports of sweetness of L-glucose (Stafford et al., 2012). As predicted, taste-blind flies (*Ir25a*-silenced *Poxn* flies), as well as flies in which only one of four other pharyngeal GRNs (*Gr32a*, *Ir60b*, *Ir67c*, and *ppk28* GRNs) were protected, showed a loss of intensity discrimination consistent with an inability to sense L-glucose (**Figure 4.6A**). Similar results were observed in feeding choice assays with 50 mM and 200 mM of D-glucose (**Figure 4.6B**). These

observations indicate that pharyngeal *Gr43a* GRNs can mediate intensity discrimination and stimulate ingestion of both L-glucose and D-glucose.

We next examined preference between D-glucose (nutritive) and L-glucose (non-nutritive) in feeding choice assays in which both tastants were presented at 50 mM. We found that w^{1118} but not *Poxn UAS-Kir2.1* control flies showed a strong preference for 50 mM D-glucose over 50 mM L-glucose, suggesting the distinct behavioral sensitivity of external taste neurons to D-glucose and L-glucose. Interestingly, we found that only *Poxn Gr43a*-protected flies among all genotypes tested in a *Poxn* mutant background exhibited a strong preference for 50 mM D-glucose over 50 mM L-glucose (**Figure 4.6C**). Similar results were observed in experiments with a higher concentration (200 mM) for each tastant or experiments with 50 mM D-glucose and 200 mM L-glucose (**Figure 4.9**). Although *Gr43a* is expressed in the few nutrient-sensing neurons in the protocerebrum (Miyamoto et al., 2012) and enteroendocrine cells in the gut (Park and Kwon, 2011), they are not intersected by *Ir25a-GAL4* and *Gr43a-LexA*, and thus unlikely to account for the observed phenotypes. Specifically, *Ir25a-GAL4* did not label any cell in the gut. When we examined *Ir25a-GAL4* and *Gr43a-LexA* expression pattern in the brain, we found that *Ir25a-GAL4* did not label any protocerebrum neurons in either 7-or 14-day-old flies (**Figure 4.10**). Thus *Gr43a* neurons in the protocerebrum would remain functional in all genotypes that were tested. In addition, *Gr43a-LexA* only labeled the protocerebrum neurons in older flies (14-day-old) but not younger flies (7-day-old) that we used for behavioral assays (**Figure 4.10**). Taken together, the results are consistent with the idea

that feeding preference for D-glucose over L-glucose in *Poxn Gr43a*-protected flies is mediated by pharyngeal sugar sensing *Gr43a* neurons.

It is possible that *Gr43a*-protected *Poxn* flies encode nutritional value and drive preference for nutritive tastants over non-nutritive ones. To test this possibility, we mixed various concentrations of D-sorbitol and D-mannose with 50 mM L-glucose and tested feeding preference for these mixtures when offered in binary choice assays with 50 mM D-glucose. Both D-sorbitol and D-mannose are nutritious but not sweet (Stafford et al., 2012). Therefore, any increase in feeding preference for L-glucose mixtures with these compounds would indicate that *Gr43a*-protected *Poxn* flies can make a decision based on caloric value rather than sweetness alone. However, we found that *Poxn Gr43a*-protected flies continued to exhibit a strong preference for 50 mM D-glucose over L-glucose/D-sorbitol and L-glucose/D-mannose mixtures at all concentrations tested (**Figure 4.6D-E**). Both control and taste-blind flies showed no feeding preference for either tastant. In contrast, when D-arabinose (sweet, non-nutritive) (Stafford et al., 2012) was mixed with L-glucose, the feeding preference in control as well as in *Poxn Gr43a*-protected flies shifted from 50 mM D-glucose to L-glucose/D-arabinose mixtures at all concentrations tested (**Figure 4.6F**). Feeding preference of taste-blind flies remained neutral in this assay. In addition, we also tested w^{1118} flies at the highest concentration of L-glucose/D-sorbitol, L-glucose/D-mannose, and L-glucose/D-arabinose mixtures and found similar results as *Poxn Gr43a*-protected flies. Altogether, these results are consistent with the

idea that pharyngeal *Gr43a* GRNs promote food choice based on sweet taste but not on the nutritional value of sugars.

Pharyngeal GRNs control parameters of micro-feeding behaviors to appetitive tastants

The internal location of pharyngeal GRNs places them in a perfect anatomical position to regulate consumption. However, it is not clear whether, and if so how, individual features of feeding behavior are controlled by pharyngeal GRNs. To investigate this, we evaluated micro-feeding parameters in response to water and four different appetitive tastants (sucrose, D-glucose, L-glucose, and 3AA) in *Poxn UAS-Kir2.1* control flies in which all pharyngeal GRNs are present, and compared them to taste-blind flies (*Ir25a*-silenced *Poxn*). Feeding responses to different tastants were recorded using the Fly Liquid-Food Interaction Counter (FLIC) assay (Ro et al., 2014) (**Figure 4.7A**). As described previously (Ro et al., 2014), tasting and feeding events were classified based on differences in output signal intensity, and we set a feeding threshold at 100 a.u. above baseline to separate the two. To exclude potential post-ingestive effects, we focused on features of the first feeding event: peak intensity, duration, interval between the first and second feeding events, and time to the first feeding event (**Figure 4.7B-E**). All feeding responses with various tastants were normalized to those obtained with water solvent alone. In comparison with control flies, peak intensity and duration of the first feeding event were significantly reduced in taste-blind flies with all four appetitive tastants (**Figure 4.7B-E**). Scrutiny of other parameters suggests possible

tastant-specific differences. The interval between the first and second feeding events was significantly greater in taste-blind flies as compared to control flies when presented with sucrose and D-glucose, but no different from controls when presented with L-glucose or the 3AA mixture (**Figure 4.7B-E**). Similarly, time to the first feeding of L-glucose was not significantly different between control and taste-blind flies, but was significantly lower in control flies for sucrose, D-glucose or 3AA. Overall, the results suggest that pharyngeal neurons control each of these four micro-feeding parameters, which are typically coupled, to promote consumption of sugars and amino acids. Consistent with differences in pharyngeal circuitry involved in behavioral sensitivity to sugars and amino acids (**Figure 4.4**), analysis of micro-feeding behaviors suggests that there may be some differences in the way that sugar and amino acid consumption are controlled.

Pharyngeal *Gr43a* GRNs alone partially restore appetitive micro-feeding responses to sugars and amino acids

We next tested how specific classes of pharyngeal neurons control features of the first feeding event in response to the four tastants. For this purpose, we genetically protected individual classes of pharyngeal GRNs (*Gr43a*, *Gr32a*, *Ir60b*, *Ir67c*) in *Ir25a*-silenced *Poxn* flies (**Figures 4.8 and 4.11**). We found that only functional restoration of *Gr43a* GRNs caused consistent increases in intensity and duration of the first feeding event in response to all four appetitive tastants. The effect of restoration of *Gr43a* GRNs on the interval between the first and second feeding events was specific to only sucrose, L-glucose, and 3AA. No effect was observed on time to the first feeding event in flies

with only *Gr43a* GRNs functional (**Figure 4.8**). We noticed that intensity and duration of the first feeding event in response to L-glucose and 3AA were slightly increased when either *Ir60b* or *Ir67c* GRNs were protected (**Figure 4.11**), suggesting that one or both of these GRN classes may confer some ability to detect L-glucose and 3AA that cannot be uncovered in the binary choice assay (**Figure 4.2F-G**). Restoration of pharyngeal *Gr32a* GRNs alone had little if any effect on micro-feeding features in response to all four appetitive tastants (**Figure 4.11**).

Tastant-specific modulation of micro-feeding features by different pharyngeal GRNs

We next tested whether other GRNs that had little to no effect of modulating micro-feeding features could modulate the ones dictated by *Gr43a* GRNs. To test this, we generated flies with *Gr43a* GRNs protected in combination with either *Ir60b* or *Ir67c* GRNs using *LexA* drivers. We chose *Ir60b* and *Ir67c* GRNs since they label only single pharyngeal GRNs in sensillum #7 of the LSO. Recombinant chromosomes with combinations of *LexA* transgenes were validated by visualizing reporter expression in three pharyngeal GRNs of the LSO (**Figure 4.12**). We found that when both *Gr43a* and *Ir60b* GRNs were protected, there was a significant increase in the duration of the first feeding event for sucrose as compared to flies in which only *Gr43a* GRNs were protected (**Figure 4.8A**). Double restoration of *Gr43a* and *Ir60b* GRNs also caused a reduction in intervals before and after the first feeding event for D-glucose but not L-glucose as compared to *Gr43a* GRNs protection alone are present (**Figure 4.8A**). These results

suggest that *Ir60b* GRNs would modulate *Gr43a* GRN-driven consumption of sucrose and glucose, via different feeding parameters. In contrast, double restoration of *Gr43a* and *Ir67c* GRNs had a more prominent effect on increasing first feeding duration and reducing intervals before and after the first feeding event for D-glucose as compared to *Gr43a* GRNs alone (**Figure 4.8B**). Therefore, *Ir60b* or *Ir67c* GRNs may differentially modulate feeding response to sucrose and glucose, respectively, when *Gr43a* GRNs are present. Altogether, these results suggest the existence of interaction between pharyngeal GRNs that regulates distinct micro-feeding features in response to sugars and amino acids.

DISCUSSION

In this study, we show that appropriate feeding responses to five different taste modalities – sweet, amino acid, bitter, acid, and salt – are abolished in "taste-blind" flies in binary choice assays. Such flies provided the means to directly test the extent to which taste input is required for appropriate food selection as well as reveal the specificity of the functional contribution of an individual type of GRN in regulating distinct features of feeding responses to appetitive stimuli. Notably, functional restoration of pharyngeal *Gr43a* neurons in "taste-blind" flies restores behavioral responses to tastants of more than one taste modality, suggesting that these pharyngeal GRNs act as sites of multimodal taste integration. We also reveal a functional redundancy in amino acid detection by both pharyngeal *Gr43a* and *Ir20a* GRNs. A closer examination of micro-feeding responses to sugars and amino acids reveals that regulation of different micro-feeding features is mainly achieved by pharyngeal *Gr43a* GRNs with other modulatory inputs of other classes of pharyngeal GRNs.

Taste input is critical for behavioral decisions in short-term feeding assays

We find that *Poxn* flies lacking all external GRNs are nevertheless capable of evaluating food substrates and making appropriate food choices, displaying sensitivity to most if not all tastant categories including sweet, bitter, salt, acid, and amino acids. Moreover, pharyngeal taste is essential for the observed taste sensitivity of *Poxn* mutants: silencing all pharyngeal GRNs via *Ir25a-GAL4* in *Poxn* flies renders them unable to discriminate tastants in binary choice assays. By extension, these results suggest that

post-ingestive mechanisms are not sufficient for appropriate food choice in short-term feeding assays. For example, the Gr43a-expressing neurons in the brain have been shown to act as a nutrient sensor to monitor hemolymph fructose level and promote feeding in starved flies (Miyamoto et al., 2012). It has been shown that consumption of sorbitol converts into fructose and elevates the hemolymph fructose level immediately after feeding (Miyamoto et al., 2012). Since *Poxn UAS-Kir2.1* flies show no preference toward L-glucose/D-sorbitol mixture over D-glucose at various concentrations tested, the Gr43a brain neurons are unlikely to be involved in detecting elevated hemolymph fructose level and mediating food choice in our short-term feeding preference assays.

Previous studies also identified other post-ingestive nutrient sensors such as diuretic hormone 44 (DH44) neurons and SLC5A11-expressing ellipsoid body R4 neurons as critical for selection of nutritive D-glucose over non-nutritive L-glucose (Dus et al., 2013, Dus et al., 2015). However, these studies did not take into account the presence of functional pharyngeal GRNs. Here, we find that pharyngeal *Gr43a* GRNs alone are sufficient for promoting food choice of D-glucose over L-glucose (**Figure 4.6D**). It remains possible that pharyngeal input is a critical component of fast-acting feedback mechanisms that engender compensatory changes in feeding behavior in response to consumption-derived changes in internal state. More recently, the identification of pharyngeal *Gr43a* interneurons that integrate information about sweet taste and fed state lends support to such a hypothesis (Yapici et al., 2016). Our recent results to characterize second-order neurons in pharyngeal circuits indicate the presence

of neurites within a region that includes DH44 neurons, but a demonstration of connectivity between pharyngeal GRNs and brain nutrient sensors awaits further investigation. Alternatively, pharyngeal GRNs may serve as substrates of nutrient-sensing mechanisms to effect behavioral changes during feeding.

Differential behavioral sensitivity between D-glucose and L-glucose in peripheral GRNs

It has been shown that flies consume more D-glucose over L-glucose but the underlying cellular basis is still unclear since the electrophysiological responses of labellar sweet GRNs and the tarsal PER behavioral responses to D-glucose and L-glucose remain the same (Fujita and Tanimura, 2011). Here, we found that flies with only *Gr43a* pharyngeal GRNs are able to select D-glucose over L-glucose, providing one of the neuronal substrates responds differentially to these two sugars. The micro-feeding features elicited by D-glucose over L-glucose were also distinct in flies with only flies with *Gr43a* pharyngeal GRNs. For example, the interval between first and second feeding events was lower in response to L-glucose but no effect to D-glucose. Such differential responses to D- or L-sugars might not be a unique feature for pharyngeal GRNs since the wild type but not *Poxn UAS-Kir2.1* control flies exhibited a preference for D-glucose over L-glucose (**Figure 4.6C**), suggesting that some external sugar sensing GRNs have differential sensitivity to these two sugars. Given that the previous study only surveys L-type labellar hairs (Fujita and Tanimura, 2011), it is possible that other types of labellar or tarsal hairs have a higher sensitivity to D-glucose over L-glucose. In addition,

differential sensory responses to D-arabinose and L-arabinose have been reported in the Gr43a GRNs in the tarsi and the LSO (Mcginnis et al., 2016), suggesting that peripheral GRNs have the ability to distinguish structurally similar enantiomers of sugars.

Multimodal integration of tastant information in taste neurons

The prevailing model of taste coding is that chemicals are separated into taste categories by their ability to activate defined, non-overlapping sub-populations of taste neurons (Accolla et al., 2007, Barretto et al., 2015, Chen et al., 2011, Harris et al., 2015). Recent observations are beginning to build a more nuanced view of this idea. For example, sweet and fatty acid tastes overlap in external GRNs (Tauber et al., 2017, Ahn et al., 2017), as do bitter and acid tastes (Charlu et al., 2013). In the context of a *Poxn* fly with a minimal taste system of 24 GRNs, genetic dissection analyses reveal that both appetitive and deterrent classes of GRNs sense chemicals belonging to more than one classically described taste category. In agreement with this idea, pharyngeal *Gr43a* GRNs can be activated by sugars and amino acids and are sufficient for promoting consumption of these tastants. In addition, our previous finding demonstrates that the sugar response of pharyngeal *Gr43a* GRNs can be inhibited by the presence of bitter compounds, high concentrations of salt, or acid, suggesting that pharyngeal *Gr43a* GRNs act as a hub to integrate information across broad tastant categories. How do pharyngeal *Gr43a* GRNs respond tastants from multiple categories? It is likely that different types of receptors detect sugars and amino acids. The amino acid response in *Gr43a* GRNs may depend on Ir76b, a broadly expressed ionotropic receptor that is required for amino acid response in

external GRNs (Ganguly et al., 2017). It will be interesting to determine the molecular basis for sensing different tastant categories in pharyngeal *Gr43a* GRNs.

How generalizable are these findings to the taste system as a whole? It is possible that taste coding properties of the pharynx may be unique, conferred by its distinctive groupings of neurons and chemosensory receptor co-expression patterns. Interestingly, some larval GRNs have been found to detect multiple tastant categories (Van Giesen et al., 2016). Among all adult taste neurons, a fraction of those residing in the pharynx is unique by virtue of their persistence through metamorphosis (Gendre et al., 2004). Thus, this organ may represent a unique site in which multimodal taste sensing properties are transferred and maintained from the larval to adult stage. However, many external GRNs also co-express members of the Gr and Ir and ppk families (Chen and Amrein, 2017, Ahn et al., 2017, Thistle et al., 2012), and may have broader functions than conceived so far. Multimodal sensing properties also invite the question of whether each GRN class can independently modulate sensitivities to different tastant categories in ways that reflect the animal's nutritional needs. It will be interesting to determine how *Gr43a* GRN response to sugar and amino acids relates to the post-mating increase in feeding preference for amino acids relative to sugars in females (Ribeiro and Dickson, 2010, Ganguly et al., 2017).

Functional redundancies between different classes of taste neurons

Behavioral analyses of flies in which only single classes of pharyngeal GRNs were active, combined with analysis of flies in which single classes of pharyngeal GRNs were silenced, uncover an unforeseen degree of functional redundancy in the pharynx. For example, although *Gr43a* GRNs were sufficient to promote amino acid feeding, preference for this tastant was abolished only upon silencing both *Ir20a* and *Gr43a* GRNs (**Figure 4.4C**). Silencing either *Ir20a* or *Gr43a* GRNs did not do so, suggesting that both GRN classes contribute to feeding preference for amino acids. These results are consistent with our previous findings of a role for the Ir20a receptor in amino acid taste (Ganguly et al., 2017). Since *Ir20a-GAL4* expression does not overlap with pharyngeal *Gr43a* GRNs, there may be at least two distinct pathways for sensing amino acids: one an *Ir20a*-independent pathway operating in pharyngeal *Gr43a* GRNs, and a second *Ir20a*-dependent pathway acting in the *Ir20a*-expressing neurons. Interestingly, silencing of *ppk28-GAL4* labeled GRNs—which include all *Ir20a*-labeled GRNs with the exception of the V3 neuron —did not significantly disrupt amino acid response. Thus, the V3 neuron may be a putative *Ir20a* GRN that acts in parallel with pharyngeal *Gr43a* GRNs to sense amino acids. Since all the experiments were performed with 3 amino acid mixtures (Ser, Thr, Phe), it remains to be determined whether these two classes of amino acid sensing pharyngeal GRNs show differential sensitivities to the individual amino acids.

There is likely an even broader view of redundant mechanisms for not only appetitive taste but also aversive taste. Recent studies have reported that feeding avoidance to many bitter compounds and acids is achieved by activation of bitter neurons and inhibition of sweet neurons in external taste sensilla (French et al., 2015, Jeong et al., 2013, Charlu et al., 2013). Our recent findings demonstrate that pharyngeal *Gr43a* GRNs are also subject to such inhibition by bitter compounds, acids and high salt, suggesting that broad cross-modality sensing mechanisms in distinct populations of GRNs act together to ensure appropriate feeding control.

Coordinated regulation of distinct micro-feeding features by different classes of pharyngeal GRNs to achieve feeding control of sugars and amino acids

The taste-blind system we have developed provides a unique opportunity to evaluate the functional profiles and behavioral contributions of different cell types in the pharynx, which may provide an understanding of the complex regulation of food choice and intake. Together with the high-resolution FLIC assays, we identify several micro-feeding features to all four appetitive tastants that are regulated by pharyngeal GRNs, such as intensity and duration of the feeding events. However, the roles of pharyngeal GRNs in intervals before and after the first feeding events seems to be tastant-specific with smaller effects for L-glucose and 3AA, evoking the possibility that different combination of pharyngeal GRNs have differential sensitivities to each appetitive tastant tested. Comparison of micro-feeding behaviors in flies with functionally restoring selected pharyngeal GRNs supports this notion since most features are partially restored

in flies with functional *Gr43a* GRNs and restoration of *Gr43a* GRNs together with either *Ir60b* or *Ir67c* GRNs have differential effects for sucrose and glucose, respectively. Thus, the phenotypes seen in control *Poxn* flies with all 24 pharyngeal GRNs appear to be achieved via multiple pharyngeal GRNs that contribute to different facets of micro-feeding features in a tastant-specific manner.

EXPERIMENTAL PROCEDURES

Fly strains. Flies were reared on standard cornmeal-dextrose-agar food at 25°C and 60-70% relative humidity under a 12 h:12 h dark:light cycle. The following fly lines were used: *Gr-GAL4* (Ling et al., 2014, Weiss et al., 2011), *Ir-GAL4* (Koh et al., 2014), *Ir76b-GAL4* (BDSC#41730), *Ir25a-GAL4* (BDSC#41728), *Ir100a-GAL4* (BDSC#41743), *ppk28-GAL4* (Cameron et al., 2010), *Gr43a-LexA* (Miyamoto and Amrein, 2014), *Gr32a-LexA* (Fan et al., 2013), *ppk28-LexA* (Thistle et al., 2012), *UAS-Kir2.1* (Baines et al., 2001), $Poxn^{\Delta M22\text{-}B5}$ (Boll and Noll, 2002), $Poxn^{70}$ (Awasaki and Kimura, 1997), *UAS-mCD8GFP* (Weiss et al., 2011), *UAS-GCaMP6s* (BDSC#42746), *UAS-CsChrimson* (BDSC#55136), *LexAop2-GAL80* (BDSC#32214), *LexAop2-6XmCherry-HA* (BDSC#52271, 52272). To generate *Ir60b-LexA* line, both the 5' and 3' flanking regions of the Ir60b gene was used as described previously (Koh et al., 2014). Assembled LexA vector was used to generate *Drosophila* strains through PhiC31 integration into attP2 landing sites (BestGene Inc.). To generate *Ir67c-LexA* line, both the 5' and 3' flanking regions of the Ir67c gene was used as described previously (Koh et al., 2014). Assembled LexA vector was used to generate *Drosophila* strains through a standard P-element transformation (BestGene Inc.). For experiments using *Poxn* mutants, we confirmed the *Poxn* mutant background in all sorted flies by observing the transformed long and bent mechanosensory hairs in the labellum, as well as the fused three tarsal segments in the legs.

Chemicals. Tastants obtained from Sigma-Aldrich are as follows: D-sucrose (S7903), D-glucose (G6152), L-glucose (G5500), D-sorbitol (85529), D-mannose (M6020), D-arabinose (A3131), L-serine (84959), L-threonine (89179), L-phenylalanine (P5482), denatonium benzoate (D5765), and L-tartaric acid (251380). Sodium chloride was obtained from Macron Chemical (7581-06). All tastants were dissolved in water.

Immunohistochemistry. Flies were anesthetized on ice, and the proboscis and brain tissue were dissected in 1X PBST (PBS with 0.3% Triton X-100) and fixed for 30 min with 4% paraformaldehyde in 1X PBST at room temperature. After three washes with 1X PBST, samples were blocked with 5% normal goat serum (Sigma, #G9023) in 1X PBST. Tissues were incubated in primary antibody solutions for 3 days at 4^{o}C. Primary antibodies were: mouse anti-nc82 (1:20; Developmental Studies Hybridoma Bank) chicken anti-GFP (1:5000; Abcam, #ab13970) and rabbit anti-DsRed (1:200; Clontech, #632496). Secondary antibodies (1:400; Invitrogen) were: goat anti-chicken Alexa Fluor 488, goat-anti-rabbit Alexa Fluor 546, and goat anti-mouse Alexa Fluor 647. Samples were mounted in VECTASHIELD antifade mounting medium (Vector Laboratories, #H-1000) and stored at 4^{o}C. Fluorescent images are acquired using a Leica SP5 confocal microscope with 400 Hz scan speed in 512x512 or 1024x1024 pixel formats. Image stacks were acquired at 1-μm optical sections. All images were presented as maximum projections of the *z* stack generated using Leica LAS AF software.

Binary choice feeding assays. Feeding preference assays were performed as described previously (Charlu et al., 2013, Chen and Dahanukar, 2017). Briefly, flies were sorted into groups of 10 males and 10 females upon eclosion and aged for 5-8 days. Since *Poxn* mutant male flies are sterile, we added 2 heterozygous males with curly wings (*Poxn/CyO*) in each group to ensure that all sorted females were mated. Heterozygous males were discarded during scoring for abdominal color. Flies were starved for 24 hr on water-saturated tissues and then placed in tight-fit Petri dishes (Falcon Cat. #35-1006) with eighteen 10 μL dots of 0.75% agarose that alternated in tastant and color using either 25 mg/mL indigo carmine (Sigma, #I8130) or 50 mg/mL sulforhodamine B (Sigma, #230162). For all experiments, we swapped dyes for each tastant with similar numbers of trials to account for any dye preference. We noted that "taste-blind" flies (i.e. *Poxn, Ir25a*-silenced flies) showed noticeable dye preferences for sulforhodamine B over indigo carmine. Although dye swap experiments annul the dye preference, the data sets reflect a high degree of variation in "taste-blind" flies. However, the observed dye bias is minimal when testing flies that have functional taste (e.g. *GAL4* and *UAS* control flies). Flies were allowed to feed for 2 hours at 25°C in a dark, humidified chamber, after which they were frozen and scored for abdomen color by dissecting the guts within 24 hours. Trials with participation lower than 50% were excluded. Preference index (PI) was calculated as ((# of flies labeled with the tastant color) – (# of flies labeled with the control color))/(total number of flies that fed). Thus, a PI of 0 would indicate equal preference between the two choices. In all cases, PI values were calculated for mixed populations of males and females, except for experiments with amino acids for which we

used only females, since they exhibit stronger feeding preference for amino acids as compared to males.

Calcium imaging. Calcium imaging on cell bodies in the pharynx were performed as described with some modifications (Joseph et al., 2017). Briefly, 1-week old male and female flies expressing *UAS-GCaMP6s* driven by *Gr43a-GAL4* were starved overnight at 25ºC and 60-70% relative humidity. Mated females were then decapitated, and the labial palps of the labellum were carefully excised using a sharp razor blade to increase access to pharyngeal sensilla. Heads were mounted in a minimal volume of water on a microscope slide with three 18x18 mm bridging slips, placed to make two channels between the bridging slips, which allowed liquid to perfuse through the sample. Then, a 22x40 mm coverslip was secured with nail polish on top of the bridging slips, positioned approximately 20 mm from the edge of microscope slide, to allow placement of tastant solution.

UAS-GCaMP6s fluorescence was viewed with an upright Zeiss 510 confocal or an inverted Leica SP5 confocal microscope. Neurons were visualized with a 10X objective, with a digital zoom of 4-5. Images were acquired at 512x512 resolution with no line averaging, with one frame scanned per second. The pinhole was calibrated to an optical slice of 100 μm, with the 488 nm laser at 25% power. Changes in fluorescent activity were recorded for 4 minutes after delivery of the stimulus. Before stimulus, focal landmarks were identified in the primary channel used to detect green fluorescent activity

of the GCaMP reporter, and in a secondary channel (either DIC or a fluorescence channel outside the activation/detection range of GCaMP) used to image the pharyngeal structure during the experiment. These focal landmarks were monitored throughout the assay, to ensure that the sample remained in the correct plane of focus. If the sample shifted slightly out-of-focus along the z-axis, the preparation was refocused to the reference landmarks. The out-of-focus frames were excluded from the $(\Delta F/F)_{MAX}$ calculations.

Fluorescence intensities were obtained with open-source Fiji/ImageJ software (https://fiji.sc). A region-of-interest (ROI) was drawn around individual cell bodies; an ROI of identical dimensions was also placed over a non-neuronal area of the image, which was used as a reference for measuring any non-specific background changes in fluorescence. Average pixel intensity for ROIs during each frame was measured with the Time-Series Analyzer Plugin, written by Balaji, J. (https://imagej.nih.gov/ij/plugins/time-series.html). A corrected average intensity for the cell body ROI was measured in each frame by subtracting the average intensity of the background ROI from the average intensity of the cell body ROI. Maximum changes in fluorescent activity were calculated as: $(\Delta F/F)_{MAX}$ = [(corrected intensity of ROI) – (average corrected intensity of 10 frames preceding stimulus)] / (average corrected intensity of 10 frames preceding stimulus). $(\Delta F/F)_{MAX}$ were then determined for either the entire 3-min sampling period or in binned 30-sec intervals, following stimulus.

Optogenetic activation. Experiments with *UAS-CsChrimson* were as described previously (Joseph et al., 2017), with the following modifications. Flies were reared on standard cornmeal-dextrose-agar food at 25°C and 60-70% relative humidity under a 12 h:12 h dark:light cycle. Four days after eclosion, flies were transferred to standard cornmeal-dextrose-agar food supplemented with 1 mM all-trans-retinal (R2500, Sigma-Aldrich, St. Louis, MO), and placed in dark at 25°C for 3 days. Before testing, flies were briefly anesthetized with low amounts of CO_2, and were gently aspirated into 1000-μL pipette tips so that their heads protruded through the end opening of the tip. Preparations were performed under low-light conditions, in which the intensity of room-lights was low enough to not stimulate *UAS-CsChrimson* activation.

Flies were placed under a standard dissecting microscope under low-light conditions and filmed with a 5.0-megapixel eyepiece digital camera with an exposure time of 500-msec (Model MD500, AmScope, Irvine, CA). Red light was provided at intensity of ~5 mW/mm^2 by 626 nm LEDs (Super Bright LEDs Inc., St. Louis, MO). The testing protocol is shown in **Figure 4.5A** and was as follows: flies were filmed in dark-conditions for 15-sec, after which red light was applied continuously for 15-sec. Flies were then subjected to dark-conditions for another 15-sec, followed by another continuous application of red light for 15-sec. Responses were classified as a full extension only if flies completely extended their proboscis, including the rostrum (**Figure 4.5C**). The order of genotypes tested on each day was randomized and tested blind to

researchers. All the responses were scored blind to researchers to eliminate bias. Approximately equal numbers of males and females were tested.

FLIC (Fly Liquid-Food Interaction Counter) assay. The FLIC Drosophila Behavior system (Sable Systems International, Las Vegas, NV) was used for measuring single-fly feeding behaviors. Feeding activities from three Drosophila Feeding Monitor (DFM) plates was collected by the FLIC Monitor software (version 2.1) that was described previously (Ro et al., 2014). In brief, mated female flies aged 5-8 days were starved for 24 hours in water-saturated vials prior to the assay. Flies were gently aspirated into individual arenas containing one of the tested compounds–water, 100 mM sucrose, 200 mM D-glucose, 200 mM L-glucose, and a mixture of 25 mM three amino acids (Ser, Thr, and Phe). The positions of tested genotypes and tastants on each DFM plate were randomly shuffled every run for genotypes, and every day for tastants. Flies were assayed for 1 hour each and the raw data of the last 55 minutes was analyzed to account for time needed to load flies into their wells.

Analysis of FLIC raw data was conducted using custom R scripts. The first script analyzed the raw electrical signal data of each well to generate feeding features described throughout this paper. A baseline electrical signal was calculated for each well by identifying the most commonly occurring electrical signal value throughout the 55-minute analysis period. Feeding events were defined as samples with electrical signal over 100 a.u. + baseline; tasting events were defined as samples with electrical signal

over the baseline but less than 100 a.u. + baseline. Two consecutive events were distinguished if they occurred more than 1 second apart.

Definition of features

- The first feeding intensity: peak electrical signal of the first feeding event
- The first feeding duration: time elapsed across the first feeding event
- Interval between the first and second feeding events: time elapsed between the first and second feeding events
- Time to the first feeding event: timestamp of the initiation of first feeding event

A second script annotated each trial with its corresponding genotype and tastant information by extracting information from accompanying text files using character matching/extracting functions. A third script performed a logistic regression analysis using a model trained on a set of 300 randomly selected and manually sorted "good" and "bad" trials to determine usable data from our larger dataset of over 3000 individual trials. We input the features generated from our data analysis code into a model that assigned weights for each feature to generate the regression. The regression predicted a continuous variable between 0 and 1 as a function of the weighted features input into the model. To minimize false positives, a value of 0.9 was selected as the threshold for binary classification. If the model assigned a trial a value of 0.9 or higher, the trial was classified as "good." If the model assigned a trial a value less than 0.9, the trial was classified as "bad." Against a test set of 300 additional randomly selected and manually

sorted trials, the regression scored about 90% accuracy and against our overall dataset, the regression provided about 67% yield of usable trials–a rate similarly reflected in the training set distribution. Source codes for the analysis can be obtained at https://github.com/vdmenon/FLIC.

Experimental design and statistical analysis. Unless otherwise noted, all data are presented as median ± interquartile range. Statistical tests were conducted using Prism 8 (GraphPad Software). All the experiments were performed in parallel with both control and experimental genotypes. Complete genotypes of flies used in each experiment are listed in **Table 4.1**. The sample size for each experiment was based on previously published reports. All independent trials were performed over 2 days.

FIGURES

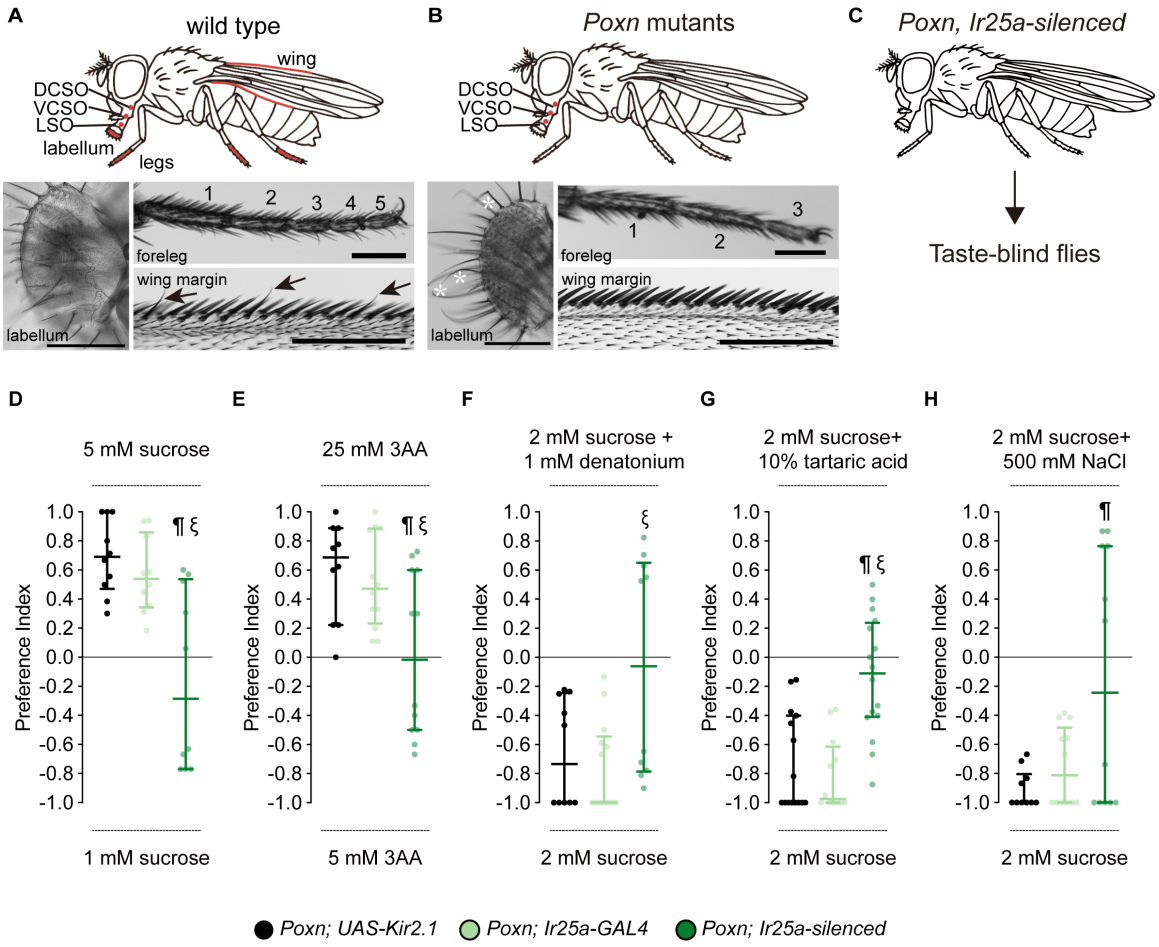

Figure 4.1. *Ir25a*-silenced *Poxn* flies are "taste-blind" to tastants from different taste modalities.

(**A-B**) Schematics (top) and bright field images of taste organs (bottom) in wild type (**A**) and *Poxn* mutant (**B**) flies. The body parts marked in red indicate locations of taste neurons. Arrows indicate taste hairs in the wing margins of wild type animals, which are absent in *Poxn* mutants. Asterisks in the bright field image of the *Poxn* labellum point to representative long, bent mechanosensory bristles, which are present in place of external

taste hairs. The five tarsal segments in wild type forelegs are indicated by numbers; these are fused into three segments in *Poxn* mutants. Scale bar: 100 μm.

(**C**) Schematic cartoon showing the generation of taste-blind flies by silencing all pharyngeal neurons via *Ir25a-GAL4* in a *Poxn* mutant background.

(**D-H**) Mean preference index values of *Poxn* ($Poxn^{\Delta M22\text{-}B5}/Poxn^{70}$) mutants carrying indicated transgenes obtained from binary choice experiments with 5 mM sucrose tested against 1 mM sucrose (**D**), 25 mM 3 amino acid mixtures (3AA) tested against 5 mM 3AA (**E**), 2 mM sucrose mixed with 1 mM denatonium (**F**), 10% tartaric acid (**G**), or 500 mM NaCl (**H**) tested against 2 mM sucrose alone. *UAS-Kir2.1* and *Ir25a-GAL4* transgenes were tested independently as indicated, or together (*Ir25a*-silenced). *n*=10-15. Error bars = interquartile range. ¶ and ξ indicate a statistically significant difference from the *UAS* and *GAL4* controls, respectively, by one-way ANOVA followed by uncorrected Fisher's LSD test or Kruskal-Wallis test followed by uncorrected Dunn's test. The One simple t test or Wilcoxon signed-rank test were used for testing whether the median values for each genotype were different from zero.

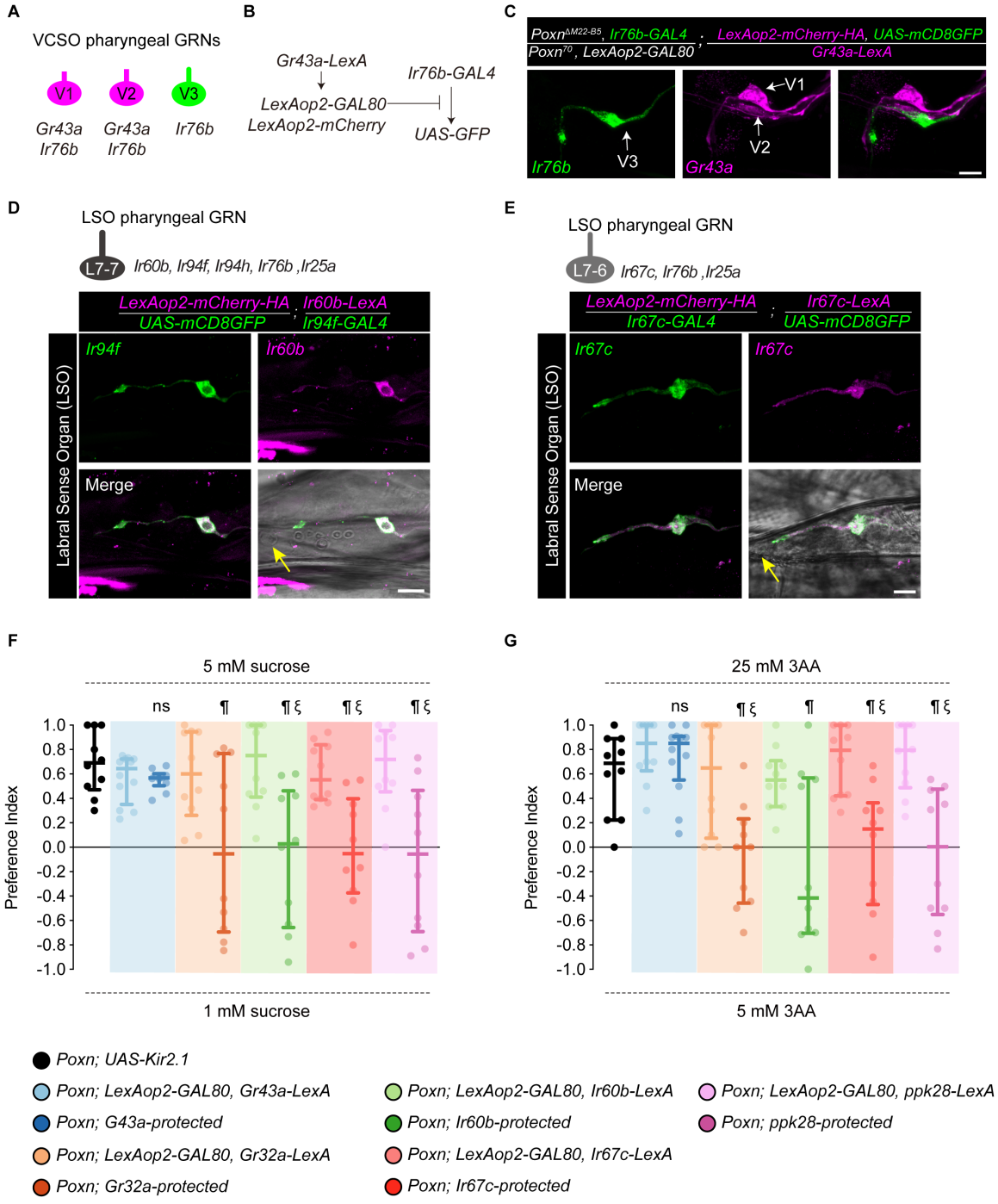

Figure 4.2. Feeding preferences of sugar and amino acids are recovered by functional restoration of pharyngeal *Gr43a* GRNs in "taste-blind" flies.

(**A**) Schematic cartoon showing the transgenic reporter expression of *Gr43a* and *Ir76b* in three pharyngeal GRNs of ventral cibarial sense organs (VCSO).

(**B**) Schematic diagram of genetic subtraction of *Gr43a-LexA* expression from *Ir76b-GAL4* with *LexAop2-GAL80* that restricts *UAS-GFP* expression to non-overlapping GRNs in the VCSO.

(**C**) Co-labeling of *Ir76b-GAL4* driven *UAS-GFP* expression in the V3 neuron and *Gr43a-LexA* driven *LexAop2-mCherry* (magenta) in the V1 and V2 neurons. Note that the GFP expression in V1 and V2 neurons is limited by the *LexAop2-GAL80* expression driven by *Gr43a-LexA*. Scale bar: 10 μm.

(**D-E**) Validation of *Ir60b-LexA* and *Ir67c-LexA* in the LSO. Expression of *Ir94f-GAL4* (green) and *Ir60b-LexA* (magenta) or *I67c-GAL4* (green) and *Ir67c-LexA* (magenta) lines in the LSO is tested with *UAS-mCD8-GFP* and *LexAop2-mCherry-HA*. The co-localization of both reporters is observed in L7-7 neuron (**D**) and L7-6 neuron (**E**). The yellow arrows mark the #7 chemosensory sensillum of the LSO.

(**F-G**) Mean preference index values of *Poxn* ($Poxn^{\Delta M22\text{-}B5}/Poxn^{70}$) mutants carrying indicated transgenes obtained from binary choice experiments with 5 mM sucrose tested against 1 mM sucrose (**F**) or 25 mM 3 amino acid mixtures (3AA) tested against 5 mM 3AA (**G**). *LexAop2-GAL80* with *Gr43a-LexA*, *Gr32a-LexA*, *Ir60b-LexA*, *Ir67c-LexA*, and *ppk28-LexA* transgene controls were tested independently as indicated, or together *Gr43a*-protected, *Gr32a*-protected, *Ir60b*-protected, *Ir67c*-protected, and *ppk28*-protected in a taste-blind background (*Poxn, Ir25a-silenced*). The *UAS-Kir2.1* transgene control data was the same as shown in **Figure 4.1D**. *n*=10-15. Error bars = interquartile

range. ¶ and ξ indicate a statistically significant difference from the *UAS* and *GAL4* controls, respectively, by Kruskal-Wallis test followed by uncorrected Dunn's test. The Wilcoxon signed-rank test were used for testing whether the median values for each genotype were different from zero.

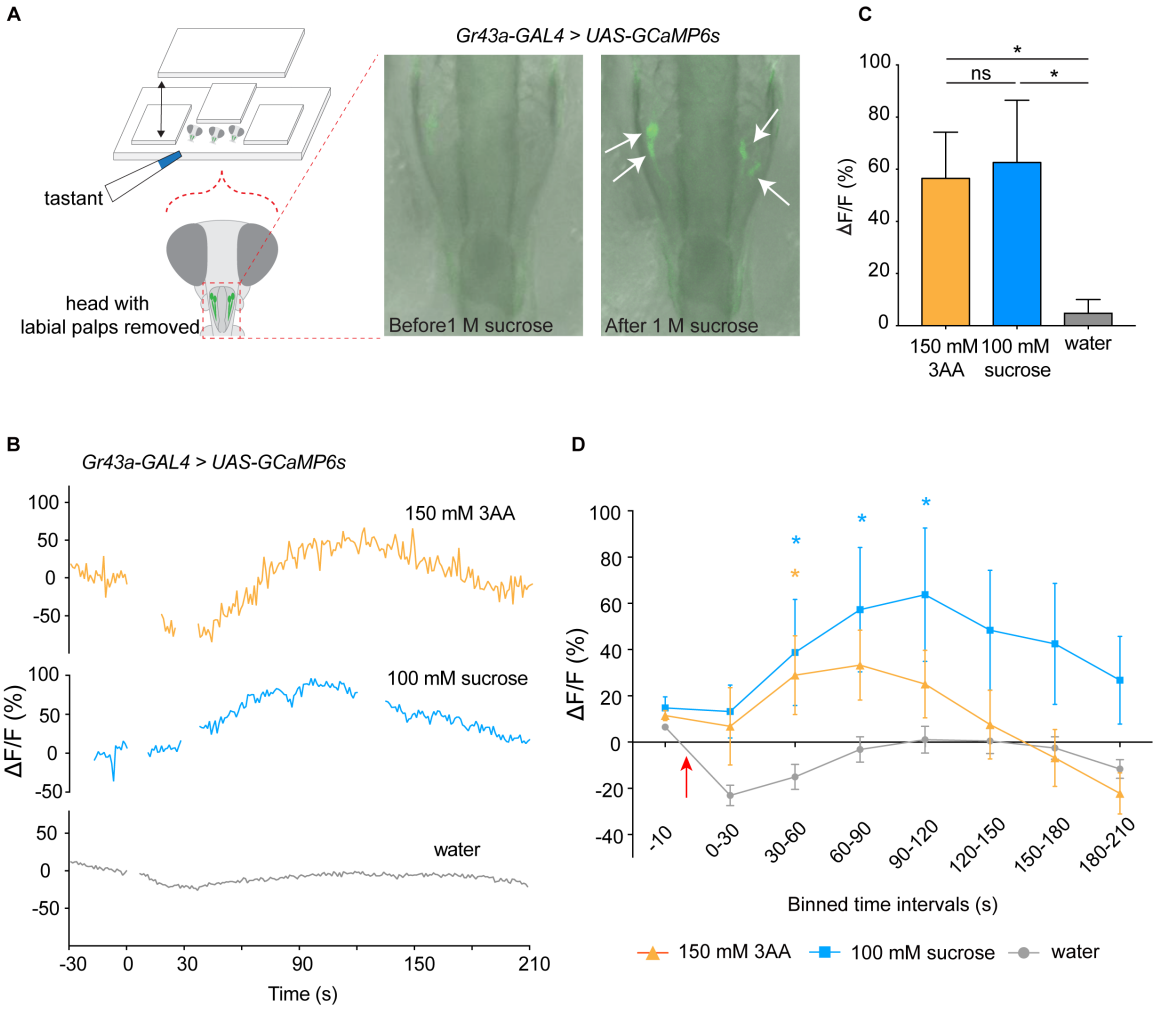

Figure 4.3. Pharyngeal calcium imaging reveals taste responses to amino acid mixtures in pharyngeal *Gr43a* neurons in the labral sense organ (LSO).

(**A**) Schematic diagram of the *ex vivo* pharyngeal calcium imaging setup (left). 22mmx22mm cover slips were placed above and on either side of the excised fly head, whose labial palps were surgically removed. A 22mmx40mm coverslip was placed on top of the heads. The tastant was applied through a P200 pipette tip. Flies with expression of GCaMP6s calcium indicator in pharyngeal *Gr43a* GRNs were imaged by confocal microscopy. Representative fluorescence images of pharyngeal *Gr43a* GRNs in the LSO

before and after 1 M sucrose stimulus (right). Arrows indicate the cell bodies of the pharyngeal *Gr43a* GRNs.

(**B**) Representative traces of GCaMP6s fluorescence in pharyngeal *Gr43a* GRNs in response to 150 mM 3AA mixture, 100 mM sucrose or water. The gaps in the traces indicate data discarded due to sample movement.

(**C**) Peak changes of GCaMP6s fluorescence in pharyngeal *Gr43a* GRNs in response to amino acid stimulus (150 mM 3AA, mixture of serine, threonine and phenylalanine), 100 mM sucrose, or solvent (water). Asterisks indicate significant difference from water by Mann-Whitney test. n=8-18. $^{**}P < 0.01$, $^{***}P < 0.001$. Error bars = SEM.

(**D**) Time course of change in fluorescence (ΔF/F) for samples that received amino acid stimulus (150 mM 3AA), 100 mM sucrose, or solvent (water). ΔF/F values are binned into 30-second intervals, after application of stimulus (at time-point indicated by the red arrow). Asterisks indicate significant difference from water by two-way ANOVA followed by Bonferroni *post hoc* test. n=8-18. $^{*}P < 0.05$. Error bars = SEM.

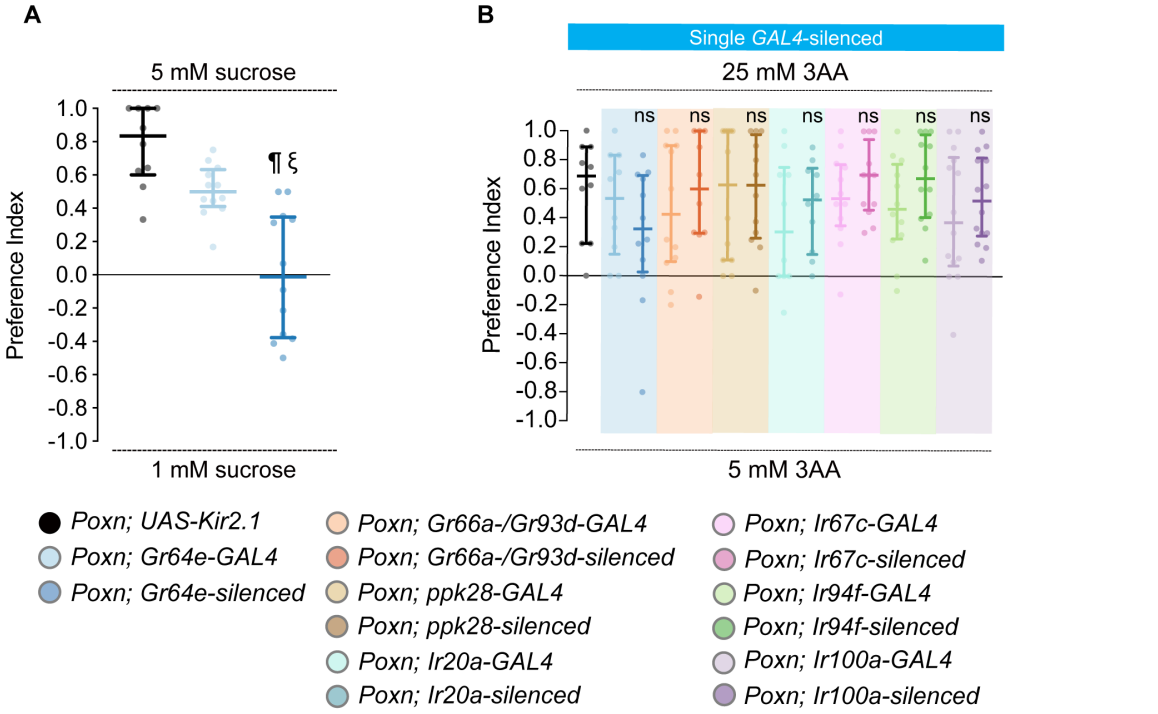
A
5 mM sucrose
1 mM sucrose
Preference Index
1.0
0.8
0.6
0.4
0.2
0.0
-0.2
-0.4
-0.6
-0.8
-1.0
¶ ξ
B
Single GAL4-silenced
25 mM 3AA
5 mM 3AA
ns
Poxn; UAS-Kir2.1
Poxn; Gr64e-GAL4
Poxn; Gr64e-silenced
Poxn; Gr66a-/Gr93d-GAL4
Poxn; Gr66a-/Gr93d-silenced
Poxn; ppk28-GAL4
Poxn; ppk28-silenced
Poxn; Ir20a-GAL4
Poxn; Ir20a-silenced
Poxn; Ir67c-GAL4
Poxn; Ir67c-silenced
Poxn; Ir94f-GAL4
Poxn; Ir94f-silenced
Poxn; Ir100a-GAL4
Poxn; Ir100a-silenced

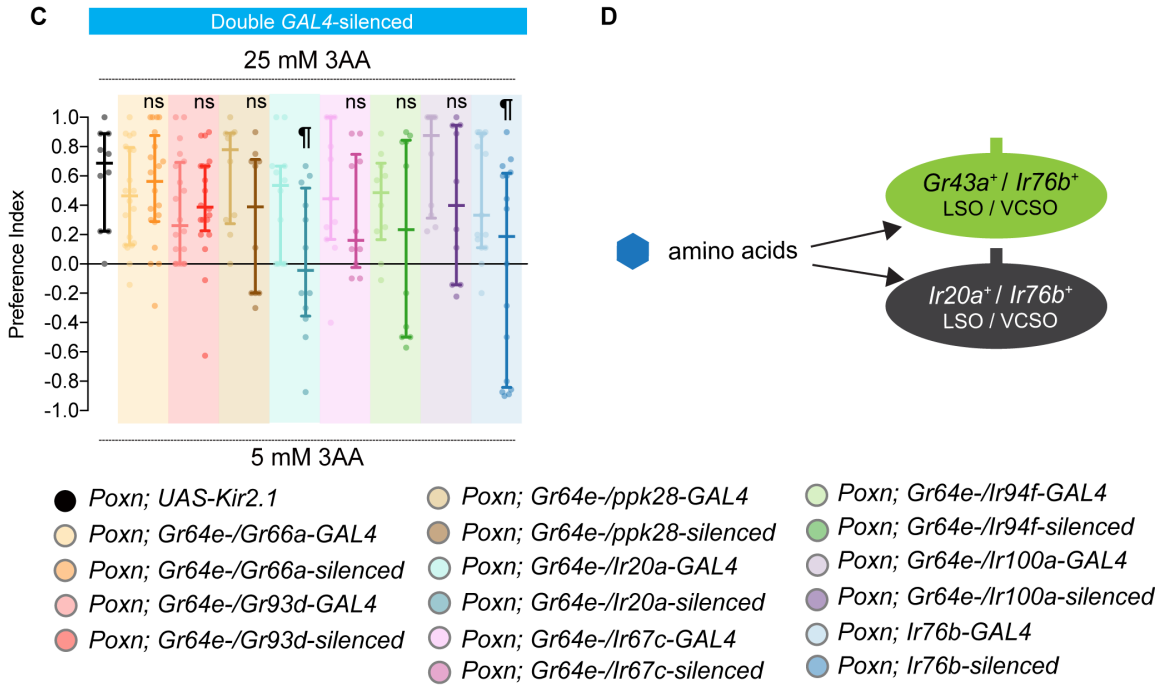
C
Double GAL4-silenced
25 mM 3AA
5 mM 3AA
Preference Index
ns
¶
D
amino acids
Gr43a+ / Ir76b+
LSO / VCSO
Ir20a+ / Ir76b+
LSO / VCSO
Poxn; UAS-Kir2.1
Poxn; Gr64e-/Gr66a-GAL4
Poxn; Gr64e-/Gr66a-silenced
Poxn; Gr64e-/Gr93d-GAL4
Poxn; Gr64e-/Gr93d-silenced
Poxn; Gr64e-/ppk28-GAL4
Poxn; Gr64e-/ppk28-silenced
Poxn; Gr64e-/Ir20a-GAL4
Poxn; Gr64e-/Ir20a-silenced
Poxn; Gr64e-/Ir67c-GAL4
Poxn; Gr64e-/Ir67c-silenced
Poxn; Gr64e-/Ir94f-GAL4
Poxn; Gr64e-/Ir94f-silenced
Poxn; Gr64e-/Ir100a-GAL4
Poxn; Gr64e-/Ir100a-silenced
Poxn; Ir76b-GAL4
Poxn; Ir76b-silenced

Figure 4.4. Pharyngeal *Gr43a* and *Ir20a* GRNs are necessary for feeding preference for amino acids.

(**A-C**) Mean preference index values of *Poxn* ($Poxn^{\Delta M22\text{-}B5}/Poxn^{70}$) mutants carrying indicated transgenes obtained from binary choice experiments with 5 mM sucrose tested against 1 mM sucrose (**A**), 25 mM 3 amino acid mixtures (3AA) tested against 5 mM 3AA (**B-C**). *UAS-Kir2.1* and *Gr/Ir-GAL4* transgenes were tested independently as indicated, or together (*Gr/Ir*-silenced). Note that the *UAS-Kir2.1* data was the same as shown in **Figure 4.1E**. *n*=10-20. Error bars = interquartile range. ¶ and ξ indicate a statistically significant difference from the *UAS* and *GAL4* controls, respectively, by Kruskal-Wallis test followed by uncorrected Dunn's test.

(**D**) Schematic diagram showing detection of amino acids through two populations of pharyngeal GRNs

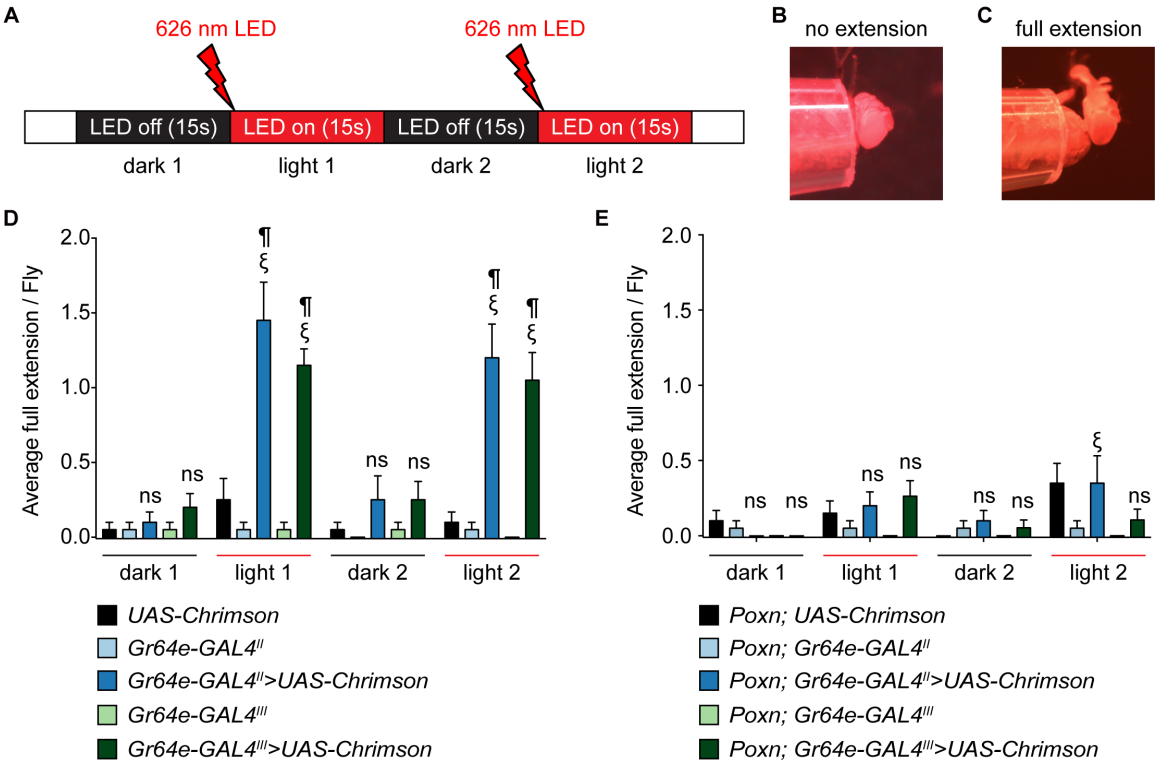

Figure 4.5. Inducible activation of pharyngeal *Gr43a* neurons does not induce proboscis extensions.

(**A**) Schematic diagram of experimental procedure to test number of proboscis extensions in 15-second period before and during two consecutive sections of red light exposure from 626 nm LEDs.

(**B-C**) Examples of negative (**B**) and positive (**C**) full proboscis extension responses.

(**D-E**) Mean full proboscis extensions during red light exposure calculated for flies with indicated transgenes in a wild type (**D**) or *Poxn* mutant background (**E**). *n*=19-21. Error bars = SEM. ¶ indicates significant difference from the corresponding *UAS* control; ξ indicates significant difference from the corresponding *GAL4* control; $P<0.05$, two-way ANOVA with *post-hoc* Tukey test. ns, not significant.

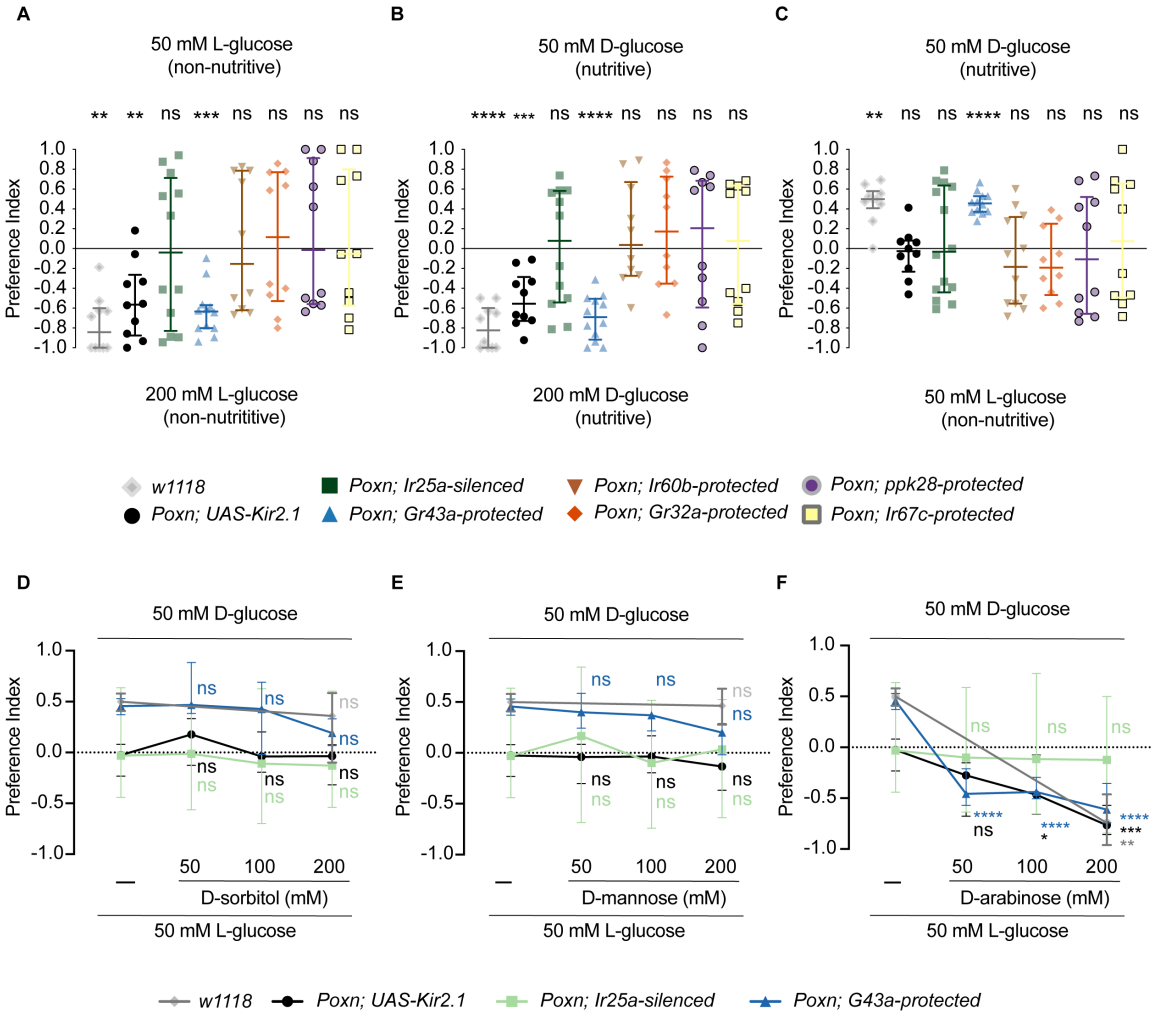

Figure 4.6. Pharyngeal *Gr43a* neurons promote food choice mainly based on sweet taste but not nutritional value of sugars.

(**A-C**) Mean preference index values of *Poxn* (*Poxn*$^{\Delta M22\text{-}B5}$/*Poxn*^{70}) mutants carrying indicated transgenes obtained from binary choice experiments with 50 mM L-glucose tested against 200 mM L-glucose (**A**), 50 mM D-glucose tested against 200 mM D-glucose (**B**), and 50 mM D-glucose tested against 50 mM L-glucose (**C**). *n*=10-14. Error bars = interquartile range. The Wilcoxon signed-rank test were used for testing whether

the median values for each genotype were different from zero. **P<0.01, ****P<0.0001. ns, not significant.

(**D-F**) Mean preference index values of *Poxn* ($Poxn^{\Delta M22\text{-}B5}/Poxn^{70}$) mutants carrying indicated transgenes obtained from binary choice experiments with 50 mM D-glucose tested against 50 mM L-glucose mixed with various concentrations of D-sorbitol (**D**), D-mannose (**E**), and D-arabinose (**F**). *n*=10-14. Error bars = interquartile range. Asterisks indicate significant difference from 50 mM L-glucose alone within the same genotype by two -way ANOVA with *post-hoc* uncorrected Fisher's LSD test. *P<0.05, ***P<0.001, ****P<0.0001. ns, not significant.

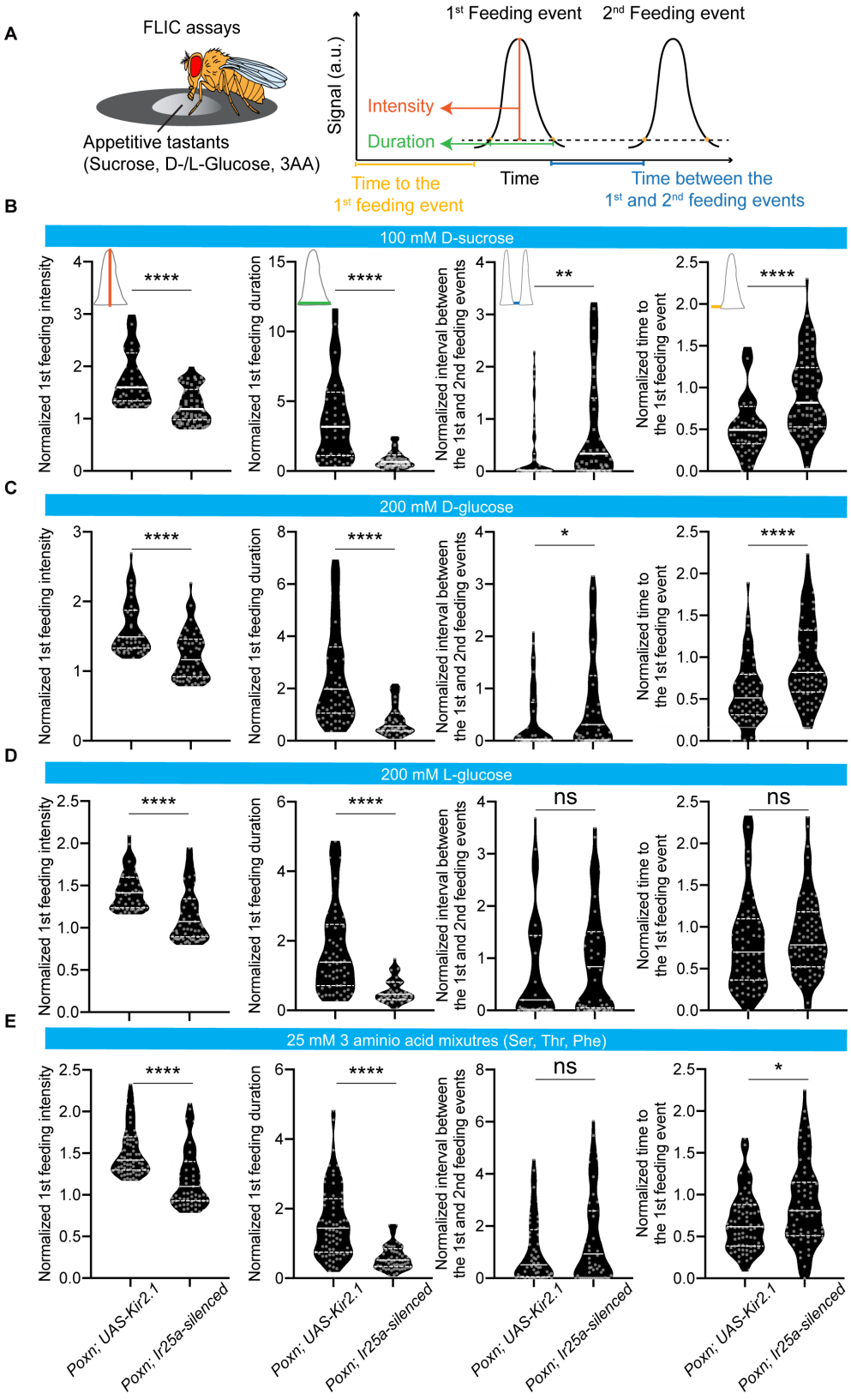
A
FLIC assays
Appetitive tastants
(Sucrose, D-/L-Glucose, 3AA)
1st Feeding event
2nd Feeding event
Signal (a.u.)
Intensity
Duration
Time
Time to the
1st feeding event
Time between the
1st and 2nd feeding events
B
100 mM D-sucrose
C
200 mM D-glucose
D
200 mM L-glucose
E
25 mM 3 aminio acid mixutres (Ser, Thr, Phe)
Normalized 1st feeding intensity
Normalized 1st feeding duration
Normalized interval between the 1st and 2nd feeding events
Normalized time to the 1st feeding event
****
**
*
ns
Poxn; UAS-Kir2.1
Poxn; Ir25a-silenced

Figure 4.7. Pharyngeal GRNs regulate micro-feeding features in response to appetitive tastants.

(**A**) Schematic diagram of Fly Liquid-Food Interaction Counter (FLIC) setup (left). Feeding responses to water and appetitive tastants (D-sucrose, D-glucose, L-glucose, and 3AA) were tested. Schematic diagram showing distinct features of micro-feeding behaviors extracted by our custom R scripts (right).

(**B-E**) Four different features of micro-feeding behaviors in respond to 100 mM D-sucrose (**B**), 200 mM D-glucose (**C**), 200 mM L-glucose (**D**), and 25 mM 3AA mixtures (**E**) was compared between *UAS* control (*Poxn; UAS-Kir2.1*) and taste-blind (*Poxn; Ir25a*-silenced), including the intensity and duration of the first feeding event, interval between the first and second feeding events, and the time to the first feeding event. All the features of micro-feeding behaviors were normalized to their corresponding water values before comparison. *n*=23-83. Error bars = interquartile range. Asterisks indicate significant difference between two groups by Mann Whitney test. *P<0.05, **P<0.01, ****P<0.0001. ns, not significant.

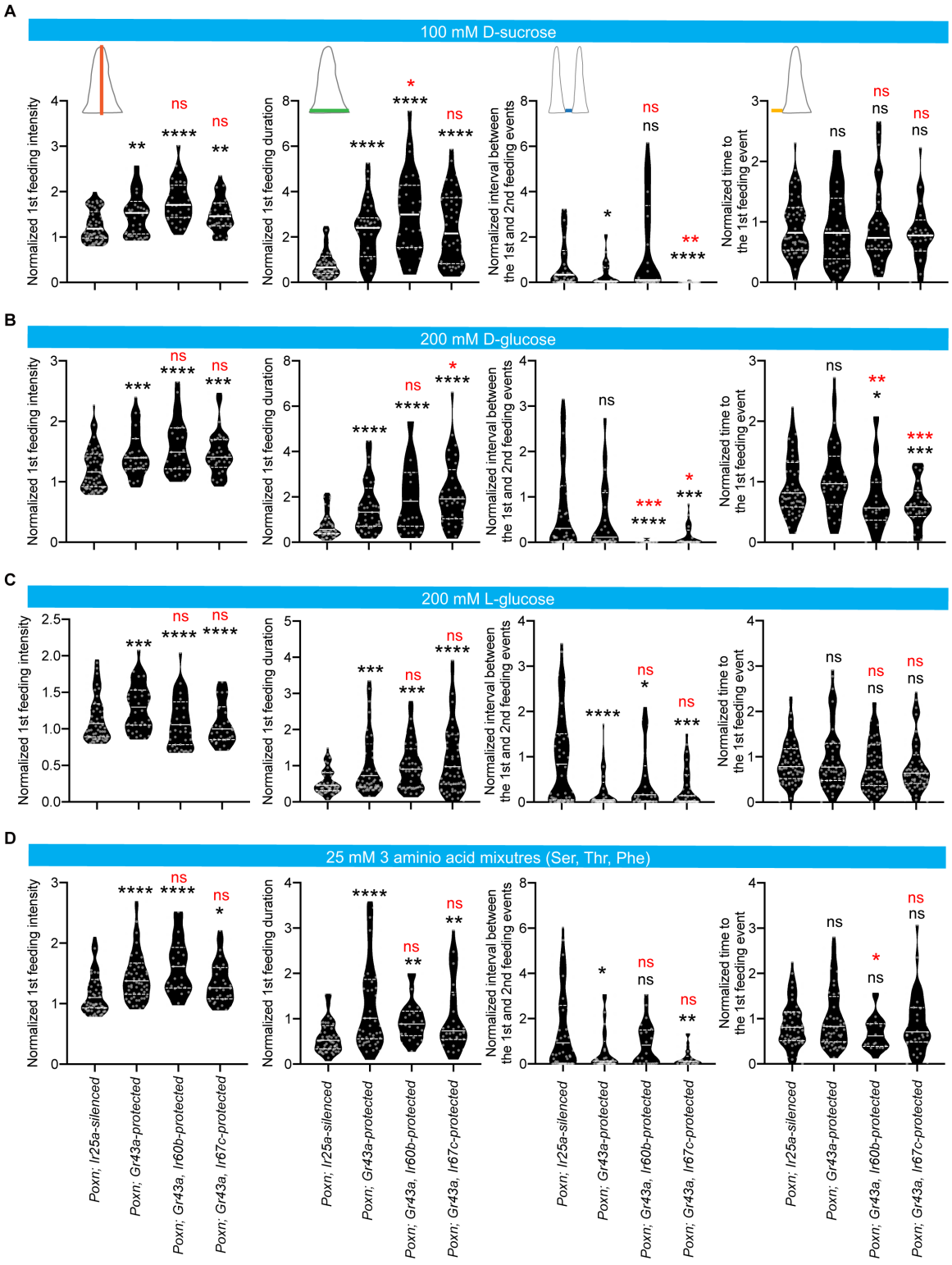
A
100 mM D-sucrose
B
200 mM D-glucose
C
200 mM L-glucose
D
25 mM 3 aminio acid mixutres (Ser, Thr, Phe)
Normalized 1st feeding intensity
Normalized 1st feeding duration
Normalized interval between the 1st and 2nd feeding events
Normalized time to the 1st feeding event
Poxn; Ir25a-silenced
Poxn; Gr43a-protected
Poxn; Gr43a, Ir60b-protected
Poxn; Gr43a, Ir67c-protected

Figure 4.8. Pharyngeal *Gr43a* GRNs along with other pharyngeal GRNs regulate micro-feeding responses to appetitive tastants in a tastant-specific manner.

(**A-D**) Four different features of micro-feeding behaviors in respond to 100 mM D-sucrose (**A**), 200 mM D-glucose (**B**), 200 mM L-glucose (**C**), and 25 mM 3AA mixtures (**D**) was compared between taste-blind (*Poxn; Ir25a*-silenced) and flies with restoring selected pharyngeal GRNs as indicated, including the intensity and duration of the first feeding event, interval between the first and second feeding events, and the time to the first feeding event. All the features of micro-feeding behaviors were normalized to their corresponding water values before comparison. *n*=23-83. Error bars = interquartile range. Asterisks (black) indicate significant difference from taste-blind (*Poxn; Ir25a*-silenced) flies by Mann Whitney test. *P<0.05, **P<0.01, ****P<0.0001. ns, not significant. Asterisks (red) indicate significant difference from (*Poxn; Gr43a*-protected) flies by Mann Whitney test. *P<0.05, **P<0.01, ****P<0.0001. ns, not significant.

SUPPLEMENTAL FIGURES

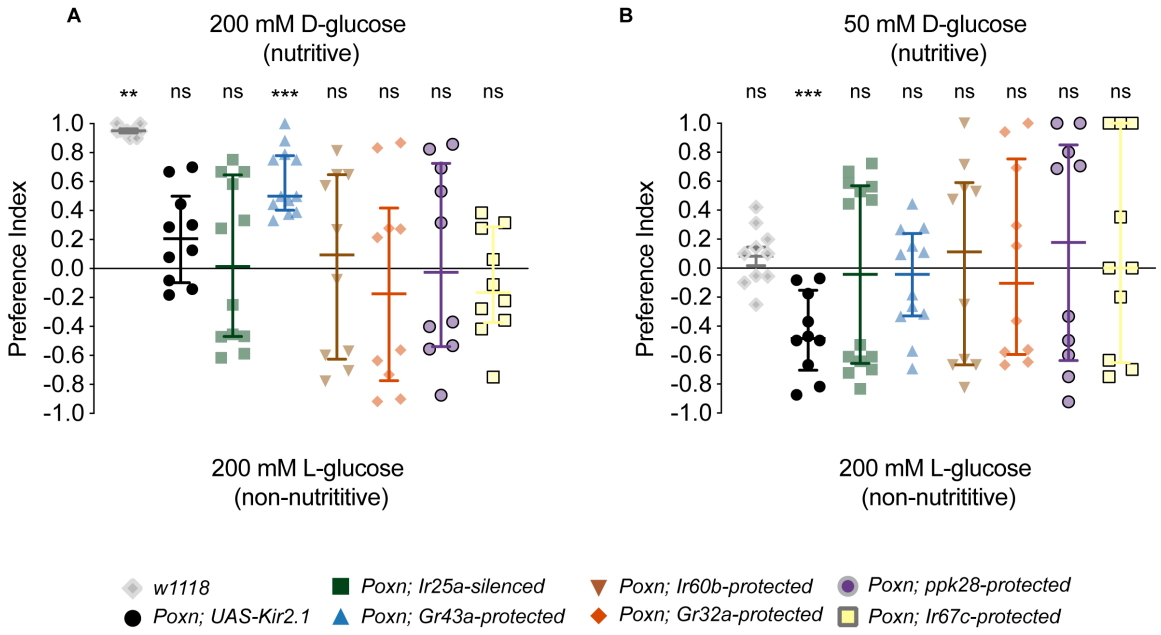

Figure 4.9. Pharyngeal *Gr43a* neurons exhibit differential behavioral sensitivity to D-glucose and L-glucose.

(**A-B**) Mean preference index values of *Poxn* ($Poxn^{\Delta M22\text{-}B5}/Poxn^{70}$) mutants carrying indicated transgenes obtained from binary choice experiments with 200 mM L-glucose tested against 200 mM L-glucose (**A**) and 50 mM D-glucose tested against 200 mM L-glucose (**B**). n=10-14. Error bars = interquartile range. The Wilcoxon signed-rank test were used for testing whether the median values for each genotype were different from zero. **P<0.01, ****P<0.0001. ns, not significant.

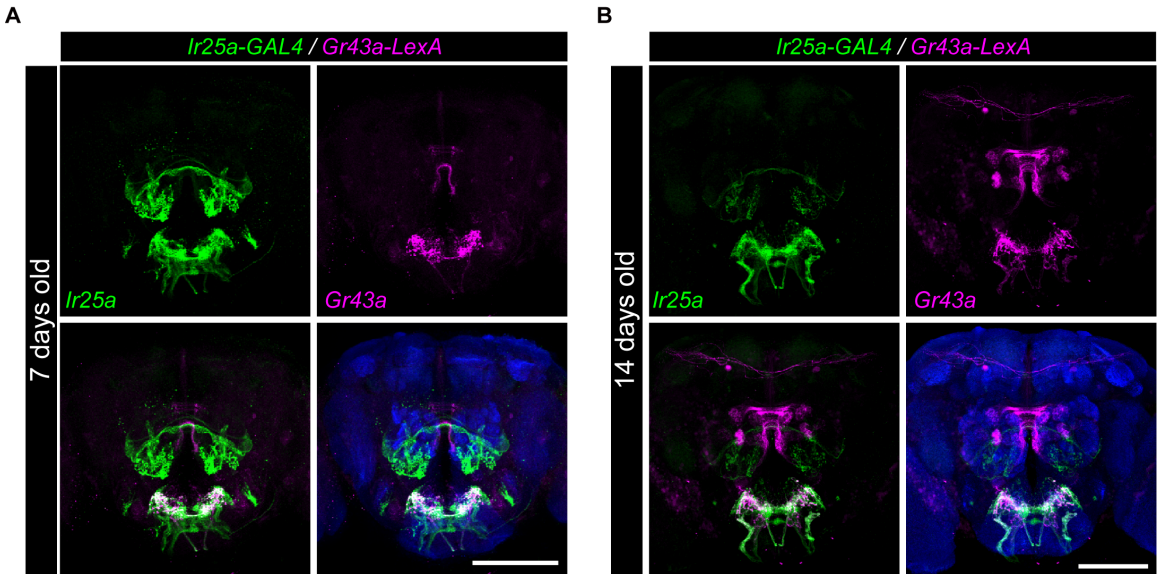

Figure 4.10. Expression of *Ir25a-GAL4* and *Gr43a-LexA* in adult *Drosophila* brain.

GFP and mCherry reporter expressions driven by *Ir25a-GAL4* (green) and *Gr43a-LexA* (magenta) drivers in the adult *Drosophila* brain in 7-day-old (**A**) and 14-day-old (**B**) flies. Neuropil is stained with anti-nc82 (blue). Scale bar: 100 μm.

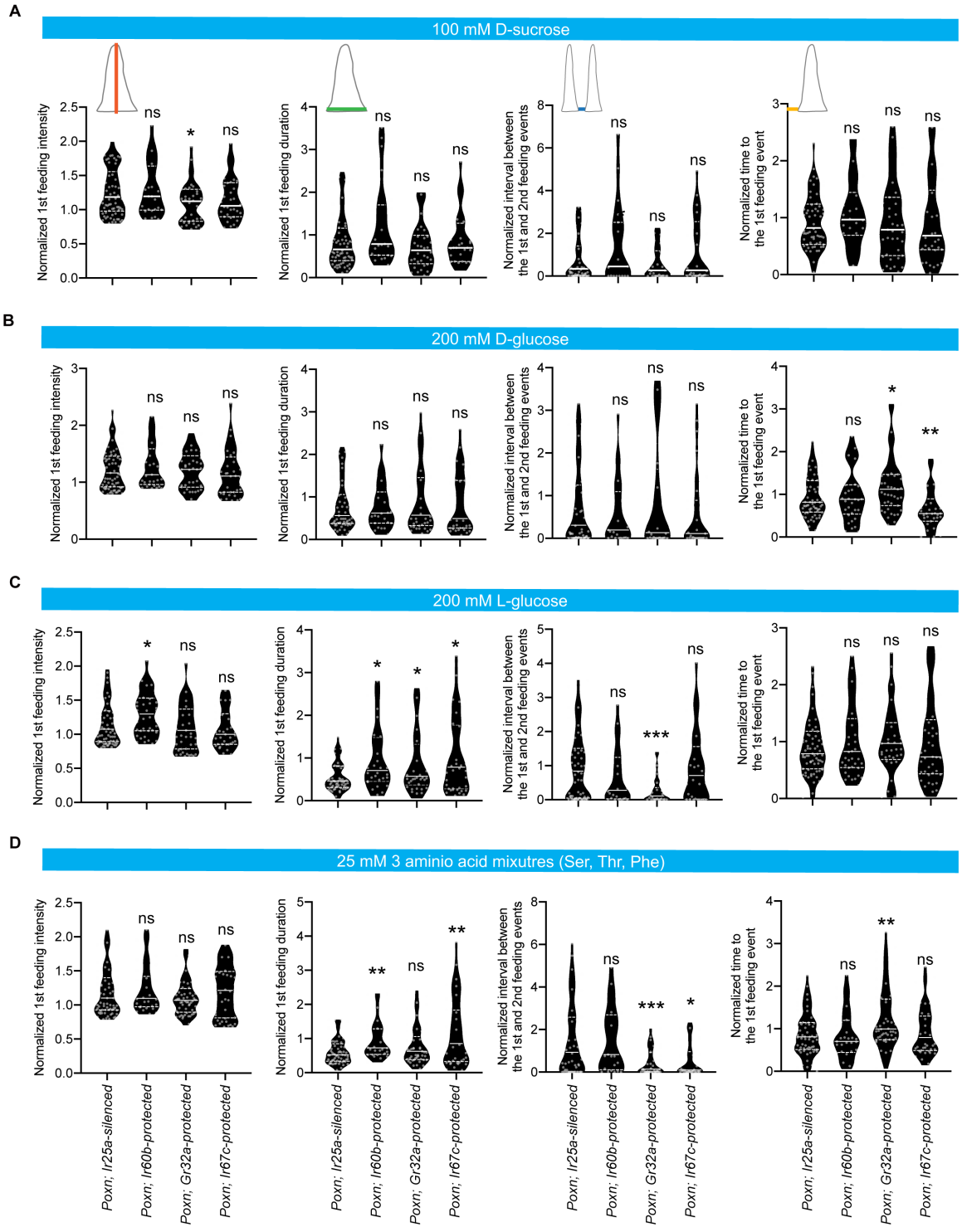

Figure 4.11. Micro-feeding responses to appetitive tastants in flies with selected pharyngeal GRNs protected (*Ir60b*, *Gr32a*, *Ir67c*) in the taste-blind background.

(**A-D**) Four different features of micro-feeding behaviors in respond to 100 mM D-sucrose (**A**), 200 mM D-glucose (**B**), 200 mM L-glucose (**C**), and 25 mM 3AA mixtures (**D**) was compared between taste-blind (*Poxn; Ir25a*-silenced) and flies with restoring selected pharyngeal GRNs as indicated, including the intensity and duration of the first feeding event, interval between the first and second feeding events, and the time to the first feeding event. All the features of micro-feeding behaviors were normalized to their corresponding water values before comparison. *n*=23-83. Error bars = interquartile range. Asterisks indicate significant difference from taste-blind (*Poxn; Ir25a*-silenced) flies by Mann Whitney test. *P<0.05, **P<0.01, ****P<0.0001. ns, not significant.

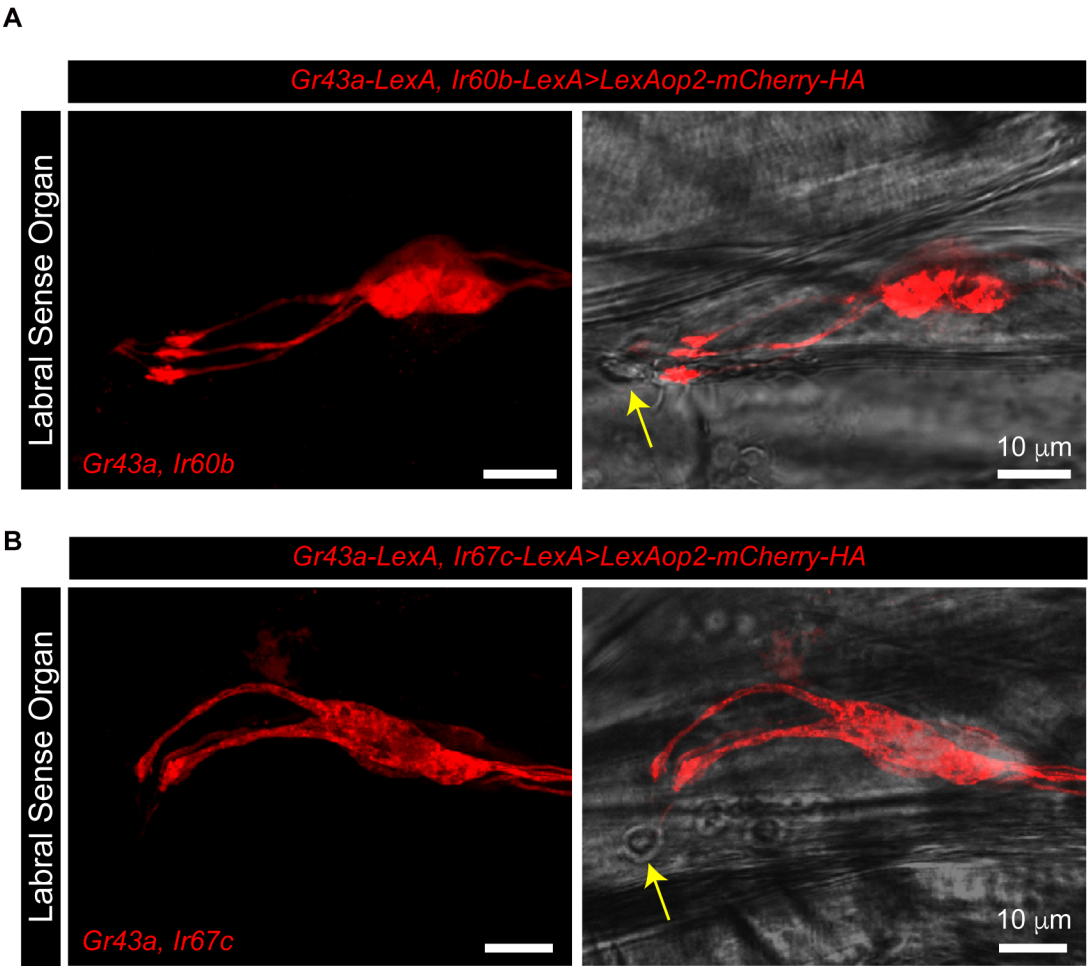

Figure 4.12. Expression of recombinant transgenes containing *Gr43a-LexA/Ir60b-LexA* and *Gr43a-LexA/Ir67c-LexA* in the #7 sensillum of LSO.

mCherry reporter expressions (red) driven by *Gr43a-LexA/Ir60b-LexA* (**A**) and *Gr43a-LexA/Ir67c-LexA* (**B**) drivers in the #7 sensillum of LSO. In both cases, three GRNs were labeled by mCherry reporter. The yellow arrows indicate the cuticular pore of the #7 sensillum of LSO. Scale bar: 10 μm.

TABLE

Table 4.1. Complete genotypes of flies used in this study.

Figure	Genotype
4.1D-H	(from left to right)
	$Poxn^{\Delta M22\text{-}B5}$/$poxn^{70}$; UAS-Kir2.1/+
	$Poxn^{\Delta M22\text{-}B5}$, Ir25a-GAL4/$Poxn^{70}$; Dr or TM3/+
	$Poxn^{\Delta M22\text{-}B5}$, Ir25a-GAL4/$Poxn^{70}$;UAS-Kir2.1/UAS-Kir2.1
4.2C	*$Poxn^{\Delta M22\text{-}B5}$, Ir76b-GAL4/$Poxn^{70}$, LexAop2-GAL80; LexAop2-mCherry-HA, UAS-mCD8-GFP/Gr43a-LexA*
4.2D	*LexAop2-mCherry-HA/UAS-mCD8-GFP; Ir60b-LexA /Ir94f-GAL4*
4.2E	*LexAop2-mCherry-HA/Ir67c-GAL4; Ir67c-LexA /UAS-mCD8-GFP*
4.2F-G	(from left to right)
	$Poxn^{\Delta M22\text{-}B5}$/$poxn^{70}$; UAS-Kir2.1/+
	$Poxn^{\Delta M22\text{-}B5}$/$Poxn^{70}$, LexAop2-GAL80; Gr43a-LexA /+
	$Poxn^{\Delta M22\text{-}B5}$, Ir25a-GAL4/$Poxn^{70}$, LexAop2-GAL80; Gr43a-LexA/UAS-Kir2.1
	$Poxn^{\Delta M22\text{-}B5}$/$Poxn^{70}$, LexAop2-GAL80; Gr32a-LexA /+
	$Poxn^{\Delta M22\text{-}B5}$, Ir25a-GAL4/$Poxn^{70}$, LexAop2-GAL80; Gr32a-LexA/UAS-Kir2.1
	$Poxn^{\Delta M22\text{-}B5}$/$Poxn^{70}$, LexAop2-GAL80; Ir60b-LexA /+
	$Poxn^{\Delta M22\text{-}B5}$, Ir25a-GAL4/$Poxn^{70}$, LexAop2-GAL80; Ir60b-LexA/UAS-Kir2.1
	$Poxn^{\Delta M22\text{-}B5}$/$Poxn^{70}$, LexAop2-GAL80; Ir67c-LexA /+
	$Poxn^{\Delta M22\text{-}B5}$, Ir25a-GAL4/$Poxn^{70}$, LexAop2-GAL80; Ir67c-LexA/UAS-Kir2.1
	$Poxn^{\Delta M22\text{-}B5}$/$Poxn^{70}$, LexAop2-GAL80; ppk28-LexA /+
	$Poxn^{\Delta M22\text{-}B5}$, Ir25a-GAL4/$Poxn^{70}$, LexAop2-GAL80; ppk28-LexA/UAS-Kir2.1
4.3	*UAS-GCaMP6s/UAS-GCaMP6s; Gr43a-GAL4/Gr43a-GAL4*
4.4A	(from left to right)
	$Poxn^{\Delta M22\text{-}B5}$/$Poxn^{70}$; UAS-Kir2.1/+
	$Poxn^{\Delta M22\text{-}B5}$, Gr64e-GAL4/$Poxn^{70}$
	$Poxn^{\Delta M22\text{-}B5}$, Gr64e-GAL4/$Poxn^{70}$; UAS-Kir2.1/+
4.4B	(from left to right)
	$Poxn^{\Delta M22\text{-}B5}$/$Poxn^{70}$; UAS-Kir2.1/+
	$Poxn^{\Delta M22\text{-}B5}$, Gr64e-GAL4/$Poxn^{70}$

	$Poxn^{\Delta M22\text{-}B5}$, Gr64e-GAL4/$Poxn^{70}$; UAS-Kir2.1/+
	$Poxn^{\Delta M22\text{-}B5}$, Gr66a-GAL4/$Poxn^{70}$; Gr93d-GAL4/+
	$Poxn^{\Delta M22\text{-}B5}$, Gr66a-GAL4/$Poxn^{70}$; Gr93d-GAL4/UAS-Kir2.1
	$Poxn^{\Delta M22\text{-}B5}$/$Poxn^{70}$; ppk28-GAL4/+
	$Poxn^{\Delta M22\text{-}B5}$/$Poxn^{70}$; ppk28-GAL4/UAS-Kir2.1
	$Poxn^{\Delta M22\text{-}B5}$, Ir20a-GAL4/$Poxn^{70}$; Dr or TM3/+
	$Poxn^{\Delta M22\text{-}B5}$, Ir20a-GAL4/$Poxn^{70}$; UAS-Kir2.1/Dr or TM3
	$Poxn^{\Delta M22\text{-}B5}$, Ir67c-GAL4/$Poxn^{70}$; Dr or TM3/+
	$Poxn^{\Delta M22\text{-}B5}$, Ir67c-GAL4/$Poxn^{70}$; UAS-Kir2.1/Dr or TM3
	$Poxn^{\Delta M22\text{-}B5}$/$Poxn^{70}$; Ir94f-GAL4/+
	$Poxn^{\Delta M22\text{-}B5}$/$Poxn^{70}$; Ir94f-GAL4/UAS-Kir2.1
	$Poxn^{\Delta M22\text{-}B5}$/$Poxn^{70}$; Ir100a-GAL4/+
	$Poxn^{\Delta M22\text{-}B5}$/$Poxn^{70}$; Ir100a-GAL4/UAS-Kir2.1
4.4C	(from left to right)
	$Poxn^{\Delta M22\text{-}B5}$/$Poxn^{70}$; UAS-Kir2.1/+
	$Poxn^{\Delta M22\text{-}B5}$, Gr64e-GAL4/$Poxn^{70}$; Gr66a-GAL4/+
	$Poxn^{\Delta M22\text{-}B5}$, Gr64e-GAL4/$Poxn^{70}$; Gr66a-GAL4/UAS-Kir2.1
	$Poxn^{\Delta M22\text{-}B5}$, Gr64e-GAL4/$Poxn^{70}$; Gr93d-GAL4/+
	$Poxn^{\Delta M22\text{-}B5}$, Gr64e-GAL4/$Poxn^{70}$; Gr93d-GAL4/UAS-Kir2.1
	$Poxn^{\Delta M22\text{-}B5}$, Gr64e-GAL4/$Poxn^{70}$; ppk28-GAL4/+
	$Poxn^{\Delta M22\text{-}B5}$, Gr64e-GAL4/$Poxn^{70}$; ppk28-GAL4/UAS-Kir2.1
	$Poxn^{\Delta M22\text{-}B5}$, Ir20a-GAL4/$Poxn^{70}$; Gr64e-GAL4/+
	$Poxn^{\Delta M22\text{-}B5}$, Ir20a-GAL4/$Poxn^{70}$; Gr64e-GAL4/UAS-Kir2.1
	$Poxn^{\Delta M22\text{-}B5}$, Ir67c-GAL4/$Poxn^{70}$; Gr64e-GAL4/+
	$Poxn^{\Delta M22\text{-}B5}$, Ir67c-GAL4/$Poxn^{70}$; Gr64e-GAL4/UAS-Kir2.1
	$Poxn^{\Delta M22\text{-}B5}$, Gr64e-GAL4/$Poxn^{70}$; Ir94f-GAL4/+
	$Poxn^{\Delta M22\text{-}B5}$, Gr64e-GAL4/$Poxn^{70}$; Ir94f-GAL4/UAS-Kir2.1
	$Poxn^{\Delta M22\text{-}B5}$, Gr64e-GAL4/$Poxn^{70}$; Ir100a-GAL4/+
	$Poxn^{\Delta M22\text{-}B5}$, Gr64e-GAL4/$Poxn^{70}$; Ir100a-GAL4/UAS-Kir2.1
	$Poxn^{\Delta M22\text{-}B5}$, Ir76b-GAL4/$Poxn^{70}$; Dr or TM3/+
	$Poxn^{\Delta M22\text{-}B5}$, Ir76b-GAL4/$Poxn^{70}$; UAS-Kir2.1/UAS-Kir2.1
4.5D	(from left to right)
	+/+; UAS-CsChrimson/+
	Gr64e-GAL4/Sp; Dr or TM3/+
	Gr64e-GAL4/Sp; UAS-CsChrimson/+
	+/Sp; Gr64e-GAL4/+

	+/Sp; Gr64e-GAL4/UAS-CsChrimson
4.5E	(from left to right)
	$Poxn^{\Delta M22\text{-}B5}$/$Poxn^{70}$; UAS-CsChrimson/+
	$Poxn^{\Delta M22\text{-}B5}$, Gr64e-GAL4/$Poxn^{70}$
	$Poxn^{\Delta M22\text{-}B5}$, Gr64e-GAL4/$Poxn^{70}$; UAS-CsChrimson/+
	$Poxn^{\Delta M22\text{-}B5}$/$Poxn^{70}$; Gr64e-GAL4/+
	$Poxn^{\Delta M22\text{-}B5}$/$Poxn^{70}$; Gr64e-GAL4/UAS-CsChrimson
4.6A-C	(from left to right)
	w1118
	$Poxn^{\Delta M22\text{-}B5}$/$Poxn^{70}$; UAS-Kir2.1/+
	$Poxn^{\Delta M22\text{-}B5}$, Ir25a-GAL4/$Poxn^{70}$;UAS-Kir2.1/UAS-Kir2.1
	$Poxn^{\Delta M22\text{-}B5}$, Ir25a-GAL4/$Poxn^{70}$, LexAop2-GAL80; Gr43a-LexA/UAS-Kir2.1
	$Poxn^{\Delta M22\text{-}B5}$, Ir25a-GAL4/$Poxn^{70}$, LexAop2-GAL80; Ir60b-LexA/UAS-Kir2.1
	$Poxn^{\Delta M22\text{-}B5}$, Ir25a-GAL4/$Poxn^{70}$, LexAop2-GAL80; Gr32a-LexA/UAS-Kir2.1
	$Poxn^{\Delta M22\text{-}B5}$, Ir25a-GAL4/$Poxn^{70}$, LexAop2-GAL80; ppk28-LexA/UAS-Kir2.1
	$Poxn^{\Delta M22\text{-}B5}$, Ir25a-GAL4/$Poxn^{70}$, LexAop2-GAL80; Ir67c-LexA/UAS-Kir2.1
4.6D-F	(from left to right)
	w1118
	$Poxn^{\Delta M22\text{-}B5}$/$Poxn^{70}$; UAS-Kir2.1/+
	$Poxn^{\Delta M22\text{-}B5}$, Ir25a-GAL4/$Poxn^{70}$;UAS-Kir2.1/UAS-Kir2.1
	$Poxn^{\Delta M22\text{-}B5}$, Ir25a-GAL4/$Poxn^{70}$, LexAop2-GAL80; Gr43a-LexA/UAS-Kir2.1
4.7B-E	(from left to right)
	$poxn^{\Delta M22\text{-}B5}$/$poxn^{70}$; UAS-Kir2.1/+
	$Poxn^{\Delta M22\text{-}B5}$, Ir25a-GAL4/$Poxn^{70}$;UAS-Kir2.1/UAS-Kir2.1
4.8	(from left to right)
	$Poxn^{\Delta M22\text{-}B5}$, Ir25a-GAL4/$Poxn^{70}$;UAS-Kir2.1/UAS-Kir2.1
	$Poxn^{\Delta M22\text{-}B5}$, Ir25a-GAL4/$Poxn^{70}$, LexAop2-GAL80; Gr43a-LexA/UAS-Kir2.1
	$Poxn^{\Delta M22\text{-}B5}$, Ir25a-GAL4/$Poxn^{70}$, LexAop2-GAL80; Gr43a-LexA, Ir60b-LexA/UAS-Kir2.1
	$Poxn^{\Delta M22\text{-}B5}$, Ir25a-GAL4/$Poxn^{70}$, LexAop2-GAL80; Gr43a-LexA, Ir67c-LexA/UAS-Kir2.1
4.9	(from left to right)

	w1118
	$Poxn^{\Delta M22\text{-}B5}$/$Poxn^{70}$; UAS-Kir2.1/+
	$Poxn^{\Delta M22\text{-}B5}$, Ir25a-GAL4/$Poxn^{70}$;UAS-Kir2.1/UAS-Kir2.1
	$Poxn^{\Delta M22\text{-}B5}$, Ir25a-GAL4/$Poxn^{70}$, LexAop2-GAL80; Gr43a-LexA/UAS-Kir2.1
	$Poxn^{\Delta M22\text{-}B5}$, Ir25a-GAL4/$Poxn^{70}$, LexAop2-GAL80; Ir60b-LexA/UAS-Kir2.1
	$Poxn^{\Delta M22\text{-}B5}$, Ir25a-GAL4/$Poxn^{70}$, LexAop2-GAL80; Gr32a-LexA/UAS-Kir2.1
	$Poxn^{\Delta M22\text{-}B5}$, Ir25a-GAL4/$Poxn^{70}$, LexAop2-GAL80; ppk28-LexA/UAS-Kir2.1
	$Poxn^{\Delta M22\text{-}B5}$, Ir25a-GAL4/$Poxn^{70}$, LexAop2-GAL80; Ir67c-LexA/UAS-Kir2.1
4.10	*Ir25a-GAL4/LexAop2-mCherry-HA; Gr43a-LexA/UAS-mCD8-GFP*
4.11	(from left to right)
	$Poxn^{\Delta M22\text{-}B5}$, Ir25a-GAL4/$Poxn^{70}$;UAS-Kir2.1/UAS-Kir2.1
	$Poxn^{\Delta M22\text{-}B5}$, Ir25a-GAL4/$Poxn^{70}$, LexAop2-GAL80; Ir60b-LexA/UAS-Kir2.1
	$Poxn^{\Delta M22\text{-}B5}$, Ir25a-GAL4/$Poxn^{70}$, LexAop2-GAL80; Gr32a-LexA/UAS-Kir2.1
	$Poxn^{\Delta M22\text{-}B5}$, Ir25a-GAL4/$Poxn^{70}$, LexAop2-GAL80; Ir67c-LexA/UAS-Kir2.1
4.12A	*LexAop2-mCherry-HA/+; Gr43a-LexA, Ir60b-LexA/+*
4.12B	*LexAop2-mCherry-HA/+; Gr43a-LexA, Ir67c-LexA/+*

REFERENCES

Accolla, R., Bathellier, B., Petersen, C. C. & Carleton, A. 2007. Differential spatial representation of taste modalities in the rat gustatory cortex. *J Neurosci,* 27**,** 1396-404.

Ahn, J. E., Chen, Y. & Amrein, H. 2017. Molecular basis of fatty acid taste in Drosophila. *Elife,* 6.

Awasaki, T. & Kimura, K. 1997. pox-neuro is required for development of chemosensory bristles in Drosophila. *J Neurobiol,* 32**,** 707-721.

Baines, R. A., Uhler, J. P., Thompson, A., Sweeney, S. T. & Bate, M. 2001. Altered electrical properties in Drosophila neurons developing without synaptic transmission. *J Neurosci,* 21**,** 1523-31.

Barretto, R. P., Gillis-Smith, S., Chandrashekar, J., Yarmolinsky, D. A., Schnitzer, M. J., Ryba, N. J. & Zuker, C. S. 2015. The neural representation of taste quality at the periphery. *Nature,* 517**,** 373-6.

Boll, W. & Noll, M. 2002. The Drosophila Pox neuro gene: control of male courtship behavior and fertility as revealed by a complete dissection of all enhancers. *Development,* 129**,** 5667-5681.

Cameron, P., Hiroi, M., Ngai, J. & Scott, K. 2010. The molecular basis for water taste in Drosophila. *Nature,* 465**,** 91-5.

Charlu, S., Wisotsky, Z., Medina, A. & Dahanukar, A. 2013. Acid sensing by sweet and bitter taste neurons in Drosophila melanogaster. *Nat Commun,* 4**,** 2042.

Chen, X., Gabitto, M., Peng, Y., Ryba, N. J. & Zuker, C. S. 2011. A gustotopic map of taste qualities in the mammalian brain. *Science,* 333**,** 1262-6.

Chen, Y. & Amrein, H. 2017. Ionotropic Receptors Mediate Drosophila Oviposition Preference through Sour Gustatory Receptor Neurons. *Curr Biol,* 27**,** 2741-2750 e4.

Chen, Y. D. & Dahanukar, A. 2017. Molecular and Cellular Organization of Taste Neurons in Adult Drosophila Pharynx. *Cell Rep,* 21**,** 2978-2991.

Dahanukar, A., Lei, Y. T., Kwon, J. Y. & Carlson, J. R. 2007. Two Gr genes underlie sugar reception in Drosophila. *Neuron,* 56**,** 503-16.

Dawydow, A., Gueta, R., Ljaschenko, D., Ullrich, S., Hermann, M., Ehmann, N., Gao, S., Fiala, A., Langenhan, T., Nagel, G. & Kittel, R. J. 2014. Channelrhodopsin-2-

XXL, a powerful optogenetic tool for low-light applications. *Proc Natl Acad Sci U S A,* 111**,** 13972-13977.

Dus, M., Ai, M. & Suh, G. S. 2013. Taste-independent nutrient selection is mediated by a brain-specific Na+ /solute co-transporter in Drosophila. *Nat Neurosci,* 16**,** 526-8.

Dus, M., Lai, J. S., Gunapala, K. M., Min, S., Tayler, T. D., Hergarden, A. C., Geraud, E., Joseph, C. M. & Suh, G. S. 2015. Nutrient Sensor in the Brain Directs the Action of the Brain-Gut Axis in Drosophila. *Neuron,* 87**,** 139-51.

Dus, M., Min, S., Keene, A. C., Lee, G. Y. & Suh, G. S. 2011. Taste-independent detection of the caloric content of sugar in Drosophila. *Proc Natl Acad Sci U S A,* 108**,** 11644-9.

Fan, P., Manoli, D. S., Ahmed, O. M., Chen, Y., Agarwal, N., Kwong, S., Cai, A. G., Neitz, J., Renslo, A., Baker, B. S. & Shah, N. M. 2013. Genetic and neural mechanisms that inhibit Drosophila from mating with other species. *Cell,* 154**,** 89-102.

Freeman, E. G. & Dahanukar, A. 2015. Molecular neurobiology of Drosophila taste. *Curr Opin Neurobiol,* 34**,** 140-8.

French, A. S., Sellier, M. J., Ali Agha, M., Guigue, A., Chabaud, M. A., Reeb, P. D., Mitra, A., Grau, Y., Soustelle, L. & Marion-Poll, F. 2015. Dual mechanism for bitter avoidance in Drosophila. *J Neurosci,* 35**,** 3990-4004.

Fujii, S., Yavuz, A., Slone, J., Jagge, C., Song, X. & Amrein, H. 2015. Drosophila sugar receptors in sweet taste perception, olfaction, and internal nutrient sensing. *Curr Biol,* 25**,** 621-627.

Fujita, M. & Tanimura, T. 2011. Drosophila evaluates and learns the nutritional value of sugars. *Curr Biol,* 21**,** 751-5.

Ganguly, A., Pang, L., Duong, V. K., Lee, A., Schoniger, H., Varady, E. & Dahanukar, A. 2017. A Molecular and Cellular Context-Dependent Role for Ir76b in Detection of Amino Acid Taste. *Cell Rep,* 18**,** 737-750.

Gendre, N., Luer, K., Friche, S., Grillenzoni, N., Ramaekers, A., Technau, G. M. & Stocker, R. F. 2004. Integration of complex larval chemosensory organs into the adult nervous system of Drosophila. *Development,* 131**,** 83-92.

Harris, D. T., Kallman, B. R., Mullaney, B. C. & Scott, K. 2015. Representations of Taste Modality in the Drosophila Brain. *Neuron,* 86**,** 1449-60.

Hiroi, M., Marion-Poll, F. & Tanimura, T. 2002. Differentiated response to sugars among labellar chemosensilla in Drosophila. *Zoolog Sci,* 19**,** 1009-18.

Inagaki, H. K., Jung, Y., Hoopfer, E. D., Wong, A. M., Mishra, N., Lin, J. Y., Tsien, R. Y. & Anderson, D. J. 2014. Optogenetic control of Drosophila using a red-shifted channelrhodopsin reveals experience-dependent influences on courtship. *Nat Methods,* 11**,** 325-32.

Jeong, Y. T., Shim, J., Oh, S. R., Yoon, H. I., Kim, C. H., Moon, S. J. & Montell, C. 2013. An odorant-binding protein required for suppression of sweet taste by bitter chemicals. *Neuron,* 79**,** 725-37.

Jiao, Y., Moon, S. J., Wang, X., Ren, Q. & Montell, C. 2008. Gr64f is required in combination with other gustatory receptors for sugar detection in Drosophila. *Curr Biol,* 18**,** 1797-801.

Joseph, R. M., Sun, J. S., Tam, E. & Carlson, J. R. 2017. A receptor and neuron that activate a circuit limiting sucrose consumption. *Elife,* 6.

Keene, A. C. & Masek, P. 2012. Optogenetic induction of aversive taste memory. *Neuroscience,* 222**,** 173-80.

Kirkhart, C. & Scott, K. 2015. Gustatory learning and processing in the Drosophila mushroom bodies. *J Neurosci,* 35**,** 5950-8.

Klapoetke, N. C., Murata, Y., Kim, S. S., Pulver, S. R., Birdsey-Benson, A., Cho, Y. K., Morimoto, T. K., Chuong, A. S., Carpenter, E. J., Tian, Z., Wang, J., Xie, Y., Yan, Z., Zhang, Y., Chow, B. Y., Surek, B., Melkonian, M., Jayaraman, V., Constantine-Paton, M., Wong, G. K. & Boyden, E. S. 2014. Independent optical excitation of distinct neural populations. *Nat Methods,* 11**,** 338-46.

Koh, T. W., He, Z., Gorur-Shandilya, S., Menuz, K., Larter, N. K., Stewart, S. & Carlson, J. R. 2014. The Drosophila IR20a clade of ionotropic receptors are candidate taste and pheromone receptors. *Neuron,* 83**,** 850-65.

Ledue, E. E., Chen, Y. C., Jung, A. Y., Dahanukar, A. & Gordon, M. D. 2015. Pharyngeal sense organs drive robust sugar consumption in Drosophila. *Nat Commun,* 6**,** 6667.

Liman, E. R., Zhang, Y. V. & Montell, C. 2014. Peripheral coding of taste. *Neuron,* 81**,** 984-1000.

Ling, F., Dahanukar, A., Weiss, L. A., Kwon, J. Y. & Carlson, J. R. 2014. The molecular and cellular basis of taste coding in the legs of Drosophila. *J Neurosci,* 34**,** 7148-64.

Mcginnis, J. P., Jiang, H., Agha, M. A., Sanchez, C. P., Lange, J., Yu, Z., Marion-Poll, F. & Si, K. 2016. Immediate perception of a reward is distinct from the reward's long-term salience. *Elife,* 5.

Miyamoto, T. & Amrein, H. 2014. Diverse roles for the Drosophila fructose sensor Gr43a. *Fly (Austin),* 8**,** 19-25.

Miyamoto, T., Chen, Y., Slone, J. & Amrein, H. 2013. Identification of a Drosophila glucose receptor using Ca2+ imaging of single chemosensory neurons. *PLoS One,* 8**,** e56304.

Miyamoto, T., Slone, J., Song, X. & Amrein, H. 2012. A fructose receptor functions as a nutrient sensor in the Drosophila brain. *Cell,* 151**,** 1113-25.

Nottebohm, E., Dambly-Chaudiere, C. & Ghysen, A. 1992. Connectivity of chemosensory neurons is controlled by the gene poxn in Drosophila. *Nature,* 359**,** 829-32.

Park, J. & Carlson, J. R. 2018. Physiological responses of the Drosophila labellum to amino acids. *J Neurogenet,* 32**,** 27-36.

Park, J. H. & Kwon, J. Y. 2011. Heterogeneous expression of Drosophila gustatory receptors in enteroendocrine cells. *PLoS One,* 6**,** e29022.

Ribeiro, C. & Dickson, B. J. 2010. Sex peptide receptor and neuronal TOR/S6K signaling modulate nutrient balancing in Drosophila. *Curr Biol,* 20**,** 1000-5.

Ro, J., Harvanek, Z. M. & Pletcher, S. D. 2014. FLIC: high-throughput, continuous analysis of feeding behaviors in Drosophila. *PLoS One,* 9**,** e101107.

Slone, J., Daniels, J. & Amrein, H. 2007. Sugar receptors in Drosophila. *Curr Biol,* 17**,** 1809-16.

Stafford, J. W., Lynd, K. M., Jung, A. Y. & Gordon, M. D. 2012. Integration of taste and calorie sensing in Drosophila. *J Neurosci,* 32**,** 14767-74.

Tauber, J. M., Brown, E. B., Li, Y., Yurgel, M. E., Masek, P. & Keene, A. C. 2017. A subset of sweet-sensing neurons identified by IR56d are necessary and sufficient for fatty acid taste. *PLoS Genet,* 13**,** e1007059.

Thistle, R., Cameron, P., Ghorayshi, A., Dennison, L. & Scott, K. 2012. Contact chemoreceptors mediate male-male repulsion and male-female attraction during Drosophila courtship. *Cell,* 149**,** 1140-51.

Thoma, V., Knapek, S., Arai, S., Hartl, M., Kohsaka, H., Sirigrivatanawong, P., Abe, A., Hashimoto, K. & Tanimoto, H. 2016. Functional dissociation in sweet taste receptor neurons between and within taste organs of Drosophila. *Nat Commun,* 7**,** 10678.

Thorne, N., Chromey, C., Bray, S. & Amrein, H. 2004. Taste perception and coding in Drosophila. *Curr Biol,* 14**,** 1065-79.

Van Giesen, L., Hernandez-Nunez, L., Delasoie-Baranek, S., Colombo, M., Renaud, P., Bruggmann, R., Benton, R., Samuel, A. D. T. & Sprecher, S. G. 2016. Multimodal stimulus coding by a gustatory sensory neuron in Drosophila larvae. *Nat Commun,* 7**,** 10687.

Wang, Z., Singhvi, A., Kong, P. & Scott, K. 2004. Taste representations in the Drosophila brain. *Cell,* 117**,** 981-91.

Weiss, L. A., Dahanukar, A., Kwon, J. Y., Banerjee, D. & Carlson, J. R. 2011. The molecular and cellular basis of bitter taste in Drosophila. *Neuron,* 69**,** 258-72.

Yapici, N., Cohn, R., Schusterreiter, C., Ruta, V. & Vosshall, L. B. 2016. A Taste Circuit that Regulates Ingestion by Integrating Food and Hunger Signals. *Cell,* 165**,** 715-29.

CHAPTER V

A subset of brain neurons controls regurgitation in adult *Drosophila melanogaster*

Work in this chapter was submitted to the Journal of Experimental Biology on August 21, 2019– **YCD Chen**, S Ahmad, K Amin, and A Dahanukar. *A subset of brain neurons controls regurgitation in adult Drosophila melanogaster.*

SUMMARY

Taste is essential for animals to evaluate food quality and make important decisions about food choice and intake. How complex brains process sensory information to produce behavior is an essential question in the field of sensory neurobiology. Currently, little is known about higher order taste circuits in the brain as compared to those of other sensory systems. Here, we use the common vinegar fly, *Drosophila melanogaster*, to screen for candidate neurons labeled by different transgenic *GAL4* lines in controlling feeding behaviors. We find that activation of one line (*VT041723-GAL4*) produces "proboscis holding" behavior (extrusion of the mouthpart without withdrawal). Further analysis shows that the proboscis holding phenotype indicates an aversive response, since flies pre-fed with either sucrose or water prior to neuronal activation exhibit regurgitation. Anatomical characterization of *VT041723-GAL4* labeled neurons suggests that they receive sensory input from peripheral taste neurons. Overall, our study identifies a subset of brain neurons labeled by *VT041723-GAL4* that may be involved in a taste circuit that controls regurgitation.

INTRODUCTION

One of the fundamental questions in the field of neuroscience is how the brain responds to different sensory inputs and mediates appropriate behaviors. To address this fundamental question, many have taken advantage of the vinegar fly, *Drosophila melanogaster*, as a neurogenetic model organism. With a numerically simpler nervous system compared to that in mammals, flies nevertheless exhibit complex behaviors. Importantly, fundamental principles of sensory coding and neuronal circuit function for processing sensory inputs and driving behaviors are often conserved across species. Therefore, *Drosophila* has been a powerful model for functional dissection of neuronal circuits underlying behaviors.

The gustatory system, which influences selection of food, egg deposition sites, and mates, among others, is an appealing sensory system to address such questions. The identification of chemosensory receptor genes (Clyne et al., 2000, Scott et al., 2001) and the development of methods to assess feeding behaviors (Ja et al., 2007, Deshpande et al., 2014, Itskov et al., 2014, Ro et al., 2014, Murphy et al., 2017, Shell et al., 2018, Park et al., 2018, Moreira et al., 2019, Yapici et al., 2016, Diegelmann et al., 2017, Shiraiwa and Carlson, 2007) provided a foundation for dissecting the functions of peripheral taste neurons with precise molecular genetic tools. Much is now known about how peripheral taste neurons detect various chemicals (Ling et al., 2014, Weiss et al., 2011, Chen and Dahanukar, 2017, Ledue et al., 2015, He et al., 2019, Raad et al., 2016, Steck et al., 2018, Jaeger et al., 2018), but higher-order gustatory processing in the central brain remains

poorly understood. A number of recent studies have utilized powerful genetic screens for higher-order neurons in the brain that process the taste information and control feeding behaviors. For example, more than a few interneurons and motor neurons have been found to selectively respond to sugars (Miyazaki et al., 2015, Kain and Dahanukar, 2015, Flood et al., 2013, Yapici et al., 2016, Gordon and Scott, 2009) or bitter compounds (Bohra et al., 2018, Kim et al., 2017) and mediate innate feeding responses such as proboscis extension and food ingestion as well as learned taste aversion. In addition, several neuromodulatory interneurons, which modulate taste responses to sugars and bitter compounds, have also been described (Ledue et al., 2016, Youn et al., 2018, Inagaki et al., 2014b, Inagaki et al., 2012). In this study, we aimed to identify candidate higher-order brain neurons involved in processing taste information and mediating feeding behaviors.

We used both *VT-GAL4* and *Janelia-GAL4* transgenic fly lines to access different subsets of neurons in the adult fly brain (Kvon et al., 2014, Jenett et al., 2012) and asked which if any can induce proboscis extension when activated. We expressed dTrpA1, a heat-activated ion channel (Kang et al., 2011), under the control of a *UAS* promoter in subsets of neurons labeled by the selected *VT-GAL4* and *Janelia-GAL4* lines and examined heat-activated proboscis extension responses (PER) (Shiraiwa and Carlson, 2007). We identified one candidate line (*VT041723-GAL4*), which labels a neuronal population that mediates regurgitation. Activation of *VT041723-GAL4* labeled neurons induces prolong proboscis extension (proboscis holding) for as long as 7 minutes without

retraction. Similar results were observed by optogenetic activation of these neurons. Flies pre-fed with sucrose or water prior neuronal activation leads to regurgitation, suggesting an aversive response for this prolonged proboscis extension. Using GFP Reconstitution Across Synaptic Partners (GRASP) technique, we find that the *VT041723-GAL4* labeled neurons have synaptic connections with peripheral taste neurons in the pharynx. Altogether, our results identify a subset of brain neurons labeled by *VT041723-GAL4* controls regurgitation. Our behavioral data also suggest that proboscis extension, a commonly used acceptance feeding behavior readout, might not be a reliable indication of appetitive feeding behavior.

RESULTS

A thermogenetic activation screen of transgenic *GAL4* lines identifies *VT041723-GAL4*, which triggers a proboscis holding behavior

To identify higher-order brain neurons involved in feeding behaviors, we took advantage of available transgenic resources in the Vienna Tiles GAL4 (*VT-GAL4*) Library at the Vienna *Drosophila* Resource Center (VDRC) and the *Janelia-GAL4* collection at the Janelia Farm Research Campus. Transgenic *GAL4* lines created with different promoter DNA sequences show different labeling patterns that can be visualized with different reporters, such as *UAS-GFP*. The expression patterns of *VT-GAL4* and *Janelia-GAL4* lines in the adult *Drosophila* brain have been well-documented (Pfeiffer et al., 2008, Jenett et al., 2012, Kvon et al., 2014). Using the Virtual Fly Brain online database (www.virtualflybrain.org) (Milyaev et al., 2012), we first did a preliminary image-based screen for neurons that arborize in and around the subesophageal zone (SEZ), the primary taste center in the fly brain, and selected several candidate lines for further analysis. Among these, *GAL4* lines that showed sparse labeling in the adult brain were prioritized for subsequent behavioral screening. To determine whether any of the selected *GAL4* lines labeled neurons involved in feeding behaviors, we expressed the *Drosophila* transient receptor potential channel, subfamily A, member 1 (dTrpA1), a heat-activated cation channel (Kang et al., 2011), using the *GAL4/UAS* binary expression system (Brand and Perrimon, 1993). By elevating the ambient temperature to 31^{o}C, we could thermogenetically activate these neurons and record the proboscis extension response (PER), in which the fly protrudes its mouthpart (proboscis), as a readout of

feeding behavior (Shiraiwa and Carlson, 2007). From a preliminary screen of 194 *GAL4* lines (155 *VT-GAL4* lines and 39 *Janelia-GAL4* lines) (**Table 5.1**), we found five lines (*VT062245-GAL4*, *VT040416-GAL4* , *VT041723-GAL4*, *VT038168-GAL4*, and *R77B08-GAL4*) that exhibited more than 40% PER (**Figure 5.1A**). Closer examination of the expression patterns of the five lines excluded three (*VT062245-GAL4*, *VT038168-GAL4*, and *R77B08-GAL4*) based on expression in peripheral taste neurons that project to the SEZ (**Figure 5.1B**) (Kwon et al., 2014). Interestingly, PER activated by the *VT041723-GAL4* line was unique in that the flies did not retract the proboscis after extension, but rather maintained it in the extended position at length (**Figure 5.1C**). We termed this unusual PER response "proboscis holding" and selected the *VT041723-GAL4* line for further analysis.

Thermogenetic activation of *VT041723-GAL4* neurons induces a sexually dimorphic proboscis holding that is independent of starvation

To determine if both males and females exhibited proboscis holding upon activation of *VT041723-GAL4* neurons, we performed the heat-activated PER assay with mated male and female flies for both experimental and control genotypes (**Figure 5.1D-E**). The proboscis holding phenotype was recorded on an all-or-nothing basis. If a fly extended its proboscis for 10 seconds or longer upon heat activation, it was considered to have "proboscis holding". If the fly did not extend its proboscis, or if the duration of proboscis extension was less than 10 seconds, it was considered to have "no proboscis holding". As expected, both male and female control flies with either *VT041723-GAL4* or

UAS-dTrpA1 transgenes did not show any proboscis holding in any test conditions. The experimental *VT041723-GAL4>UAS-dTrpA1* flies demonstrated varying levels of proboscis holding between sexes. We found that 10.7% of male flies (N = 56) and 54.5% of mated female flies (N = 66) showed the proboscis holding response (**Figure 5.1D-E**). Since starvation increases PER response in flies (Dethier, 1976), we next accessed whether *VT041723-GAL4* neuron-activated proboscis holding behavior is modulated by starvation. We tested flies that were starved for 24 hours (N = 63 for males and N = 74 for females) and found that similar fractions of fed and starved flies exhibited proboscis holding (**Figure 5.1D-E**).

To further investigate the nature of proboscis holding in *VT041723>dTrpA1* flies, we recorded the duration of proboscis holding in fed and starved flies that showed this behavior. For feasibility, we capped measurement of proboscis holding time at 7 minutes. Our results showed that the average proboscis holding duration was not significantly different between fed and starved flies of the same sex (unpaired *t* test for males and Mann-Whitney test for females, $P > 0.05$). However, mated female flies showed significantly longer times of proboscis holding as compared to males in both fed and starved conditions (unpaired *t* tests, $P < 0.05$) (**Figure 5.1F**). In fact, many female flies held the proboscis in the extended position for the maximum recording time (7 min). Together, our results show that activation of *VT041723-GAL4* neurons induces proboscis holding in a sexually dimorphic manner, with females exhibiting proboscis holding at a higher frequency and longer duration.

Optogenetic activation of *VT041723-GAL4* neurons induces a sexually dimorphic partial proboscis holding response.

We next verified the role of *VT041723-GAL4* neurons in proboscis holding in an independent optogenetic activation paradigm using a red-shifted channelrhodopsin, *CsChrimson* (Klapoetke et al., 2014). Experimental flies were transferred to food supplemented with all-trans retinal (ATR) for 2-3 days in dark and tested for behavioral responses with 626 nm red LED stimulation. Consistent with the results of thermogenetic activation experiments (**Figure 5.1**), optogenetic activation of *VT041723-GAL4* neurons resulted in proboscis holding (**Figure 5.2A**). We noted, however, that in most cases the proboscis was not fully extended (partial proboscis holding) by optogenetic activation. Nonetheless, these flies also maintained the partial proboscis holding for up to 7 minutes under continuous red LED exposure, at which point the trial was completed. Further, the partial proboscis holding responses were sexually dimorphic; 4.3% of male flies (N = 47) and 39.1% of mated female flies (N = 69) exhibited the phenotype (**Figure 5.2B**). Control flies that were not given ATR food (-ATR) showed little if any proboscis holding upon light stimulation. (N = 36 for males and N = 71 for females).

***VT041723-GAL4* neurons in the dorsolateral protocerebrum and anterior SEZ**

We next examined the expression pattern of *VT041723-GAL4* in the brain using *UAS-GFP*. Similar to the expression pattern described previously (Kvon et al., 2014), we found labeling in neurons that showed dense innervation in the antennal mechanosensory and motor center (AMMC), and some labeled neurites traveling across the midline

between the SEZ and the pars intercerebralis regions (**Figure 5.3A**). Some weakly labeled cell bodies were observed within the SEZ. Notably, one pair of neurons in the dorsolateral protocerebrum was strongly labeled, and their anatomical characteristics were reminiscent of previously reported *Gr43a*$^{+}$ fructose-sensing neurons in the brain (Miyamoto et al., 2012). To confirm whether *VT041723-GAL4* labeled *Gr43a*$^{+}$ neurons, we performed double-labeling experiments with two fluorescent reporters driven by *VT041723-GAL4* and *Gr43a-LexA*, respectively (**Figure 5.3B**). We found no overlap between expression of the two reporters, indicating that *VT041723-GAL4* labeled a different set of neurons in the brain.

To characterize the neuroanatomy of *VT041723-GAL4* neurons in more detail, we expressed the presynaptic marker Syt-GFP (Zhang et al., 2002) and the postsynaptic marker DenMark (Nicolai et al., 2010) and examined their distribution in the brain (**Figure 5.3C**). We found the Syt-GFP signal was located medially relative to DenMark in the protocerebrum region. Both Syt-GFP and DenMark signals were observed in the AMMC and the SEZ. In the AMMC, DenMark was distributed across the whole neuropil whereas Syt-GFP was confined to the lateral AMMC region. Altogether, the *VT041723-GAL4* line labels neurons in the anterior SEZ as well as dorsolateral protocerebrum of the fly brain, consistent with a role in controlling proboscis extension and holding.

Post-consumption activation of *VT041723-GAL4* neurons induces regurgitation

We next aimed to determine whether *VT041723-GAL4*-activated proboscis holding phenotype is modulated by prior feeding experience. To test this possibility, we starved the *VT041723-GAL4>UAS-dTrpA1* flies for 24 hours and then pre-fed the flies with a fixed amount of 100 mM sucrose (0.5 μL) immediately before transferring them onto the 31°C heat block for thermogenic activation (**Figure 5.4A**). Surprisingly, we found that more than half of the male (49.1%) and mated female (76.3%) flies exhibited regurgitation (**Figure 5.4B**), which was apparent by the formation of a liquid bubble at the tip of the proboscis (**Figure 5.4A**). In addition, about 10% of the flies showed proboscis holding without regurgitation. These results suggest that activation of *VT041723-GAL4* neurons conveys an aversive signal that causes regurgitation of an ingested meal.

Regurgitation mediated by *VT041723-GAL4* neurons is independent of starvation state and meal quality

We next asked if starvation time affects the regurgitation phenotype. For this purpose, we performed mild starvation (4 hours) before pre-feeding flies with 0.5 μL of 100 mM sucrose. Similar to the results obtained with 24-hour starvation, we found more than half of the male (72.3%) and mated female (50%) flies exhibited regurgitation upon activation of *VT041723-GAL4* neurons (**Figure 5.4C**). In addition, regurgitation behavior was also observed when flies were pre-fed with 0.5 μL of water after starvation on dry tissue paper, suggesting that the observed behavioral response is independent of tastants

in the pre-fed meal (**Figure 5.4D**). Thus, *VT041723-GAL4*-induced regurgitation of a meal appears to be independent of starvation state and meal quality.

VT041723-GAL4 neurons have synaptic proximity with pharyngeal GRNs

We next investigated the possibility that *VT041723-GAL4* neurons may be part of taste circuits by performing GFP reconstitution across synaptic partners (GRASP) experiments (Fan et al., 2013). We first examined the expression of both *VT041723-GAL4* and *Ir76b-LexA* in the fly brain. *Ir76b-LexA* labels some olfactory neuronal projections in the antennal lobes as well as projections in the SEZ from many gustatory receptor neurons (GRNs) from different taste organs, including those in labellar taste hairs, labellar taste pegs, pharynx, and legs (Ganguly et al., 2017, Zhang et al., 2013, Hussain et al., 2016, Chen and Dahanukar, 2017, Steck et al., 2018, Jaeger et al., 2018, Chen and Amrein, 2017, Ahn et al., 2017). We found that neurites of *VT041723-GAL4* neurons and *Ir76b*$^{+}$ pharyngeal GRNs appeared to be in close proximity to each other in the SEZ (**Figure 5.5A**). We then performed a GRASP experiment by expressing split GFP1-10 fused with a transmembrane protein involved in synapse formation (Knight et al., 2011), neurexin, in *VT041723-GAL4* neurons, and split GFP11 fused with CD4 in *Ir76b*$^{+}$ neurons. We stained the neuropil using anti-nc82 and visualized direct GFP fluorescence. Controls lacking either *VT041723-GAL4* or *Ir76b-LexA* did not show any GFP signal. A different candidate line from our screen (**Figure 5.1A-B**), *VT040416-GAL4*, that labeled extensive neurite arborization in the SEZ (**Figure 5.6**), also did not show any positive GRASP signal with *Ir76b*$^{+}$ GRNs. Notably, we observed

reconstitution of GFP fluorescence in the SEZ when *VT041723-GAL4* and *Ir76b-LexA* were used to express the two split GFP components (**Figure 5.5B**), suggesting that termini of *VT041723-GAL4* neurons are in close proximity with those of *Ir76b-LexA* GRNs, and may receive taste input from *Ir76b*$^{+}$ neurons.

One previous study has shown that thermogenetic activation of *Gr66a*-expressing taste neurons in the mouthpart caused regurgitation (Kang et al., 2011), which raised the possibility that *VT041723-GAL4* neurons receive input from pharyngeal *Gr66a*$^{+}$ GRNs. To test this possibility, we used *Pox-neuro* (*Poxn*) mutants in which all external taste hairs are transformed into mechanosensory hairs leaving pharyngeal taste neurons intact (Chen et al., 2018, Chen and Dahanukar, 2017, Ledue et al., 2015). Consistent with our previous report (Chen and Dahanukar, 2017), *Poxn* mutants retained *Ir76b*$^{+}$ projections from the pharynx and a few taste pegs, while lacking projections from all external taste organs. GRASP experiments in a *Poxn* mutant background revealed positive GRASP signal between *VT041723-GAL4* and *Ir76b-LexA* GRNs in the SEZ (**Figure 5.5D**). The results support the idea that *VT041723-GAL4* neurons receive taste inputs from pharyngeal GRNs and regulate regurgitation.

DISCUSSION

Knowledge about how neural circuits are wired in the brain is crucial for understanding how sensory information is translated into behavior. In *Drosophila*, higher-order brain regions that process olfactory information, such as the lateral horn and mushroom body, have been described in detail (Dolan et al., 2019, Jefferis et al., 2007, Marin et al., 2002, Wong et al., 2002), but much less is known about processing of gustatory information after the first relay in the SEZ, with reports of only a few central neurons that have been anatomically or functionally characterized (Bohra et al., 2018, Kim et al., 2017, Yapici et al., 2016, Miyazaki et al., 2015, Kain and Dahanukar, 2015, Flood et al., 2013). In this study, we have identified a subset of brain neurons labeled by *VT041723-GAL4* whose activation causes a proboscis holding and regurgitation behavior in adult *Drosophila*.

Proboscis extension has been characterized as an appetitive behavioral response and widely used as a read-out of food acceptance (Shiraiwa and Carlson, 2007). Several previous reports have shown that activation of external sweet taste neurons via *Gr5a-GAL4* causes proboscis extension (Inagaki et al., 2012, Inagaki et al., 2014a, Dawydow et al., 2014, Du et al., 2016, Kain and Dahanukar, 2015, Yapici et al., 2016, Keene and Masek, 2012). Under these conditions, flies usually exhibit proboscis extensions followed by quick retractions. Since activation of *VT041723-GAL4* neurons resulted in a single extension without retraction for the duration of the assay, we considered that it may not be indicative of an appetitive response but rather that it represented an aversive response.

Consistent with this idea, post-consumption activation of *VT041723-GAL4* neurons induced regurgitation, similar to that observed in flies with stimulation of deterrent taste neurons (Kang et al., 2011) or with overconsumption (Pool et al., 2014). However, *VT041723-GAL4* neurons induced regurgitation often accompanied by proboscis holding, and sustained proboscis extension is observed only when the fly is actively ingesting. We cannot, therefore, exclude the possibility that proboscis holding and regurgitation are controlled by different subset of *VT041723-GAL4* neurons. Alternatively, proboscis holding may be a common feature of feeding and regurgitation behaviors.

In this study, we found that the frequency of proboscis holding behavior is strikingly higher in females than in males. In *Drosophila*, *doublesex* (*dsx*) and *fruitless* (*fru*) are known as sex-determining transcription factors that specify sexually dimorphic neuronal circuits and behaviors (Erdman and Burtis, 1993, Ito et al., 1996, Ryner et al., 1996, Auer and Benton, 2016, Asahina, 2018). Although we found no sexual dimorphism in the pattern of *VT041723-GAL4* expression in the brain (data not shown), a closer look at the expression of sex-specific *fru* and *dsx* in *VT041723-GAL4* neurons would provide further insight into possible mechanisms underlying sexual dimorphism. In addition, sex-specific differences in feeding responses to salt (Walker et al., 2015), yeast (Ribeiro and Dickson, 2010), amino acids (Ganguly et al., 2017), and sugars (Chandegra et al., 2017) have been reported. Given the possibility of functional connectivity between *VT041723-GAL4* neurons and peripheral taste neurons, it will be of interest to determine whether specific gustatory input is involved in sex-dependent variation in the proboscis holding

phenotype. Moreover, since the sexual difference is lost when flies are pre-fed with either water or sucrose and tested in thermogenetic activation experiments, it appears that prior feeding experience differentially influences the proboscis holding phenotype in males and females.

VT041723-GAL4 labels multiple neurons that can be largely separated into two anatomical groups, one near the dorsolateral protocerebrum and a second around the SEZ with extensive neurite arborization in the AMMC. Although our study does not identify which of the two populations is involved in regurgitation behavior, GRASP experiments implicate the latter, which are poised to receive input from pharyngeal $Ir76b^{+}$ GRNs, which encompass $Gr66a^{+}$ GRNs in the #8 and #9 sensilla of the labral sense organ (LSO) (Chen and Dahanukar, 2017) that induce regurgitation (Kang et al., 2011). *Gr66a* is broadly expressed in many bitter taste neurons and mediates feeding avoidance of various aversive compounds (Weiss et al., 2011, Moon et al., 2006, Marella et al., 2006, Wang et al., 2004, Thorne et al., 2004). It is plausible, therefore, that pharyngeal $Gr66a^{+}$ GRNs act as a final checkpoint for food consumption and sense cues that induce regurgitation of unsavory meals via activation of *VT041723-GAL4* neurons.

PER requires precise coordination of various motor programs, including rostrum lifting, haustellum extension, labella extension, and labella spreading. Recently, motoneurons controlling individual motor sequence of the PER have been described at the single-cell level (Schwarz et al., 2017). However, motor circuits controlling

regurgitation have not been explored and consequently, little is known about whether PER and regurgitation share common motor programs. Based on our observations, we posit that *VT041723-GAL4* neurons provide a good starting point to address such questions. Future experiments using genetic intersectional strategies may identify the minimum subset of *VT041723-GAL4* neurons that are required for regurgitation behavior. Overall, our results lay the groundwork to analyze a simple behavior and the neuronal circuits and conditions that control it.

EXPERIMENTAL PROCEDURES

Fly strains. Flies were reared on standard cornmeal-dextrose-agar food at 25°C and 60-70% relative humidity under a 12 hour: 12 hour dark: light cycle. The following fly strains were used in this study: *VT041723-GAL4* (Vienna Drosophila Resource Center) (Kvon et al., 2014), *Gr43a-LexA* (Miyamoto and Amrein, 2014), *Ir76b-LexA* (Ganguly et al., 2017), $Poxn^{\Delta M22\text{-}B5}$ (Boll and Noll, 2002), $Poxn^{70}$ (Awasaki and Kimura, 1997), *UAS-mCD8-GFP (Weiss et al., 2011)*, *UAS-Syt-GFP, UAS-DenMark* (BDSC #33064) *UAS-dTrpA1* (BDSC #26263), *UAS-CsChrimson* (BDSC#55135), *UAS-spGFP1-10::Nrx* (Fan et al., 2013), *LexAop-spGFP11::CD4* (Gordon and Scott, 2009), *LexAop2-6XmCherry-HA* (BDSC#52271, 52272).

Immunohistochemistry. Flies aged 4-8 days were anesthetized on ice, and brain tissues were dissected in 1X PBST (PBS with 0.3% Triton X-100) followed by fixing with 4% paraformaldehyde in 1X PBST for 30 min at room temperature. After three washes with 1X PBST, samples were blocked with 5% normal goat serum (Sigma, #G9023) in 1X PBST. Tissues were incubated in primary antibody solutions for 3 days at 4°C. Primary antibodies were: chicken anti-GFP (1:5000; Abcam, #ab13970), rabbit anti-DsRed (1:200; Clontech, #632496), and mouse anti-nc82 (1:20; Developmental Studies Hybridoma Bank). Secondary antibodies (1:400; Invitrogen) were: goat anti-chicken Alexa Fluor 488, goat-anti-rabbit Alexa Fluor 546, goat-anti-mouse Alexa Fluor 568, and goat anti-mouse Alexa Fluor 647. Samples were mounted in VECTASHIELD antifade mounting medium (Vector Laboratories, #H-1000) and stored at 4°C. Fluorescent images

were acquired using a Leica SP5 confocal microscope with 400 Hz scan speed in 512x512 or 1024x1024 pixel formats. Image stacks were acquired at 1-μm optical sections. All images were presented as maximum projections of the *z* stack generated using Leica LAS AF software.

GFP Reconstitution Across Synaptic Partners (GRASP). Immunofluorescence staining procedures were similar as described above with the following minor modifications for detecting GRASP signals between *Ir76b-LexA* peripheral taste neurons and *VT041723-GAL4* central neurons in the brain. To detect native reconstituted GFP signal, only the primary antibody of mouse anti-nc82 (1:20; Developmental Studies Hybridoma Bank) was used for staining neuropil. Both transgene controls were stained together with experimental genotypes at the same time and imaged with the same settings using a Leica SP5 confocal microscope. Image stacks were acquired at 1-μm optical sections. All images were presented as maximum projections of the *z* stack generated using Leica LAS AF software.

Thermogenetic-activated proboscis extension response (PER) assay. Flies of both sexes, aged 4-8 days, were immobilized on glass coverslips with drops of clear, non-toxic nail polish and then allowed to acclimate for 30-60 mins in a humidified chamber prepared by filling a pipette tip box with water and placing damp Kimwipes (Kimberly-Clark Kimtech) on top. One by one, each coverslip containing an individual fly was placed on a 31^{o}C heat block and proboscis extensions were observed under a light

microscope. In the initial screening of 194 *VT-GAL4* and *Janelia-GAL4* lines (**Figure 5.1A**), we scored flies showing full proboscis extension as an indication of food acceptance. In subsequent experiments focusing on the *VT041723-GAL4* line (**Figures 5.1C-F, 5.2, 5.4**), we recorded trial number, sex, proboscis extension, and extension duration for each experimental trial. Proboscis holding was scored when flies fully extended their proboscis for more than 10 seconds without retraction. For the experiments examining regurgitation phenotype, flies were starved for 24 hours on either water-saturated tissues and then pre-fed 0.5 μL of 100 mM sucrose (Sigma-Aldrich, #S7903) (**Figure 5.4B-C**), or dry tissues and then pre-fed 0.5 μL of distilled water (**Figure 5.4D**). Flies that did not consume the pre-feeding tastant solutions in entirety were excluded from the analysis. Flies that consumed all of the pre-feeding tastant solutions were transferred to a 31^{o}C heat block and the number of flies showing regurgitation was recorded. Regurgitation was defined by the presence of a liquid bubble at the tip of the proboscis (**Figure 5.4A**). In all experiments, we tested both *GAL4* and *UAS* controls together with experimental flies in parallel, in random order, and genotypes were blinded to the experimenters. Among all control flies, we did not observe any that showed proboscis holding or regurgitation behaviors.

Optogenetic-activated proboscis extension response (PER) assay. Flies were reared on standard cornmeal-dextrose-agar food at 25°C and 60-70% relative humidity under a 12 hour: 12 hour dark: light cycle. Two to four days after eclosion, flies were transferred to standard cornmeal-dextrose-agar food supplemented with 1 mM all-trans-retinal (Sigma-

Aldrich, #R2500), and placed in aluminum foil-wrapped vials at 25°C for 2-3 days. Sibling flies were transferred to the same food vials without all-trans-retinal to serve as controls. Flies were prepared as for the thermogenetic-activated PER assay described above with the exception that they were prepared under low-light conditions, in which the intensity of room-lights was too low to activate CsChrimson. Flies were then stimulated with 626 nm LED light (Super Bright LEDs Inc.), and the number of flies showing proboscis holding was recorded. In all experiments, we performed both control and experimental flies on each day, in random order, and fly genotypes and rearing conditions were blinded to the experimenters.

Statistical analyses. All data are presented as median ± interquartile range. Statistical tests were conducted using Prism 8 (GraphPad Software). Differences between means of different groups were evaluated for statistical significance with unpaired *t* tests. All control and experimental genotypes were always tested in parallel, and all genotypes and rearing conditions were blinded to the experimenters. All independent trials were performed over 2 days.

FIGURES

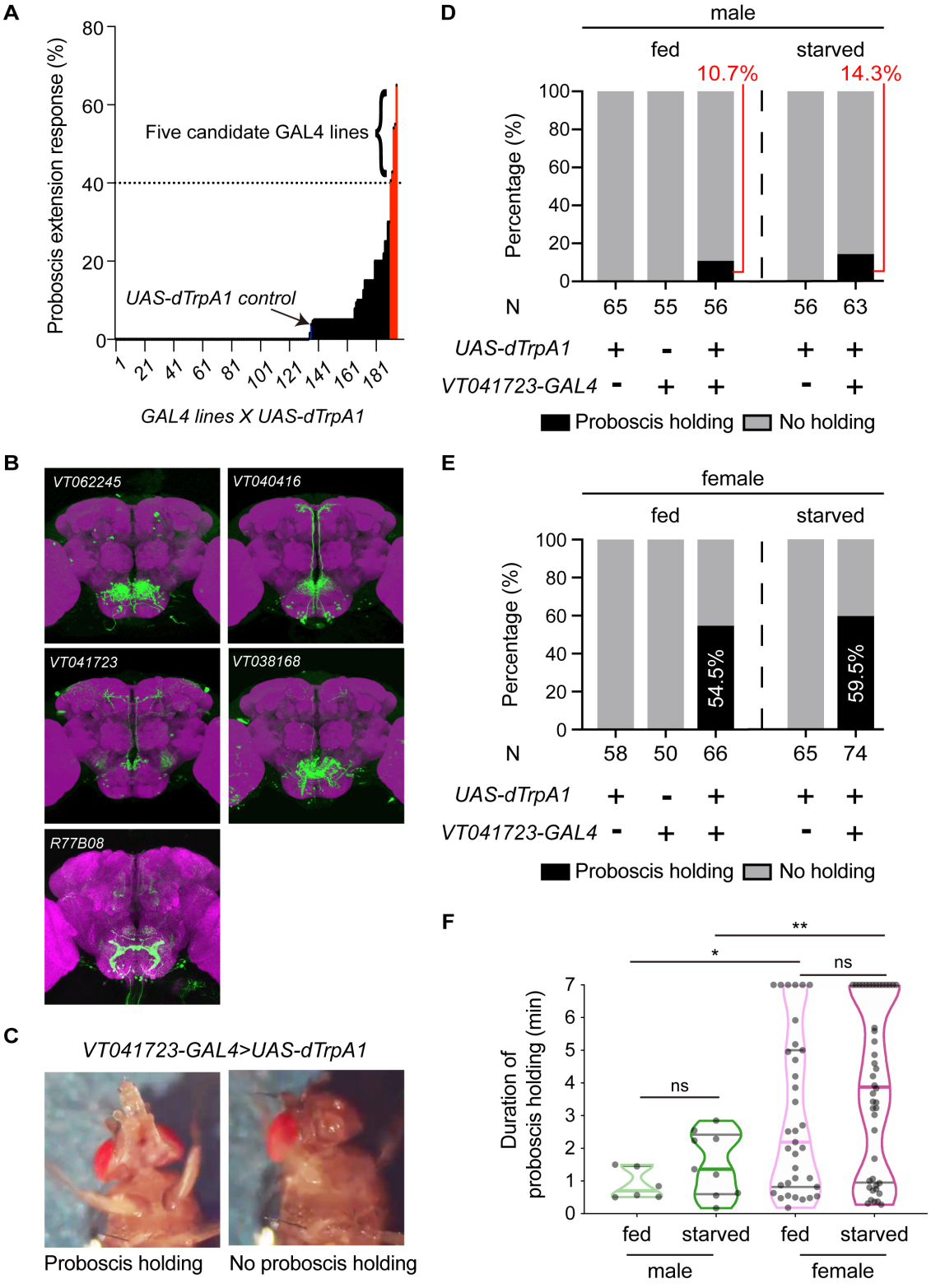
A
Proboscis extension response (%)
Five candidate GAL4 lines
UAS-dTrpA1 control
GAL4 lines X UAS-dTrpA1
B
VT062245
VT040416
VT041723
VT038168
R77B08
C
VT041723-GAL4>UAS-dTrpA1
Proboscis holding
No proboscis holding
D
male
fed
starved
10.7%
14.3%
Percentage (%)
N
65 55 56 56 63
UAS-dTrpA1
VT041723-GAL4
Proboscis holding
No holding
E
female
54.5%
59.5%
58 50 66 65 74
F
Duration of proboscis holding (min)
ns
*
**
male
female

Figure 5.1. A proboscis extension screen of *GAL4* transgenic lines from the VDRC and Janelia Research campus identifies *VT041723-GAL4* neurons as candidates for higher-order taste neurons controlling feeding behavior. (**A**) Heat-activated proboscis extension responses of 195 *GAL4>dTrpA1* lines. The *UAS-dTrpA1* control is shown in blue (arrow). Red bars indicate the five candidate *GAL4* lines with >40% PER. (**B**) Green Fluorescent Protein (GFP) expression patterns in the adult *Drosophila* brain driven by the 5 candidate *GAL4* lines. Images were taken from the Virtual Fly Brain (www.virtualflybrain.org) (Milyaev et al., 2012). (**C**) Sample images of proboscis holding upon thermogenetic activation of *VT041723-GAL4* neurons. (**D-E**) Results of thermogenetic activation experiments with male (**D**) and female (**E**) flies of the indicated genotypes, tested without starvation (fed) or after 24-hr starvation on wet tissues (starved). *UAS* and *GAL4* controls were tested in parallel with the experimental flies, and genotypes were blinded to the experimenters. N = 50-74. (**F**) Duration of the proboscis holding in a 7-minute thermogenetic activation assay. N = 6-44. * $p<0.05$, ** $p< 0.01$. ns, not significant, unpaired *t* tests.

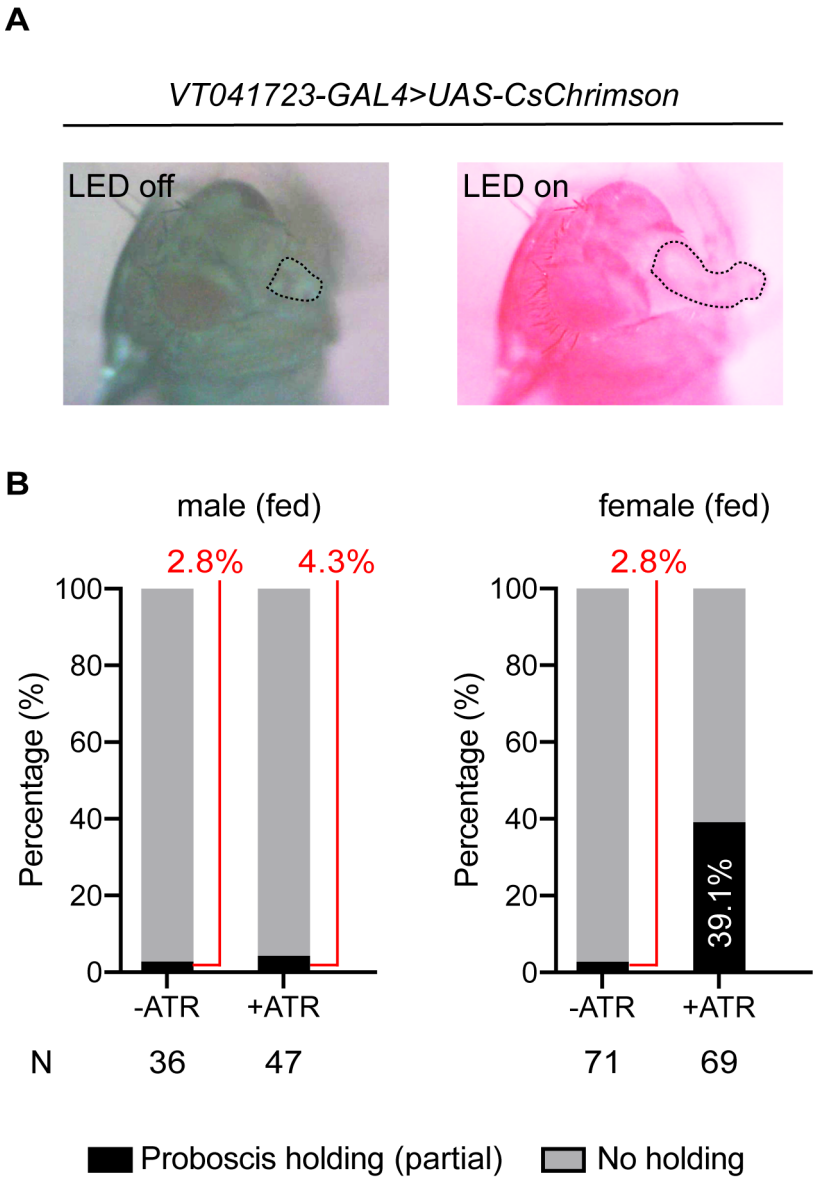

Figure 5.2. Optogenetic activation of *VT041723-GAL4* neurons induces proboscis holding. (**A**) Sample images of the head before (left) and after (right) optogenetic activation of *VT041723-GAL4* neurons with 626 nm LED. The dashed line outlines the proboscis. Note that the proboscis is not fully extended as compared to **Figure 5.1C**, however, flies hold it in the partially extended position for the 7-minute duration of the assay. (**B**) Percentage of *VT041723-GAL>UAS-CsChrimson* flies fed with food with

(+ATR) or without (-ATR) ATR showing proboscis holding upon red LED activation. The fed states of the flies were blinded to the experimenters. N = 36-71.

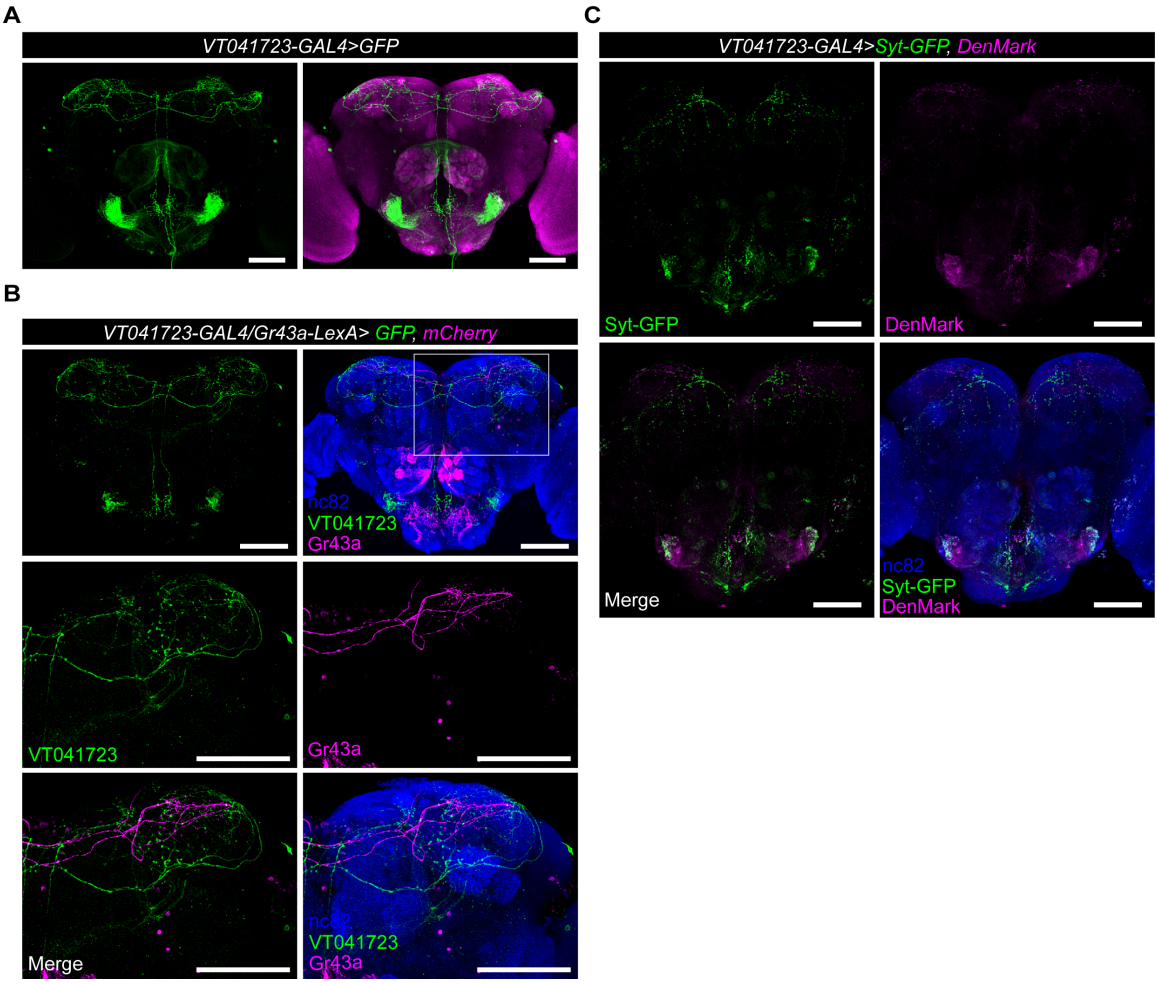

Figure 5.3. Neuroanatomical analysis of *VT041723-GAL4* neurons. (**A**) Expression of a GFP reporter driven by *VT041723-GAL4* in the adult *Drosophila* brain. Neuropil is stained with anti-nc82 (magenta). Scale bar: 100 µm. (**B**) GFP and mCherry reporter expression driven by *VT041723-GAL4* (green) and *Gr43a-LexA* (magenta) in the adult *Drosophila* brain. Neuropil is stained with anti-nc82 (blue). Region of the white rectangle is enlarged and shown in the images below. Scale bar: 100 µm. (**C**) Expression of the pre-synaptic marker Syt::GFP (green) and dendritic marker DenMark (magenta) in

VT041723-GAL4 neurons in the adult *Drosophila* brain. Neuropil is stained with anti-nc82 (blue). Scale bar: 100 μm.

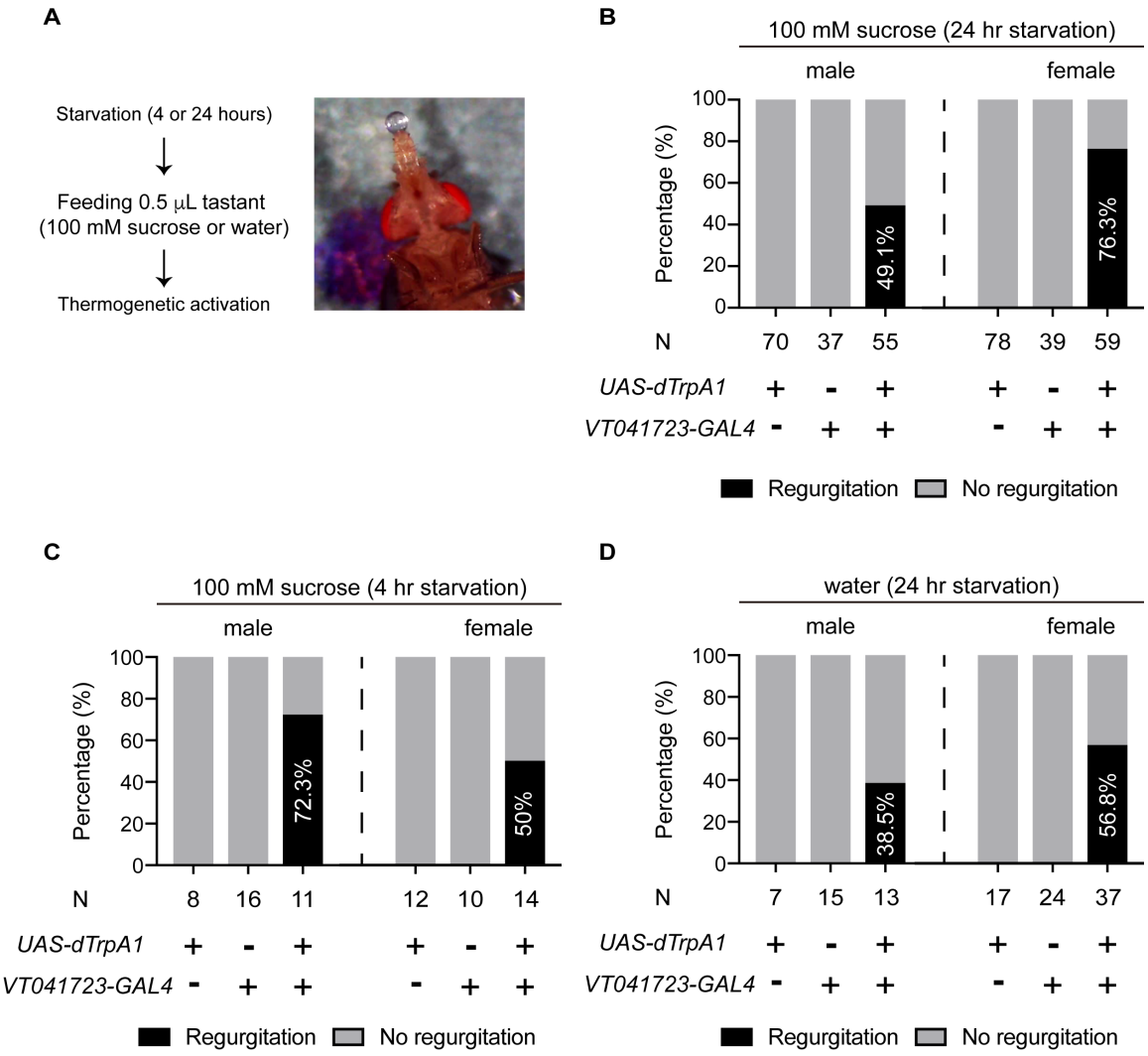

Figure 5.4. Thermogenetic activation of *VT041723-GAL4* neurons induces regurgitation after ingestion (**A**) Summary of experimental procedure for the regurgitation assays (left), and an image of a fly having regurgitation (right). (**B-C**) Distribution of phenotypes upon heat activation after sucrose feeding. No significant difference was observed between flies with 24-hour (**B**) and 4-hour starvation (**C**) prior to sucrose feeding. N = 8-78. (**D**) Distribution of phenotypes upon heat activation after water ingestion following 24-hour starvation on dry tissues. N = 7-37. In all experiments,

UAS and *GAL4* controls were tested in parallel with experimental flies, and genotypes were blinded to the experimenters. No regurgitation was seen in any of the transgenic control flies.

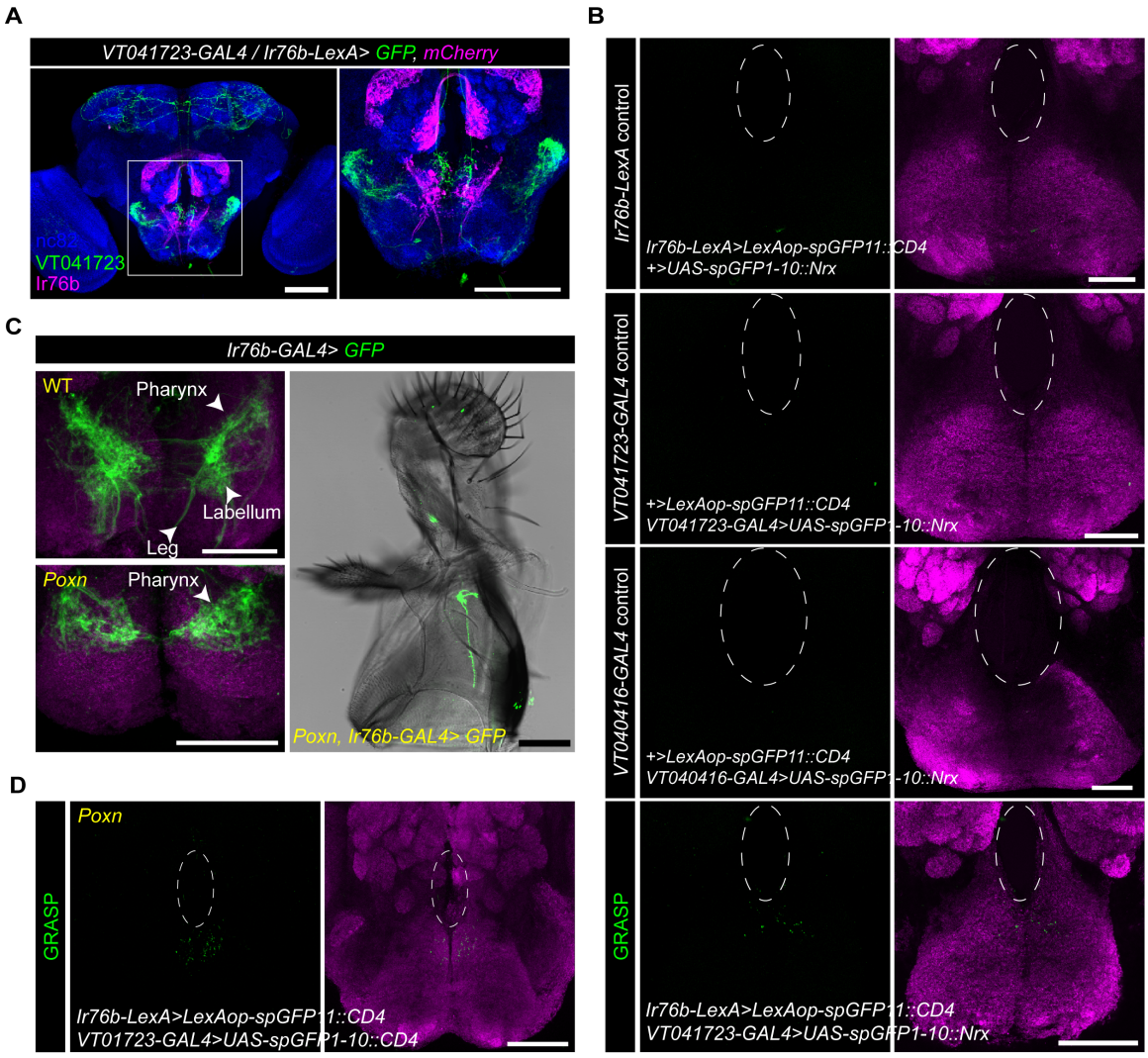

Figure 5.5. *VT041723-GAL4* neurons show a GRASP signal with *Ir76b*$^{+}$ pharyngeal GRNs. (**A**) GFP and mCherry reporter expression driven by *VT041723-GAL4* (green) and *Ir76b-LexA* (magenta) in the adult *Drosophila* brain. Region of the white rectangle in the left image is enlarged and shown on the right. Neuropil is stained with anti-nc82 (blue). Scale bar: 100 μm. (**B**) GRASP signal (green) in the brains of flies with indicated transgenes. Neuropil is stained with anti-nc82 (magenta). Dashed line outlines the region of the esophagus. Scale bar: 50 μm. (**C**) Images of the SEZ showing axonal termini

(green) labeled by *Ir76b-GAL4>GFP* in wild type (WT, w^{1118}) and *Poxn* ($Poxn^{\Delta M22\text{-}B5}/Poxn^{70}$) flies. Scale bar: 50 μm (left). Bright field images of the proboscis showing GRNs (green) labeled by *Ir76b-GAL4>GFP* in the pharynx and a few taste pegs in a *Poxn* mutant background. Scale bar: 100 μm (right). (**D**) GRASP signal (green) in the brain of a *Poxn* mutant flies with indicated transgenes. Scale bar: 50 μm.

SUPPLEMENTAL FIGURE

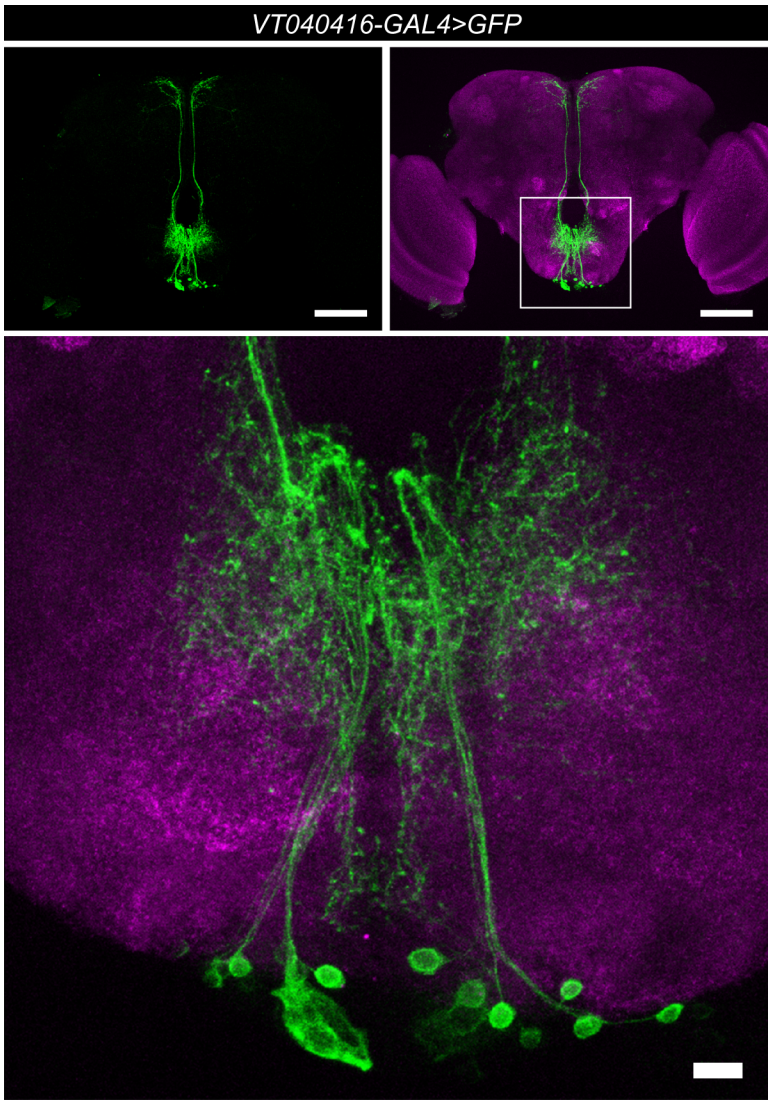

Figure 5.6 Expression of *VT040416-GAL4* in the brain. (**A**) GFP expression in the adult *Drosophila* brain of *VT040416-GAL4>GFP* flies. Neuropil is stained with anti-nc82 (magenta). Scale bar: 100 μm (top), 10 μm (bottom).

TABLE

Table 5.1 Summary of PER results in the thermogenetic activation screen with 194 selected *VT-GAL4* and *Janelia-GAL4* lines.

Line number	Stock number	Inserted construct	PER (%)
1	BDSC 48723	GMR16D02-GAL4	0
2	BDSC 39332	GMR65A10-GAL4	0
3	BDSC 48522	GMR12G03-GAL4	0
4	BDSC 49238	GMR10G07-GAL4	0
5	BDSC 48891	GMR20D04-GAL4	0
6	BDSC 48755	GMR17B03-GAL4	0
7	BDSC 50020	GMR38G08-GAL4	0
8	BDSC 39898	GMR75F02-GAL4	0
9	BDSC 50326	GMR47G06-GAL4	0
10	BDSC 39288	GMR64A07-GAL4	0
11	BDSC 48527	GMR12G12-GAL4	0
12	BDSC 46435	GMR60F03-GAL4	0
13	BDSC 39316	GMR64G05-GAL4	0
14	BDSC 47335	GMR23F01-GAL4	0
15	BDSC 50039	GMR39C07-GAL4	0
16	BDSC 49700	GMR32B04-GAL4	0
17	BDSC 49004	GMR22H09-GAL4	0

18	BDSC 47839	GMR10A11-GAL4	0
19	BDSC 39885	GMR75B11-GAL4	0
20	BDSC 50296	GMR47B12-GAL4	0
21	BDSC 50034	GMR39A11-GAL4	0
22	BDSC 48367	GMR81E10-GAL4	0
23	BDSC 50291	GMR47A12-GAL4	0
24	BDSC 48515	GMR12F05-GAL4	0
25	BDSC 50297	GMR47C03-GAL4	0
26	BDSC 47253	GMR94C10-GAL4	0
27	BDSC 50207	GMR44D07-GAL4	0
28	VDRC 207671	VT057287	0
29	VDRC 206433	VT057286	0
30	VDRC 200916	VT057280	0
31	VDRC 200828	VT057294	0
32	VDRC 206712	VT043663	0
33	VDRC 205899	VT043688	0
34	VDRC 204490	VT043670	0
35	VDRC 202967	VT043685	0
36	VDRC 202712	VT043658	0
37	VDRC 201610	VT043686	0
38	VDRC 201134	VT043678	0

39	VDRC 200755	VT043699	0
40	VDRC 201193	VT043701	0
41	VDRC 200285	VT043698	0
42	VDRC 207582	VT046252	0
43	VDRC 205020	VT056866	0
44	VDRC 203856	VT023747	0
45	VDRC 206542	VT029749	0
46	VDRC 204934	VT043645	0
47	VDRC 206065	VT039485	0
48	VDRC 207679	VT063218	0
49	VDRC 207662	VT042573	0
50	VDRC 204287	VT043697	0
51	VDRC 201032	VT017247	0
52	VDRC 203341	VT031562	0
53	VDRC 203183	VT010262	0
54	VDRC 207777	VT021853	0
55	VDRC 207746	VT062774	0
56	VDRC 204334	VT037601	0
57	VDRC 207914	VT017745	0
58	VDRC 204710	VT048649	0
59	VDRC 202764	VT058427	0

60	VDRC 204652	VT023783	0
61	VDRC 204475	VT022100	0
62	VDRC 205316	VT041269	0
63	VDRC 201067	VT034804	0
64	VDRC 204569	VT026174	0
65	VDRC 201918	VT050226	0
66	VDRC 205643	VT063191	0
67	VDRC 200494	VT002857	0
68	VDRC 201761	VT014604	0
69	VDRC 203479	VT026020	0
70	VDRC 208182	VT038884	0
71	VDRC 202173	VT008279	0
72	VDRC 204924	VT032280	0
73	VDRC 203610	VT048140	0
74	VDRC 201756	VT002210	0
75	VDRC 201439	VT040540	0
76	VDRC 201230	VT015784	0
77	VDRC 205866	VT007768	0
78	VDRC 204711	VT048651	0
79	VDRC 204949	VT048656	0
80	VDRC 205136	VT039361	0

81	VDRC 207835	VT016057	0
82	VDRC 200076	VT012300	0
83	VDRC 205765	VT009667	0
84	VDRC 202860	VT027938	0
85	VDRC 200626	VT037726	0
86	VDRC 202148	VT049374	0
87	VDRC 201299	VT058699	0
88	VDRC 207526	VT022224	0
89	VDRC 206883	VT015971	0
90	VDRC 203133	VT007359	0
91	VDRC 206930	VT026759	0
92	VDRC 202180	VT008480	0
93	VDRC 202959	VT028872	0
94	VDRC 206202	VT026782	0
95	VDRC 204216	VT043928	0
96	VDRC 200348	VT038814	0
97	VDRC 205738	VT056808	0
98	VDRC 206660	VT013039	0
99	VDRC 202186	VT008489	0
100	VDRC 206852	VT041658	0
101	VDRC 208087	VT030526	0

102	VDRC 201715	VT017415	0
103	VDRC 206982	VT026753	0
104	VDRC 203106	VT016969	0
105	VDRC 203875	VT050233	0
106	VDRC 201792	VT025779	0
107	VDRC 203086	VT007709	0
108	VDRC 203039	VT014724	0
109	VDRC 202909	VT007767	0
110	VDRC 201324	VT049500	0
111	VDRC 201212	VT006395	0
112	VDRC 203757	VT007747	0
113	VDRC 200786	VT039997	0
114	VDRC 200755	VT043699	0
115	VDRC 204493	VT044843	0
116	VDRC 202191	VT003238	0
117	VDRC 203180	VT009835	0
118	VDRC 204287	VT043697	0
119	VDRC 201907	VT040033	0
120	VDRC 203008	VT010054	0
121	VDRC 206753	VT029822	0
122	VDRC 207897	VT015256	0

123	VDRC 207668	VT054815	0
124	VDRC 204630	VT044175	0
125	VDRC 202663	VT046307	0
126	VDRC 207554	VT058854	0
127	VDRC 206455	VT045791	0
128	VDRC 203935	VT016848	0
129	VDRC 202538	VT032907	0
130	VDRC 203984	VT062245	0
131	VDRC 205034	VT060196	0
132	VDRC 207789	VT041298	0
133	VDRC 206418	VT049371	0
134	VDRC 203267	VT029203	0
135	VDRC 203267	VT029203	1.5625
136	BDSC 26263	UAS-dTrpA1	3.84615
137	VDRC 206660	VT013039	4.6875
138	BDSC 49961	GMR37F05-GAL4	5
139	BDSC 50146	GMR42B10-GAL4	5
140	BDSC 38810	GMR52A06-GAL4	5
141	BDSC 39973	GMR77F07-GAL4	5
142	BDSC 40458	GMR86D08-GAL4	5
143	VDRC 201830	VT043635	5

144	VDRC 207088	VT050546	5
145	VDRC 207914	VT017745	5
146	VDRC 202842	VT059229	5
147	VDRC 206712	VT043663	5
148	VDRC 205377	VT049112	5
149	VDRC 203901	VT063556	5
150	VDRC 201617	VT049245	5
151	VDRC 206420	VT049570	5
152	VDRC 204187	VT062763	5
153	VDRC 204778	VT028452	5
154	VDRC 200252	VT034795	5
155	VDRC 201744	VT056509	5
156	VDRC 208860	VT030527	5
157	VDRC 204797	VT030528	5
158	VDRC 204931	VT038156	5
159	VDRC 202537	VT032906	5
160	VDRC 204703	VT046912	5
161	VDRC 200084	VT019428	5
162	VDRC 206523	VT020016	5
163	VDRC 203128	VT021366	5
164	VDRC 201412	VT045153	5

165	VDRC 207611	VT037802	5
166	VDRC 208087	VT030526	7.8125
167	VDRC 204949	VT048656	9.375
168	BDSC 47826	GMR88C04-GAL4	10
169	VDRC 202269	VT025803	10
170	VDRC 203052	VT017205	10
171	VDRC 200911	VT041424	10
172	VDRC 201230	VT015784	12.5
173	BDSC 49396	GMR53D04-GAL4	15
174	VDRC 205453	VT036779	15
175	VDRC 203966	VT040981	15
176	VDRC 205806	VT000456	15
177	VDRC 200309	VT050245	15
178	VDRC 206939	VT037470	15
179	VDRC 204317	VT030091	15
180	BDSC 50149	GMR42C05-GAL4	20
181	BDSC 50386	GMR48G07-GAL4	20
182	BDSC 48967	GMR22B01-GAL4	20
183	VDRC 204407	VT059796	20
184	VDRC 203800	VT038168	20
185	VDRC 206142	VT058927	20

186	VDRC 204139	VT017376	21.875
187	VDRC 204934	VT043645	25
188	VDRC 203186	VT013509	25
189	BDSC 48016	GMR9A03-GAL4	30
190	VDRC 20055	VT064520	30
191	VDRC 203984	VT062245	40.625
192	VDRC 204969	VT040416	42.85
193	VDRC 202699	VT041723	54.117
194	VDRC 203800	VT038168	55
195	BDSC 39951	GMR77B08-GAL4	65

REFERENCES

Ahn, J. E., Chen, Y. & Amrein, H. 2017. Molecular basis of fatty acid taste in Drosophila. *Elife,* 6.

Asahina, K. 2018. Sex differences in Drosophila behavior: Qualitative and Quantitative Dimorphism. *Curr Opin Physiol,* 6**,** 35-45.

Auer, T. O. & Benton, R. 2016. Sexual circuitry in Drosophila. *Curr Opin Neurobiol,* 38**,** 18-26.

Awasaki, T. & Kimura, K. 1997. pox-neuro is required for development of chemosensory bristles in Drosophila. *J Neurobiol,* 32**,** 707-21.

Bohra, A. A., Kallman, B. R., Reichert, H. & Vijayraghavan, K. 2018. Identification of a Single Pair of Interneurons for Bitter Taste Processing in the Drosophila Brain. *Curr Biol,* 28**,** 847-858 e3.

Boll, W. & Noll, M. 2002. The Drosophila Pox neuro gene: control of male courtship behavior and fertility as revealed by a complete dissection of all enhancers. *Development,* 129**,** 5667-81.

Brand, A. H. & Perrimon, N. 1993. Targeted gene expression as a means of altering cell fates and generating dominant phenotypes. *Development,* 118**,** 401-15.

Chandegra, B., Tang, J. L. Y., Chi, H. & Alic, N. 2017. Sexually dimorphic effects of dietary sugar on lifespan, feeding and starvation resistance in Drosophila. *Aging (Albany NY),* 9**,** 2521-2528.

Chen, Y. & Amrein, H. 2017. Ionotropic Receptors Mediate Drosophila Oviposition Preference through Sour Gustatory Receptor Neurons. *Curr Biol,* 27**,** 2741-2750 e4.

Chen, Y. D. & Dahanukar, A. 2017. Molecular and Cellular Organization of Taste Neurons in Adult Drosophila Pharynx. *Cell Rep,* 21**,** 2978-2991.

Chen, Y. D., Park, S. J., Ja, W. W. & Dahanukar, A. 2018. Using Pox-Neuro (Poxn) Mutants in Drosophila Gustation Research: A Double-Edged Sword. *Front Cell Neurosci,* 12**,** 382.

Clyne, P. J., Warr, C. G. & Carlson, J. R. 2000. Candidate taste receptors in Drosophila. *Science,* 287**,** 1830-4.

Dawydow, A., Gueta, R., Ljaschenko, D., Ullrich, S., Hermann, M., Ehmann, N., Gao, S., Fiala, A., Langenhan, T., Nagel, G. & Kittel, R. J. 2014. Channelrhodopsin-2-

XXL, a powerful optogenetic tool for low-light applications. *Proc Natl Acad Sci U S A,* 111**,** 13972-7.

Deshpande, S. A., Carvalho, G. B., Amador, A., Phillips, A. M., Hoxha, S., Lizotte, K. J. & Ja, W. W. 2014. Quantifying Drosophila food intake: comparative analysis of current methodology. *Nat Methods,* 11**,** 535-40.

Dethier, V. G. 1976. *The hungry fly : a physiological study of the behavior associated with feeding,* Cambridge, Mass., Harvard University Press.

Diegelmann, S., Jansen, A., Jois, S., Kastenholz, K., Velo Escarcena, L., Strudthoff, N. & Scholz, H. 2017. The CApillary FEeder Assay Measures Food Intake in Drosophila melanogaster. *J Vis Exp*.

Dolan, M. J., Frechter, S., Bates, A. S., Dan, C., Huoviala, P., Roberts, R. J., Schlegel, P., Dhawan, S., Tabano, R., Dionne, H., Christoforou, C., Close, K., Sutcliffe, B., Giuliani, B., Li, F., Costa, M., Ihrke, G., Meissner, G. W., Bock, D. D., Aso, Y., Rubin, G. M. & Jefferis, G. S. 2019. Neurogenetic dissection of the Drosophila lateral horn reveals major outputs, diverse behavioural functions, and interactions with the mushroom body. *Elife,* 8.

Du, E. J., Ahn, T. J., Wen, X., Seo, D. W., Na, D. L., Kwon, J. Y., Choi, M., Kim, H. W., Cho, H. & Kang, K. 2016. Nucleophile sensitivity of Drosophila TRPA1 underlies light-induced feeding deterrence. *Elife,* 5.

Erdman, S. E. & Burtis, K. C. 1993. The Drosophila doublesex proteins share a novel zinc finger related DNA binding domain. *EMBO J,* 12**,** 527-35.

Fan, P., Manoli, D. S., Ahmed, O. M., Chen, Y., Agarwal, N., Kwong, S., Cai, A. G., Neitz, J., Renslo, A., Baker, B. S. & Shah, N. M. 2013. Genetic and neural mechanisms that inhibit Drosophila from mating with other species. *Cell,* 154**,** 89-102.

Flood, T. F., Iguchi, S., Gorczyca, M., White, B., Ito, K. & Yoshihara, M. 2013. A single pair of interneurons commands the Drosophila feeding motor program. *Nature,* 499**,** 83-7.

Ganguly, A., Pang, L., Duong, V. K., Lee, A., Schoniger, H., Varady, E. & Dahanukar, A. 2017. A Molecular and Cellular Context-Dependent Role for Ir76b in Detection of Amino Acid Taste. *Cell Rep,* 18**,** 737-750.

Gordon, M. D. & Scott, K. 2009. Motor control in a Drosophila taste circuit. *Neuron,* 61**,** 373-84.

He, Z., Luo, Y., Shang, X., Sun, J. S. & Carlson, J. R. 2019. Chemosensory sensilla of the Drosophila wing express a candidate ionotropic pheromone receptor. *PLoS Biol,* 17**,** e2006619.

Hussain, A., Zhang, M., Ucpunar, H. K., Svensson, T., Quillery, E., Gompel, N., Ignell, R. & Grunwald Kadow, I. C. 2016. Ionotropic Chemosensory Receptors Mediate the Taste and Smell of Polyamines. *PLoS Biol,* 14**,** e1002454.

Inagaki, H. K., Ben-Tabou De-Leon, S., Wong, A. M., Jagadish, S., Ishimoto, H., Barnea, G., Kitamoto, T., Axel, R. & Anderson, D. J. 2012. Visualizing neuromodulation in vivo: TANGO-mapping of dopamine signaling reveals appetite control of sugar sensing. *Cell,* 148**,** 583-95.

Inagaki, H. K., Jung, Y., Hoopfer, E. D., Wong, A. M., Mishra, N., Lin, J. Y., Tsien, R. Y. & Anderson, D. J. 2014a. Optogenetic control of Drosophila using a red-shifted channelrhodopsin reveals experience-dependent influences on courtship. *Nat Methods,* 11**,** 325-32.

Inagaki, H. K., Panse, K. M. & Anderson, D. J. 2014b. Independent, reciprocal neuromodulatory control of sweet and bitter taste sensitivity during starvation in Drosophila. *Neuron,* 84**,** 806-20.

Ito, H., Fujitani, K., Usui, K., Shimizu-Nishikawa, K., Tanaka, S. & Yamamoto, D. 1996. Sexual orientation in Drosophila is altered by the satori mutation in the sex-determination gene fruitless that encodes a zinc finger protein with a BTB domain. *Proc Natl Acad Sci U S A,* 93**,** 9687-92.

Itskov, P. M., Moreira, J. M., Vinnik, E., Lopes, G., Safarik, S., Dickinson, M. H. & Ribeiro, C. 2014. Automated monitoring and quantitative analysis of feeding behaviour in Drosophila. *Nat Commun,* 5**,** 4560.

Ja, W. W., Carvalho, G. B., Mak, E. M., De La Rosa, N. N., Fang, A. Y., Liong, J. C., Brummel, T. & Benzer, S. 2007. Prandiology of Drosophila and the CAFE assay. *Proc Natl Acad Sci U S A,* 104**,** 8253-6.

Jaeger, A. H., Stanley, M., Weiss, Z. F., Musso, P. Y., Chan, R. C., Zhang, H., Feldman-Kiss, D. & Gordon, M. D. 2018. A complex peripheral code for salt taste in Drosophila. *Elife,* 7.

Jefferis, G. S., Potter, C. J., Chan, A. M., Marin, E. C., Rohlfing, T., Maurer, C. R., Jr. & Luo, L. 2007. Comprehensive maps of Drosophila higher olfactory centers: spatially segregated fruit and pheromone representation. *Cell,* 128**,** 1187-203.

Jenett, A., Rubin, G. M., Ngo, T. T., Shepherd, D., Murphy, C., Dionne, H., Pfeiffer, B. D., Cavallaro, A., Hall, D., Jeter, J., Iyer, N., Fetter, D., Hausenfluck, J. H., Peng, H., Trautman, E. T., Svirskas, R. R., Myers, E. W., Iwinski, Z. R., Aso, Y., Depasquale, G. M., Enos, A., Hulamm, P., Lam, S. C., Li, H. H., Laverty, T. R., Long, F., Qu, L., Murphy, S. D., Rokicki, K., Safford, T., Shaw, K., Simpson, J. H., Sowell, A., Tae, S., Yu, Y. & Zugates, C. T. 2012. A GAL4-driver line resource for Drosophila neurobiology. *Cell Rep,* 2**,** 991-1001.

Kain, P. & Dahanukar, A. 2015. Secondary taste neurons that convey sweet taste and starvation in the Drosophila brain. *Neuron,* 85**,** 819-32.

Kang, K., Panzano, V. C., Chang, E. C., Ni, L., Dainis, A. M., Jenkins, A. M., Regna, K., Muskavitch, M. A. & Garrity, P. A. 2011. Modulation of TRPA1 thermal sensitivity enables sensory discrimination in Drosophila. *Nature,* 481**,** 76-80.

Keene, A. C. & Masek, P. 2012. Optogenetic induction of aversive taste memory. *Neuroscience,* 222**,** 173-80.

Kim, H., Kirkhart, C. & Scott, K. 2017. Long-range projection neurons in the taste circuit of Drosophila. *Elife,* 6.

Klapoetke, N. C., Murata, Y., Kim, S. S., Pulver, S. R., Birdsey-Benson, A., Cho, Y. K., Morimoto, T. K., Chuong, A. S., Carpenter, E. J., Tian, Z., Wang, J., Xie, Y., Yan, Z., Zhang, Y., Chow, B. Y., Surek, B., Melkonian, M., Jayaraman, V., Constantine-Paton, M., Wong, G. K. & Boyden, E. S. 2014. Independent optical excitation of distinct neural populations. *Nat Methods,* 11**,** 338-46.

Knight, D., Xie, W. & Boulianne, G. L. 2011. Neurexins and neuroligins: recent insights from invertebrates. *Mol Neurobiol,* 44**,** 426-40.

Kvon, E. Z., Kazmar, T., Stampfel, G., Yanez-Cuna, J. O., Pagani, M., Schernhuber, K., Dickson, B. J. & Stark, A. 2014. Genome-scale functional characterization of Drosophila developmental enhancers in vivo. *Nature,* 512**,** 91-5.

Kwon, J. Y., Dahanukar, A., Weiss, L. A. & Carlson, J. R. 2014. A map of taste neuron projections in the Drosophila CNS. *J Biosci,* 39**,** 565-74.

Ledue, E. E., Chen, Y. C., Jung, A. Y., Dahanukar, A. & Gordon, M. D. 2015. Pharyngeal sense organs drive robust sugar consumption in Drosophila. *Nat Commun,* 6**,** 6667.

Ledue, E. E., Mann, K., Koch, E., Chu, B., Dakin, R. & Gordon, M. D. 2016. Starvation-Induced Depotentiation of Bitter Taste in Drosophila. *Curr Biol,* 26**,** 2854-2861.

Ling, F., Dahanukar, A., Weiss, L. A., Kwon, J. Y. & Carlson, J. R. 2014. The molecular and cellular basis of taste coding in the legs of Drosophila. *J Neurosci,* 34**,** 7148-64.

Marella, S., Fischler, W., Kong, P., Asgarian, S., Rueckert, E. & Scott, K. 2006. Imaging taste responses in the fly brain reveals a functional map of taste category and behavior. *Neuron,* 49**,** 285-95.

Marin, E. C., Jefferis, G. S., Komiyama, T., Zhu, H. & Luo, L. 2002. Representation of the glomerular olfactory map in the Drosophila brain. *Cell,* 109**,** 243-55.

Milyaev, N., Osumi-Sutherland, D., Reeve, S., Burton, N., Baldock, R. A. & Armstrong, J. D. 2012. The Virtual Fly Brain browser and query interface. *Bioinformatics,* 28**,** 411-5.

Miyamoto, T. & Amrein, H. 2014. Diverse roles for the Drosophila fructose sensor Gr43a. *Fly (Austin),* 8**,** 19-25.

Miyamoto, T., Slone, J., Song, X. & Amrein, H. 2012. A fructose receptor functions as a nutrient sensor in the Drosophila brain. *Cell,* 151**,** 1113-25.

Miyazaki, T., Lin, T. Y., Ito, K., Lee, C. H. & Stopfer, M. 2015. A gustatory second-order neuron that connects sucrose-sensitive primary neurons and a distinct region of the gnathal ganglion in the Drosophila brain. *J Neurogenet,* 29**,** 144-55.

Moon, S. J., Kottgen, M., Jiao, Y., Xu, H. & Montell, C. 2006. A taste receptor required for the caffeine response in vivo. *Curr Biol,* 16**,** 1812-7.

Moreira, J. M., Itskov, P. M., Goldschmidt, D., Baltazar, C., Steck, K., Tastekin, I., Walker, S. J. & Ribeiro, C. 2019. optoPAD, a closed-loop optogenetics system to study the circuit basis of feeding behaviors. *Elife,* 8.

Murphy, K. R., Park, J. H., Huber, R. & Ja, W. W. 2017. Simultaneous measurement of sleep and feeding in individual Drosophila. *Nat Protoc,* 12**,** 2355-2366.

Nicolai, L. J., Ramaekers, A., Raemaekers, T., Drozdzecki, A., Mauss, A. S., Yan, J., Landgraf, M., Annaert, W. & Hassan, B. A. 2010. Genetically encoded dendritic marker sheds light on neuronal connectivity in Drosophila. *Proc Natl Acad Sci U S A,* 107**,** 20553-8.

Park, A., Tran, T. & Atkinson, N. S. 2018. Monitoring food preference in Drosophila by oligonucleotide tagging. *Proc Natl Acad Sci U S A,* 115**,** 9020-9025.

Pfeiffer, B. D., Jenett, A., Hammonds, A. S., Ngo, T. T., Misra, S., Murphy, C., Scully, A., Carlson, J. W., Wan, K. H., Laverty, T. R., Mungall, C., Svirskas, R., Kadonaga, J. T., Doe, C. Q., Eisen, M. B., Celniker, S. E. & Rubin, G. M. 2008. Tools for neuroanatomy and neurogenetics in Drosophila. *Proc Natl Acad Sci U S A,* 105**,** 9715-20.

Pool, A. H., Kvello, P., Mann, K., Cheung, S. K., Gordon, M. D., Wang, L. & Scott, K. 2014. Four GABAergic interneurons impose feeding restraint in Drosophila. *Neuron,* 83**,** 164-77.

Raad, H., Ferveur, J. F., Ledger, N., Capovilla, M. & Robichon, A. 2016. Functional Gustatory Role of Chemoreceptors in Drosophila Wings. *Cell Rep,* 15**,** 1442-1454.

Ribeiro, C. & Dickson, B. J. 2010. Sex peptide receptor and neuronal TOR/S6K signaling modulate nutrient balancing in Drosophila. *Curr Biol,* 20**,** 1000-5.

Ro, J., Harvanek, Z. M. & Pletcher, S. D. 2014. FLIC: high-throughput, continuous analysis of feeding behaviors in Drosophila. *PLoS One,* 9**,** e101107.

Ryner, L. C., Goodwin, S. F., Castrillon, D. H., Anand, A., Villella, A., Baker, B. S., Hall, J. C., Taylor, B. J. & Wasserman, S. A. 1996. Control of male sexual behavior and sexual orientation in Drosophila by the fruitless gene. *Cell,* 87**,** 1079-89.

Schwarz, O., Bohra, A. A., Liu, X., Reichert, H., Vijayraghavan, K. & Pielage, J. 2017. Motor control of Drosophila feeding behavior. *Elife,* 6.

Scott, K., Brady, R., Jr., Cravchik, A., Morozov, P., Rzhetsky, A., Zuker, C. & Axel, R. 2001. A chemosensory gene family encoding candidate gustatory and olfactory receptors in Drosophila. *Cell,* 104**,** 661-73.

Shell, B. C., Schmitt, R. E., Lee, K. M., Johnson, J. C., Chung, B. Y., Pletcher, S. D. & Grotewiel, M. 2018. Measurement of solid food intake in Drosophila via consumption-excretion of a dye tracer. *Sci Rep,* 8**,** 11536.

Shiraiwa, T. & Carlson, J. R. 2007. Proboscis extension response (PER) assay in Drosophila. *J Vis Exp***,** 193.

Steck, K., Walker, S. J., Itskov, P. M., Baltazar, C., Moreira, J. M. & Ribeiro, C. 2018. Internal amino acid state modulates yeast taste neurons to support protein homeostasis in Drosophila. *Elife,* 7.

Thorne, N., Chromey, C., Bray, S. & Amrein, H. 2004. Taste perception and coding in Drosophila. *Curr Biol,* 14**,** 1065-79.

Walker, S. J., Corrales-Carvajal, V. M. & Ribeiro, C. 2015. Postmating Circuitry Modulates Salt Taste Processing to Increase Reproductive Output in Drosophila. *Curr Biol,* 25**,** 2621-30.

Wang, Z., Singhvi, A., Kong, P. & Scott, K. 2004. Taste representations in the Drosophila brain. *Cell,* 117**,** 981-91.

Weiss, L. A., Dahanukar, A., Kwon, J. Y., Banerjee, D. & Carlson, J. R. 2011. The molecular and cellular basis of bitter taste in Drosophila. *Neuron,* 69**,** 258-72.

Wong, A. M., Wang, J. W. & Axel, R. 2002. Spatial representation of the glomerular map in the Drosophila protocerebrum. *Cell,* 109**,** 229-41.

Yapici, N., Cohn, R., Schusterreiter, C., Ruta, V. & Vosshall, L. B. 2016. A Taste Circuit that Regulates Ingestion by Integrating Food and Hunger Signals. *Cell,* 165**,** 715-29.

Youn, H., Kirkhart, C., Chia, J. & Scott, K. 2018. A subset of octopaminergic neurons that promotes feeding initiation in Drosophila melanogaster. *PLoS One,* 13**,** e0198362.

Zhang, Y. Q., Rodesch, C. K. & Broadie, K. 2002. Living synaptic vesicle marker: synaptotagmin-GFP. *Genesis,* 34**,** 142-5.

Zhang, Y. V., Ni, J. & Montell, C. 2013. The molecular basis for attractive salt-taste coding in Drosophila. *Science,* 340**,** 1334-8.

CHAPTER VI

Conclusion and Perspective

Some parts of this chapter have been published previously – **YCD Chen**, SJ Park, WW Ja, and A Dahanukar. Using Pox-neuro (Poxn) mutants in Drosophila gustation research: a double-edged sword. *Frontiers in Cellular Neuroscience*, October 24, 2018; 12(382).

In this thesis, I report the use of molecular, genetic, and behavioral tools to investigate the organization and function of the pharyngeal taste organs in adult *Drosophila*. Given the anatomical location of pharyngeal taste organs, it has long been assumed that they act as gatekeepers for monitoring food quality and controlling ingestion, but there is little direct knowledge of the functional roles of sensory neurons that reside within. There are recent studies hinting at the function of pharyngeal taste neurons in detecting bacterial lipopolysaccharides (Soldano et al., 2016) and high concentrations of salt (NaCl) (Kim et al., 2017), but a systematic analysis of pharyngeal taste in feeding behaviors is lacking. We took advantage of *Poxn* mutants that offer a minimal taste model for probing the roles of pharyngeal taste in feeding control. *Poxn* mutants are capable of selecting appetitive tastants such as sugars and amino acids (Chapter IV), and rejecting aversive tastants such as bitter compounds, high salt concentration, and very low pH (Chapter III), providing support for the idea that pharyngeal taste organs pose an important link between taste sensory input and feeding behavioral output. Guided by the pharyngeal receptor-to-neuron maps described in Chapter II (Chen and Dahanukar, 2017), we used genetic dissection strategies to interrogate the function of different neuronal subsets in driving behavioral responses to various tastants (Chapter III and IV). These experiments demonstrate the contributions of pharyngeal taste neurons in controlling food intake, and also to provide a platform for probing sensory functions of the many remaining orphan neurons.

Cell-type specific tools for labeling pharyngeal GRNs

The *chemoreceptor-GAL4* lines mapped to three pharyngeal taste organs have full coverage of all 24 pharyngeal GRNs. However, most of the *chemoreceptor-GAL4* lines labeled more than one neuron. Our behavioral data suggested a complex functional heterogeneity among pharyngeal GRNs. Thus, manipulating groups of pharyngeal GRNs via the *chemoreceptor-GAL4* lines described here may not always be suitable for assessing functional roles of individual neurons in feeding control. A recent study has generated many *Ir-GAL4* lines (Sanchez-Alcaniz et al., 2018), many of which show expression in pharyngeal taste organs. Incorporation of these newly generated *Ir-GAL4* lines in our pharyngeal receptor-to-neuron maps would provide more tools for dissecting distinct subsets of pharyngeal GRNs. In addition, use of genetic intersectional strategies such as split-GAL4 or GAL80 together with other binary expression systems (Pfeiffer et al., 2010, Lee and Luo, 1999, Luan et al., 2006) to further expand the pharyngeal genetic toolkit might ultimately achieve cell-type specific labeling at a single neuron level in the pharynx.

We also established taste-blind flies and a neuronal function restoration toolkit to protect selective classes of pharyngeal GRNs in otherwise taste-blind flies. These experiments allowed us to probe neuronal "sufficiency" for feeding behaviors and have uncovered complex patterns of sensory integration in pharynx. The functional protection toolkit could also be expanded in the future by generation of *chemoreceptor-GAL80* lines using a recently developed homology-assisted CRISPR knock-in (HACK) technique (Xie

et al., 2018), which would allow for *in vivo* conversion of existing *GAL4* insertions into those expressing GAL80. A significant advantage of HACK is that *GAL80* is likely to be expressed in the same pattern as each characterized *GAL4* line, by virtue of its placement in the same genomic location. Such an expanded toolkit would allow functional restoration of smaller subsets of pharyngeal GRNs, possibly at the single neuron resolution.

Considerations in using *Poxn* mutants for gustation research

Although we demonstrated the advantage of using *Pox-neuro* (*Poxn*) mutants to study the organization and function pharyngeal taste circuits, *Poxn* is also expressed in various postmitotic neurons in the developing brain, including a protocerebral dorsal cluster and a deutocerebral ventral cluster (Minocha et al., 2017). The former is crucial for connections of the bulb with the ellipsoid body, while the latter is important for connections between the antennal lobe and lateral horn. In *Poxn* mutants, the *Poxn*-expressing brain neurons cannot establish proper connections with their targets. The behavioral consequences of the central nervous system defects are not clear and await further characterization. Although the wiring defects were observed in *Poxn* mutants homozygous for the *ΔM22-B5* allele, created by an imprecise excision spanning over 17 kb that removes part of the *Poxn* gene and promoter as well as an adjacent gene encoding a sugar transporter homolog, CG8249 (Boll and Noll, 2002), a recent study pinpoints a 1442 kb upstream fragment as an important enhancer for brain function (Minocha et al., 2017). In addition to the defects in the central nervous system, mutants homozygous for

the *ΔM22-B5* allele also have defects in leg/antenna segmentation, male courtship, male fertility, and flight (Boll and Noll, 2002). Although defined enhancer regions have been implicated for specific functions (Boll and Noll, 2002), little is known about involvement of the adjacent gene that is removed in the *ΔM22-B5* allele in fly behavior. An ethyl methanesulfonate (EMS)-generated allele, $Poxn^{70}$, has been reported to be an amorphic allele (Awasaki and Kimura, 1997) with adjacent genes likely intact. Thus, the transheterozygous allelic combination of $Poxn^{\Delta M22\text{-}B5}$/ $Poxn^{70}$ in recent studies might circumvent some of the defects described in flies homozygous for the *ΔM22-B5* allele (Chen and Dahanukar, 2017, Ledue et al., 2015), although this remains unconfirmed.

Given that *Poxn* mutants are defective in external taste sensing, care must be taken in selecting appropriate assays for quantifying food intake. An increasing number of assays have been developed for measuring food intake in *Drosophila*, including the quantification of food labeled with radiotracers or colorimetric dyes, or direct monitoring of consumed volume of liquid diet (solutions of yeast or sugar) in the Capillary Feeder (CAFE) assay (Deshpande et al., 2014). *Poxn* mutants have been shown to ingest food as either liquid (i.e. in the CAFE assay) (Devineni and Heberlein, 2009) or solid (i.e. radiolabeling or colorimetric dyes in agar-based medium) (Deshpande et al., 2015, Chen and Dahanukar, 2017, Ledue et al., 2015). However, a recent report showed that *Poxn* mutant flies have difficulty in finding food sources with increased distance between them in binary choice assays (Abu et al., 2018), suggesting a context-dependent foraging deficiency in *Poxn* flies. In our study (Chapter IV), we used recently developed FLIC

assays to perform quantification of feeding parameters at high resolution, thus offering another alternative for evaluating mechanisms of feeding control in *Poxn* mutants.

In addition to the effects of different *Poxn* mutant alleles on the development of the central nervous system, another precaution in using *Poxn* mutants in gustatory research is that there has been no assessment of whether the supernumerary mechanosensory bristles have any function in mechanosensing and thus impart hypersensitivity to mechanical stimuli. Indeed, recent studies have identified at least two different neuronal populations that mediate feeding preference on the basis of texture. One class is the mechanosensory neurons in labellar taste sensilla, which express a mechanosensory receptor, NOMPC (Sanchez-Alcaniz et al., 2017). The second is multidendritic neurons in the labellum (md-L), expressing the transmembrane channel-like (TMC) protein (Zhang et al., 2016). It is not clear how these two mechanosensing mechanisms interact, but the contribution of mechanosensation in feeding behaviors cannot be ignored. In sum, given the potential functions of *Poxn* outside the taste system and its role in the developing nervous system, care should be taken to ensure that all genetic manipulations and comparisons use the same *Poxn* mutant background. In this way, it will help to minimize or rule out hypersensitivity in mechanosensation and other potential defects that confound the interpretation of results.

Sufficiency and necessity of pharyngeal taste in feeding control

Poxn mutant flies that lack all external taste hairs still exhibit qualitatively similar food choice and intake behaviors to both appetitive and aversive compounds, suggesting that pharyngeal taste alone is sufficient to determine these behavioral outcomes. However, reciprocal experiments to test the necessity of pharyngeal taste in feeding control have not been performed. The *Ir25a-GAL4* driver used here to label all 24 pharyngeal GRNs is also broadly expressed in the labellum, tarsi and wing margins (Chen and Amrein, 2017, Ahn et al., 2017, Sanchez-Alcaniz et al., 2018, Lee et al., 2018), disqualifying it for use in silencing pharyngeal GRNs specifically in otherwise wild type flies. It is possible that flies without all pharyngeal GRNs will behave similarly to wild type flies in different feeding assays, suggesting functional redundancies between external and internal GRNs. Alternatively, one might observe defects in feeding assays when pharyngeal taste input is absent, indicating selective roles of pharyngeal taste in regulating feeding behaviors. Given the current paucity of genetic tools for ablating taste input from internal pharyngeal GRNs without affecting external GRNs, resolution of such questions awaits the future.

The observation that the *Poxn* mutation did not affect cell fate in pharyngeal taste sensilla posits that other transcription factors might act specifically in pharyngeal taste sensilla during development. With recent advances in single-cell RNA sequencing technologies, it will be possible to identify specific markers for pharyngeal GRNs and achieve pharynx-specific genetic manipulations. Alternatively, two olfactory binding

proteins (OBPs), OBP19c and OPB56b have been shown to be exclusively expressed in support cells of taste sensilla in LSO, VCSO, and DCSO (Galindo and Smith, 2001). Genetic ablation of these support cells via expression of pro-apoptotic genes (e.g. Reaper, Hind, and Grim) might disrupt function of entire pharyngeal taste sensilla, thereby providing another potential genetic strategy to investigate the necessity of pharyngeal taste in feeding control.

Pharyngeal taste circuits in the *Drosophila* brain

To understand taste coding in the brain and the relationships between sensory input and behavioral output, it is essential to explore the brain circuits processing pharyngeal taste information. The recently developed circuit-tracing technique, trans-Tango, has been applied to identify second-order sweet taste neurons in the fly (Talay et al., 2017). However, the presence of over 100 sweet GRNs in peripheral organs resulted in labeling of a large number of secondary neurons, creating challenges for further studies. The combination of a genetic toolkit for labeling pharyngeal GRNs and the minimal taste system in *Poxn* mutants provides a unique opportunity for detailed neuroanatomical and functional characterization of pharyngeal second-order neurons in the brain (Chapter III). As proof-of-principle, we traced secondary neurons processing appetitive (sugars and amino acids) or aversive (bitter, acids, and high salts) information and found their projections in several common brain regions, including the pars intercerebralis, a functional homolog of the mammalian hypothalamus. In many cases, single pharyngeal GRNs showed connections with multiple second-order neurons that projected to distinct

brain regions, suggesting that even specific gustatory information may be broadly conveyed across several brain regions. In addition, one noticeable difference between second-order neuron labeling in wild type and *Poxn* flies is the absence of trans-Tango-labeled neurons above the antennal lobes in *Poxn* flies, suggesting that these may specifically connect with external GRNs. Intriguingly, the external taste-specific second-order neurons seem to project to the mushroom body, the primary learning and memory center, evoking the possibility that external GRNs but not internal GRNs may provide the primary input for forming gustatory memory. However, it is still possible that internal pharyngeal GRNs are able to contribute to gustatory memory formation through synaptic connections beyond the second-order neurons. Future studies using the genetic reagents generated here to investigate gustatory memory will help to clarify the roles of external and internal GRNs in gustatory memory formation. In addition, a refined genetic toolkit for each pharyngeal GRN class would facilitate the creation of a comprehensive map of pharyngeal circuits in the brain. Functional imaging and manipulation of second-order pharyngeal GRNs could be achieved by incorporating *QUAS-CaMPARI2*, *QUAS-GCaMP*, *QUAS-CsChrimson*, and *QUAS-GRASP* transgenes into the trans-Tango system. Altogether, these experiments will provide further insight into how taste information is processed in higher-order brain circuits to control food intake.

Broader impact

Most insects have internal taste sensilla on the epipharyngeal and hypopharyngeal organs of the alimentary canal. Previous anatomical studies have suggested that these

sensilla are chemosensory (Pontes et al., 2014, Backus and Mclean, 1985, Jefferies, 1987, Foster et al., 1983, Eaton, 1979, Chapman and Boer, 1995, Mciver and Siemicki, 1981, Dethier, 1976, Nayak and Singh, 1983, Stocker and Schorderet, 1981). In *Rhodnius prolixus*, the internal gustatory sensilla of the epipharynx have been shown to detect various bitter compounds and inhibit ingestion (Pontes et al., 2014). In other insects, structures with similar functions have been observed. For example, chemosensory sensilla of leafhoppers are found in precibarium, a canal links food passage and the cibarial pump. These precibarial sensilla function in discriminating chemicals produced by host plants (Backus and Mclean, 1985). It has been proposed that internal chemosensory input likely influences the threshold of behavioral response to gustatory stimuli and contributes to various steps of feeding behaviors such as food ingestion, although their physiological role in gustation have been mostly speculative due to their poor accessibility with recording electrodes. By using *Drosophila* as an insect model, we establish a minimal pharyngeal taste system in *Poxn* mutants and lay a foundation for dissecting the function of pharyngeal GRNs. Combined with the genetic toolkit derived from the map of pharyngeal taste neurons described here, we now have the means to evaluate the sensory function of a taste organ that has often been overlooked while interpreting results of feeding behavior experiments. Such knowledge would be applicable to other insect species given the internal taste organs are wildly present in insects.

My research in the pharyngeal taste system could be extended to study mechanisms involved in meal size control, maintenance, termination of feeding, and integration between taste and hunger signals. Recent findings highlight the roles of distinct populations of pharyngeal GRNs in driving and limiting sugar consumption, respectively (Joseph et al., 2017, Ledue et al., 2015). The neuronal circuits identified here might be shared between flies and mammals and will play key roles in controlling over-eating behaviors and metabolic diseases, like obesity and diabetes. Alteration of feeding behaviors via targeting insect pharyngeal GRNs could also have vast applications in curbing the spread of diseases by insect vectors and reducing crop damage by agricultural pests.

REFERENCES

Abu, F., Wang, J. G., Oh, Y., Deng, J., Neubert, T. A. & Suh, G. S. B. 2018. Communicating the nutritional value of sugar in Drosophila. *Proc Natl Acad Sci U S A,* 115**,** E2829-E2838.

Ahn, J. E., Chen, Y. & Amrein, H. 2017. Molecular basis of fatty acid taste in Drosophila. *Elife,* 6.

Awasaki, T. & Kimura, K. 1997. pox-neuro is required for development of chemosensory bristles in Drosophila. *J Neurobiol,* 32**,** 707-21.

Backus, E. A. & Mclean, D. L. 1985. Behavioral evidence that the precibarial sensilla of leafhoppers are chemosensory and function in host discrimination. *Entomologia Experimentalis et Applicata,* 37**,** 219-228.

Boll, W. & Noll, M. 2002. The Drosophila Pox neuro gene: control of male courtship behavior and fertility as revealed by a complete dissection of all enhancers. *Development,* 129**,** 5667-81.

Chapman, R. F. & Boer, G. d. 1995. *Regulatory mechanisms in insect feeding,* New York, Chapman & Hall.

Chen, Y. & Amrein, H. 2017. Ionotropic Receptors Mediate Drosophila Oviposition Preference through Sour Gustatory Receptor Neurons. *Curr Biol,* 27**,** 2741-2750 e4.

Chen, Y. D. & Dahanukar, A. 2017. Molecular and Cellular Organization of Taste Neurons in Adult Drosophila Pharynx. *Cell Rep,* 21**,** 2978-2991.

Deshpande, S. A., Carvalho, G. B., Amador, A., Phillips, A. M., Hoxha, S., Lizotte, K. J. & Ja, W. W. 2014. Quantifying Drosophila food intake: comparative analysis of current methodology. *Nat Methods,* 11**,** 535-40.

Deshpande, S. A., Yamada, R., Mak, C. M., Hunter, B., Soto Obando, A., Hoxha, S. & Ja, W. W. 2015. Acidic Food pH Increases Palatability and Consumption and Extends Drosophila Lifespan. *J Nutr,* 145**,** 2789-96.

Dethier, V. G. 1976. *The hungry fly : a physiological study of the behavior associated with feeding,* Cambridge, Mass., Harvard University Press.

Devineni, A. V. & Heberlein, U. 2009. Preferential ethanol consumption in Drosophila models features of addiction. *Curr Biol,* 19**,** 2126-32.

Eaton, J. L. 1979. Chemoreceptors in the cibario-pharyngeal pump of the cabbage looper moth, Trichoplusia ni (Lepidoptera: Noctuidae). *J Morphol,* 160**,** 7-15.

Foster, S., Goodman, L. J. & Duckett, J. G. 1983. Sensory receptors associated with the stylets and cibarium of the rice brown planthopper, Nilapavarta lugens. *Cell and Tissue Research,* 232**,** 111-119.

Galindo, K. & Smith, D. P. 2001. A large family of divergent Drosophila odorant-binding proteins expressed in gustatory and olfactory sensilla. *Genetics,* 159**,** 1059-72.

Jefferies, D. 1987. Labrocibarial sensilla in the female of the black fly Simulium damnosum s.l. (Diptera: Simuliidae). *Canadian Journal of Zoology,* 65**,** 441-444.

Joseph, R. M., Sun, J. S., Tam, E. & Carlson, J. R. 2017. A receptor and neuron that activate a circuit limiting sucrose consumption. *Elife,* 6.

Kim, H., Jeong, Y. T., Choi, M. S., Choi, J., Moon, S. J. & Kwon, J. Y. 2017. Involvement of a Gr2a-Expressing Drosophila Pharyngeal Gustatory Receptor Neuron in Regulation of Aversion to High-Salt Foods. *Mol Cells,* 40**,** 331-338.

Ledue, E. E., Chen, Y. C., Jung, A. Y., Dahanukar, A. & Gordon, M. D. 2015. Pharyngeal sense organs drive robust sugar consumption in Drosophila. *Nat Commun,* 6**,** 6667.

Lee, T. & Luo, L. 1999. Mosaic analysis with a repressible cell marker for studies of gene function in neuronal morphogenesis. *Neuron,* 22**,** 451-61.

Lee, Y., Poudel, S., Kim, Y., Thakur, D. & Montell, C. 2018. Calcium Taste Avoidance in Drosophila. *Neuron,* 97**,** 67-74 e4.

Luan, H., Peabody, N. C., Vinson, C. R. & White, B. H. 2006. Refined spatial manipulation of neuronal function by combinatorial restriction of transgene expression. *Neuron,* 52**,** 425-36.

Mciver, S. & Siemicki, R. 1981. Innervation of cibarial sensilla of Aedes aegypti (L.) (Diptera: Culicidae). *International Journal of Insect Morphology and Embryology,* 10**,** 355-357.

Minocha, S., Boll, W. & Noll, M. 2017. Crucial roles of Pox neuro in the developing ellipsoid body and antennal lobes of the Drosophila brain. *PLoS One,* 12**,** e0176002.

Nayak, S. V. & Singh, R. N. 1983. Sensilla on the Tarsal Segments and Mouthparts of Adult Drosophila-Melanogaster Meigen (Diptera, Drosophilidae). *International Journal of Insect Morphology & Embryology,* 12**,** 273-291.

Pfeiffer, B. D., Ngo, T. T., Hibbard, K. L., Murphy, C., Jenett, A., Truman, J. W. & Rubin, G. M. 2010. Refinement of tools for targeted gene expression in Drosophila. *Genetics,* 186**,** 735-55.

Pontes, G., Minoli, S., Insaurralde, I. O., De Brito Sanchez, M. G. & Barrozo, R. B. 2014. Bitter stimuli modulate the feeding decision of a blood-sucking insect via two sensory inputs. *J Exp Biol,* 217**,** 3708-17.

Sanchez-Alcaniz, J. A., Silbering, A. F., Croset, V., Zappia, G., Sivasubramaniam, A. K., Abuin, L., Sahai, S. Y., Munch, D., Steck, K., Auer, T. O., Cruchet, S., Neagu-Maier, G. L., Sprecher, S. G., Ribeiro, C., Yapici, N. & Benton, R. 2018. An expression atlas of variant ionotropic glutamate receptors identifies a molecular basis of carbonation sensing. *Nat Commun,* 9**,** 4252.

Sanchez-Alcaniz, J. A., Zappia, G., Marion-Poll, F. & Benton, R. 2017. A mechanosensory receptor required for food texture detection in Drosophila. *Nat Commun,* 8**,** 14192.

Soldano, A., Alpizar, Y. A., Boonen, B., Franco, L., Lopez-Requena, A., Liu, G., Mora, N., Yaksi, E., Voets, T., Vennekens, R., Hassan, B. A. & Talavera, K. 2016. Gustatory-mediated avoidance of bacterial lipopolysaccharides via TRPA1 activation in Drosophila. *Elife,* 5.

Stocker, R. F. & Schorderet, M. 1981. Cobalt filling of sensory projections from internal and external mouthparts in Drosophila. *Cell Tissue Res,* 216**,** 513-23.

Talay, M., Richman, E. B., Snell, N. J., Hartmann, G. G., Fisher, J. D., Sorkac, A., Santoyo, J. F., Chou-Freed, C., Nair, N., Johnson, M., Szymanski, J. R. & Barnea, G. 2017. Transsynaptic Mapping of Second-Order Taste Neurons in Flies by trans-Tango. *Neuron,* 96**,** 783-795 e4.

Xie, T., Ho, M. C. W., Liu, Q., Horiuchi, W., Lin, C. C., Task, D., Luan, H., White, B. H., Potter, C. J. & Wu, M. N. 2018. A Genetic Toolkit for Dissecting Dopamine Circuit Function in Drosophila. *Cell Rep,* 23**,** 652-665.

Zhang, Y. V., Aikin, T. J., Li, Z. & Montell, C. 2016. The Basis of Food Texture Sensation in Drosophila. *Neuron,* 91**,** 863-877.